Distribution Agreement

In presenting this thesis or dissertation as a partial fulfillment of the requirements for an advanced degree from Emory University, I hereby grant to Emory University and its agents the non-exclusive license to archive, make accessible, and display my thesis or dissertation in whole or in part in all forms of media, now or hereafter known, including display on the world wide web. I understand that I may select some access restrictions as part of the online submission of this thesis or dissertation. I retain all ownership rights to the copyright of the thesis or dissertation. I also retain the right to use in future works (such as articles or books) all or part of this thesis or dissertation.

Signature:

_____ _____

Li-Ting Chien Date

Functional Characterization of *Drosophila* Bestrophin 1

By

Li-Ting Chien
Doctor of Philosophy

Graduate Division of Biological Biomedical Sciences
Program in Neuroscience

_____
Criss Hartzell, Ph.D.
Advisor

_____ _____
Randy Hall, Ph.D. Kenneth Moberg, Ph.D.
Committee Member Committee Member

_____ _____
Junmin Peng, Ph.D. Steve Traynelis, Ph.D.
Committee Member Committee Member

Accepted:

_____
Lisa A. Tedesco
Dean of Graduate School

_____
Date

Functional Characterization of *Drosophila* Bestrophin 1

By

Li-Ting Chien

B.S., National Taiwan University, 2000

Advisor: Criss Hartzell, Ph.D.

An abstract of
A dissertation submitted to the Faculty of the Graduate School of Emory University
In Partial fulfillment of the requirements for the degree of
Doctor of Philosophy
In
Graduate Division of Biological and Biomedical Sciences
Neuroscience
2008

Abstract

Functional Characterization of *Drosophila* Bestrophin 1

By Li-Ting Chien

Mutations in the human bestrophin-1 gene are genetically linked to Best vitelliform macular degeneration, which often leads to childhood blindness. The pathogenesis is unclear because the function of hBest1 is not fully understood. In this dissertation, I report the functional characterization of endogenous bestrophin currents and the identification of the physiological role of bestrophins in *Drosophila*. Here I show that (1) bestrophins clearly are the pore-forming subunit of a Cl^- channel; (2) the bestrophin Cl^- channel is regulated by both cytoplasmic Ca^{2+} and hyposmotic cell swelling; and (3) dBest1 is very likely involved in salt balance in the fly. The *Drosophila* S2 cell line expresses four bestrophins and exhibits endogenous Cl^- currents (I_{Cl}) that are stimulated by Ca^{2+} or swelling. The I_{CaCl} and $I_{Clswell}$ exhibit similar electrophysiological properties and are both suppressed by non-overlapping RNAis to dBest1, but not dBest2-4. The I_{Cl} in the dBest1 RNAi-treated S2 cells are rescued by expressing dBest1 cDNA. To determine if dBest1 is the pore-forming subunit but not just an accessory subunit of a Cl^- channel, we rescue the S2 I_{Cl} with a mutant dBest1 with altered biophysical properties. As expected for an ion channel with a mutant pore, biophysical properties of the rescued dBest1-F81C current differ significantly from the native I_{Cl}. Moreover, when F81 is substituted with a negatively charged glutamate, the anion permeability is reversed. The fact that mutating F81 alters intrinsic properties of the I_{Cl} suggests that dBest1 forms the pore of the S2 Cl^- channel. At the cellular level, dBest1 is characterized to regulate cell volume by mediating regulatory volume decrease in response to hyposmotic stimuli. Dysfunctional dBest1 is further found to associate with increased fly mortality on salty food. These studies provide important insights into the possible role of bestrophins in macular degeneration.

Functional Characterization of *Drosophila* Bestrophin 1

By

Li-Ting Chien

B.S., National Taiwan University, 2000

Advisor: Criss Hartzell, Ph.D.

A dissertation submitted to the Faculty of the Graduate School of Emory University
In Partial fulfillment of the requirements for the degree of
Doctor of Philosophy
In
Graduate Division of Biological and Biomedical Sciences
Neuroscience
2008

Acknowledgement

I whole-heartedly thank my advisor, Dr. Criss Hartzell for his assistance, mentorship, and guidance. Criss has worked side-by side with me through this entire process. Criss' approach to my training fostered my growth both as a scientist and as a person. His generous nature and creativity are truly an example for all scientists.Special thanks to former and present members of the Hartzell lab, especially Rodolphe Fischmeister, Zhiqiang Qu, Ilva Putzier, Kuai Yu, Qinghuan Xiao, Yuanyuan Cui, Charity Duran, Pat Whitworth, Liana Artinian, and Yihan Yang for their friendship and support.

I am also very grateful to my thesis committee members Dr. Kenneth Moberg, Dr. Randy Hall, Dr. Stephen Traynelis, and Dr. Junmin Peng, who have all provided me with valuable feedback and discussion for this work. I thank our collaborator Dr. Edward Blumenthal and people in the Moberg lab for their suggestions and assistance on my fly work. Thanks are also due to Dr. Wun-Shaing Wayne Chang and Dr. Chin-Tin Chen for giving me the opportunity to experience science as an undergraduate student and as a research asistant.

I also wish to thank my previous advisor Dr. Steven Estus, Dr. Wally Whiteheart, Dr. Jane Harrison, and Sandy Akay and Dr. Yoland Smith for their encouragement and support. I also wish to acknowledge Dr. Harish Joshi for introducing the beauty of Cell Biology to me and Dr. Victor Fundez for his generous advice. Thanks to the faculty and students of the Department of Cell Biology, Graduate Program in Neuroscience, and the entire Emory University for providing a friendly and open place to do scientific research.

I am especially thankful for the love and support that I have received from my family in Taiwan. Special thanks to my mom and my mother in law, who volunteer to share their time to care for my son, allowing me to accomplish my research and thesis. I send endless appreciation to my husband and my best friend, Tai-De Li, for always being there whether I needed him or not. Thanks to my baby, Benjamin, for making this not an ending, but a new beginning.

This dissertation is dedicated to my parents, Mei-Chi Li and Min-Ren Chien.

Table of Contents

Figures

Tables

CHAPTER 1

INTRODUCTION AND BACKGROUND

Mutations in the human bestrophin 1 have been genetically linked to the inherited Best Vitelliform Macular Dystrophy (Best Disease). The etiology of Best Disease remains unclear primarily because the function of bestrophin is not fully understood. Bestrophins might be a Cl^- channel because Best Disease patients lack a component of the electrooculogram that might be due to a Cl^- conductance. In this chapter, I will introduce the history of the discovery of ion channels first. I will then describe the properties of different types of Cl^- channels. This will be followed by a comprehensive introduction of Best Disease and the rationales of my thesis research.

Ion Channel in Biological Membranes

At some time in Earth's early history, primitive organisms began to acquire a protective lipid envelope to separate cytoplasm from their environment. Such biological membrane, although providing necessary segregation of the vital components from the primordial extracellular medium, also form a diffusion barrier to prevent exchange of essential metabolites, especially charged ions that are essential for cells' vitality. Specialized membrane-spanning proteins, therefore, have evolved to selectively control the movement of all the major physiological ions. There are three types of transport machinery on biological membranes: pumps, transporters, and ion channels. Pumps are molecular catalysts that drive ions and other permeant molecules against their electro-chemical gradients by coupling the pump with the energy of ATP hydrolysis. Transporters promote the transmembrane movement of one type of ion against its gradient using the energy of the electrochemical gradient of another kind of ion or permeant species. Both pumps and transporters promote transmembrane ion movement by employing

vectorial conformational change to expose the substrate binding side alternatively to the inner and outer side of the membrane. Thus, transporters and exchangers express a slow turnover rate of ~10^2/sec and ~10^4/sec respectively. Ion channels, on the other hand, form hydrophilic pores on the membrane that greatly expedite the passive flux of permeant ion down its electrochemical gradients without input of additional energy sources. Thus, the rate that ions pass through ion channels can be as high as ~10^8/sec. Therefore, ion channels can be viewed as efficient catalysts designed to speed the transit rate of ions across the lipid bilayer membrane.

The discovery of ion channels began about 50 years ago. Hodgkin and Huxley's famous Nobel Prize study in squid giant axon established that both Na^+ and K^+ contribute to the action potential but in opposing directions (Hodgkin & Huxley, 1952b, Hodgkin & Huxley, 1952a). Their studies suggested pore-forming channels as the ionic pathway across the plasma membrane. Subsequently, the discovery of patch clamping technique in 1976 by Neher and Sakmann (Neher & Sakmann, 1976), which was honored by the 1991 Nobel Prize, allowed real-time measurement of single channel currents from patches of living cell membranes and permitted the assessment of how ion channel function was altered by different stimuli. Another breakthrough invention came in 1981 when Hamill *et al.* (Hamill *et al.*, 1981) developed the giga-ohm seal and whole cell patch-clamping techniques, approaches that have been particularly used in the study of isolated cells and in brain slices. More recently, the cartoon structure of ion channels have gradually become substantiated after Mackinnon *et al.* (Doyle *et al.*, 1998) had overcome the major daunting problem of purifying membrane-spanning ion channels and crystallizing them. The term ion channel is no longer merely a plausible hypothesis now but has become substantiated in

molecular entities.

Typical molecular characteristics of ion channels are that they are composed of an assembly of integral proteins with hydrophobic amino acids gathered at the exterior protein-membrane interface and hydrophilic residues lining the inner ion conducting pore. With the exception of gap junctions (Nicholson *et al.*, 2000) and porins (Duy *et al.*, 2007), the channel-forming proteins of the outer membranes of Gram negative bacteria, mitochondria, and chloroplasts which have relatively large and permissive pores, most ion channels have narrow, highly selective pores that can open and close. Therefore, a typical ion channel is distinguished from other transport proteins by three major properties. First, the ion channel shows ion selectivity, permitting ions of specific identity to get into the pore. In fact, the atomic resolution structures of ion channels have shown that their pores are narrow enough in places to force permeant ions into intimate contact with the walls of the channel so that only ions of appropriate charge and size can pass through (Bass *et al.*, 2002, Chang *et al.*, 1998, Cowan *et al.*, 1992, Doyle *et al.*, 1998, Jiang *et al.*, 2002, Jiang *et al.*, 2003, Kuo *et al.*, 2003, Long *et al.*, 2005, Weiss *et al.*, 1991). The second important feature of ion channels is that the pore is not continuously open. Instead, they are gated, which allow ion channels to open up briefly and close again. In most cases, the gate opens in response to specific stimuli such as ligand binding (ligand-gated), electrical signals (voltage-gated), second messengers (i.e. Ca^{2+}-activated or cyclic nucleotide-gated), or mechanical force (i.e. volume-regulated or mechanically-gated), depending on the type and function of the host cell (for reviews see: (Nilius & Droogmans, 2003, Suzuki *et al.*, 2006). Therefore, ion channels can be categorized based on their gating mechanisms. The third feature of ion channels is that the direction of the ion flow is determined by the

difference between the membrane potential of the cell and the equilibrium potential (Nernst potential) of that ion which is defined by the ratio of the concentration of that type of ion at the two sides of the membrane. For example, when a Cl^- channel opens, the Cl^- flows out to depolarize the cell if the resting membrane potential is more negative than the equilibrium potential of Cl^- (E_{Cl}), therefore, providing a net outward driving force for Cl^-. In contrast, Cl^- flows into the cell to hyperpolarize a cell if the resting membrane potential is more positive than the E_{Cl}.

Chloride channel Overview

With the incorporation of multidisciplinary approaches in electrophysiology, pharmacology, molecular biology, biochemistry, bioinformatics, and structure determination, the list of ion channels has expanded exponentially during the past few decades. Based on the charge of the ions that are allowed to pass through the pore, ion channels are categorized into two super families: cation channels and anion channels. Cation channels can be subcategorized based on their gating mechanisms. The families of voltage-gated Na^+, K^+, and Ca^{2+} channels are activated by deviation in the membrane potential from the resting state and are involved mostly in electrical signaling in nerves and muscles. Ligand-gated cation channels such as the nicotinic acetylcholine receptor and glutamate receptors gate open by binding with the diffusible chemical ligand and mediate fast synaptic transmission.

While cation channels have received much attention, the study of anion channels has lagged behind. This is mainly because the most abundant physiological anion, Cl^-, unlike cations, was long thought to be distributed passively in electrochemical equilibrium across

the cell membrane. If Cl^- was passively distributed in equilibrium, it seemed useless: it could not provide energy for transport of other substances and its passive distribution precluded a signaling function (Hartzell *et al.*, 2008). For decades, the belief in the existence of Cl^- channels remained a somewhat unique interest with little physiological relevance. Nevertheless, this situation began to change with the discovery of active Cl^- transport mechanisms in cells with low resting Cl^- permeability and most importantly, with the molecular cloning of $GABA_A$ and ClC-0 chloride channels from the bovine brain (Schofield *et al.*, 1987) and the electric organ of *Torpedo* fish (Jentsch *et al.*, 1990) respectively. To date, there are ~35 mammalian genes that have been found to encode for Cl^- channel activities (compared to hundreds of genes found in cation channels) (Hartzell *et al.*, 2008).

Based on the gating mechanism, Cl^- channels are categorized into four major families: ligand-gated Cl^- channels, voltage-gated Cl^- channels, Ca^{2+}-activated Cl^- channels, and volume-regulated anion channels. Each family of Cl^- channel does not share significant homology in protein sequence with the other families, indicating that they've evolved independently of each other from various ancestor genes. Cl^- channels are ubiquitously expressed, with each family of Cl^- channels involved in different physiological processes at different developmental stages and in different tissues. Examples of physiological functions of Cl^- channels include transcellular transport of electrolytes and fluid, cell volume regulation, regulation of cytoplasmic Cl^- concentration, and stabilization of membrane potential. A more elaborate description on the discovery, biological function, activation mechanism, and structure of each family of Cl^- channel will be introduced in the following section.

Ligand-Gated Cl^- Channels

Ligand-gated Cl^- channels are heteromeric plasma membrane proteins that are activated by binding with extracellular ligands. Once bound to the ligand, the channels change conformation within the membrane, opening the pore in order to allow Cl^- to flux down its electrochemical gradient. This family of Cl^- channels is known as ionotropic receptors and are concentrated in the plasma membrane of postsynaptic cells in the region of chemical synapses. They are involved in rapid inhibitory synaptic transmission between electrically excitable cells by converting chemical signals to electrical ones. Their ability to "put a cell to rest" has a big deal to do with the co-residing Cl^- active transporters (KCC, NDAE, for example) in the plasma membrane of the same cell that build up a Cl^- gradient across the cell membrane by extruding Cl^- out to the extracellular medium. Therefore, Cl^- will flow inwardly following its electrochemical gradient upon opening of the ligand-gated Cl^- channels. The outcome of Cl^- influx is to bring the membrane potential closer to the equilibrium potential of Cl^-. The resulting change in membrane potential makes it more difficult for the cell to fire an action potential. In other word, the cell becomes hyperpolarized.

Examples of ligand-gated Cl^- channels that are involved in inhibitory synaptic transmission include the $GABA_A$ (gamma aminobutyric acid) receptor and Glycine receptor found in vertebrate central nervous system and the invertebrate Glutamate-gated Cl^- channel which is found extrajunctionally in the plasma membrane of muscle (Delgado *et al.*, 1989, Fraser *et al.*, 1990) and the neuronal cell body (Giles & Usherwood, 1985, Horseman *et al.*, 1988, Wafford *et al.*, 1989) of insects and nematodes but not in vertebrates, thus, serving as an insecticide target (Cully *et al.*, 1996).

One major feature of ligand-gated channels in action is that the changes in Cl^- permeability (and hence the changes of membrane potential) produced by activation of these Cl^- channels upon binding the ligand is relatively local and are graded according to how much neurotransmitter is released at the synapse and how long it persists there. Therefore, many neuro-psychiatric therapeutic chemicals have been developed to aim at fine tuning the activity of these ligand-gated Cl^- channels by prolonging either the opening state (agonistic drugs) or closing state (antagonistic drugs) of these channels. Several human diseases are caused by defective ligand-gated Cl^- channels and are either inherited in Mendelian fashion or are caused by sporadic genetic mutation. These diseases include epilepsy and juvenile myoclonous epilepsy (reduced $GABA_A$ activity; (Jones-Davis & Macdonald, 2003)), schizophrenia (defective trafficking of $GABA_A$; (Jacob *et al.*, 2008)), and hyperekplexia or startle disease (defects in glycine function; (Lapunzina *et al.*, 2003)).

Voltage-Gated Cl^- Channels

Voltage-gated Cl^- channel often refers to the canonical and most studied family of Cl^- channels: the ClCs. While classical ClC currents are activated by changes in membrane potential (Fahlke, 2001), some can also be activated by cell swelling and moderate extracellular acidification (Arreola *et al.*, 2002, Jordt & Jentsch, 1997, Thiemann *et al.*, 1992). ClC-0 is the founding member of the ClC family. It is enriched in the electric organ of the electric ray, *Torpedo*, and was first described electrophysiologically as a "double-barrel" Cl^- channel when reconstituted in planar lipid bilayer (Miller & White, 1980). Ten years later the gene was finally expression cloned (Jentsch *et al.*, 1990). Immediately afterwards many mammalian homologous were identified and their

physiological functions have been extensively studied (for reviews, see: (Jentsch *et al.*, 2005)).

There are nine ClC genes in mammals, with only four of them (ClC-1, -2, -Ka, and –Kb) being located in the plasma membrane. In contrast, although ClC-3, -4, and -5 mediated currents could be measured in the plasma membrane when expressed heterologously in *Xenopus* oocytes or in other transfected cells (Friedrich *et al.*, 1999, Li *et al.*, 2000, Steinmeyer *et al.*, 1995), the rest of the five ClCs (ClC-3, -4, -5, -6, and -7) are predominantly found in the membrane of intracellular organelles, in particular, vesicles in the lysosome-endosomal pathway (Buyse *et al.*, 1998, Kornak *et al.*, 2001, Picollo *et al.*, 2004, Scheel *et al.*, 2005). ClC-1, 2, 3, Ka, and Kb have been unambiguously shown to function as voltage-gated Cl^- channels. The other mammalian ClC proteins are either characterized as H^+/Cl^- exchangers or are still functionally unclear (Picollo & Pusch, 2005, Scheel *et al.*, 2005). In the subsequent section, I will only elaborate on those ClC members that function as voltage-gated Cl^- channels.

The diverse physiological functions of mammalian ClCs were demonstrated by pathologies resulting from their mutational inactivation in several human genetic diseases. In mammals, ClC-1 is exclusively expressed in skeletal muscles (Steinmeyer *et al.*, 1991), ClC-K in kidney, whereas ClC-2 is widely expressed (Thiemann *et al.*, 1992). Like ClC-0 in the electric organ (derived from skeletal muscle) of Torpedo, the Cl^- equilibrium potential in mammalian skeletal muscle is close to that of K^+. Therefore, the repolarizing Cl^- current through both ClC-0 (in fish) and ClC-1 (in mammals) stabilizes the membrane potential of the skeletal muscle. As a result, natural disruptions in ClC-1 gene have been characterized to cause myotonia, a form of muscle hyperexcitability/ stiffness in human

(Pusch, 2002, George *et al.*, 1993, Koch *et al.*, 1992, Mankodi *et al.*, 2002) and mouse (Steinmeyer *et al.*, 1991). Defective ClC-K causes Bartter's syndrome, a rare but inherited human disease associated with excessive renal salt and water wasting because this channel is critical in NaCl reabsorption in certain segment of the nephron (Matsumura *et al.*, 1999, Vandewalle *et al.*, 1997). Despite its broad expression pattern, elimination of ClC-2 in knockout mice leads to very limited and specific phenotypes in testis and retina (Bosl *et al.*, 2001), and mutation in ClC-2 has not yet correlated with any significant human disease so far. The ClCs described above are Cl^- channels at the cell surface. ClC-3, on the other hand, is predominantly found in the endosomal-lysosomal compartments and is correlated with the acidification of these vesicles by compensating currents of vesicular H^+/ATPases (Jentsch *et al.*, 2005). Similar to ClC-2, ClC-3 is broadly expressed, and there is not a clear correlation between defective ClC-3 with any human disease. However, ClC-3 aberrant mice exhibit progressive degeneration of the retina, hippocampus, and ileal mucosa and showed manifestations similar to human neuronal ceroid lipofuscinosis (Kasper *et al.*, 2005, Moreland *et al.*, 2006, Yoshikawa *et al.*, 2002).

Ca^{2+}-activated Cl^- Channels (CaCCs)

The permeability of Ca^{2+}-activated Cl^- channels for Cl^- is modulated by changes in the cytosolic Ca^{2+} concentration. On average, an increase of cytosolic [Ca^{2+}] to 0.2-5 μM is needed to activate CaCC (Hartzell *et al.*, 2005a). The first CaC current was described in Xenopus oocytes in the early 1980s. Increases in $[Ca^{2+}]_i$ upon fertilization activates CaC currents that depolarize the oocyte cell membrane that somehow prevents the entry of additional sperm (Barish, 1983, Miledi, 1982).

Cl^- currents associated with an increase of cytoplasmic Ca^{2+} were subsequently discovered in many different cell types including various non-excitable cells such as epithelial cells (Begenisich & Melvin, 1998, Kidd & Thorn, 2000, Melvin *et al.*, 2005), exocrine glands (Botelho & Dartt, 1980, Hunter *et al.*, 1983, Melvin *et al.*, 1991, Worrell & Frizzell, 1991), and immune cells (Holevinsky *et al.*, 1994, Nishimoto *et al.*, 1991), and many other excitable cells such as neurons (Andre *et al.*, 2003, Bader *et al.*, 1987, Currie *et al.*, 1995, Frings *et al.*, 2000, Hussy, 1992, Nishimoto *et al.*, 1991, Schlichter *et al.*, 1989, Scott *et al.*, 1988, Stapleton *et al.*, 1994), olfactory (Delay *et al.*, 1997, Firestein & Shepherd, 1995, Kleene & Gesteland, 1991, Kurahashi & Yau, 1994, Lowe & Gold, 1993, Pifferi *et al.*, 2006, Sato & Suzuki, 2000, Sorota & Du, 1998), taste (Herness & Sun, 1999, McBride & Roper, 1991), and photo-receptors (Bader *et al.*, 1982, Barnes, 1994, Barnes & Bui, 1991, Maricq & Korenbrot, 1988, Okada *et al.*, 1995); cardiac (Han & Ferrier, 1992, Han & Ferrier, 1996, Nakayama & Fozzard, 1988, Zygmunt *et al.*, 1998) and smooth muscles (Large & Wang, 1996, Wang *et al.*, 1997). CaCCs are involved in epithelial secretion of electrolytes and water (Boucher *et al.*, 1989, Grubb & Gabriel, 1997, Wagner *et al.*, 1991), membrane excitability in cardiac muscle and neurons (Frings *et al.*, 2000, Kawano *et al.*, 1995, Zygmunt, 1994), sensory transduction (Barnes & Hille, 1989, Frings *et al.*, 2000, Maricq & Korenbrot, 1988, Thoreson & Burkhardt, 1991), regulation of vascular tone (Large & Wang, 1996), and probably other not-yet clarified physiological functions as well.

Grossly speaking, CaC channels can be further separated into two classes (even though these need not be mutually exclusive) based on the mechanism of activation/gating: channels activated by directly binding to micromolar or submicromolar of cytosolic Ca^{2+}

and channels that are activated indirectly via $Ca2^{2+}$-binding proteins or Ca^{2+}-dependent enzymes such as Ca^{2+}/calmodulin-dependent kinase II (CAMKII). The distinction between these two classes of CaC channel is reflected in the observation that some CaC currents can be stably activated in excised patches by Ca^{2+}_i in the absence of ATP (Collier *et al.*, 1996, Frizzell *et al.*, 1986, Gomez-Hernandez *et al.*, 1997, Koumi *et al.*, 1994, Martin, 1993, Takahashi *et al.*, 1987, Zhang *et al.*, 1995) suggesting phosphorylation is not required, whereas in other preparations channel activity runs down quickly after excision, suggesting the possibility that components in addition to Ca^{2+} are required to open the channel (Klockner, 1993, Morris & Frizzell, 1993, Nilius *et al.*, 1997b, Reisert *et al.*, 2003, Schlenker & Fitz, 1996, Van Renterghem & Lazdunski, 1993).

At the macroscopic level, CaC currents have very similar overall properties in a variety of cell types, including *Xenopus* oocytes (Kuruma & Hartzell, 1999), various secretory epithelial cells (Arreola *et al.*, 1996, Evans & Marty, 1986, Piper *et al.*, 2002, Reinsprecht *et al.*, 1995, Wang *et al.*, 1997, Zhang *et al.*, 1995), hepatocytes (Koumi *et al.*, 1994), vascular, airway and gut smooth muscle cells (Large & Wang, 1996), Jurkat T cells (Nishimoto *et al.*, 1991), and pulmonary artery endothelial cells (Nilius *et al.*, 1997b). Generally speaking, these CaC currents exhibit Ca^{2+}-sensitivity, activate slowly with depolarization, are relatively non-selective among anions and have a higher permeability to I^- than to Cl^-, and are voltage-sensitive with linear instantaneous current-voltage (I-V) relationship and an outwardly rectifying steady state I-V curve. At the single channel level, CaC channels can be further categorized into three classes based on their single channel conductance. The small conductance CaC channels have 1-3 pS of single channel conductance, express a linear or outwardly rectifying I-V relationship, and have been

described in Xenopus oocytes (Takahashi *et al.*, 1987), cardiac myocytes (Collier *et al.*, 1996), arterial smooth muscle (Hirakawa *et al.*, 1999, Klockner, 1993, Piper & Large, 2003), A6 kidney cell line (Marunaka & Eaton, 1990), and endocrine cells (Taleb *et al.*, 1988). Some of these currents run down after excision of the patch. The mid-conductance CaC channels are 8-15 pS in conductance, exhibit a linear I-V relationship, and are found in colon (Morris & Frizzell, 1993), hepatocytes (Koumi *et al.*, 1994), endothelial cells (Nilius *et al.*, 1997b), and biliary cell line (Schlenker & Fitz, 1996). CaM antagonists block some members of these channels. The big-conductance CaC currents express 40-50 pS of conductance. The currents are outwardly rectifying and were identified in Jurkat T cell (Nishimoto *et al.*, 1991), airway epithelial cells (Frizzell *et al.*, 1986), vascular smooth muscle cells (Piper & Large, 2003), and Xenopus spinal neurons (Hussy, 1992). CaMKII activates some of these channels. Whether this diversity of single-channel conductance truly reflects the variety of single channels that underlie the typical macroscopic $I_{Cl.Ca}$ remains ambiguous because rarely have investigators carefully linked single-channel measurements with macroscopic currents (Hartzell *et al.*, 2005a).

Three molecular candidates have been proposed to be CaC channels. One of these is the CLCA protein (Cunningham *et al.*, 1995, Gaspar *et al.*, 2000). Transfection of various types of cells with cDNA encoding various CLCA proteins induces Ca^{2+}-dependent Cl^- currents (Elble *et al.*, 1997, Gandhi *et al.*, 1998, Gruber *et al.*, 1998, Pauli *et al.*, 2000). However, several lines of evidence suggest that CLCAs are cell-adhesion proteins (Elble *et al.*, 1997) and at least one member of this family is a secreted protein (Gruber & Pauli, 1999, Pauli *et al.*, 2000). The ClC-3 of the ClC Cl^- channel family was also proposed to be a Ca^{2+}-dependent Cl^- channel that required CaMKII for activation (Hu & Bok, 2001,

Robinson *et al.*, 2004). But recent evidence has shown that ClC-3 exhibits significant distinct biophysical properties than those reported previously on the same protein. Instead, ClC-3 has been proposed to be an ion transporter with largely intracellular localization (Li *et al.*, 2000, Li *et al.*, 2002). The third CaCC candidate is the *Tweety* family of proteins (Suzuki & Mizuno, 2004, Suzuki *et al.*, 2006). Two human homologs (*hTTY2* and *hTTY3*) of this family exhibit maxi-conductance (260pS) CaC currents while one other human isotype (*hTTY1*) expresses currents that are Ca-independent (Suzuki & Mizuno, 2004). Reports about the currents related with *Tweety* are scarce. More independent and unbiased studies are needed to establish the function and the identity of this family of proteins.

Volume-Regulated Anion Channels (VRACs)

Gram negative bacteria and plant cells have semi-rigid cell wall that surround the plasma membrane to prevent cell bursting when subjected to an osmotic shock. In the single cell organism amoeba, the excess water that flows in by osmosis is collected in contractile vacuoles, which periodically discharge their contents to the exterior. In most animal cells, however, the swollen cell undergoes subsequent shrinkage known as regulatory volume decrease (RVD). RVD is mediated by swell-activated Cl^- currents (VRAC current) together with a co-activation of K^+ current that allows a large efflux of osmolytes, which is followed by loss of water (Hoffmann & Dunham, 1995, Nilius *et al.*, 1997a, Nilius *et al.*, 1996, Nilius *et al.*, 1995, Strange *et al.*, 1996). Activation of a Cl^- efflux pathway by cell swelling was first demonstrated by Hoffman *et al.* in Ehrlich ascites tumor cells (Hoffmann *et al.*, 1979) and subsequently in lymphocytes (Grinstein *et al.*, 1984), epithelial cells (Kubo & Okada, 1992, Strange *et al.*, 1996, Zhang & Jacob, 1997),

renal collecting duct cell line (Schwiebert *et al.*, 1994), cardiac myocytes (Hirakawa *et al.*, 1999), endothelial cells (Nilius *et al.*, 1994), osteoblast-like cells (Gosling *et al.*, 1995), and a great variety of other types of animal cells (Nilius *et al.*, 1997a, Okada, 1997).

In fact, volume-regulated Cl^- currents are ubiquitously expressed in most animal cells. Besides regulation of cell volume, VRAC channels have been implicated in numerous other physiological functions including vectorial transport of Cl^- and consequently, salt and fluid secretion (Hoffmann & Dunham, 1995, McEwan *et al.*, 1993, Strange *et al.*, 1996), suppression of cell proliferation (Chou *et al.*, 1995, Phipps *et al.*, 1996, Villaz *et al.*, 1995, Voets *et al.*, 1997) in lymphocytes and myeloblastic leukemia cells (Phipps *et al.*, 1996, Schumacher *et al.*, 1995), endothelial cells (Nilius *et al.*, 1997c, Voets *et al.*, 1995) and in undifferentiated myogenic and neuronal cell lines (Nilius *et al.*, 1997c, Voets *et al.*, 1997), and providing a pathway for amino acid (i.e. taurine and glycine) and other macromolecular organic osmolyte (i.e. myoinositol, sorbitol, and methylamines) transport across the plasma membrane (Nilius *et al.*, 1996, Strange & Jackson, 1995) in glial and glioma cells (Jackson & Strange, 1993, Roy, 1995), erythrocytes (Kirk *et al.*, 1992), endothelial cells (Manolopoulos *et al.*, 1997), MDCK kidney epithelial cell line (Banderali & Roy, 1992), and IMCD inner medullary collecting duct cell line (Boese *et al.*, 1996).

Generally speaking, VRAC channels described in various types of cells exhibit some common macroscopic electrophysiological properties. These include moderate outward rectifying current-voltage relationships, Ca^{2+}-independence, inactivation at positive potentials, and high selectivity for anions over cations, low anion selectivity with a permeability sequence of $I^- > Br^- > Cl^-$ (Okada, 1997). However, it is not clear how the cell senses changes in volume and how these changes are transduced to channel activation. The

exact gating mechanism is also obscure. Nevertheless, many speculative gating mechanisms have been proposed, including those of mechano-sensitive ion channels. These include the direct gating of the channel by membrane stretch as a result of cell swelling (Hamill & McBride, 1994, Ingber, 1997) and indirect gating mechanisms like the involvement of a volume-sensitive phosphorylation cascade (Nilius *et al.*, 1997a), lipid soluble mediators or intracellular second messengers generated after cell swelling (Hoffmann & Dunham, 1995, Sackin, 1995), rearrangement of channel subunits (Hamill & McBride, 1994), and insertion of cytosolic channel components to the plasma membrane (Hamill & McBride, 1994, Opsahl & Webb, 1994, Strange *et al.*, 1996). To date, the exact gating mechanism is still unclear, primarily because the VRAC channels have not been cloned.

VRAC channels can be roughly classified to three groups based on single channel conductance. The small conductance VRAC channels (0.1-8 pS) are described in choroid plexus cells (Christensen *et al.*, 1989), Ehrlich ascites (Christensen & Hoffmann, 1992), chromatin cells (Doroshenko & Neher, 1992), neutrophils (Stoddard *et al.*, 1993), lymphocytes (Lewis *et al.*, 1993, Schumacher *et al.*, 1995), and endothelial cells (Nilius *et al.*, 1994). However, for many of the currents described above, the intracellular [Ca^{2+}] was neither well controlled nor measured. The possibility that these channels are activated by a swelling-induced rise in cytoplasmic Ca^{2+} cannot be excluded (Nilius *et al.*, 1997b, Nilius *et al.*, 1997a). Most VRAC channels fall into the category of intermediate conductance (20-80 pS). This group of VRAC currents have been identified in HeLa S2 cervical carcinoma cell line (Anderson *et al.*, 1995), T84 epithelial cells (Solc & Wine, 1991, Worrell *et al.*, 1989), rat renal collecting duct cell line IMCD (Boese *et al.*, 1996), BC3H1

myoblast cell line (Voets *et al.*, 1997), and C6 glioma cell line (Jackson & Strange, 1995). The maxi conductance VRAC channels have been found in astrocytes (Jalonen, 1993), neuroblastoma cells (Falke & Misler, 1989), renal cortical collecting duct cells (Schwiebert *et al.*, 1994), and neonatal cardiac myocytes (Coulombe & Coraboeuf, 1992). They exhibit bell-shaped voltage dependence with high open probabilities in the range of $\pm$ 40 mV (Falke & Misler, 1989, Jalonen, 1993). Overall, it should be noted that cells could possess a variety of volume-sensitive Cl^- channels (Nilius *et al.*, 1997a). VRAC currents with significantly different single channel conductance have been reported in A6 epithelial cells (Banderali & Ehrenfeld, 1996, Nilius *et al.*, 1997a) and in both pigment and non-pigment ciliary epithelial cells in the bovine eye (Zhang & Jacob, 1997).

To date, four molecular candidates have been proposed to be VRAC channels. Two members of the ClC family, ClC-2 and ClC-3, were proposed to be VRAC channels. ClC-2 is activated by cell swelling and is shown to contribute to volume regulation in some cell types (Bond *et al.*, 1998, Furukawa *et al.*, 1998). However, the electrophysiological features of ClC-2 current (hyperpolarization activation and inward rectification) are distinct from the VRAC current, the role of ClC-2 as a VRAC channel seems unlikely. ClC-3 is shown to be involved in cell volume regulation in several types of cells, (Duan *et al.*, 1997, Hermoso *et al.*, 2002). But cardiomyocytes isolated from ClC-3 knockout mice still preserved functionally active VRAC currents on the plasma membrane (Gong *et al.*, 2004). Over expression of p-glycoprotein, the protein product of the multiple drug resistant 1 (*MDR1*) gene, induced VRAC currents that recapitulate many key phenotypes of typical VRAC currents in epithelial cell (Valverde *et al.*, 1992). However, the volume-sensitive Cl^- currents are not dependent on endogenous p-glycoprotein in a human epithelial cell line

(Okada, 1997, Tominaga *et al.*, 1995). Expression of nucleotide-sensitive Cl^- channels (ICln) in Xenopus oocytes also induced typical VRAC currents in response to hyposmotic challenge (Paulmichl *et al.*, 1992). This result was questioned because another group was able to separate the over-expressed ICln current from the native VRAC current in Xenopus oocytes by criteria including anion selectivity and volume sensitivity (Voets *et al.*, 1996).

Although the Cl^- currents activated by Ca^{2+} or by cell swelling have been widely described in many cells types, the controversy about the molecular identity of VRAC and CaC channels still exists. The fact that multiple different proteins generate Cl^- currents that exhibit sensitivities to Ca^{2+} or cell swelling suggests a redundancy in these two families of channels that indicates the physiological processes that they are involved in are inherently important and complex.

Bestrophin, a novel family of Cl^- channels?

Macular Degeneration and Clinical Presentation

Age-related macular degeneration (ARMD) is the leading cause of central vision loss (blindness) in the United States for those over the age of fifty years (de Jong, 2006, Jager *et al.*, 2008, Penfold *et al.*, 2001). Approximately 15 million Americans and many millions more around the world suffer from this disorder, and the overall prevalence of advanced macular degeneration is projected to increase by more than 50% by the year of 2020 (Friedman *et al.*, 2004). While ARMD is mostly sporadic with mixed etiology, there are a number of early onset-forms of macular degeneration that are largely or exclusively genetic. These inherited forms of macular degeneration have provided invaluable models for the speculation of the etiology underlying all forms of macular degeneration.

These degenerative visual disorders affect the macula, a small area near the center of the retina that is densely packed with light-sensitive photoreceptor cone cells. The cone cells are responsible for high acuity and color vision. Therefore, the most common early sign of macular degeneration is blurred vision. Generally speaking, macular degeneration develops gradually and painlessly. Symptoms subsequent to blurred vision include increasing difficulty adapting to low levels of light, slow recovery of visual function after exposure to bright light, a decrease ability in discerning in the intensity or brightness of colors, haziness or missing areas in the center of the visual field (central scotomas) combined with a profound drop in the central vision acuity, and finally loss of vision (de Jong, 2006, Jager *et al.*, 2008). Additional associated symptoms include visual hallucinations (Charles Bonnet Syndrome) that arise from distorted high acuity vision (Khan *et al.*, 2008, Rovner, 2006).

Familial Macular Degeneration

As mentioned above, a small portion of macular degeneration is inherited in a Mendelian fashion. One example of which is the Best vitelliform macular dystrophy (Best Disease; Best macular dystrophy). Best Disease was first described and named by a German ophthalmologist Dr. Franz Best (Best, 1905). Different from most macular degenerations that are age-related, Best Disease typically presents with juvenile onset with an autosomal dominant inheritance. The first signs of the condition usually present before puberty, but there are also later-onset cases. Mutations in the human bestrophin 1 gene (*BEST1*) have been identified to associate with Best Disease (Allikmets *et al.*, 1999, Bakall *et al.*, 1999, Caldwell *et al.*, 1999, Eksandh *et al.*, 2001, Kramer *et al.*, 2003, Lotery *et al.*,

2000, Marchant *et al.*, 2002, White *et al.*, 2000, Petrukhin *et al.*, 1998, Ponjavic *et al.*, 1999, Pollack *et al.*, 2005, Wabbels *et al.*, 2006, Yanagi *et al.*, 2002, Yu *et al.*, 2007). Unfortunately, there is no effective therapy for slowing or stopping the progression of the disease besides supportive treatment. The only possible exception is a laser photocoagulation treatment used to ablate subretinal neovascular membranes in an attempt to avoid complications of subretinal hemorrhages (Blodi & Stone, 1990). Presently, genetic evaluation of family members to identify carriers and pedigree analysis remain the most important preventive approaches with vitelliform macular dystrophy. Although Best Disease remains a rare form of macular degeneration, it may be a model for understanding of the molecular mechanisms underlying most forms of macular degeneration.

Symptoms and Progression of Best Disease

Best disease causes progressive vision impairment that can be divided into six stages (Blodi & Stone, 1990, Gutman *et al.*, 1982, Lachapelle *et al.*, 1988). The first stage is the previtelliform stage, which is often asymptomatic. In this stage, although the vision is unaffected and the eye fundus remains normal, an electrooculogram test (EOG) starts to reveal abnormalities. The second stage is the vitelliform stage, during which a yellow egg yolk-like deposition in the macular region is detected by fundus eye examination. The fundus abnormalities are usually bilateral and vision is usually unaffected at this stage. The following stage is the pseudohypopyon stage. At this level, the layer of cells in the vicinity of the outer segments of photoreceptor, the retinal pigment epithelial cells (RPE), start to degenerate. Therefore, disease carriers start to notice a decline in visual abilities. The fourth stage is the vitelliruptive stage, during which the yellow deposits become irregular

in shape and can disperse outside of the macula. This “rupture” of the deposition severely devastates the visual ability and the color vision (Chung *et al.*, 2001). The final stages include the atrophic stage and the subretinal neovascular stage. During the atrophic stage, both the photoreceptor and the RPE begin to degenerate and visual impairment is usually severe. When the disease progresses to the subretinal neovascular stage, new but fragile blood vessels start to proliferate from the choroid. These vessels break easily, causing accumulation of blood in the retina that eventually triggers the formation of scar tissues. Patients at this stage may suffer from the predominant symptom of loss of vision at this final stage (Gutman *et al.*, 1982, Lachapelle *et al.*, 1988, Loewenstein *et al.*, 1993).

Pathophysiology of Best Vitelliform Macular Degeneration

Although Best Disease and most other macular degenerative disorders share some histological similarities and are primarily characterized by rather selective degeneration of the macula, Best Disease and other adult-onset macular dystrophies are generally considered distinct entities (Brecher & Bird, 1990, Felbor *et al.*, 1997, Kramer *et al.*, 2000). While Best Disease is characterized by mutations in the *BEST1* gene, most age-related vitelliform macular dystrophy is linked to mutations in the peripherin/RDS gene, which encodes a photoreceptor-specific membrane glycoprotein (Felbor *et al.*, 1997).The retinal pigment epithelium (RPE) cells appear to have degenerative changes in some cases and secondary atrophy of photoreceptor cells has been noted. Macrophages containing lipofuscin have been found to migrate into the outer retina and choroidal neovasculization has been reported (de Jong, 2006). A common feature of these disorders is the striking appearance of a yellow egg yolk-like (vitelliform) lipofuscin

deposition/lesion within and around the RPE (Braley, 1966, Hartzell *et al.*, 2005b), particularly in the macula.

Lipofuscin is primarily composed of partially oxidized lipid and proteins of both photoreceptor and RPE origins (Schutt *et al.*, 2002). The major fluorescent component of lipofuscin is a metabolite of retinal pigment called A2E (N-retinylidene-N-retinylethanolamine), which has been shown to disrupt cell membrane integrity by a detergent-like effect (Eldred & Lasky, 1993), to perturb lysosomal function (Finnemann *et al.*, 2002, Shamsi & Boulton, 2001), and to promote apoptosis (Sparrow & Cai, 2001). Some research groups suggest that the accumulation of lipofuscin may be the result of an imbalance between formation and disposal mechanisms (Katz *et al.*, 1999), while others propose that once lipofuscin is formed, it is not degradable (Elleder *et al.*, 1995, Terman & Brunk, 1998). In any case, lipofuscin seems to be a noxious material (Hartzell *et al.*, 2005b) that is thought to be the major causal factor of age-related macular degeneration because it correlates to the severity of the photoreceptor degeneration (Young, 1987). To date, the mechanism of lipofuscin formation and the link of lipofuscin deposition to macular degeneration are still unknown.

Diagnosis of Best Disease

The characteristic feature of Best Disease is the accumulation of yellow lipofuscin deposition in the macula by eye fundus examination. However, if the disorder has progressed to a later stage that involves breakdown of photoreceptors and degeneration of RPE cells, the morphological appearance may be difficult to distinguish from other forms of macular degeneration. The hallmark diagnostic feature of Best Disease is a markedly

abnormal electrooculogram (EOG) in all stages of progression and even in asymptomatic carriers (Wajima *et al.*, 1993). The EOG is measured by placing electrodes on either side of the eye. The subject is allowed to adapt to darkness and is asked to fixate on one of two light-emitting diodes 30 degree apart that illuminate alternately at a frequency of ~0.2/sec. The difference in voltage measured when the eyes are fixated on the right versus the left light-emitting diode is thought to represent the voltage across the RPE indirectly (Hartzell *et al.*, 2005b). The voltage becomes small in during adaptation to the dark and will increase gradually over ~5-15 minutes when the ambient lights are turned on. In normal subjects, the light to dark ratio is ~1.8. Typically, this ratio is greatly diminished or abolished in Best Disease patients and carriers (Francois *et al.*, 1967, Petrukhin *et al.*, 1998).

The fact that the light peak is substantially reduced even in asymptomatic Best Disease carriers and occurs before the onset of the disease symptoms indicates that the light peak reflects a physiological entity that the defect of which is intrinsically associated with (and possibly causes) the disorder rather than a consequence of the degenerative processes in the course of the disease (Deutman, 1969, Francois *et al.*, 1967, Petrukhin *et al.*, 1998, Tsunenari *et al.*, 2006). EOG and genetic analysis of mutations of the *BEST1* gene together are so far the most promising approaches to confirm the diagnosis long before any visual impairment has occurred.

Discovery of the Bestrophin Gene

Although the disease was originally reported in 1905, the gene responsible for Best Disease remained unknown for decades. The identification of the inheritance pattern of Best Disease was facilitated by a study in the 1970s in a large Swedish family suffered

from the disease. More than 250 cases were traced back to a gene source in the 17th century (Nordstrom & Barkman, 1977). The locus for Best Disease was determined by linkage analysis (Forsman *et al.*, 1992, Stone *et al.*, 1992) and refined to be located at chromosome loci 11q13 (Cooper *et al.*, 1997, Stohr *et al.*, 1998, Weber *et al.*, 1994). The gene responsible for Best Disease was later cloned and named as *BEST1* (previously *VMD2*) by recombination breakpoint analysis (Petrukhin *et al.*, 1998, Marquardt *et al.*, 1998). Approximately 100 point mutations have been identified in human *BEST1* gene in Best Disease patients. Details of these mutations are listed in several databases including: the Retinal Scientific International Database at http://www.retina-international.org/sci-news/vmd2mut.htm, the Online Mendelian Inheritance in Man in the public domain by the National Center for Biotechnology Information (BVMD, OMIM 153700) at http://www.ncbi.nlm.nih.gov/entrez/dispomim.cgi?id=153700, VMD2 Gene Mutation Database at http://www.uni-wuerzburg.de/humangenetics/vmd2.html, and the Human Gene Mutation Database at University of Regensburg at http://www-huge.uni-regensburg.de/VMD2_database/index.php?select_db=VMD2. In brief, almost all of these mutations are missense mutations that result in single amino acid substitution. These mutations are dispersed throughout the first 8 exons (totally 11 exons) in the human *BEST1* gene, which correlates to the first 310 amino acids of the bestrophin protein where the highest homology among bestrophins from all creatures is located.

To date, bestrophins are a family of genes that are unambiguously identified throughout different phyla including human, non-human primates, pigs, rodents, birds, bony fish, amphibians, echinoderms, insects, flat worms, and nematodes such as *C.*

elegans. All mammals have three to four bestrophin paralogs. The human genome contains four bestrophin paralogs (*hBest1, hBest2, hBest3, and hBest4*) (Stohr *et al.*, 1998, Tsunenari *et al.*, 2003) while in mouse there are three bestrophin paralogs and one pseudogene (Kramer *et al.*, 2004). Among the arthropod bestrophins, there are 3 bestrophin genes in *Drosophila melanogaster* (and possibly one more pseudogene), 2 in mosquito (*Aneopheles Gambia*), and 25 in *Caenorhabditis elegans* (Tsunenari *et al.*, 2003). All of the bestrophin genes share a conserved gene structure, with almost identical sizes of the 8 transmembrane domain (TMD)-encoding exons and highly conserved exon-intron boundaries.

The bestrophin proteins share conserved RFP amino acid motif (Arg-Phe-Pro) with a family of proteins with unknown function originally identified in Caenorhabditis elegans. Besides, bestrophin does not express any homology to any other protein of known function. bestrophin proteins from all evolutionarily distinct species are divided into a conserved N terminal domain containing 4 to 6 putative transmembrane regions and a C terminal domain that is highly variable among homologs and paralogs in both sequence and length. When comparing the 4 of human and mouse bestrophin orthologs, for example, the N and C terminal domains show 69-95 % and 34-74 % identity, respectively while in pair-wise comparison among all non-orthologs bestrophins from human and mouse, the N and C termini show 44-67 % and 4-19 % identity, respectively (Tsunenari *et al.*, 2003).

According to hydropathy analysis and transmembrane domain (TMD) prediction algorithms, bestrophins are predicted to be membrane proteins that contain 4 to 6 transmembrane domains (Marmorstein & Kinnick, 2007, Milenkovic *et al.*, 2007, Sun *et al.*, 2002, Tsunenari *et al.*, 2006). Transmembrane domain number 2, 5, and 6 are highly

conserved from bacteria to human (Hartzell *et al.*, 2008). However, the precise location and number of transmembrane domains are still controversial mainly because experimental data from independent groups are not yet in agreement. Expressed bestrophins can form either homo- or hetero-oligomeric complexes (Sun *et al.*, 2002). Stoichiometry of bestrophin oligomeric complex has not been fully resolved. Dimer to tetramer or pentamer have been reported in bestrophins purified from animal RPE cells (Stanton *et al.*, 2006) and over-expressed HEK cells (Sun *et al.*, 2002) respectively.

Characterization of the Function of Bestrophin Proteins

The etiological mechanism of Best Disease is not clear mainly because the function of bestrophin is not elucidated. When the bestrophin gene was first discovered in 1998, it was proposed to be a transporter of the lipid component of the lipofuscin (Petrukhin *et al.*, 1998). By immunohistochemistry, human, macaque, porcine, and mouse bestrophins are found to locate in the basolateral membrane of the RPE cells (Marmorstein *et al.*, 2000, Marmorstein *et al.*, 2002). The same group of researchers also identified similar pattern of membrane distribution of bestrophins in the rat RPE after injection of a viral vector containing human Best1 cDNA (Marmorstein *et al.*, 2004). Trans-RPE transport plays an important role in maintaining both the electrolyte and fluid composition of the fluid surrounding the photoreceptors and RPE (Steinberg, 1985). Because Cl^- flux is generally associated with the transepithelial transport of substances, it is reasonable to think that bestrophin, with its purported location, has an important role in such function of RPE cells (Tsunenari *et al.*, 2006). Since the diagnostic feature of Best Disease patients and carriers is the reduction of the light peak component of the EOG, which is associated with a Cl^-

conductance in the basolateral membrane of RPE cells, the mutant bestrophin is likely to play a role in generating the altered EOG of individuals with Best Disease (Gomez *et al.*, 2001, Marmorstein *et al.*, 2000). In addition, it has been suggested that the increase in the basal RPE Cl^- conductance associated with the EOG light peak is triggered by an intracellular second messenger such as Ca^{2+} (Joseph & Miller, 1992, Ueda & Steinberg, 1994). These observations together made it intriguing to propose that hBest1 is a Ca^{2+}-activated Cl^- channel. Studies on characterizing the function and regulation of bestrophin proteins have been conducted with bestrophins from multiple animals including human, mouse, Xenopus, and fruit fly and have continued to contribute to elucidating the pathogenic mechanism of Best Disease.

Human Bestrophins

The human genome contains four paralogs of bestrophin that are localized on different chromosomes (Human GenBank: *hBest1*-11q13*, hBest2*-19q13*, hBest3*-12q14*, and hBest4*-1p33). Bestrophin genes share a conserved gene structure, with almost identical sizes of the 8 TMD-encoding exons and highly conserved exon-intron boundaries, but each of the four hBest proteins has a unique C' tail of variable length (Stohr *et al.*, 1998, Tsunenari *et al.*, 2003). Nevertheless, in pair-wise comparisons, the four human bestrophin proteins share up to 66 % identity in amino acid sequence within the conserved N terminal ~360 amino acids but show minimal homology within the C terminal domains (Tsunenari *et al.*, 2003).

Human bestrophin 1 (GenBank ID: AF057169) protein is a 68 kDa protein composed of 585 amino acids. By RT-PCR and Northern blot assays, the transcript of hBest1 is

predominantly expressed in the RPE cells and to a much lesser extent in the brain and testis (Petrukhin *et al.*, 1998, Marquardt *et al.*, 1998). The function of human bestrophin 1 was first studied by Sun et al. with hBest1 cloned from human ocular cDNA (Sun *et al.*, 2002). When untransfected HEK cells are patch clamped with an intracellular solution containing micromolar free Ca^{2+}, the currents are very small (<100 pA) whereas hBest1-transfected cells showed large currents (Sun *et al.*, 2002, Yu *et al.*, 2006). Ca^{2+} dependence was also examined in hBest1-transfected HEK cells using the photolyzable caged-Ca^{2+} compound, Ca^{2+}-NPEGTA (Sun *et al.*, 2002). In cells preloaded with BAPTA (Ca^{2+} chelator), the release of caged Ca^{2+} did not exhibit measurable currents.

The current induced by hBest1 in response to elevated intracellular Ca^{2+} intracellular Ca^{2+} was carried by Cl^- because of the following criteria: (1) the reversal potential of the whole cell current falls at 0 mV when equimolar of Cl^- was present in both the intracellular and extracellular solutions, as would be predicted with the Nernst equation if the current is mediated by Cl^- (Sun *et al.*, 2002, Yu *et al.*, 2006); (2) lowering the Cl^- concentration in the extracellular solution by replacing Cl^-_o with gluconate shifted the reversal potential to more positive values, suggesting a substantial Cl^- permeability (Sun *et al.*, 2002, Kowdley *et al.*, 1994) the Ca^{2+}-activated current is reversibly blocked by 0.5 mM of DIDS (4,4'-diisthiocyanostilbene-2,2'-disulfonate), a compound that suppresses many Cl^- channels (Sun *et al.*, 2002). The electrophysiological properties of the macroscopic Cl^- currents induced by hBest1 include (Sun *et al.*, 2002, Yu *et al.*, 2006, Tsunenari *et al.*, 2003, Fischmeister & Hartzell, 2005): (1) an elevated intracellular Ca^{2+} is required to activate the current; (2) the Cl^- current is suppressed by hyperosmotic cell shrinkage and runs down over time with a mean decline ratio of 50% in 10-15 minutes; (4) this current shows slight

outward (Sun *et al.*, 2002, Yu *et al.*, 2006) or inward (Tsunenari *et al.*, 2003) rectification; (5) the current is time-independent; (6) the induced channel exhibits a relative anionic permeability sequence of $NO_3^- > I^- > Br^- > Cl^-$. Notably, the Cl^- currents generated by hBest1 expressed in multiple different cell lines could be modulated by osmotic differences across the plasma membrane. Cl currents related to hBest1 are greatly suppressed by hyperosmotic cell shrinkage and stimulated, but non-systematically and to a lesser extent, by hyposmotic extracellular solution (Fischmeister & Hartzell, 2005). This suggests that hBest1 could be involved in the volume sensitivity of RPE cells during phagocytosis of photoreceptor outer segments. Consequently, distinct functional properties of hBest1 may contribute to RPE dysfunction and thus may explain the variable phenotypes associated with mutant hBest1 protein (Milenkovic *et al.*, 2008).

The topology and stoichiometry of functional hBest1 protein complex are still elusive. Two different topology models have been proposed for hBest1 (Marmorstein & Kinnick, 2007, Milenkovic *et al.*, 2007, Stanton *et al.*, 2006, Tsunenari *et al.*, 2006). One model proposes that the predicted TMD 1, 2, 5, and 6 traverse the cell membrane while TMD 3 and 4 together form an intracellular loop (Milenkovic *et al.*, 2007). The other model implies that hBest1 contains 4 TMDs that are composed of the predicted TMD 1, 2, 4, and 6 and that TMD 5 is a reentering loop from the extracellular side (Tsunenari *et al.*, 2003). Both models show that hBest1 is membrane protein that traverses the membrane four times and both N and C termini are cytoplasmic. Quaternary structure analysis suggests that functional hBest1 is likely to exist as multimeric complexes of four or five subunits by forming either homo- or heteromeric associations between bestrophin paralogs (Sun *et al.*, 2002).

All of the mutations that are linked to Best Disease are autosomal dominant and almost all are missense mutations cause by single amino acid substitution. Over 97% of these disease-causing mutations cluster within or near the putative transmembrane domains of hBest1, implying important functional properties (Bakall *et al.*, 1999, Kramer *et al.*, 2000, Lotery *et al.*, 2000, Marchant *et al.*, 2002, Marquardt *et al.*, 1998, Petrukhin *et al.*, 1998, White *et al.*, 2000). Around 1/3 of these 100 disease-causing mutations have been carefully examined, and they all exhibit depressed Cl^- function (Marchant *et al.*, 2007, Qu *et al.*, 2003, Sun *et al.*, 2002, Tsunenari *et al.*, 2003, Yu *et al.*, 2006, Yu *et al.*, 2007). In addition, many of these mutations also inhibit wild type hBest1 currents during co-expression (Yu *et al.*, 2007), as expected for the dominant negative pattern of inheritance of the disease and oligomeric nature of the channel.

Human bestrophin 2 (GenBank ID: AF440756) is 57 kDa in size and is made up with 509 amino acids. By fluorescent in situ hybridization (Lotery *et al.*, 2000) approach, BEST2 gene was mapped in human chromosome 19q13 (Stohr *et al.*, 2002). hBest2 transcript is predominantly expressed in RPE and colon (Stohr *et al.*, 2002) and in the parotid salivary gland (Nakamoto *et al.*, 2007). When over-expressed in HEK cells, hBest2 also induces a Cl^- current. However, different from hBest1, the Cl^- current induced by hBest2 is not Ca^{2+}-sensitive. Generally speaking, the macroscopic Cl^- currents associated with expression of hBest2 exhibit time-independence and linear I-V relationship (Sun *et al.*, 2002). hBest2 can form heteromeric protein complex with hBest1 when expressed in HEK cells (Sun *et al.*, 2002). The physiological significance of such interaction is unclear because it is unknown if both hBest1 and hBest2 are expressed in the same tissue and the functional recording data for hBest1 and hBest2 co-transfected cells is lacking.

Human bestrophin 3 (GenBank ID: AY515706) is the longest member (668 amino acids) of the hBest family of proteins with a size of 67 kDa. mRNA of hBest3 is enriched in skeletal muscle and is weakly expressed in brain, spinal cord, bone marrow, retina, thymus, and testis (Stohr *et al.*, 2002). hBest3 cDNA was cloned from testes and retina for functional assays (Tsunenari *et al.*, 2003). When over-expressed in HEK cells, hBest3 elicits Ca^{2+}-stimulated Cl^- currents that are the most atypical among all human bestrophins. The Cl^- current induced by hBest3 is strong inwardly rectifying and shows strong time-dependent activation of prolonged (~20 seconds) and steady increase in conductance at hyperpolarizing membrane potentials (Tsunenari *et al.*, 2003).

Human bestrophin 4 (GenBank ID: AF440757) is 54 kDa in size and contains 474 amino acids. It is highly expressed in colon and weakly in fetal brain, spinal cord, retina, lung, trachea, testis, and placenta (Stohr *et al.*, 2002). Cells expressing human bestrophin 4 cDNA cloned from testes and fetal brain induces Cl^- currents that are on average greater than all of the other human bestrophin paralogs in magnitude (Tsunenari *et al.*, 2003). For example, hBest4 expressed in CHO-K1 cells manifested Cl^- currents that often exceeds ~20 nA whereas Cl^- currents associated with expression of hBest1 is typically ~1 nA in magnitude (Tsunenari *et al.*, 2006). The Cl^- currents associated with expressed hBest4 respond to negative voltages with a rapid and roughly linear current-voltage relationship followed by a time-dependent inactivation (Tsunenari *et al.*, 2006, Tsunenari *et al.*, 2003). In an effort to elucidate the activation mechanism by Ca^{2+}, excised patch of cells transfected with hBest4 was examined for its Ca^{2+} sensitivity. Tsunenari *et al.* reported that hBest 4 could be activated by free Ca^{2+} on the cytoplasmic side (Reisert *et al.*, 2003, Tsunenari *et al.*, 2006) although the kinetics of the activation/deactivation is much slower

than for typical Ca^{2+}-activated chloride currents (Reisert *et al.*, 2003). Activation through Ca^{2+}-dependent phosphorylation seemed unlikely because the solutions for excise patch recording of hBest4 were ATP-free. Ca^{2+} could either be activating hBest4 by directly binding to the cytoplasmic domains of the protein or it is modulating hBest4 through indirect pathways through membrane bound messengers (Tsunenari *et al.*, 2006). Although hBest2, 3, and 4 can all induce Cl^- currents when expressed in the HEK cell, only hBest1 mutations are correlated with Best Disease.

Mouse Bestrophins

The mouse genome contains three bestrophin paralogs and a pseudogene that are located on different chromosomes (*mBest1*: 19B, *mBest2*: 8 syntenic, *mBest3*: 10 syntenic). The same as human bestrophins, mouse bestrophin paralogs are conserved in first ~360 amino acids at the N terminal and are highly divergent in both length and sequence in their C termini. Based on a consensus of multiple different prediction algorithms, mouse bestrophins are predicted to be membrane proteins with four transmembrane domains that correspond well to the four predicted TMDs of hBest1 protein (Bakall *et al.*, 2003).

Mouse bestrophin 1 (NM_011913) is a 64 kDa protein that contains 551 amino acid residues and exhibits 63 % identity and 74 % homology to the overall sequence of hBest1 (Bakall *et al.*, 1999, Bakall *et al.*, 2003, Milenkovic *et al.*, 2007). The expression pattern of mBest was determined with RT-PCR in RNA isolated from mouse RPE at different developmental stages. mBest transcript level is most prominent during early postnatal development stage (P2 to P5). However, mBest protein level detected by immunohistochemistry showed an initiation of mBest expression at the RPE cells very late

in postnatal development (> P10). Nevertheless, This time point matches the onset of time-evoked electrical responses in the outer retina (ERG) (P10-P12), and the results support a role for bestrophin in RPE response to ionic changes that accompany retinal activity (Bakall *et al.*, 2003). Besides RPE, mBest1 is broadly expressed in other epithelia including the intestine, kidney, and airway (Barro Soria *et al.*, 2006). To date, there is no reliable report showing that mBest1 carries Cl^- currents. Alternatively to functioning as a Cl^- channel, mBest1 may act as an accessory molecule in the regulation of the voltage-gated Ca^{2+} channels (Marmorstein *et al.*, 2006, Rosenthal *et al.*, 2006, Yu *et al.*, 2008).

Mouse bestrophin 2 (AA509923) is made up with 465 amino acids that exhibit a molecular mass of 57 kDa. Heterologous Cl^- currents induced by over-expression of mBest2 are the most extensively studied among mouse paralogs (Bakall *et al.*, 2008, Barro Soria *et al.*, 2006, Duta *et al.*, 2004, Fischmeister & Hartzell, 2005, Kunzelmann *et al.*, 2007, Pifferi *et al.*, 2006, Qu *et al.*, 2006a, Qu *et al.*, 2004, Qu & Hartzell, 2004). When expressed in HEK cells, mBest2 induces Cl^- currents that manifests sensitivity to elevated cytoplasmic Ca^{2+}, linear current-voltage relationship, time independency, and a lack of discrimination between among permeant anions with a lyotropic permeability sequence of $SCN^- > NO_3^- > I^- > Br^- > Cl^- > F^-$ (Qu *et al.*, 2004). The lyotropic permeability sequence suggests that electrostatic interaction of the permeant ion with the pore is less important than hydrophobic interactions (Eisenman & Horn, 1983). This explains the observation that larger ions such as SCN^-, which are more easily dehydrated, are more permeant than smaller ions (F^-) (Hartzell *et al.*, 2008, Qu & Hartzell, 2004). In addition, like the Cl^- currents induced by expressing hBest1 in HEK cells, Cl^- currents associated with the

expression of mBest2 are also strongly inhibited by hyperosmotic extracellular recording solution (Fischmeister & Hartzell, 2005). Furthermore, studies in the mouse olfactory neurons suggest that mBest2 is responsible for the CaC current that is downstream of the activation of the cyclic nucleotide-gated (CNG) cation channel (Pifferi *et al.*, 2006), implying a physiological role of mBest2 in mediating the olfactory transduction. However, the expression of mBest2 at the olfactory neuron is not reproducible by other labs and the biological function of mBest2 remains unclear.

Recently, mBest2 knockout mice were generated by replacing exon 1, 2, and part of exon 3 with LacZ gene (Bakall *et al.*, 2008). By RT-PCR, mBest2 mRNA is found in the eye, olfactory sensory neurons, colon, trachea, brain, lung, kidney, and parotid acinar cells (Bakall *et al.*, 2008, Pifferi *et al.*, 2006, Srivastava *et al.*, 2008). X-gal staining confirms the localization of mBest2 in colon epithelia and refines the expression of mBest2 in the non-pigment epithelial cells (NPE) of the eye, but not in RPE cells (Bakall *et al.*, 2008). The absence of mBest2 had no obvious deleterious effect on the mouse. However, mBest2 plays a role in the generation of intraocular pressure (IOP) by regulating formation of aqueous humor because the mBest2-disrupted mouse exhibits significantly diminished IOP when compared to wild type and heterozygous littermates (Bakall *et al.*, 2008). This observation matches the functional localization of mBest2 in the NPE, the tissue that is in charge of aqueous humor secretion. Thus, inhibition of Best2 function may represent a putative new avenue for regulating IOP in individuals suffering from glaucoma (Bakall *et al.*, 2008).

Mouse bestrophin 3 (AY450426) contains 669 amino acids and weighs 76 kDa. The Cl^- currents induced by mBest3 in HEK cells are not stimulated by intracellular Ca^{2+} and

the overall amplitude of the macroscopic currents is small relatively to the currents induced by other Ca^{2+}-sensitive bestrophins (Qu *et al.*, 2006b). Qu *et al.* discovered an autoinhibitory (AI) domain at the C terminus of mBest3 (Qu *et al.*, 2006b) and further refined it to seven critical residues (amino acid 356-362) (Qu *et al.*, 2007). Replacing any residues except Proline 357 within this domain with Alanine greatly enhanced Cl^- currents and substituting a residue within this domain altered the current rectification, suggesting that the AI domain is associated with the channel pore or gating mechanism (Qu *et al.*, 2007). Full length mBest3 is transcribed in the heart. A splice variant of mBest3 that lacks exon 2, 3, and 6 was recently discovered in salivary gland, parotid gland, lung, testis, and kidney (Srivastava *et al.*, 2008). The truncated mBest3 does not induce Cl^- currents when expressed in HEK cell and does not affect the Cl^- currents of full length mBest3 or mBest2 when co-expressed in HEK cells, suggesting that the splice variant does not have functional roles in regulating mBest3 or mBest2 (Srivastava *et al.*, 2008). The physiological function of the truncated mBest3 remains unclear.

Xenopus Bestrophins

It is known that CaC channels are expressed at high levels in Xenopus oocytes (Hartzell *et al.*, 2005a). Based on sequences obtained from mammalian bestrophins, Qu *et al.* successfully cloned two bestrophin cDNAs from Xenopus oocyte (Qu *et al.*, 2003). By RT-PCR, xBest2 mRNA is highly expressed in RPE, liver, and spleen and to a lesser extent in the neural retina and the lung. Relatively little transcript was found in the brain, heart, and gut. A 54 kDa protein band corresponding to xBest2 was revealed in neural retina, liver, gut, and spleen but not in the RPE. Heterologous expression of xBest2 in HEK cells

induced CaC currents. The xBest2 associated Cl^- currents resemble Cl^- currents induced by mBest2 that show time-independence, linear I-V relationship (voltage-independence) at saturating Ca^{2+} concentration, an EC_{50} for Ca^{2+} of 210 nM, and a selective anion permeability with a lyotropic permeability sequence of $I^- > Br^- > Cl^- >> Asp^-$. Disease-causing mutations (W93C and G299E) introduced to xBest2 do not produce functional currents and exhibit dominant negative effect when co-expressed with wild type xBest2, implying that these conserved amino acids are involved with important basal function of the bestrophin family.

Limitations Associated with the Present Study of Bestrophins

An the functional level, over-expression of a variety of different bestrophins in HEK cells induces novel Cl^- currents (Chien *et al.*, 2006, Qu *et al.*, 2006a, Qu *et al.*, 2006b, Qu *et al.*, 2004, Qu & Hartzell, 2004, Qu *et al.*, 2003, Sun *et al.*, 2002, Tsunenari *et al.*, 2006, Tsunenari *et al.*, 2003, Barro Soria *et al.*, 2006, Srivastava *et al.*, 2008), suggesting that Bestrophins act as transporters of chloride ions across epithelial borders. However, the characterization of bestrophin function faces similar limitations that have universally hampered the identification of Cl^- currents. Based on the often redundant nature of Cl^- channel exhibition in biological systems, the major limitation to differentiate Cl^- channels from mixtures of currents is the lack of specific blockers or high affinity ligands.

Secondly, although functional association of an upregulated current with the heterologous expression of a protein is a powerful tool for showing that a specific gene encodes an ion channel, this approach is not without pitfalls. One concern is that expression of exogenous proteins could induce the up-regulation of endogenous ion

channels. Lessons on this are well documented in Xenopus oocytes, where expression of a wide variety of exogenous ion channels including nonconducting potassium channel mutants or other membrane proteins induces up-regulation of an endogenous current (Attali *et al.*, 1993, Kowdley *et al.*, 1994, Shimbo *et al.*, 1995, Tzounopoulos *et al.*, 1995).

Another limitation is that many model cell lines that are widely used for functional studies of ion channels such as Xenopus oocytes and HEK cells, express endogenous Cl^- channels (Ackerman *et al.*, 1994, Arellano & Miledi, 1995, Kuruma & Hartzell, 2000, Voets *et al.*, 1996). The presence of background Cl^- currents have greatly hampered the unambiguous characterization and screening of CaC and VRAC channels especially and many other protein candidates that encode for Cl^- conductance.

In addition to the limitations mentioned above, the nature of exogenous proteins in heterologous over-expressed cells such as HEK and Xenopus oocytes may not be well preserved and can be greatly affected by of the lack of optimal regulatory subunits in host cells. For example, Tsunenari *et al.* reported that they were unable to detect new Cl^- currents in Xenopus oocyte following injection of synthetic hBest1 mRNA, whereas control injection of ClC-0 mRNA with identical 5'- and 3'- untranslated regions (UTRs) produced large Cl^- currents (Tsunenari *et al.*, 2003). However, these researchers were able to record Cl^- currents when hBest1 was expressed in HEK cells, suggesting that HEK cells may contain chaperones, trafficking proteins, and/or ion channel subunits that are required for bestrophins from human to function or to properly targeted to the plasma membrane. Another more extreme example is reported by Schmieder *et al.* that the currents induced by expression of Xenopus homologue of ClC-5 (xClC-5) in Xenopus oocyte depend significantly on the vector used (Schmieder *et al.*, 1998). If the cRNA was flanked by

Xenopus beta-globin 5'- and 3' UTRs, the anion selectivity and sensitivity to Cl^- channel blockers was different than when the cRNA contained the native xClC-5 UTR regions. The authors suggest that the current induced by the beta-globin-UTR-flanked cRNA was authentic xClC-5 current, whereas the current induced by the native cRNA was due to upregulation of endogenous Cl^- currents. Therefore, interpretations should be made carefully with data obtained from heterologous over-expression systems (Kuruma & Hartzell, 2000).

Besides these common limitations for the characterization of most types of Cl^- channel mentioned above, the study of bestrophin function has also encountered several obstacles, both at the cellular level and at the animal level. The etiology of Best Disease is highly related to mutant bestrophin in the RPE cells. Therefore, cultured RPE cells are theoretically the most suitable model for studying the function of bestrophins and their involvement in visual disorders. Unfortunately, cultured RPE cells often lose their differentiated phenotype and the expression of bestrophins (Rak *et al.*, 2006) unless unusually complicated culture methods are involved (Hu & Bok, 2001, Ohno-Matsui *et al.*, 2006). These limitations greatly hamper the use of isolated RPE cells as an in vitro model for their in vivo function. Although RPE cell lines are available and may represent an alternative systems to work with, these cell lines do not express endogenous bestrophins.

At the animal level, restricted numbers of Best Disease patients/families as well as the legal and ethical issues with human subjects greatly impede the direct study of the pathogenic mechanism of Best Disease. Mice are so far the most widely used vertebrate model animals for studying the inherited diseases of humans, with whom they share 99% of their genes (Rosenthal & Brown, 2007). Advantages of using mice as a genetic model

system to study the physiological function of bestrophins mainly rely on the homology of genes and the conserved developmental and gross anatomical features between mice and humans. Ours and other labs are currently using bestrophin knockout/mutant mice to explore the physiological function of bestrophins (Bakall *et al.*, 2008, Marmorstein *et al.*, 2006). However, phenotypes related to disrupted bestrophin have not been identified in mBest1 -R218C, mBest1 KO, mBest2 KO, and double KO mice (Marmorstein *et al.*, 2006). This can be explained by the often redundant protein expression profiles in mammals (Grubb & Boucher, 1999, Pilewski & Frizzell, 1999, Snouwaert *et al.*, 1992). In addition, each bestrophin gene has a unique overall pattern of expression, in many tissues these patterns overlap. This raises another potential complication of gene compensation, such that removal of a particular isoform of a gene family causes upregulation of other isoform(s) or, in the case of bestrophin, even other kind of Cl^- transport modules. Researchers now have begun to search for phenotypes in mouse tissues other than the eye.

Drosophila melanogaster and its Cell Line as Model Systems for Bestrophin Study

Drosophila S2 cell line is derived from undifferentiated fly embryos (Schneider, 1972). The major discoveries that made S2 cell ideal for the study of bestrophin function is that they express physiological level of native bestrophins and endogenous Cl^- currents (Chien & Hartzell, 2007, Chien *et al.*, 2006). Detailed description of the characterization of S2 native bestrophins and Cl^- currents will be covered in the following Chapters. In addition, the ease of genetics in silencing the expression of a particular gene by interference RNA approach is another appealing advantage of using S2 cells as a model system to study bestrophins. Most importantly, S2 cells are exquisitely sensitive to RNAi

and thus conducive for use in genomic analyses (Clemens *et al.*, 2000, Ramet *et al.*, 2002). The RNAi treatment in S2 cells does not require transfection reagents that are often toxic to the cells and the complication of immune responses induced by RNAi is absent in S2 cells. Furthermore, morphological and functional studies of S2 cells have revealed that S2 cells belong to a phagocytic hematocyte lineage (Cheng & Portnoy, 2003, Elwell & Engel, 2005, Mansfield *et al.*, 2003). This resemblance between the feature of S2 cells and the physiological functions of RPE cells where mammalian bestrophins locate makes this cell line a plausible tool for studying the conserved physiological processes mediated by bestrophins.

Drosophila melanogaster is the one of the most popular organisms in biological research. It is easily cultured in mass, has a short generation time, and has simple genomic component that has been fully sequenced. The fly is an especially powerful tool for understanding the function of a novel gene by means of reverse genetics. This is because the fly is one of the small sets of organisms in which transgenics are feasible. Moreover, the mutant flies are readily obtainable from several *Drosophila* stock centers around the world, such as the Bloomington *Drosophila* Stock Center at the University of Indiana and the fly bank at the National Institute of Genetics in Japan. In Chapter 5 of this dissertation, I will present some of my preliminay data that imply a defective Cl^- transport phenotype as a consequence of disrupted dBest1 function in the fly.

Rationale and Organizational Overview

The common limitations with rodent animal models in the study of human genetic disorders including Best Disease were mentioned above. Another major concern that hampers the identification of Cl^- channels, as described earlier with the characterization of

CaC and VRAC channels, is that many favorite cell lines used for patch clamping exhibit background Cl^- currents. Due to the lack of pharmacological reagents, these endogenous Cl^- currents are often indiscernible from the currents carried by exogenous proteins. In addition, another concern with the over-expression system is whether the currents induced by over-expressing a protein can truthfully recapitulate its physiological function as an ion channel. Extensive studies are often required to rule out the possibility that the expressed protein is up-regulating or unmasking an endogenous Cl^- conductance. Nevertheless, the discovery that mouse and human bestrophins are associated with the expression of Cl^- currents in heterologous cells has opened new avenues to understand the pathogenic of Best Disease. However, progress has been hampered by the critical information concerning:

(1) the biophysical function of native bestrophin,

(2) the direct correlation between bestrophin and the Cl^- currents in native cells,

(3) the regulation of endogenous bestrophin currents,

(4) the cellular process regulated by bestrophins,

(5) and a phenotype associated with mutant dBest1 in the fly.

In this dissertation, I focus on the functional characterization of *Drosophila* bestrophins with an obvious goal to facilitate the process of elucidating the pathogenic mechanisms of Best Disease and to provide implications to the treatment of macular degeneration. I provide answers to these outstanding questions listed above and test the hypothesis that bestrophins are Cl^- channels physiologically, bestrophin currents are dually regulated/activated by Ca^{2+} and by cell swelling, bestrophins are physiologically crucial in the regulation of cell volume homeostasis, and bestrophins may play a role in

osmoregulation in the intact fly by mediating Cl^- homeostasis.

CHAPTER 2

ENDOGENOUS *DROSOPHILA* BESTROPHIN MEDIATES CALCIUM-ACTIVATED CHLORIDE CURRENTS

Summary

Mutations in the human bestrophin 1 (hBest1) gene are responsible for Best vitelliform macular dystrophy (Best Disease). However, the underlying pathogenic mechanisms linking mutated hBest1 to Best Disease are unknown majorly because the function of hBest1 is not fully understood. When over-expressed in heterologous cells, hBest1 and several other mammalian bestrophins elicit Cl^- currents that are stimulated by elevated cytoplasmic Ca^{2+}. While much is known about the molecular function of heterologously-expressed bestrophins, little is known about the properties of endogenous bestrophins. We report here the discovery that native bestrophins function as Ca^{2+}-activated Cl^- channels in *Drosophila* S2 cell line. S2 cells express four endogenous *Drosophila* bestrophin paralogs (dBest1-4) and exhibit native CaC currents. To determine if the native S2 CaC currents are mediated by bestrophins, we applied interfering RNA (RNAi) to silence the expression of each bestrophin. The CaC current was abolished by RNAi constructs to dBest1, whereas RNAi to dBest2, dBest3, and dBest4 did not affect the CaC current. These studies demonstrated for the first time that endogenous bestrophins function as CaC channels. Moreover, dBest1 expressed heterologously in HEK cells induced Cl^- currents that recapitulated major phenotypic characteristics of the S2 native CaC currents. The role of dBest1 in forming the channel was further supported by the observation that some basic biophysical properties such as the relative anionic permeability and conductance of heterologous dBest1 Cl^- current was altered when a point mutation was introduced to a putative pore-lining amino acid (F81C). These data provide additional support that dBest1 is a Cl^- channel and implies that Best Disease might be a Cl^- channelopathy.

Introduction

Best vitelliform macular dystrophy (BVMD, Best Disease) is an inherited debilitating visual disorder characterized by the relatively selective degeneration of cells in the macula of human eyes (Best, 1905). In 1998, mutations in the human bestrophin 1 gene (*hBest1*) were first identified from families of affected pedigree as the genetic defect responsible for this progressive, early-onset, autosomal dominant form of macular degeneration by positional cloning (Marquardt *et al.*, 1998, Petrukhin *et al.*, 1998). Since then, accumulating evidence has suggested that BVMD is associated with mutations in the hBest1 gene (White *et al.*, 2000). To date, approximately 100 different mutations in the hBest1 gene have been reported to link to Best Disease (White *et al.*, 2000). Despite the established link between mutations in the hBest1 gene to Best Disease, the exact pathogenic mechanism by which mutated hBest1 leads to macular degeneration remains unknown. This is mainly because the function of hBest1 has not been fully characterized.

The molecular function of bestrophins have been implicated from both clinical and experimental observations. The hallmark diagnostic feature of Best Disease is a reduction of a component in the electrooculogram (EOG) that is believed to be mediated by a Cl^- conductance across the retinal pigment epithelium (RPE) in the eye (Gallemore & Steinberg, 1993, Wajima *et al.*, 1993). Using immunohistochemical approaches, researchers have demonstrated that bestrophins from multiple different vertebrates including macaque, pig, and mouse are distributed on the basolateral plasma membrane of the RPE cells (Marmorstein *et al.*, 2000, Marmorstein *et al.*, 2004). These observations have led to the hypothesis that bestrophin is mediating the Cl^- transport in the RPE.

The study of the pathogenic mechanism of BVMD with human subjects has been

complicated by the limited tissue availability and is hampered by the rare occurrence of this genetic disease. The identification of the molecular function of bestrophins in RPE cells is also hampered by the fact that RPE cells in culture are deprived of their native morphological properties and do not express bestrophins unless very unusual and complicated culture conditions are applied (Hu & Bok, 2001). Moreover, primary cultures of RPE cells cannot be transfected by conventional methods. These limitations have hampered the use of RPE for the identification of the function of bestrophins.

A great amount of effort has been invested in determining the function of bestrophins in model cell lines that have been widely used for cell biological and electrophysiological studies such as the HEK cell. When transfected to HEK cells, the expression of various mammalian bestrophin orthologs and paralogs is associated with an induction of Cl^- currents that are sensitive to intracellular [Ca^{2+}] (Qu *et al.*, 2006a, Qu *et al.*, 2006b, Qu *et al.*, 2004, Qu & Hartzell, 2004, Qu *et al.*, 2003, Sun *et al.*, 2002, Tsunenari *et al.*, 2006, Tsunenari *et al.*, 2003). In addition, co-expression of disease-causing mutants from either hBest1 or mBest2 greatly reduces wild type Cl^- currents induced by bestrophins in HEK cells (Marchant *et al.*, 2007, Sun *et al.*, 2002, Yu *et al.*, 2006, Yu *et al.*, 2007). This finding is consistent with the dominant negative trait of Best Disease. These studies in heterologous expression systems have prompted speculations that Best Disease is a channelopathy caused by a defective Cl^- channel function.

The coincident upregulation of CaC currents and the over-expression of bestrophins in HEK cells suggests that bestrophins are CaC channels. I have already described several limitations with the use of heterologous expression cells for the study of Cl^- channels in the previous chapter. Besides these limitations, the finding that a transmembrane protein could

elicit Cl^- currents when expressed in heterologous systems, but it does not mediate Cl^- currents in native cells (Tominaga *et al.*, 1995) has further highlighted the need to compare bestrophin-associated Cl^- currents in heterologous cells and in endogenous cells.

To determine if endogenous bestrophins function as CaC channels and to compare the property of heterologous currents induced by bestrophins to the endogenous bestrophin currents, we use the *Drosophila* S2 cell line as a model. We report here that *Drosophila* S2 cells express bestrophins physiologically and exhibit native Cl^- currents that are activated by elevated cytoplasmic Ca^{2+}. The accessibility of a post-transcriptional gene silencing approach by interfering RNA in S2 cells allows us to directly test if the macroscopic CaC currents are carried by the endogenous bestrophins. Using this RNAi approach, we have identified that dBest1 is responsible for S2 native CaC currents. These data provide strong evidences that bestrophins function as CaC channels physiologically. In addition, we report here that the expression of dBest1 in HEK cells elicited Cl^- currents that recapitulate many phenotypic characteristics of the S2 CaC currents. Introduction of a point mutation at the putative pore-forming site (F81C) change the biophysical properties of the heterologous dBest1 current. These results provide additional support that dBest1 is a substantial Cl^- channel.

Results

Characterization of Native CaC Currents in *Drosophila* S2 Cells

Drosophila S2 cells express an endogenous CaC current (Fig. 2-1). When S2 cells were subjected to whole cell recording, the initial whole-cell currents observed immediately after patch break were on average smaller than 250 pA at +100mV (n= 52)

with either zero Ca^{2+} (< 20 nM free) or high Ca^{2+} (~ 4.5 μM) intracellular recording solutions. The Cl^- currents recorded with zero Ca^{2+} remained stably smaller than 250 pA throughout the ~5-minute recording (Fig. 2-1B, C, and F). In a small portion of cells that were patched with zero Ca^{2+}, the Cl^- currents ran up transiently to a few hundred pA and then ran down and stabilized (data not shown) to approximately the same amplitude as the currents measured at the initiation of patch break. The reason for this transient run-up is not clear, but may be due to a spike of cytosolic Ca^{2+} associated with making or breaking the membrane patch.

In contrast, the currents recorded with the pipette solution containing high Ca^{2+} (Fig. 2-1A and F) ran up gradually with a mean half time of ~2 min (Fig. 2-1C) before reaching a plateau of stabilized currents that were on average 17.1 ± 3.2-fold (mean ± SEM, n = 25) greater than the initial current. This Ca^{2+}-sensitive current is carried by Cl^- because the measured reversal potential (0 mV) matched the calculated Nernst potential of Cl^- (E_{Cl}) in symmetrical [Cl^-] solutions. In addition, the CaC currents are unaffected if cations in both the intracellular and extracellular recording solutions were replaced by the relatively large and membrane-impermeant cation, $NMDG^+$ (N-methyl-d-glucamine) and the outward currents were blocked if extracellular Cl^- was replaced with the relatively large anion SO_4^{2-} (data not shown).

Like the CaC currents mediated by overexpression of hBest1, hBest2, and mBest2 in HEK cells (Qu *et al.*, 2004, Sun *et al.*, 2002, Tsunenari *et al.*, 2003), the fully activated CaC currents recorded in *Drosophila* S2 cells did not show any significant time-dependent activation or inactivation in response to voltage steps (Fig. 2-1D and E). However, the S2 CaC currents had small voltage dependence at the extremes of the voltage range that gave

the I-V relationship a characteristic "S" shape (Fig. 2-1 A and E).

Mechanisms of Slow Activation by Intracellular Ca^{2+}

The exact mechanisms for the run-up remain unknown. The run-up of S2 CaC currents takes minutes of time, suggesting an indirect role of Ca^{2+} in activating the current, possibly through a Ca^{2+}-sensitive kinase. Our preliminary data suggest that phosphorylation might be involved because the run-up of S2 CaC currents was accelerated and the macroscopic CaC current was enhanced in amplitude when Mg-ATP (3 mM) was included in the internal recording solution in addition to Ca^{2+}. The external solution contained glucose, so that the cell was capable of synthesizing ATP. Pre-incubating the S2 cells with either of the two non-selective kinase inhibitors staurosporin (0.1 mM) and k252a (1 μM) significantly prevented the CaC currents from activating (Fig. 2-2). Pre-treating S2 cells with a non-selective phosphatase inhibitor, calyculin (0.1 mM), suppressed the run-up phase of the S2 CaC current. These data suggest that the activation mechanism of S2 CaC current is regulated by phosphorylation. Moreover, our recent unpublished data show that a Ca^{2+}/calmodulin-dependent protein kinase II (CaMKII) inhibitor KN-93 (1 μM) suppresses the S2 CaC currents (Personal correspondence, Charity Duran), suggesting the involvement of an indirect activation mechanism by Ca^{2+} through a kinase pathway.

Pharmacology of *Drosophila* S2 CaC Currents

Although specific and potent CaC channel blockers are not available, we tested a few reagents that have been reported to inhibit CaC channels on S2 CaC currents (Figure 2-3).

The Cl^- channel blocker ($\geq$ 100 μM) was applied extracellularly to the cell when the CaC current reached a steady state. One of the most common blockers for native CaC channels is NFA (niflumic acid) (White & Aylwin, 1990). Although 10 μM NFA potently blocked native *Xenopus* CaC currents (Qu & Hartzell, 2001), 100 μM NFA does not inhibit S2 CaC currents. We also examined the effect of other commonly used Cl^- channel blockers, such as A9C (anthracene-9-carboxylic acid), DIDS (4,4'-diisothiocyanato- stilbene-2,2'-disulfonic acid), and NPPB (5-nitro-2-(3-phenylpropylamino)-benzoic acid), and relatively non-specific Cl^- channel blockers such as NEM (N-ethylmaleimide) and Zn^{2+}. 100 μM A9C, NFA, and DIDS and 1 mM of Zn^{2+} did not inhibit or inhibited slightly (~30%) the S2 CaC currents, whereas 100 μM NEM blocked ~ 50% of the currents. NPPB blocked S2 CaC currents in a voltage-dependent manner. At –100 mV, 100 μM NPPB blocked ~ 70% of the inward currents, whereas it suppressed only ~ 30% of the S2 CaC currents at +100 mV. The effect of NPPB is more potent at both voltage extremes at 300 μM. Approximately 70% and ~ 90% of the S2 CaC currents were blocked at +100 mV and –100 mV, respectively.

Identification of Endogenous Bestrophin Expression in S2 Cells

To determine whether S2 cells express endogenous bestrophins, we performed reverse-transcriptase PCR using total RNA extracted from S2 cells. RT-PCR primers were designed to span exon–exon boundaries to ensure the specificity to mRNA transcripts but not genomic DNA (Table 2-1). Using several different sets of primers, transcripts for dBest1 (AAR99659), dBest2 (AAF50668), dBest3 (AAF49648), and occasionally dBest4 (AAF49649) were detected by RT-PCR (Fig. 2-4B). The sequences of the PCR products

matched GenBank/EMBL/DDBJ sequences for individual *Drosophila* bestrophin.

Interfering RNA Knocks Down Both dBest Expression and S2 CaC Currents

The lack of specific blockers to Cl^- channels is one of the major problems that impedes the identification and isolation of Cl^- currents. To test whether S2 CaC currents are mediated by bestrophins, we adapted the approach of RNA interference. Since all four *Drosophila* bestrophins are highly conserved in the first ~360 amino acids and ~65% identical at the nucleotide level, our initial attempt was aimed at reducing nonselectively all *Drosophila* bestrophins at once with a conserved N-terminal bestrophin domain-targeting RNAi. To do so, we treated S2 cells with mixtures of RNAis to conserved N-terminal regions of both dBest1 and dBest2 (Fig. 2-4A; Table 2-2). Figure 2-4B shows the results of RT-PCR of cells treated with a mixture of the 1N and 2N dsRNAs. The level of transcript for all four *Drosophila* bestrophins was dramatically knocked down by 1N/2N RNAi treatment, in comparison with cells treated with control RNAi bearing the sequence of an intron of mBest2 gene.

Most importantly, cells treated with the 1N/2N RNAi mixture did not express CaC currents (Fig. 2-4C, D, and E). Typically, CaC currents in 1N/2N RNAi-treated cells remained less than <100 pA indefinitely after the initiation of whole cell recording with high Ca^{2+} pipette solution. In contrast, cells treated with control RNAi were indistinguishable from untreated cells as shown in Fig. 2-1; the currents ran up from <100 pA to ~1 nA with a mean half time of ~2 min. Control and 1N/2N RNAi-treated cells were prepared from the same passage of S2 cells and patch clamped in parallel on the same day. RNAi-treated cells had no apparent morphological differences from control cells. The lack

of CaC currents was not due to cell death because trypan blue exclusion assay did not show any difference in cell vitality ratio between control RNAi- and bestrophin RNAi-treated cells (data not shown).

To identify specifically which bestrophins were responsible for the CaC currents in S2 cells, RNAi was made to C-terminal regions of bestrophins that were divergent from one another (Fig. 2-4A; Table 2-2). The nucleotide sequence at the C terminus differs substantially between *Drosophila* bestrophins and account for the paralog specificity of RNAi molecules. Four RNAis were made to regions encoding parts of the unique C termini of dBest1 (1S and 1C) and dBest2 (2S and 2C). Two others were made to regions of dBest3 (3C) and dBest4 (4C) that spanned conserved and unique regions. As shown in Fig. 2-5A, these dsRNAs reduced or eliminated the respective transcripts. RNAi to dBest4 had inconsistent effects on dBest4 mRNA levels (data not shown).

To examine the efficiency and specificity of RNAi on bestrophins at the protein level, we made polyclonal antibodies to a fusion protein containing amino acids 440–718 of the C-terminus domain of dBest1. The specificity of the antibody was characterized using tissue extracts from fruit flies in which the *dBest1* gene was completely removed by recombination ($dBest^{1\text{-}2}$ line, (Tavsanli *et al.*, 2001)) with flies in which the knockout was rescued by a transposon containing an 18-kb genomic fragment encompassing the entire *dBest1* gene (λ*5*; $dBest1^{1\text{-}2}$ line, (Tavsanli *et al.*, 2001)). The antibody recognized specifically a band near the predicted size of dBest1 (79.6 kD) in dBest1 rescued flies while the band was absent in the $dBest1^{1\text{-}2}$ knockout flies (Fig. 2-5B). These results show that the antibody we developed was specific for dBest1 protein. In the S2 cells, dBest1-1S RNAi efficiently and specifically knocked out the expression of dBest1 while a single

dBest1 band was observed in cells treated with control RNAi (Fig. 2-5C). Because high quality antibodies are not available for other *Drosophila* bestrophins, we were not able to assess effects of the RNAi on other dBests protein levels.

It should be emphasize that the effect of dBest2 RNAi on S2 CaC current is not always consistent. It seems that the two dBest2 RNAi constructs (2C and 2S) described here sometimes exhibit off-target effect on dBest1 expression level. dBest2 RNAi data and a detailed discussion of the role of dBest2 in mediating the S2 Cl^- current will be depicted in the following chapter. In brief, we have discovered a correlation between an off-target suppression of dBest1 by dBest2 RNAi and the reduction of S2 Cl^- current in some batches of S2 cells, whereas in most other recent experiments in which dBest2 RNAi did not affect dBest1 expression, the S2 Cl^- current remained similar to the control current. Fig. 2-5D shows the plateau current amplitudes ~5 min after patch break in patch-clamped S2 cells. In all cases, the current immediately after patch break was ~100 pA. However, each of the two RNAi constructs to dBest1 abolished native CaC currents in S2 cells while the RNAi constructs to dBest3 and dBest4 had no effect on CaC currents. As mentioned above, it seems that dBest2 is not responsible for S2 CaC currents. Therefore, the most cautious conclusion is that the principal component of the S2 CaC channel is dBest1.

Heterologous Currents Associated with dBest1

As a further attempt to examine if dBest1 is the principal subunit of the functional CaC channels, we transiently transfected dBest1 in HEK cells for whole cell recording. We discovered that HEK cells transfected with dBest1 alone expressed Cl^- currents that recapitulated several key characteristics of native S2 cells: (a) the Cl^- current activated

gradually after patch break and stabilized at a plateau level with a half time similar to native dBest1 CaC currents in S2 cells (~2 minute) (Fig. 2-6A and B); (b) the current had slight voltage dependence at both voltage extremes ($\pm$100 mV) and therefore, exhibited "S" shaped current-voltage relationship (Fig. 2-6A and D); (c) the current was time-independent and exhibited high current noise at negative membrane potentials like the native current (Fig. 2-6C); (d) the rectification ratio of the dBest1 current in HEK cell was slightly outward rectifying, which is similar to the S2 native CaC currents; (e) the relative permeability and conductance between SCN^- (thiocyanate) and Cl^- (P_{SCN}/P_{Cl} and G_{SCN}/G_{Cl}) were the same for the dBest1 current expressed in HEK cells and the endogenous S2 cell current (Fig. 2-7C and D).

Transfection of dBest2 alone in HEK cells, on the other hand, did not produce any Cl^- currents (Fig. 2-8B and D). It is possible that dBest2 is not expressed or properly trafficked to the plasma membrane. Since we do not have an antibody for dBest2, these hypotheses were not tested. Another possibility is that there is an endogenous bestrophin in HEK cells that can form a functional channel with dBest1 but not with dBest2. However, HEK cells do not express hBest1 or hBest2 (Data not shown).

Regardless of the preservation of many key biophysical properties of S2 CaC currents in the Cl^- currents induced by dBest1 alone in HEK cells, the Cl^- currents induced by heterologously expressed dBest1 were Ca^{2+}-independent. Cl^- currents induced by dBest1 in HEK cells both exhibited similar rate of activation and plateau current amplitude regardless of the presence of Ca^{2+} in the pipet solution. It is possible that dBest1 is the α subunit (pore-forming domain) of the channel while the Ca^{2+}-sensing β subunit that is required for the CaC channel to be fully functional is missing in HEK cells. Co-expressing

dBest1 and dBest2 in HEK cells, however, did not restore the Ca^{2+}-sensitivity of the Cl^- current, but the current activated twice faster than expressing dBest1 alone (not depicted). This suggests that dBest2 might exhibit some regulatory roles on dBest1.

Mutation in dBest1 Altered the Biophysical Properties of the Cl^- Current

Cl^- currents are ubiquitously expressed, including HEK cells (Helix *et al.*, 2003, Nilius & Droogmans, 2003, Sardini *et al.*, 2003). To verify further that the Cl^- currents induced by dBest1-transfected HEK cells were carried by dBest1 and not by an up-regulated endogenous channel, we mutated phenylalanine 81 to cysteine (F81C) and examined the effect on the current. F81C was chosen because mutation of the homologous amino acid (F80) in mBest2 alters conductance and permeability (Qu & Hartzell, 2004), indicating that this residue is in the vicinity of the ion conducting pore. Significantly different from wild-type dBest1 and endogenous S2 CaC currents, the F81C current inwardly rectified (Fig. 2-8A and B), indicating a more favored outward flux of Cl^- than the inward direction. In addition, both P_{SCN}/P_{Cl} and G_{SCN}/G_{Cl} were increased by the F81C mutation (Fig. 2-8C and D). The changes in dBest1 currents resulting from the mutagenesis support the hypothesis that the currents were mediated by dBest1 and further suggest that dBest1 either contained the ion selectivity filter or controlled channel gating.

Discussion

Endogenous *Drosophila* Bestrophins are CaC Channels

Although inherited forms of macular degeneration are rare, studies of the bestrophin gene products continue to provide valuable insights into the pathogenic mechanisms

underlying the inherited Best Disease. In over-expression systems, bestrophins from various species have been shown to induce Cl^- currents, and many of these currents are stimulated by cytoplasmic Ca^{2+} (Qu *et al.*, 2004, Qu & Hartzell, 2004, Qu *et al.*, 2003, Sun *et al.*, 2002, Tsunenari *et al.*, 2006, Tsunenari *et al.*, 2003). In this study, we aimed at examining whether endogenous bestrophins function as Cl^- channels. The *Drosophila* S2 cell line expresses endogenous bestrophins. By RT-PCR, transcripts of four *Drosophila* bestrophins were identified from S2 cell RNA extracts. With whole cell patch-clamping, we discovered that S2 cells express native Cl^- currents that are stimulated by elevated cytoplasmic Ca^{2+}. However, these native S2 CaC currents are not blocked by many of the commonly used pharmacological reagents that suppress Cl^- currents, unless unusually high concentrations of blockers were applied.

To test if the S2 CaC currents are mediated by bestrophins, we used RNAi. A mixture of RNAi that targets the conserved N terminal domains of dBest1 and dBest2 greatly suppressed the expression of all four bestrophin paralogs and abolished the native CaC currents in S2 cells, suggesting that S2 native CaC currents are mediated by bestrophins. To specifically identify the molecular composition of the CaC channel, we made RNAi constructs to the divergent C termini that are unique to individual dBest paralogs. RNAis to dBest1 specifically abolished native S2 CaC currents whereas RNAi to dBest3 and dBest4 did not affect the currents. Specificity of dBest1 RNAi were confirmed by Western blotting with a polyclonal antibody made for dBest1. These results unambiguously demonstrated for the first time that native bestrophins are essential components of CaC channels. The observation that heterologously expressed dBest1 alone induced a Cl^- current that recapitulates most phenotypic characteristics of the endogenous S2 CaC currents and that

mutation of a putative pore-lining residue (F81C) alters the rectification properties and P_{SCN}/P_{Cl} and G_{SCN}/G_{Cl} of the heterologous current lend additional confidence to the conclusion that bestrophins are CaC channels.

There are three (or four) bestrophin paralogs in *Drosophila melanogaster* genome. *dBest1* (AY061546) is located at chromosome 3R and encodes for a 79.6 kDa protein that contains 721 amino acids. The molecular function of dBest1 was first reported by Sun et al. that when over-expressed in HEK cells, dBest1 induces a Cl^- current (Sun *et al.*, 2002). We further demonstrated here that endogenous bestrophins expressed by a fly cell line function as Cl^- channels that are stimulated by elevated cytoplasmic Ca^{2+} in whole cell patch clamping configuration (Chien *et al.*, 2006). Additional evidence supporting the idea that *Drosophila* bestrophins encode for a functional CaC channel is provided by our by inside-out excised patch recording data. Single channel analysis of the S2 bestrophin currents revealed a ~2 pS single channel conductance with fast gating kinetics and linear current –voltage relationship. A similar current was also observed in CHO cells transfected with dBest1, but no such channel activity was seen in S2 cells treated with RNAi to dBest1 and in untransfected CHO cells (Chien *et al.*, 2006). This single channel data together with the macroscopic functional analysis of the S2 Cl^- currents carried by *Drosophila* bestrophins provide definitive evidence that bestrophins are components of native CaC channels at the plasma membrane. In addition, the rate of single channel activation exhibited a mean half time of ~ 30 seconds, which is close to the scale of the macroscopic current activation rate. This relatively slow activation rate exhibited by single S2 CaC channels implies an indirect activation mechanism by Ca^{2+}, maybe through phosphorylation by a Ca^{2+}-sensitive kinase. This suggestion is supported by our

preliminary observation that application of a CaMKII inhibitor to S2 cells suppressed the dBest CaC currents.

dBest2, *3*, and *4* genes are all located on fly chromosome arm 3L. dBest2 (BT010012) protein has 809 amino acids and is 89.8 kDa in molecular mass. dBest3 (AAF49648) is 62.7 kDa in size with 535 amino acids. dBest4 (AAF49649) is predicted to have 526 amino acids with an estimated size of 61.5 kDa. Whether *dBest4* gene encodes for a protein is not clear, and some researchers have proposed that dBest4 is a pseudo gene (personal communication, Dr. Edward Blumenthal). To date, the molecular function of dBest2, 3, and 4 and the biological processes in which they are involved are unknown. Our experimental results contribute to the understanding of the function of dBest1 in forming the CaC channel dBest1 physiologically.

Other Endogenous Cl^- currents expressed by *Drosophila* S2 Cells

We report here that the native CaC currents in S2 cells are mediated by bestrophins. However, while we were measuring the endogenous macroscopic dBest currents in S2 cells, we noticed the occasional appearance of another Cl^- conductance in ~10% of the cells recorded. Although this Cl^- current of another kind might be contaminating the currents carried by bestrophins, we feel that this concern is minimized due to the following reasons: (1) the amplitude of this other Cl^- current is obviously smaller (< -200 pA) than bestrophin currents (-500 to -2000 pA), (2) this other Cl^- current is not sensitive to intracellular Ca^{2+}, this small background Cl^- current exhibits significantly different electrophysiological properties from bestrophin currents in that it is pronouncedly inwardly-rectifying and is activated by negative voltages in a time-dependent manner, making the two Cl^- currents

readily distinguishable, (4) this other Cl^- current is not affected by RNAi to bestrophins and still exists in ~10 % of S2 cells after bestrophin RNAi treatment. Many of these properties resemble a native Cl^- current in the *Drosophila* S2 cell line reported previously (Asmild & Willumsen, 2000). However, similar to what we have described above, these authors concluded that this Cl^- conductance is small enough (< 100 pA) and manifests obvious biophysical properties that differ from many other known Cl^- currents. Therefore, the effect of this inwardly-rectifying Cl^- conductance can be ignored when studying other Cl^- channel activities in the S2 cell line (Asmild & Willumsen, 2000).

Comparison of endogenous dBest currents and heterologous dBest1 currents

Our RNAi data suggested that native S2 CaC channels are composed predominantly of dBest1. Expressing dBest1 in HEK cell induces Cl^- currents that exhibit similar current-voltage relationship, noises at negative potentials, time course of activation, and time-independence as the endogenous Cl^- current in S2 cells. The fact that the dBest1-associated Cl^- currents in HEK cells recapitulate most key characteristics of native S2 CaC currents is consistent with the conclusion drawn from the RNAi experiment. However, similar to what we described above, Sun *et al.* reported that the Cl^- currents induced by dBest1 in HEK cells are not sensitive to Ca^{2+}_i (Sun *et al.*, 2002). These data together suggest that either an essential regulatory molecule for dBest1 is missing in the HEK cell, or the over-expressed dBest1 has saturated the regulatory mechanism and uncouples dBest1 current from the regulation by Ca^{2+}.

Comparison of CaC currents mediated by *Drosophila* and vertebrate Bestrophins

Endogenous *Drosophila* bestrophins induce Cl^- currents that are stimulated by elevated cytoplasmic Ca^{2+}. However, the macroscopic CaC currents carried by dBest1 show some characteristics that are different from those induced by vertebrate bestrophins. These differences include: (1) dBest1 currents are <100 pA at the initiation of the recording and activate slowly with a mean half time of 2-4 minutes, whereas vertebrate bestrophin CaC currents are either fully activated immediately (mBest2) or activate significantly faster than dBest1 (hBest1) after the initiation of whole cell recording; (2) dBest1 CaC currents are slightly voltage dependent at plus and negative voltage extremes and therefore exhibit an S-shaped current-voltage relationship and slight outward rectification, while vertebrate bestrophins exhibit dissimilar voltage dependences including linear (mBest2), outwardly rectifying (hBest1), and inward rectification (hBest3 and mBest3); (3) dBest1 CaC currents do not run down in either endogenous or heterologous cells, whereas hBest1 and mBest2 currents run down significantly during patch clamping. These differences could arise from the significantly different amino acid composition in the C terminal tails of bestrophin orthologs. A detailed examination of the C terminal sequences reveals a highly conserved Ser358 residue in all bestrophins except dBest1 (E358). This Serine residue is predicted as a putative phosphorylation site. Site-directed mutagenesis of Ser358 to Glutamate in hBest1 significantly prolongs the time needed for hBest1 to become fully activated (personal communication, Dr. Qinghuan Xiao). The average half time for the mutant hBest1 is 2 minutes, which resembles the activation rate of dBest currents. Our pilot analysis with non-selective kinase and phosphatase inhibitors also indicate the involvement of phosphorylation events during the activation phase of dBest currents. The activation of dBest CaC currents are significantly prolonged by kinase inhibitors, whereas

the currents are already activated at the initiation of whole cell recording by pre-treating S2 cells with phosphatase inhibitors. These observations suggest that phosphorylation is involved in regulating the activation of dBest currents, probably through a Ca^{2+}-sensitve kinase pathway.

In conclusion, our comprehensive analysis of endogenous bestrophins has demonstrated for the first time that bestrophins function as CaC channels physiologically. Our data have also revealed the similarity and the different Ca^{2+} sensitivity between heterologously expressed dBest1 and native bestrophin channels. Our findings that the expression of S2 CaC current is associated with dBest1 by RNAi plus the observation that expressing dBest1 alone in HEK cell induces Cl^- currents that recapitulate most phenotypes of the S2 Cl^- currents consistently suggest that the dBest1 is the principal component of the S2 CaC channel. Together, these data provide strong support that *Drosophila* bestrophins function as substantial CaC channels physiologically.

Materials and Methods

Cell Culture

Drosophila S2 cells were cultured in Schneider's *Drosophila* Medium (GIBCO BRL) with 10% heat-inactivated FBS, 50 U/ml penicillin, and 50 μg/ml streptomycin in air at 22-24 °C. S2 cells were seeded at a density of ~1 x 10^6 cells/ml in 10-cm petri dishes and were split 1:4 weekly. HEK-293 cells (American Type Culture Collection) were cultured in Eagle's Minimum Essential Medium with L-glutamine (Cellgro Co.), 10% heat-inactivated FBS (GIBCO BRL), and 50 U/ml penicillin and 50 μg/ml streptomycin (GIBCO BRL) in 5% CO_2/95% O_2 at 37 °C.

Solutions for Whole Cell Recording

The nominally "zero" Ca^{2+} intracellular solution used for patch clamping S2 cells contained (in mM) 143 CsCl, 8 $MgCl_2$, 10 EGTA-NMDG, and 10 HEPES, pH 7.3 (with NMDG) (free Ca^{2+} < 20 nM). The "high" Ca^{2+} intracellular solution was the same, except 10 mM EGTA-NMDG was replaced by 10 mM Ca-EGTA-NMDG. The Ca-EGTA stock solution was made by mixing 95 mM $CaCO_3$ and 100 mM EGTA at pH 7 (adjusted with CsOH) and titrating the final [Ca^{2+}] to make it equal to [EGTA] by the pH-metric method (Tsien and Pozzan, 1989) and was estimated to have ~ 40 μM free Ca^{2+}. The external solution used for patch clamp recording of S2 cells contained (in mM) 150 NaCl, 2 $CaCl_2$, 1 $MgCl_2$, 10 HEPES, 15 sucrose, and 10 glucose (pH 7.3 with NaOH). Osmolarity of all solutions was adjusted with water or sucrose to 320 mOsM. The standard pipette solution for HEK-293 recording contained (in mM) 146 CsCl, 2 $MgCl_2$, 5 Ca-EGTA, 8 HEPES, 10 sucrose, pH 7.3 (with NMDG). HEK-293 extracellular solution contained 140 NaCl, 5

KCl, 2 $CaCl_2$, 1 $MgCl_2$, 15 glucose, and 10 HEPES (pH 7.4 with NaOH). Osmolarity of both solutions was adjusted to 304 mOsM. With these recording solutions, Cl^- Currents would be expected to have reversal potentials near zero (symmetrical [Cl^-]), while cation currents would have extreme nonzero reversal potentials.

Whole Cell Recording

Patch-clamp was performed at room temperature (22-24°C). S2 cells were allowed to adhere to the bottom of the recording chamber for 10 min and were then washed twice prior to whole cell recording. Fire polished pipettes pulled from borosilicate glass (Sutter Instrument Co.) had resistances of 2-3 MΩ when filled with intracellular solution. For whole-cell recording, cells were usually voltage clamped with ~1-sec duration ramps from -100 to +100 mV run at 10-s intervals or 750-ms voltage steps from -100 mV to +100 mV in 20-mV increments. Whole cell recording data were filtered at 2-5 kHz and sampled at 5-10 kHz by an Axopatch 200A amplifier controlled by Clampex 8.2 via a Digidata 1322A data acquisition system (Axon Instruments Inc.). In all cases, sampling was at least twice the filtering frequency. Data were not corrected for liquid junction potentials, which were calculated to be ~ 4 mV. Series resistance compensation was not routinely employed, but cells were discarded if the series resistance was > 10 MΩ (typically 5 MΩ). The average capacitance of the S2 cells was 14.2 ± 0.4 (n =89).

Data Analysis

Data were analyzed using pClamp 9 software and Origin 7.0 (Microcol). Analyzed results were presented as mean ± SEM and *n* refers to the number of patches or repeats in each

experiment. Curve fitting was performed using the iterative algorithms in Origin. Relative anion permeability of the channels was determined by measuring the shift in E_{rev} upon changing the solution on one side of the membrane from one containing 150 mM Cl^- to another with 150 mM thiocyanate (SCN^-). The permeability ratio was estimated using the Goldman-Hodgkin-Katz (GHK) equation (Hille, 2001).

$$P_{SCN}/P_{Cl} = \exp(\Delta E_{rev}F/RT)$$

where ΔE_{rev} is the difference between the reversal potential with the test anion SCN^- and that observed with symmetrical Cl^- (E_{rev}= 0 mV), and F, R, and T have their normal thermodynamic meanings. In the calculations of relative anion permeability, the cation permeability was assumed negligible. As mentioned by (Qu & Hartzell, 2000), this could introduce an error into the relative permeability ratios if relative cation permeability is high. If cation permeability is independent of the permeability of the permeant anion, this error will be largest for anions with low permeability. The cation permeability was not corrected because (Franciolini & Nonner, 1994) have shown that cation permeability in a type of Cl^- channel is tightly coupled to the relative permeability of the permeant anion. If this were also true in the CaCC channel, corrections based on the assumption that cation permeability is independent of anion permeability would also be in error and would significantly confuse the situation. Thus, until whether cation and anion permeabilities are coupled in the CaCC is elucidated, this simplification of not applying any correction was adopted.

Reverse Transcriptase PCR

The efficiency of gene silencing by RNAi was evaluated by reverse transcriptase PCR

(RT-PCR). Total RNA was purified by the Trizol (Invitrogen) method. Bestrophin gene-specific primers were designed to span exon/exon boundaries to ensure that genomic DNA was not amplified (Table 2-1). RT-PCR was conducted using SuperScript III One-Step RT-PCR with Platinum Taq (Invitrogen). PCR band densities on agarose gel were quantified using an AlphaImager Imaging System (Alpha Innotech). Each PCR band was excised, gel-purified, and cloned into pCRII-TOPO (Invitrogen) for sequencing.

Interfering RNA (RNAi)

Double stranded interference RNA was synthesized using dBest cDNAs as template. Control dsRNA was prepared from mBest2 intron 9. PCR primers (Table 2-2) consisted of bestrophin gene-specific sequences with the T7 promoter sequence added to the 5' ends (Van Gelder *et al.*, 1990). Each primer was BLASTed against the *Drosophila* nucleotide database (NCBI) to ensure specificity. The PCR products were amplified with *Pfx* DNA polymerase (Invitrogen), gel-purified (QIAquick gel extraction kit, QIAGEN), and used for in vitro RNAi synthesis (mMESSAGE mMACHINE high yield capped RNA transcription kit, Ambion). RNAs were heated to 65 centigrade for 10 min and annealed by slowly cooling to room temperature. For RNAi transfection, 10^6 adherent S2 cells in a 35-mm Petri dish were washed twice with serum free medium before incubating with 40 µg of dsRNA in 1 ml of serum-free medium for 30 min at room temperature. The cells were supplemented with 2 ml of medium containing serum and cultured for 2 days for RT-PCR analysis and 6 days before whole recording.

Generation of dBest1 Antibody

Antibodies were raised in rabbits against amino acids 440-718 of dBest1 with $(His)_6$ tags. The construct for the His-tagged dBest1 was made by amplifying the dBest1 nucleotide sequence encoding amino acids 440-718 using *Pfx* DNA polymerase and primers to which EcoRI (forward) and NotI (reverse) restriction sites had been added. The PCR product was then subcloned into EcoRI and NotI sites of pET28a (Novagen). Protein expression was induced in BL21 *Escherichia coli* by IPTG, the bacteria were lyzed with Bug Buster Protein Extraction Reagent (Novagen), and the His-tagged protein was purified by chromatography on a Ni-NTA-His bind affinity column (Novagen) for immunizing rabbits. The specificity of the antibody was confirmed with the absence of a band in the dBest1 knockout fly (*dBest1*$^{1-2}$ and rescued λ*5; dBest1*$^{1-2}$ lines were obtained from Dr. Graeme Mardon, Baylor College of Medicine, Houston, TX).

Western Blotting

Crude membrane extracts of S2 cells treated with control, dBest1, and dBest2 RNAis were equally loaded (25 μg) and separated by SDS-PAGE on 10% Tris-HCl polyacrylamide gels before blotting to PDVF membrane. The polyclonal dBest1 antibody was used at 1:5,000 dilutions and ECL (Pierce Co.) chemiluminescent signal was detected by exposing X-ray films (Kodak).

Cloning of *Drosophila* Bestrophins

The sequences of the *Drosophila* bestrophins used in this study agreed with GenBank/EMBL/DDBJ sequences for dBest1 (AY061546), dBest2 (BT010012), dBest3 (AAF49648), and dBest4 (AAF49649). dBest1 full-length cDNAs was purchased from

Drosophila Gene Collection (Lawrence Berkeley National Laboratory). The open reading frame of dBest1 cDNA was amplified by PCR using *Pfx* DNA polymerase and subcloned into the KpnI (5') and NotI (3') sites of pcDNA3.1. Amplified DNA constructs were sequenced for confirmation.

Transfection of dBest1 in HEK-293 Cells

dBest1 in pcDNA3.1 was transfected into HEK-293 cells along with pEGFP (Invitrogen) in 2:1 ratio using Fugene-6 Transfection Reagent (Marchant *et al.*). To obtain modest amplitude of whole cell CaC currents (1-2 nA), 0.01-0.05 μg of dBest1 cDNA was used to transfect one 35-mm culture dish of confluent HEK-293 cells. After 24 hours, cells were dissociated and re-plated onto glass coverslips and cultured for another 16-24 hours before electrophysiological recording. Transfected cells were identified by EGFP fluorescence and were recorded within 3 days after transfection.

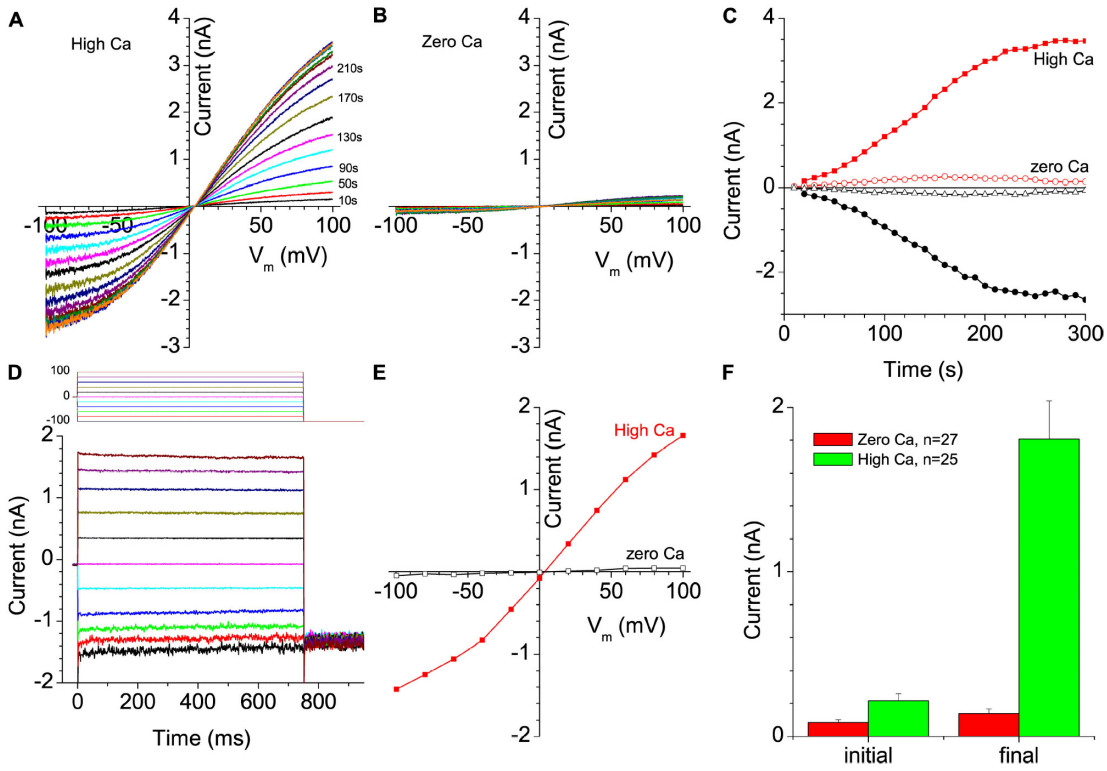

Figure 2-1: Native chloride currents of *Drosophila* S2 cells. (A-C) Time-dependent activation of a Cl^- current with (A) high or (B) zero intracellular Ca^{2+}. Current-voltage relationships were recorded by voltage ramps at 10-s intervals after establishing whole-cell recording. (C) Current amplitudes with time after patch break at +100 mV (red) and -100 mV (black) for high Ca^{2+} (solid symbols) and 0 Ca^{2+} (open symbols). (D) Current traces in response to voltage steps recorded after the currents had reached their peak (>5 min after patch break). (E) Steady-state current-voltage relationship in high Ca^{2+} (solid symbols) and 0 Ca^{2+} (open symbols). (F) Average current amplitudes at +100 mV at the onset of whole cell recording (Initial) and after the currents have reached a steady state (final) in high (green) and 0 (red) Ca^{2+}.

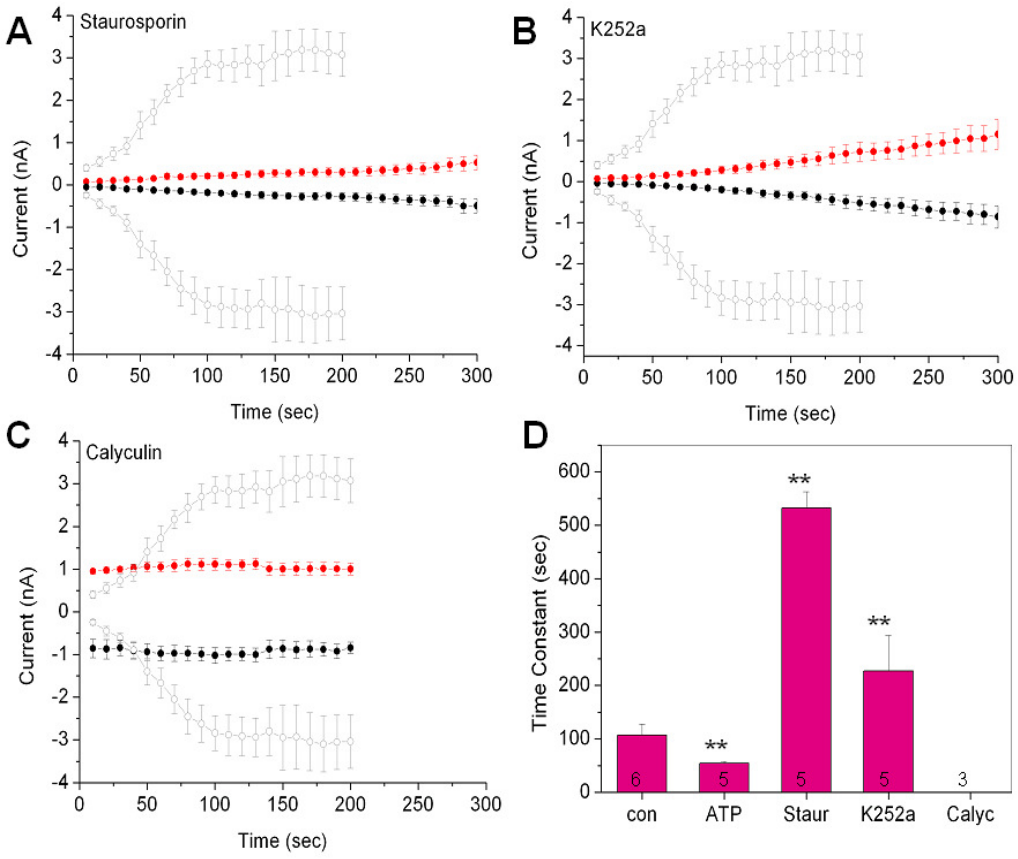

Figure 2-2: S2 CaC currents are modulated by phosphorylation. S2 cells are pre-incubated with kinase or phosphatase inhibitors for 5 minutes before patch clamping. The recording pipette contained high-Ca^{2+} supplemented with 3 mM of ATP. The same inhibitor is present in both the intracellular and extracellular recording solutions during recordings. (A-C) The time course of S2 CaC currents in the presence of kinase or phosphatase inhibitors. S2 CaC currents are suppressed by kinase inhibitors (A) staurosporin (0.1mM) or (B) k252a (1µM). At these concentrations, the effect of both kinase inhibitors is non-selective. (C) When S2 cells are treated with calyculin (0.1mM)

which non-selectively inhibits protein phosphatases, the S2 CaC currents were activated at the initiation of whole cell recording. The native S2 CaC current recorded with supplemented ATP in the absence of any inhibitor is shown in open circles, whereas the current recorded with the presence of inhibitors are shown in red (V_m=100mV) and black (V_m=-100mV) circles. (D) Average time constant of the activation of S2 CaC current with high-Ca^{2+}_i (control), high-Ca^{2+}_i plus ATP (ATP), and with high-Ca^{2+}_i plus ATP and kinase or phosphatase inhibitors. The number of data collected for each group is indicated in the bar graph. Data are presented as mean $\pm$ S.E.M. ** means that the mean value is significantly different from the control group with $p<0.01$.

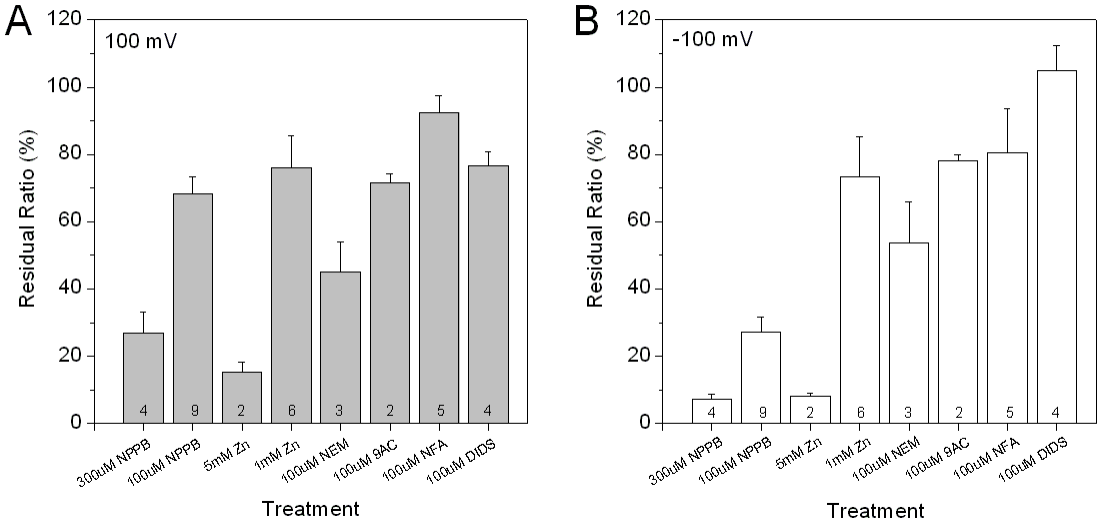

Figure 2-3: Pharmacology of S2 CaC currents. S2 cell whole cell patch clamping was established with high-Ca^{2+} intracellular solution. The pharmacological blockers were added in the extracellular solution when the S2 CaC currents reached steady states. The concentration of each blocker is indicated in the figure. The effect of the blockers on S2 CaC currents are presented as residual ratios (%), which is calculated as $I_{after\ drug}$ / $I_{before\ drug}$ * 100 %. The potency of each reagent on blocking S2 CaC currents are calculated at the two voltage extremes and are shown when (A) V_m =100 mV and (B) V_m = -100 mV, respectively. Data are presented as mean $\pm$ S.E.M. The number of data collected for each group is indicated in the bar graph.

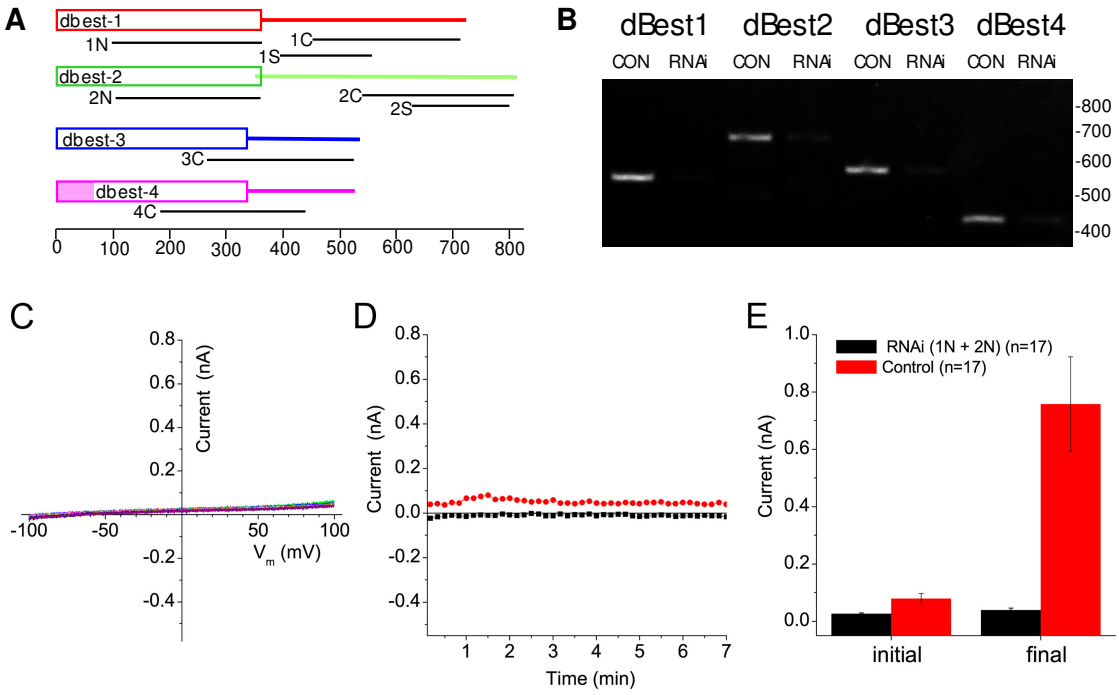

Figure 2-4: RNAi inhibition of dBest expression and CaC currents. (A) RNAi strategy. The conserved N-terminal regions of the four dBests are shown as boxes and the variable C-terminal regions shown as lines. The ruler shows amino acid number. The location of the RNAi constructs is shown by black lines below the dBests. (B) Expression of dBests by RT-PCR in cells treated with non-interfering dsRNA (CON) or a mixture of 1N and 2N RNAi (RNAi). Experiment was repeated three times. (C) Current-voltage relationship of RNAi-treated cell (superimposed traces spanning 6 min after patch break). (D) Time course of current activation in RNAi-treated cell after patch break. (E) Average current amplitudes at +100 mV immediately after patch break (initial) or after ~5 min (final) for cells treated with control dsRNA (red) and 1N+2N RNAi (black).

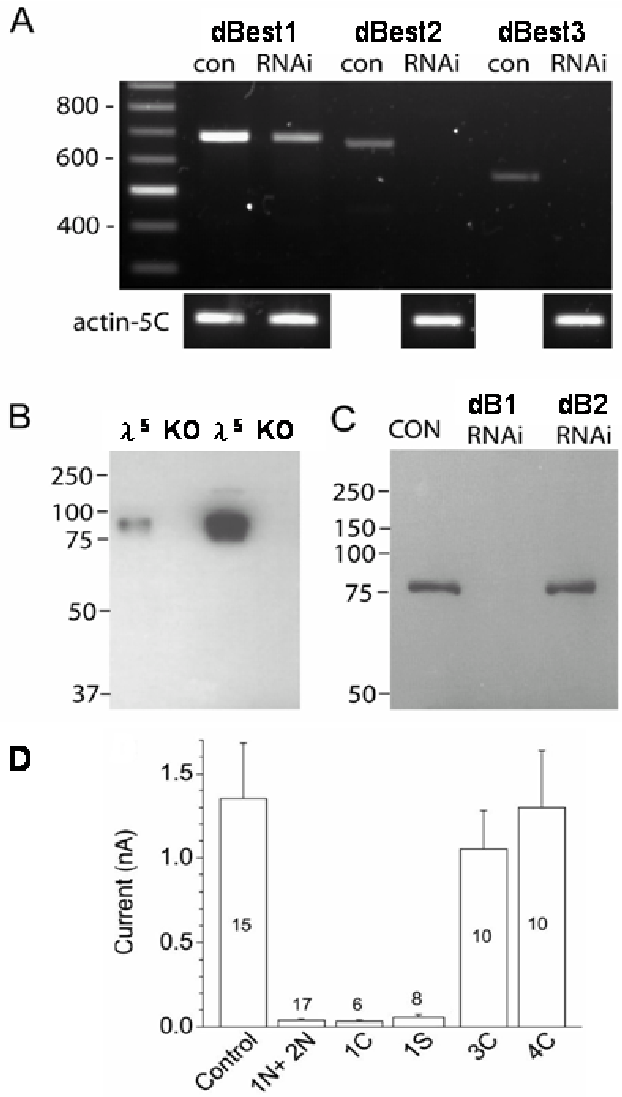

Figure 2-5: Specific RNAi inhibition of S2 CaC currents. (A) Quantification of dBest expression by RT-PCR in cells treated with non-interfering dsRNA (con) or specific RNAi to dBest1 (1C, 679 bp), dBest2 (2C, 665 bp), or dBest3 (3C, 565 bp). The actin-5 bands (426 bp) in the bottom panel show equal loading. These bands were obtained by RT-PCR of aliquots of the same RNAs used for the bestrophin RT-PCR in the top panel. The

actin-5C PCRs were run in separate lanes on the same gel as the bestrophin RT-PCR products, but for clarity they are shown below their respective bestrophin lanes. (B) Specificity of the dBest1 antibody. Western blot of SDS extracts from Malpighian tubules of knockout dBest1$^{1-2}$ (KO) and rescued λ^5; dBest$^{1-2}$ (λ^5) flies. Lane 1 and 2 were loaded with 5 µl extract, whereas lane 3 and 4 were loaded with 30 µl. Wild-type flies gave the same pattern as rescued flies (not depicted). (C) Western blot of S2 cell extracts from cells treated with control dsRNA (CON), dBest1 (2S), or dBest2 (2S) RNAi. Blot was probed with dBest1 antibody in cells that did not exhibit cross reactivity of dBest2 to dBest1. In other batches of S2 cells where S2 CaC current was suppressed by dBest2 RNAi (2C or 2S), dBest1 protein level was also decreased (not shown). (D) S2 CaC currents recorded at +100 mV ~5 min after currents reached their plateau level in control cells and cells treated with RNAi as indicated. Numbers above bars indicate number of cells studied.

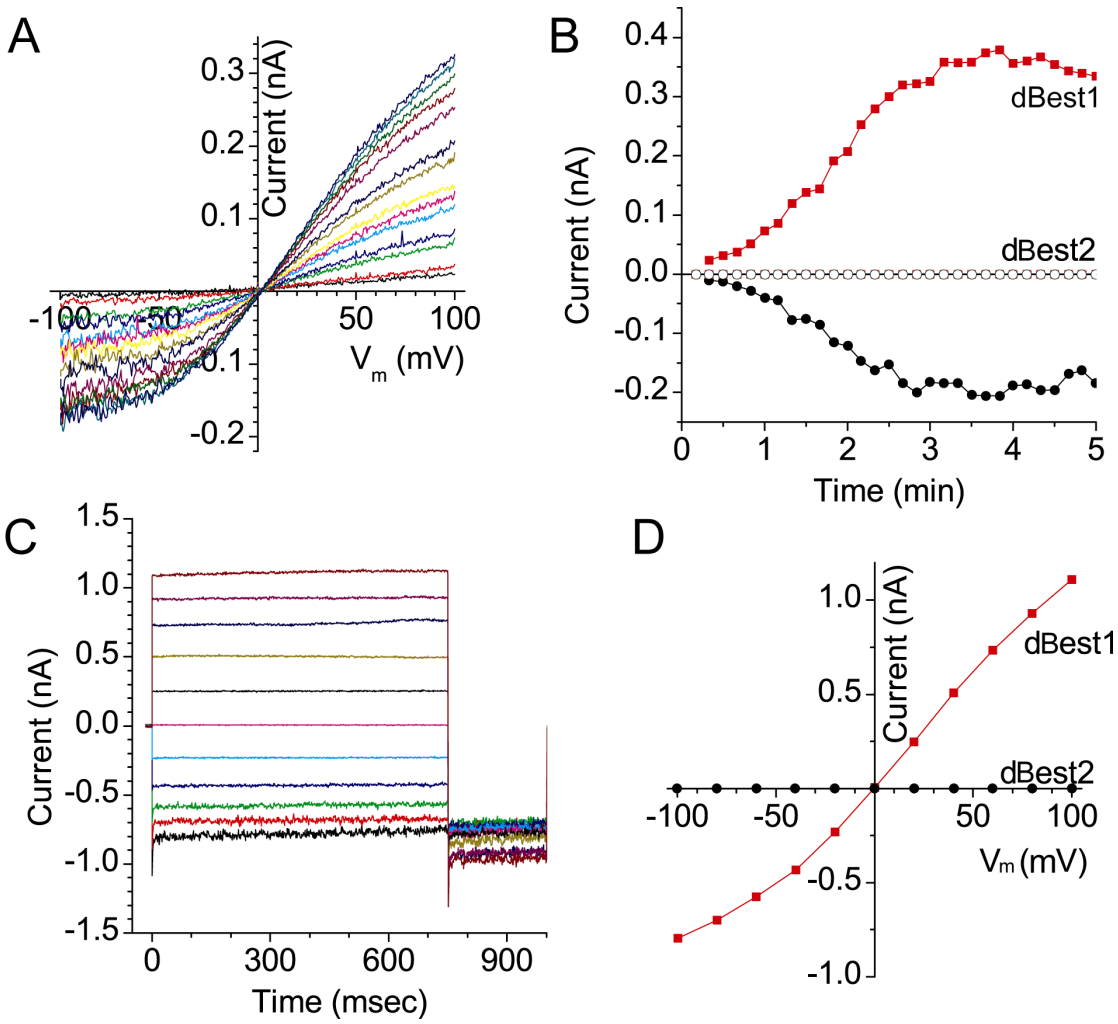

Figure 2-6: Expression of dBest1 and dBest2 in HEK cells. (A) Currents in HEK cells expressing dBest1 in response to voltage ramps delivered once every 10 sec. after patch break as in Fig. 1 A. (B) Activation of CaC current after patch break in HEK cells expressing dBest1 (filled symbols) or dBest2 (open symbols) at +100 mV (squares) and -100 mV (circles). (C) Cl currents in cells expressing dBest1 induced by step voltages between -100 mV and +100 mV at 20-mV intervals. (D) I-V curve from step protocols.

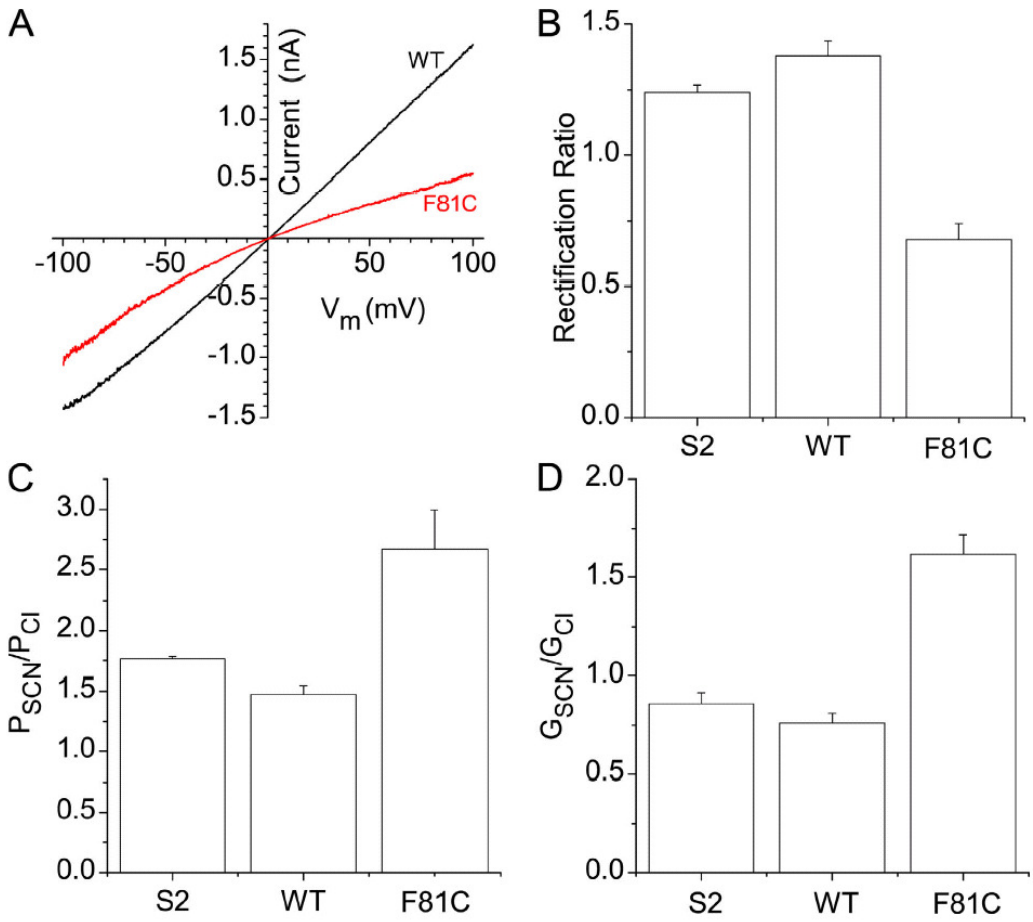

Figure 2-7: Effect of mutagenesis of dBest1 F81 to cysteine. (A) I-V currents from voltage ramps for wild-type dBest1 and dBest1-F81C in HEK cells. (B-D) Comparison of the electrophysiological properties of endogenous S2 CaC currents with wild-type dBest1 and dBest1-F81C expressed in HEK cells. (B) Rectification ratio calculated by dividing the amplitude of the current at +100 mV by the absolute value of the current at –100 mV. (C) Permeability and (D) conductance of the SCN^- relative to Cl^- for native S2 cells and HEK cells expressing wild-type (WT) or F81C dBest1.

Table 2-1. Exon-exon spanning RT-PCR primers for *Drosophila* bestrophins

Primer	Sequence	Product Size
Act5C	Forward: 5'-TCAGCCAGCAGTCGTCTAATCCAG-3' Reverse: 5'-GCGGGGCCTCGGTCAGC-3'	426 bp
dBest1	Forward: 5'-TGGCGAAGACGATGATGATTTTGA-3' Reverse: 5'-CTGGTTTTCCGGCCGATGTAGC-3'	533 bp
dBest1'	Forward: 5'-TCGATGAAATGGCCGATGATG-3' Reverse: 5'-ATGCTCTCCACTGTCTCTCG-3'	679 bp
dBest2	Forward: 5'-CGCGGACTATGAAAGCGTGG-3' Reverse: 5'-CTGGAATACTGCTCGGCGTG-3'	665 bp
dBest3	Forward: 5'-TCGATAAGCCTGTTTTCGAGGA-3' Reverse: 5-AGGGTGACGACCTGTGTATAG-3'	565 bp
dBest4	Forward: 5'-TGACGACTTCGAGCTCAACTG-3' Reverse: 5'-ATCGTTAAAGTCAATTGTGGATTG-3'	433 bp

Table 2-2. Primers for *Drosophila* bestrophins RNAi synthesis

Primer	Sequence	Product size
CON	Forward: 5'-TCGGGGCTGTGGCTGAGGT-3' Reverse: 5'-TGGTGCTTCGCGTTGATGTGT-3'	785 bp
1N	Forward: 5'-ATCCCATCGCCGTGTTTGT-3' Reverse: 5'-ACCTCGATCTTGGCAGTGGAC-3'	814 bp
1C	Forward: 5'-GCAACGCCCAGTCAGGA-3' Reverse: 5'-TCATCGTCGAATTGGAGAAC-3'	793 bp
1S	Forward: 5'-TGATGCCAGTGGCATTCAC-3' Reverse: 5'-CGCCAGGTGGAAATAGGTT-3'	509 bp
2N	Forward: 5'-GATACGTTGGCCCTGTTCATAA-3' Reverse: 5'-GCTCGTCTTTCCGGTAGTGTTC-3'	793 bp
2C	Forward: 5'-CCAGCTCGGTCCTAATG-3' Reverse: 5'-CCTCTCCGGTCTTTTGTT-3'	798 bp
2S	Forward: 5'-AAACATCACCACTCTGTCGT-3' Reverse: 5'-TTGAGGGGGCCGAGGAT-3'	503 bp
3C	Forward: 5'-GATCGGGATATTAAGCACTACA-3' Reverse: 5'-GTCCTCCTCCTTTCTCTTTTTC-3'	783 bp
4C	Forward: 5'-TGGCCACGTACTCCTTCTTCCT-3' Reverse: 5'-GCTCTGTCCCCCGCTTCCT-3'	784 bp

T7 sites (5'-CTAATACGACTCACTATAGGGAG-3') were added to 5' ends of both forward and reverse primers.

CHAPTER 3

DUAL ACTIVATION MECHANISMS OF DBEST1 Cl^- CURRENT

Summary

Mutations in the human bestrophin 1 (*VMD2*) gene are linked to Best vitelliform macular degeneration. However, the pathogenic mechanisms have not yet been determined because the function of the bestrophin protein is not fully understood. Bestrophins have been proposed to comprise a new family of Cl^- Channels that are activated by cytosolic Ca^{2+}. While a great deal of efforts have been focused on the identification of bestrophins being CaC channels, it has also been shown that Cl^- currents induced by heterologously expressed hBest1 and mBest2 in HEK cells were sensitive to osmotic pressure. Fischmeister *et al.* reported that the heterologous bestrophin currents stimulated by hyposmotic cell swelling were not quantifiable because of the expression of endogenous VRAC currents in HEK cells (Fischmeister & Hartzell, 2005). To overcome this problem, we decided to examine if bestrophins function as VRAC channels physiologically in *Drosophila* S2 cells. Here we demonstrate that Cl^- currents in *Drosophila* S2 cells, which we have previously shown are mediated by bestrophins, are dually regulated by Ca^{2+} and by cell volume. The bestrophin Cl^- currents were activated in a dose-dependent manner by osmotic pressure differences between the internal and external solutions. The increase in the current was accompanied by cell swelling. The volume-regulated Cl^- current was abolished by treating cells with each of four different RNAi constructs that diminished dBest1 expression. The volume-regulated current was rescued by transfecting with dBest1. Furthermore, cells not expressing dBest1 were severely depressed in their ability to regulate their cell volume. Volume regulation and Ca^{2+} regulation can occur independently of one another: the volume-regulated current could be activated in the complete absence of Ca^{2+} and the Ca^{2+}-activated current could be activated independently of alterations in cell

volume. However, these two bestrophin activation pathways can interact; intracellular Ca^{2+} potentiates the magnitude of the current activated by changes in cell volume. We conclude that in addition to being regulated by intracellular Ca^{2+}, *Drosophila* bestrophins are also novel members of the volume-regulated anion channel (VRAC) family that are necessary for maintaining cell volume homeostasis.

Introduction

Mutations in the gene encoding human bestrophin 1 (*VMD2*) are linked to a form of juvenile-onset blindness called Best vitelliform macular dystrophy (Best Disease) (Marquardt *et al.*, 1998, Petrukhin *et al.*, 1998). Recently, mutations in hBest1 have also been identified from a small fraction of cases of adult onset vitelliform macular dystrophy (Allikmets *et al.*, 1999, Kramer *et al.*, 2000, Seddon *et al.*, 2001), autosomal dominant vitreoretinochoroidopathy (Yardley *et al.*, 2004), autosomal recessive Bestrophinopathy (Burgess *et al.*, 2008), and canine multifocal retinopathy (Guziewicz *et al.*, 2007). Several bestrophin homologs from human and mouse have been proposed to comprise a new family of Cl^- channels in heterologous cells, many of which are activated by cytoplasmic Ca^{2+} (Qu *et al.*, 2004, Sun *et al.*, 2002, Tsunenari *et al.*, 2003). As described in the previous Chapter, *Drosophila* bestrophin have also been demonstrated to mediate Cl^- currents both in heterologous cells and in endogenous cells (Chien *et al.*, 2006).

It remains unclear, however, whether defects in the CaC channel activity of bestrophin is enough to completely explain the disease (Marmorstein *et al.*, 2006, Yu *et al.*, 2006, Yu *et al.*, 2007). Experiments with knock-out mice suggest that this explanation alone is not sufficient (Hartzell *et al.*, 2008). Accumulating lines of evidence have implicated the complexity of the function of bestrophin. Besides functioning as a CaC channel, some investigators have described that bestrophin could regulate Ca^{2+} signaling by inhibiting Ca_v channel activity (Marmorstein *et al.*, 2006, Rosenthal *et al.*, 2006, Yu *et al.*, 2008). In addition, bestrophins may also involve in cell volume regulation by functioning as VRAC channels (Fischmeister & Hartzell, 2005). Fischmeister *et al.* have demonstrated that the expression of hBest1 and mBest2 in HEK cells correlate with an

induction of Cl^- currents that are sensitive to osmolality differences between two sides of the plasma membrane. A 20% increase in extracellular osmolality almost completely inhibits hBest1 or mBest2 currents expressed in HEK cells. Conversely, decrease in the extracellular osmolality increases the current (Fischmeister & Hartzell, 2005). These data suggest that bestrophin currents are also sensitive to deviations in homeostatic cell volume.

VRAC channels play a central role in maintaining cell volume homeostasis. These channels activate in response to cell swelling probably through a mechanism similar to that which gates open mechano-sensitive ion channels. The common outcome of VRAC channel activation is the efflux of Cl^- followed by the out flow of water (Hoffmann & Simonsen, 1989, Lang *et al.*, 1998, Nilius *et al.*, 1997a). This results in a decrease in cell volume known as regulatory volume decrease (RVD). Although the functional characterization and physiological consequence of activation of VRAC channels has been known for decades, the molecular identity of the VRAC channel remains elusive (Eggermont *et al.*, 2001, Hoffmann & Simonsen, 1989, Lang *et al.*, 1998, Nilius *et al.*, 1997a). As described in Chapter 1, a major limitation in the identification of Cl^- channels is the lack of specific blockers.

To facilitate a comprehensive analysis of the regulation of endogenous bestrophin currents and to elucidate the physiological processes in which bestrophins are involved, we used the *Drosophila* S2 cell line as the model system. We have previously demonstrated that bestrophins are responsible for CaC currents using RNAi strategy (Chien *et al.*, 2006). In this Chapter, we characterized that endogenous bestrophin currents are stimulated by cell swelling induced by osmotic differences across the plasma membrane. Using a similar post-transcriptional gene silencing approach described previously, we demonstrate that the

swell-activated Cl^- currents were abolished when dBest1 expression in S2 cells is knocked down by RNAi. We will also describe in this Chapter that the activation of bestrophin currents by hyposmotic cell swelling does not require cytoplasmic Ca^{2+}, but an increase in intracellular Ca^{2+} facilitates the amplitude of the volume-sensitive bestrophins currents. Furthermore, the physiological consequence of dBest1 activation in response to cell swelling is to reduce the cell volume to close to its original value through a process called regulatory volume decrease (RVD). RVD is clearly mediated by dBest1 because cells treated with dBest1 RNAi exhibited significantly defective volume regulation ability. These data extend the knowledge of the activation mechanism of bestrophin currents and indicate that bestrophin is a novel member of the VRAC family. Our results also provide valuable insights into the physiological process that is regulated directly by bestrophin and prompt speculations that defective electrolyte and cell volume homeostasis may underlie the pathogenic mechanism of Best Disease.

Results

Osmotic Sensitivity of dBest1 CaC Currents

To test whether native bestrophin currents are sensitive to osmolality, S2 cells were voltage clamped under isosmotic conditions with an intracellular solution that contained high Ca^{2+} (~4.5 μM). The current was small (0.04 nA) immediately after patch break and then slowly activated with a half time of ~2 min to reach a plateau of 3.6 nA, as we have described previously (Fig. 3-1). We have previously concluded that this Ca^{2+}-activated current is mediated by dBest1 and possibly by dBest2 because this current is abolished by RNAi to dBest1 (Chien *et al.*, 2006). Increasing extracellular osmolality by 30% caused a

dramatic reduction of the current to 0.2 nA (Fig. 3-1). This suppression effect of extracellular hyperosmotic solution was similar to that described for hBest1 and mBest2 expressed in HEK cells (Fischmeister & Hartzell, 2005). When the extracellular solution was returned to isosmotic, the current usually increased very slowly and did not return to the initial current amplitude even after ~5 min. Fischmeister *et al.* have also observed a similar sluggish reversibility of mBest2 current once it has been suppressed by hyperosmotic solutions (Fischmeister & Hartzell, 2005). We suspect that this relative irreversibility can be caused by the relatively non-physiological magnitude of osmotic pressure changes, which results in disruption of the coupling between the volume sensor and the bestrophin current. Under our usual recording conditions (<5 min), the current does not run down in isosmotic conditions.

Characterization of Native Osmotically-Activated Cl^- Currents in S2 Cells

To test whether osmotic pressure could activate bestrophin currents independently of Ca^{2+}, we measured Cl^- currents in S2 cells under anisosmotic conditions with zero Ca^{2+} in the recording pipette. S2 cells were allowed to adapt to the extracellular solution (E300) for 15 min before recording. The cells were then patch-clamped with nominally 0 Ca^{2+} (<20 nM) intracellular solutions that were either isosmotic (I300) or hyperosmotic (I320, Δ20 mosmol kg^{-1} or I340, Δ40 mosmol kg^{-1}). Fig. 3-2A shows the traces of Cl^- currents of a typical S2 cell activated with Δ20 mosmol kg^{-1} osmotic pressure. The time course of the development of the osmotically activated Cl^- current is shown in Fig. 3-2B. Similar to the native Ca^{2+}-activated dBest Cl^- currents in S2 cells, the initial whole cell current immediately after patch break was on average <0.1 nA regardless of the osmotic pressure.

With isosmotic solutions, the current remained stably small at <0.2 nA indefinitely after patch break (n = 6, ~9 min). In contrast, with an internal solution having a higher osmolality than the extracellular solution, the current ran up briskly with a mean half time of 2.4 ± 0.1 min (n = 28) before reaching a peak that was on average 45.1 ± 7.3-fold (Δ20 mosmol kg^{-1}, n = 13) or 60.1 ± 15.2-fold (Δ40 mosmol kg^{-1}, n = 9) greater than the initial current amplitude (Fig. 3-2B). The osmotically sensitive currents are carried by Cl^- because the measured reversal potential is close to the calculated E_{Cl} (0 mV) in equimolar of [Cl^-] at both sides of the membrane and the currents were blocked by SO_4^- applied in the bath. However, about half of the S2 Cl^- currents activated by hyposmotic conditions ran down within one minute after reaching a plateau magnitude. The precise mechanism of the run-down is unclear.

Voltage steps from −100 mV to +100 mV in 20-mV steps were applied to the cell after the ramp current had reached a peak value (~4 min) to examine the time-dependence of the osmotically sensitive Cl^- current at fixed membrane potential (Fig. 3-2C). Cl^- currents activated by Δ20 or Δ40 mosmol kg^{-1} osmotic pressure did not show time-dependent activation or inactivation. The same as dBest CaC current, the steady-state current-voltage curve of this osmotic sensitive Cl^- current also showed slight voltage dependence at voltage extremes and showed a characteristic S shape (Fig. 3-2D).

The osmotically activated Cl^- currents share many key characteristics with the Ca^{2+}-activated dBest Cl^- currents described previously in S2 cells; (a) the currents activate slowly with time after patch break; (b) the half time of the activation of both currents is similar; (c) the currents are carried out by Cl^- because the measured reversal potential is close to the calculated E_{Cl} which is 0 mV in under equimolar [Cl^-] at both sides of the

membrane; (d) both currents are S-shaped in their current-voltage relationships; (e) both currents manifest noises at negative membrane potentials; (f) the currents do not show time-dependency.

S2 Osmotically-Activated Cl^- Currents is Coupled with Cell Swelling

To determine whether activation of the bestrophin current was related to osmotically induced changes in cell volume, we simultaneously imaged while patch-clamping the cells at a fixed time interval (imaged and voltage ramp applied every 10 seconds). The average time course of the development of the hyposmotically activated S2 Cl^- current and corresponding cell volume increase in response to Δ20 mosmol kg^{-1} is shown in Fig. 3-3A. Cell swelling preceded the activation of the Cl^- current and both the cell volume as well as the magnitude of the Cl^- current reached plateau levels with similar half time (~2 min). In addition, the magnitude of the Cl^- current is well coupled to cell swelling in a dose-dependent manner. Cells recorded in isosmotic solutions remained stable in volume indefinitely or shrank slightly (−7.7 ± 6.9%) (n = 4). The cell volume and the current were coordinately larger with greater osmotic pressure differences (Fig. 3-3B). At the peak of hyposmotic swelling, the cell volume increased 50.3 ± 11.6% (n = 4) with Δ20 mosmol kg^{-1} and 118.9 ± 38.8% (n = 3) with Δ40 mosmol kg^{-1}. These data shown in Fig. 3-1 to 3-3 suggest that S2 cells express native VRAC channel, which might be mediated by bestrophins.

It should be pointed out that our cell volume measurement method may not be perfect. The S2 cell volume was determined by measuring the circumference of the cell assuming that the shape of S2 cells is spherical. This approach may not be perfectly accurate in

determining cell volume and errors could possibly arise from the choice of focal plain, the limitation in the image resolution, the precision in circumference determination, and the assumption that S2 cells are spherical. Theoretically speaking, with Δ40 mosmol kg^{-1} osmotic pressure, an ideal osmometer predicts a 13.8% increase in cell volume. In our hands, however, the measured cell volume is much greater than predicted. This might be explained by the fact that cell swelling is not spherically symmetrical, as assumed. If cell swelling is constrained in the z-plane by mechanical pressure from the patch pipet, the change in cell volume may appear to be larger than it actually is. For this reason, the estimates of cell volume may be subject to some quantitative error and the magnitude of swelling may be overestimated.

RNAi Knocks Down dBests and VRAC Expressions in S2 Cells

The biophysical properties of the current activated by hyposmotic solutions in *Drosophila* S2 cells are virtually identical to the Cl^- current stimulated by Ca^{2+} that we described in the previous chapter. These similarities strongly suggest that anisosmotic pressures can activate the same current in the absence of elevated intracellular Ca^{2+}. Here, the RNAi approach is used again to test if bestrophins mediate the osmotically activated Cl^- current in S2 cells. S2 cells were treated with bestrophin subtype-specific RNAi or control dsRNA mentioned previously. To avoid possible unintended off-target effect with the use of long double stranded RNAi in *Drosophila* cells (Cullen, 2006, Echeverri *et al.*, 2006, Moffat *et al.*, 2007), we performed RNAi experiment with previously designed constructs (1C, 1S, 2C, 2S) in conjunction with two additional non-overlapping RNAis. To do this, we designed two additional RNAi constructs to the 3' and 5' untranslated regions (UTRs)

of dBest1 (1U5 and 1U3) and dBest2 (2U5 and 2U3) respectively. These new RNAi constructs will also be useful for the purpose of performing rescue experiments, because the UTR-targeting RNAi is not going to counteract the effect of transfected cDNA that contains only the open reading frame of the gene.

Six days after the RNAi treatment, S2 osmotically activated Cl^- currents were measured with Δ20 mosmol kg^{-1} (I320, E300) osmotic pressure. Cells that were treated with control dsRNA exhibited plateau currents of 1.07 ± 0.12 nA (n = 25) (Fig. 3-4A, open bars). Two of the dBest1 RNAi constructs including dB1C and dB1S that have previously been shown to abolish the CaC currents in S2 cells plus the two additional UTR-targeting RNAis (dB1U5 and dB1U3) all reduced the osmotically activated Cl^- current (recorded with the zero Ca^{2+} intracellular solution) significantly (Fig. 3-4A) to less than 0.2 nA. These four different RNAi constructs to dBest1 also abolished, or greatly reduced the CaC currents (under isosmotic condition) in S2 cells (Fig. 3-4B, open bars).

The efficiency and specificity of dBest1 RNAis were examined by Western blot (Fig. 3-4C) and RT-PCR (Fig. 3-4D). In 22 independent RNAi treatments, all of these four different dBest1 RNAi constructs greatly knocked down or abolished dBest1 protein and mRNA transcript level. However, we sometimes observed some “off-target” effects of dB1C and dB1U5 RNAi constructs on dBest2 transcripts. We do not understand the mechanism of these effects because the identity among dBest1 and dBest2 RNAis is subtle (Table 3-1). Nevertheless, the fact that both the Cl^- currents as well as dBest1 protein and transcript levels are abolished or significantly reduced with multiple different RNAi constructs to dBest1 strongly suggests that dBest1 is a substantial mediator of the VRAC and CaC currents in S2 cells.

Similar to the dBest1 RNAi design, four dBest2 RNAi constructs were made: two to sequences coding for parts of the C terminus of dBest2 (dB2C and dB2S) as mentioned in the previous chapter, and two others to the 5' (dB2U5) and 3' (dB2U3) UTRs respectively. dB2U3 and dB2U5 reduced dBest2 message levels, but had no significant effect on the VRAC or CaC current (Fig. 3-4A, B, and D). dB2C and dB2S, on the other hand, reduced both CaC and VRAC currents ~50%, but the effects were not statistically significant (at either the 0.05 or 0.01 level), except for the effect of dB2S on the VRAC current (Fig. 3-4A). In any case, the specificity of dBest2 RNAi on dBest2 level could only be accessed by RT-PCR because of the lack of dBest2 specific antibody. As briefly mentioned in Chapter 2, the effect of dB2C and dB2S to reduce the S2 Cl^- currents can be explained by a variable off-target effect of these RNAi constructs on dBest1 level. To go into details, in 4 out of 13 different RNAi treatment with the dB2C and dB2S RNAis, dBest1 protein levels were reduced to <10% of the control level. In six separate experiments where dBest1 protein was apparently the same as control, the mean current magnitudes in dB2C- and dB2S- RNAi-treated cells were identical to control (CaCC: 1.84 $\pm$ 0.19 nA, n = 23, VRAC: 0.75 $\pm$ 0.16 nA, n = 10; Fig. 3-4A and B, gray bars).

Recently, it is reported that matches as short as 6 or 7 nucleotides can cause translational repression of unintended targets (Birmingham *et al.*, 2006, Jackson *et al.*, 2006, Lin *et al.*, 2005, Moffat *et al.*, 2007). We think this may explain the cross reactivity between dBest1 and dBest2 RNAis reported here because the largest cluster of matching bases was 14 with 3 mismatches in these designs. An additional possibility may be that dBest1 and dBest2 are co-regulated so that knocking down either of these two proteins affect the expression of the other one. With careful and comprehensive comparison of all of

our data accumulated over the years, we now believe that the cross-reactivity of dBest2 RNAi constructs on dBest1 expression level underlies the inhibition of S2 CaC and VRAC currents. We conclude that dBest1 is the principal protein that mediate both the VRAC and CaC currents in S2 cells.

The sensitivity as well as specificity of dBest3 RNAi on dBests transcript level seems relatively consistent; dBest3 mRNA is consistently knocked down while dBest1 protein and dBest2 mRNA levels remain unaltered (Fig. 3-4A and D). dBest3 RNAi also did not affect either the CaC and VRAC currents. dBest4 RNAi also did not produce any effect on either of the S2 Cl^- currents. However, because dBest4 expression level varied from culture to culture as mentioned in previous chapter, the role of dBest4 remains inconclusive. Nevertheless, these data provide additional support that the dBest1 is the major player of the native CaC and VRAC currents in S2 cells and other bestrophins are not necessary in forming the ion channel.

Rescue of VRAC Currents by Expression of dBest1

To ascertain the specificity of dBest1 RNAi, we further tested the role of dBest1 in forming the S2 Cl^- channels by performing rescue experiments. To do this, we first knocked down native S2 dBest1 with UTR-targeting RNAi constructs and then expressed the open reading frame cDNA of dBest1 in these nominally dBest1-null cells. S2 cells were treated with dB1U5 RNAi for 4 days. The cells were then transfected with *Drosophila* expression constructs encoding either GFP alone or dBest1 plus GFP (Fig. 3-5). VRAC currents were measured in response to Δ20 mosmol kg^{-1} (nominally 0 Ca^{2+} I320, E300) hyposmolality. CaC currents were measured in isosmotic conditions with ~4.5 μM free

internal Ca^{2+} as described previously. dB1U5-treated cells transfected with GFP alone exhibited virtually no VRAC or CaC currents (Fig. 3-5A, C, and F). In contrast, dB1U5-treated cells transfected with dBest1 expressed apparent VRAC and CaC currents that exhibited typical phenotypes of the endogenous S2 CaC and VRAC currents (Fig. 3-5B, D, and F). The rescued currents activated slowly after patch break (Fig. 3-5 E), exhibited S-shaped I-V curves (Fig. 3-5B and D), showed noisy currents at negative potentials (Fig. 3-5B and D), and were time-independent in response to voltage steps (data not shown). Despite that the rescued CaC and VRAC currents activated slowly after initiation of patch break, these currents on average activated about twice as fast as the endogenous currents (Fig. 3-5 E, τ = 1 min). This might be related to the high level of dBest1 expression as depicted in Fig. 3-4C. Rescue with dBest1 resulted in a significant overexpression of dBest1 protein level while transfection of GFP only did not provide any affect on the dBest1 level in cells pre-treated with dB1U5 RNAi..

The Effect of Cytosolic Ca^{2+} and Cell Swelling on Surface dBest1 Level

Regardless of the activation mechanism, dBest1 currents showed a common characteristic: slow activation with a mean half time of 2-3 minutes. We have demonstrated in the previous chapter that the activation of bestrophin currents might involve phosphorylation of the channel protein by Ca^{2+}-dependent kinases. Besides phosphorylation, an increase in cell surface expression level has also been proposed to underlie the slow activation of VRAC currents (Jackson & Strange, 1995, Nilius *et al.*, 1997a). To test if changes in the cell surface level of dBest1 underlies the minute-scale activation mechanism of dBest1 Cl^- currents, we performed semi-quantitative analysis to

determine the surface expression ratio of dBest1. To do this, S2 cells were treated with either hyposmotic stimuli (40 mosm kg^{-1}) or with Calcimycin (Ca^{2+} ionophore) to increase cytoplasmic [Ca^{2+}] first. Then surface protein was labeled with biotin and pulled down by avidin-coated beads. Purified cell surface protein fraction and whole cell lysates were then Western blotted for dBest1 (Fig. 3-6A). The relative surface expression ratio of dBest1 is shown in Fig. 3-6B. In control untreated cells, approximately 20% of the total dBest1 was found expressed on the cell surface. This is in agreement with our unpublished immunocytochemistry data as well as those published (Fischmeister & Hartzell, 2005, Tsunenari *et al.*, 2003), which showed that the majority of transiently transfected hBest1 and native mBest2 was localized intracellularly. In any case, surface expression levels of dBest1 did not appear to be affected by hyposmotic stimuli or increment of cytoplasmic Ca^{2+}. These results suggested that the increase in protein trafficking/expression to the cell surface is not the primary mechanism that caused the slow activation of both volume-regulated and Ca^{2+}-activated bestrophin currents in S2 cells. This conclusion is further supported by our observation that the membrane capacitance, the parameter that correlates with the amount of the lipid bilayer of a cell, is not increased when the dBest1 current is fully activated be cell swelling.

The Role of Cytoplasmic Ca^{2+} on dBest1 VRAC Current

Although typical VRAC channels are Ca^{2+}-independent, hyposmotic cell swelling can elicit an increase of intracellular [Ca^{2+}] in several types of cells (McCarty & O'Neil, 1992). This increase in cytoplasmic Ca^{2+} in response to cell swelling may underlie the activation of dBest1 currents. Our result shown in Fig. 3-4 suggests that activation of dBest1 currents

can occur in the absence of intracellularly applied Ca^{2+}. However, an enhanced $[Ca^{2+}]_i$ may also result from Ca^{2+} influx from the extracellular recording solution, which contains 2mM of Ca^{2+} when cell swells. To test more rigorously whether the volume-regulated bestrophin current required Ca^{2+} for activation, Ca^{2+} was removed from all solutions and Ca^{2+} chelators were added to both intra and extracellular solutions. $CaCl_2$ in the E300 extracellular solution was replaced with 2 mM $MgCl_2$ and 1 mM EGTA was added to chelate residual free Ca^{2+}. Furthermore, 5 mM BAPTA was added to the already zero Ca^{2+} intracellular solution. With Δ20 mosmol kg^{-1} and nominally Ca^{2+}-free extracellular and intracellular solutions, bestrophin current activated with approximately the same rate (t/2 = 1.6 ± 0.2 min) as in control cells recorded with 2 mM Ca^{2+} in the bath (2.3 ± 0.1 min), but the peak amplitude of the volume-activated Cl^- currents in nominally zero Ca^{2+} conditions was significantly smaller (0.36 ± 0.07 nA) than in controls (1.14 ± 0.12 nA) (Fig. 3-7A). Despite the magnitude of the current, the swell-activated Cl^- current measured with (Fig. 3-7B) and without $Ca^{2+}{}_i$ (Fig. 3-7C) exhibited virtually identical I-V curves to native dBest1 current, indicating that they are both mediated by the same channel. These results suggest that although Ca^{2+} is not required for activation of dBest1 current by hyposmotic cell swelling, Ca^{2+} is facilitatory. This finding is consistent with reports that VRAC currents are not activated by raising cytoplasmic $[Ca^{2+}]$ (Doroshenko & Neher, 1992, Hazama & Okada, 1988, Nilius *et al.*, 1997a) but may require a basal level of $[Ca^{2+}]$i for full activation (Altamirano *et al.*, 1998, Chen *et al.*, 2007, Nilius *et al.*, 1997a, Park *et al.*, 2007, Szucs *et al.*, 1996).

The Role of Cell Volume on dBest1 CaC Current

Although Ca^{2+} is not required for the activation of swelling-activated dBest1 currents, we wanted to test whether high intracellular Ca^{2+} stimulated dBest1 current by inducing cell swelling. Bestrophin currents were activated by patch clamping under isosmotic conditions with solutions used for stimulating dBest1 CaC currents mentioned previously mentioned. Changes in cell volume was calculated as the percent difference between the volume measured at the beginning and at the plateau phase of the CaC current recording. Cells recorded with high-Ca^{2+}_i solution (~4.5 μM) exhibited typical Ca^{2+}-regulated bestrophin currents that were small initially (0.12 ± 0.03 nA) and slowly developed to a plateau value of 2.48 ± 0.38 nA with a mean half time of 2.5 ± 0.2 min (Fig. 3-8A). The corresponding cell volume change in the same cells is shown in Fig. 3-8B. Cell volume was normalized to the initial volume measured at the initiation of whole cell recording. Cell volume recorded with high intracellular Ca^{2+} did not change during the recording. This result excludes the involvement of swelling in Ca^{2+}-dependent activation of bestrophin current and indicates that volume and Ca^{2+} are parallel pathways regulating bestrophin currents.

When cells were patched with zero-Ca^{2+} intracellular (<20 nM) solution (described in previous CaCC chapter) under isosmotic conditions, both initial and steady-state currents were <0.2 nA. While half of the cells had currents <0.2 nA indefinitely, the other half increased transiently to 0.47 ± 0.06 nA with a half time of 1.4 ± 0.2 min before declining and stabilizing at levels <0.2 nA for the rest of the recording (up to 5 min). The mechanism of this transiently increased Cl^- current in zero-Ca^{2+}_i solution is not known. However, this transient activation of Cl^- currents could result from the effect of a transient Ca^{2+} leak from the external source when breaking the membrane in the patch right before

the initiation of whole cell recording. It could also be caused by some partially activated dBest1 CaC channels by a portion of Ca^{2+} in the cytoplasm that was not yet fully chelated by the slowly diffusible EGTA at the initial stage of the whole cell recording. The cell volume in all cells patched with zero-Ca^{2+} solution decreased gradually during the recording regardless of whether the currents transiently activated or not. One would expect that the cell volume remains unchanged in isosmotic condition. However, we observed ~ 15% reduction instead. This could possibly be caused by the dilution of cytoplasmic macro-osmolytes (i.e. proteins and/or nucleotides) into the recording pipet. As a result, the amount of net osmolyte in the cytoplasm is reduced and the cell would shrink accordingly.

In any case, we conclude that cell swelling is not a factor causing the activation of Ca^{2+}-regulated bestrophin currents. Together, it seems that cell swelling and elevated Ca^{2+}_i are two independent mechanisms that could activate bestrophin current. However, as discussed below, these two activation mechanisms may not necessarily be mutually exclusive.

Physiological Function of dBest1 VRAC

VRAC channels have been shown to be responsible for regulatory volume decrease (RVD) and cell volume control during hyposmotic stress in a variety of cell types (Kubo & Okada, 1992, Nilius *et al.*, 1995, Schwiebert *et al.*, 1994). To determine whether bestrophins play a role in RVD, we compared the cell volume between control cells and cells treated with bestrophin-specific RNAi. To elaborate on the measurement of RVD, S2 cells were first allowed to equilibrate in *Drosophila* saline (320 mosm kg^{-1}) for 15 min before the application of hyposmotic saline (~170 mosm kg^{-1}) to stimulate cell swelling.

The cells were allowed to incubate in the hyposmotic saline for 30 minutes before the extracellular solution was brought back to isosmotic saline for another 15 minutes at the end. Time-lapse images were taken throughout the entire process described above. Cell volume was calculated from the measured circumference of the S2 cells and was normalized to the initial volume measured in isosmotic solution.

Control S2 cells exhibited robust RVD under these conditions (Fig. 3-9). In cells treated with control dsRNA, the hyposmotic solution caused the cells to swell to ~150% of their initial volumes within 1–2 min. The volume then decreased gradually over a period of 30 min with an average cell volume recovery ratio of ~75%. Cells treated with RNAi to dBest3 or dBest4 had the similar magnitude and time course of swelling and RVD as control cells. In contrast, S2 cells lacking dBest1 showed a suppression of RVD. Cells treated with three different dBest1 RNAis (dB1S, dB1C, and dB1U5) all swelled to a larger extent in hyposmotic solution and exhibit a significantly slower time course and magnitude of RVD (Fig. 3-9).

In response to the osmotic stimuli, control cells swelled less than dBest1 RNAi-treated S2 cells. This can be explained by the fact that control cells were able to start regulating their volume even when these cells are swelling. When the extracellular solution was returned to the isosmotic solution at the end of the 30 minute challenge course, the control cells shrank to a volume that was ~20% less than their initial volume in isosmotic saline (Fig. 3-9B). In contrast, upon returning to isosmotic solution, the volume of dBest1 RNAi-treated S2 cells returned to a value close to the initial volume but did not decrease below this level. This is consistent with the absence of RVD in S2 cells null of dBest1. These data demonstrate for the first time the physiological process that is regulated by

dBest1 as a VRAC channel.

Discussion

dBest1 is a new member of the VRAC channel family

Previously, we discovered that native *Drosophila* bestrophins function as CaC channels physiologically in S2 cell. In this Chapter, I described that endogenous bestrophin Cl^- currents in S2 cell are also regulated by cell swelling as a consequence of osmotic difference across the plasma membrane. Our data suggest that dBest1 is a new member of the of VRAC channel family that is involved in cell volume control. The data supporting this suggestion include the following: (1) cell swelling precedes activation of the osmotically sensitive Cl^- current in S2 cells; (2) the osmotically sensitive currents is abolished or dramatically suppressed by RNAi treatment that knocked down dBes1 protein expression, the inhibition of the Cl^- currents by dBest1 RNAi can be rescued by overexpression of dBest1 cDNA; (3) dBest1 knocked down cells exhibit an impaired ability to regulate their cell volume in response to hyposmotic cell swelling; and (4) there is an excellent correlation between the VRAC current and the ability of cells to undergo regulatory volume decrease (RVD).

The VRAC current is apparently mediated by the same ion channel that mediates S2 CaC currents, because the same RNAi treatment reduced both currents. Furthermore, both CaC and VRAC currents were rescued by the same cDNA construct in cells pre-treated with dBest1 RNAi. These results provide strong support that the S2 endogenous CaC and VRAC channels are both mediated by dBest1. Our previous observation that expressing dBest1 alone in HEK cells was sufficient to produce Cl^- currents that recapitulated most of

the phenotypic characteristics of the native S2 CaC (Chien *et al.*, 2006) provide additional support to this conclusion.

Comparison of the osmotically sensitive dBest1 and vertebrate bestrophin currents

Previously, hBest1 and mBest2 expressed in several kinds of cells including HEK cell line induced novel Cl^- currents that exhibit sensitivity to cell volume (Fischmeister & Hartzell, 2005). The currents induced by these vertebrate bestrophins are strongly inhibited by hyperosmotic cell shrinkage and stimulated, but non-systematically and to a much lesser extent to hyposmotic solutions. The authors found that the later effect could not be quantified because of a simultaneous activation of an inseparable endogenous VRAC current in the host cells. The fact that VRAC channels are ubiquitously expressed makes it very difficult to arrive at a molecular identification of VRAC in model cell lines such as HEK cells. Our approach of studying the volume sensitivity of native bestrophins in *Drosophila* S2 cells bypassed this limitation. The native S2 VRAC currents are abolished by multiple RNAi construct to dBest1 and are rescued by transfection of dBest1 cDNA. In intact S2 cells, the dBest1 VRAC currents are highly sensitive to hyposmotic challenge, and cells null of dBest1 show impaired cell volume control (RVD). These dBest1 RNAi results plus the rescue experiment provide us more confidence to propose that dBest1 is a new member of the VRAC family. In addition to the difference in osmotic sensitivity, the dependence on intracellular Ca^{2+} is also different between dBest1 and vertebrate bestrophin volume-sensitive currents. dBest1 VRAC currents are activated independently of Ca^{2+}, whereas a permissive level of cytoplasmic Ca^{2+} is a pre-requisite for the hBest1 and mBest2 Cl^- currents to respond to changes in cell volume (Fischmeister & Hartzell,

2005). The activation of canonical VRAC channel is usually considered to be independent of Ca^{2+} (Nilius *et al.*, 1997a), but a permissive level of Ca seems to be required for VRAC activation in some types of cells (Nilius *et al.*, 1997a, Szucs *et al.*, 1996, Altamirano *et al.*, 1998, Chen *et al.*, 2007, Park *et al.*, 2007).

Dual regulatory mechanisms of dBest1 Cl^- current

To further refine the dependence of intracellular Ca^{2+} and hyposmotic cell swelling on the activation of dBest1 current, we examined these two regulatory mechanisms one at a time. When Ca^{2+} was removed from both the intracellular and the extracellular solutions, the dBest1 Cl^- current still activate in response to hyposmotic cell swelling. This is consistent with previous reports that the activation of VRAC currents does not require an increase of intracellular Ca^{2+} (Doroshenko & Neher, 1992, Hazama & Okada, 1988, Nilius *et al.*, 1997a, Okada *et al.*, 1998). When dBest1 current was activated by Ca^{2+}_i, the cell volume was not altered. These data indicate that cell volume and Ca^{2+} are independent activators to bestrophins. However, these two activation mechanisms are not mutually exclusive because Ca^{2+} facilitates dBest1 VRAC current and hyposmotic cell swelling could augment Ca^{2+}-activated dBest1 conductance. As mentioned above, there is considerable evidence that although elevation of Ca^{2+} is not necessary, a basal level of intracellular Ca^{2+} (~50-100 nM) is required for VRAC activation in certain types of cells (Altamirano *et al.*, 1998, Chen *et al.*, 2007, Nilius *et al.*, 1997a, Park *et al.*, 2007, Szucs *et al.*, 1996). hBest1 has an EC_{50} for Ca^{2+} of ~150 nM, which is very close to the permissive level for VRAC activation. Also, increases in cell volume are often accompanied by increase in intracellular Ca^{2+}, although the role of Ca^{2+} remains controversial and unsolved

(McCarty & O'Neil, 1992). It remains to be studied whether these two activators are truly independent or whether they converge on some common regulatory signaling pathway.

Materials and Methods

Solutions for Whole Cell Recording

Unless indicated otherwise, the standard extracellular solution (E300) used for patch clamping S2 cells contained (in mM) 115 NaCl, 2 $CaCl_2$, 1 $MgCl_2$, 5 KCl, 10 HEPES (pH 7.2 with NaOH), and 48 mannitol to achieve 300 mosmol kg^{-1}. The intracellular solution (I300, nominally zero-Ca^{2+}) contained (in mM): 110 CsCl, 10 EGTA-NMDG, 8 $MgCl_2$, 10 HEPES (pH 7.2 with NMDG), and 20 mannitol to achieve 300 mosmol kg^{-1}. Intracellular solutions of other osmolalities (such as I320 and I340) were prepared by adding mannitol until the desired osmolality was achieved. Osmotic pressure differences are expressed as Δ mosmol kg^{-1} (osmolality inside minus osmolality outside). For zero-Ca conditions, $CaCl_2$ in the E300 solution was replaced with 2 mM $MgCl_2$ and 1 mM EGTA was added. In addition, 5 mM BAPTA was added to the I300 solution prior to adjusting the osmolality to 320 mosmol kg^{-1} with mannitol. *Drosophila* saline contained (mM) 117.5 NaCl, 20 KCl, 2 $CaCl_2$, 8.5 $MgCl_2$, 20 glucose, 10.2 $NaHCO_3$, 4.3 NaH_2PO_4, and 8.6 HEPES pH7.4 (330 mosmol/kg).

Imaging and Cell Volume Determination

For monitoring regulatory volume decrease (RVD), day-6 RNAi-treated S2 cells were washed and allowed to equilibrate for 15 min in *Drosophila* saline. Cells that were round with a bright membrane were chosen for cell volume measurement. The average diameter of the selected cells was 15.5 ± 0.8 μm (n=56). Phase contrast images of the cells were taken at 5-sec intervals and were analyzed with MetaMorph Imaging software (Universal Imaging Co.). The volume of the cell was calculated from the measured circumference

assuming that the shape of S2 cells is spherical. After 1 min, the cells were exposed to hypo-osmotic saline (166 mosmol kg^{-1}) that was made by mixing equal amount of *Drosophila* Saline with de-ionized H_2O. The imaging was continued for ~30 min before returning to isosmotic *Drosophila* saline for another 15 minutes. RVD was expressed as % recovery = $(Vol_{peak} - Vol_{30min}) / Vol_{peak}$, where Vol_{peak} is the maximum cell volume and Vol_{30min} is the volume 30 min after switching to hyposmotic solution. For measuring cell volume during whole cell patch clamping, images were taken synchronizedly with the application of the commend voltages every 10 seconds. Changes in cell volume were expressed as % difference to the initial cell volume measured immediately after patch break.

Interfering RNA

Double-stranded interference RNA was synthesized using the Megascript High-Yield Transcription Kit (Ambion). Cells were treated the same way as mentioned in Chapter 2. In addition to some of the *Drosophila* bestrophin RNAi constructs that were described previously in Chapter 2, RNAis to both 3' and 5' UTR of dBest1 and dBest2 were prepared. The information of all RNAi constructs is listed in Table III. Possible off-target effects of each RNAi were evaluated by BLASTing the RNAi sequence against the *Drosophila* genome. Off-target hits >17 nucleotides in length are listed in Table 3-2.

Cloning and Rescue of dBest1 in S2 Cells

The dBest1 open reading frame was PCR'd and introduced into KpnI (5') and NotI (3') sites of pAc5.1/V5-HisA *Drosophila* expression vector (Invitrogen). For the rescue

experiment, a mixture of 2-4 µg of purified pAC5.1-dBest1 and 0.5-1 µg of pAC5.1-EGFP was used to transfect 4.2 x 10^5 S2 cells that were treated with dB1U5 RNAi for 4 days with calcium phosphate. Cells treated with dB1U5 RNAi and transfected with 2-4 µg of pAC5.1-EGFP were used as controls. Green cells were patch-clamped at day 2-4 after transfection.

Western Blotting

For Western blot, whole cell lysate collected from S2 cells treated with different RNAi was equally loaded (5µg) and separated by SDS-PAGE on 10% Tris-HCl polyacrylamide gels before blotting to PDVF membrane. The polyclonal dBest1 antibody and monoclonal mouse actin antibody (Chemicon Co.) were used at 1:1000 and 1:5000 dilutions respectively. The ECL signal was detected by enhanced chemiluminescence (Super Signal, Pierce Chemical Co.).

Reverse Transcriptase PCR

The effectiveness of the RNAi treatment on dBest2 and dBest3 transcript level was evaluated by RT-PCR using SuperScript III One-Step RT-PCR with Platinum Taq (Invitrogen). RT-PCR was done using the dBest1' and dBest2 primer sets mentioned previously in previous chapter and with dBest3 primer pair: (Forward) 5'-GTAACAAGGGCTCGAAAGGAAGGT-3' and (Reverse) 5'-CACGGCATATGG CAACTCAGC-3'.

Cell Surface Protein Level Quantification

For hyposmotic treatment (40 mosmkg^{-1}), S2 cells were placed in E300 extracellular solution for 15 minutes then E260 extracellular solution for another 10 minutes. For Ca^{2+} ionophore treatment, S2 cells were incubated with 2 μM of Calcimycin (Frementeck Co.) in standard extracellular recording solution for 10 minutes. Then all reaction was stopped by placing the cells on ice. Cells were washed three times with ice cold PBS and biotinylated with 0.5 mg/ml Ez-Link Sulfo-NHS-LC Biotin (Pierce Co.) in PBS for 30 minutes. The cells were then washed with PBS containing Ca^{2+} and Mg^{2+} and incubated in 100mM glycine in PBS to quench unreacted biotin. The cells were washed three times with PBS and resuspended from the culture dish for centrifugation with 1200 rpm for 5 minutes at 4 °C. Cell pellets were lyzed and sonicated in the lysis buffer (250 μl per 10cm culture dish) containing 150 mM NaCl, 5 mM EDTA, 50 mM Hepes (pH7.2), 1% Triton X-100, 0.5% protease inhibitor cocktail III (Calbiochem Co.) and 10 μM PMSF. 200 μl of whole cell lysate was incubated with 50μl of streptavidin beads (UltraLink Immobilized Streptavidin; Pierce Co.) at 4 °C for an overnight. The beads were washed with the lysis buffer containing 200 mM NaCl for three times, and the bound proteins were eluted with 200 μl of 2X Laemmli buffer. Equal amount of cell lysate was loaded and Western blotted for dBest1 (1:1000; 05280 polyclonal antibody). Mouse anti-fibrillarin/Nop1p antibody (1:2000; EnCor Biotechnology Inc.) was used as the loading control for cell membrane fraction and mouse anti-actin antibody (1:2000; Chemicon/Millipore Co.) was used as the loading control for whole cell extract. Densities of the blotted bands were determined by densitometry (FlourChem; Alpha Innotech Co.) and relative cell surface expression ratio was calculated as: $Protein_{surface}/Protein_{total} \times 100\%$.

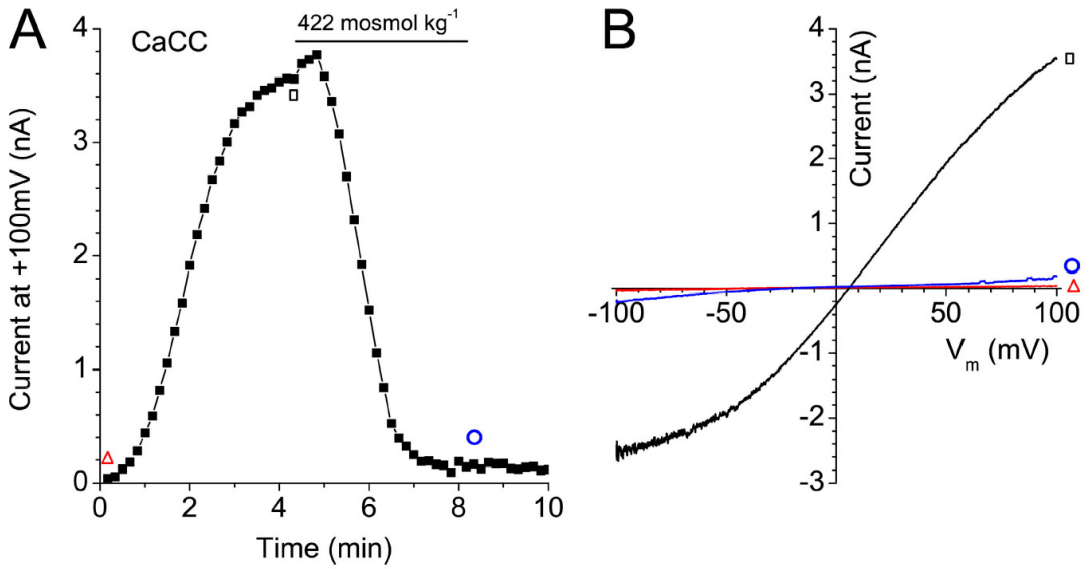

Figure 3-1: Native Drosophila S2 Ca^{2+}-activated Cl^- currents are sensitive to osmotic pressure. (A) Time course of typical S2 endogenous CaC currents. Whole cell patch clamping was initiated in *Drosophila* S2 cells with isosmotic (320 mosmol kg^{-1}) intracellular (~4.5 μM free Ca^{2+}) and external solutions. Voltage ramps from -100 to +100 mV were given from a holding potential of 0 mV at 10-sec intervals. After the CaC currents had reached a plateau amplitude, the bath was replaced with a hyperosmotic external solution (422 mosmol kg^{-1} by addition of mannitol). (B) Current-voltage relationship of the CaC current measured at the beginning (open triangle), the plateau (open square), and after hyperosmotic shock (open circle). Internal solution (in mM) was 165 CsCl, 8 $MgCl_2$, 10 Ca-EGTA, 10 HEPES, pH 7.4. External solution: 150 NaCl, 1 $MgCl_2$, 2 $CaCl_2$, 10 HEPES, pH 7.4, 20 mannitol (320 msomol kg^{-1}).

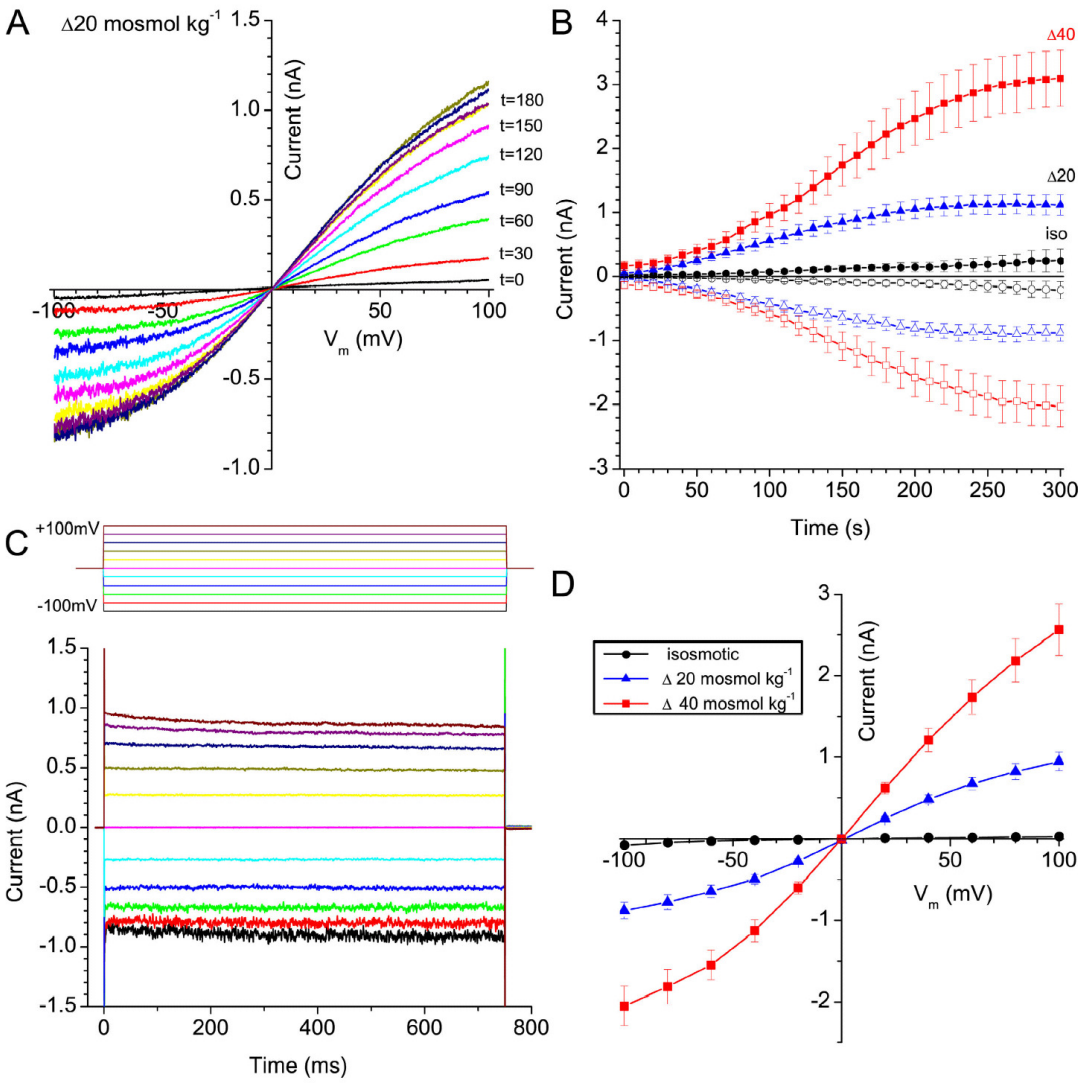

Figure 3-2: Drosophila S2 cells express endogenous osmotically-activated Cl^- currents. (A and B) Time-dependent activation of the osmotically-activated Cl^- currents in S2 cells. (A) Traces of a typical S2 osmotically activated Cl^- current recorded by voltage ramps from -100 to +100 mV at 10-sec intervals after establishing whole cell recording with Δ20 mosmol kg^{-1} (intracellular solution: nominally 0 Ca^{2+} I320; external solution: E300). (B) Time course of the osmotically-activated Cl^- currents measured at -100 mV

(open symbols) and +100 mV (solid symbols) at Δ 40 mosmol kg^{-1} (squares, $n = 9$), Δ 20 mosmol kg^{-1} (triangles, $n = 13$), and Δ0 mosmol kg^{-1} (circles, $n = 6$). (C) Current traces of a typical osmotically-activated (Δ 20 mosmol kg^{-1}) Cl^- current in response to voltage steps (20 mV intervals from -100 to +100 mV) after the ramp current had reached a peak (~4 min). (D) Steady-state current-voltage relationship with Δ 40 mosmol kg^{-1} ($n = 9$), Δ 20 mosmol kg^{-1} ($n = 16$), and Δ 0 mosmol kg^{-1} ($n = 5$). All averaged data are represented as mean ± SEM.

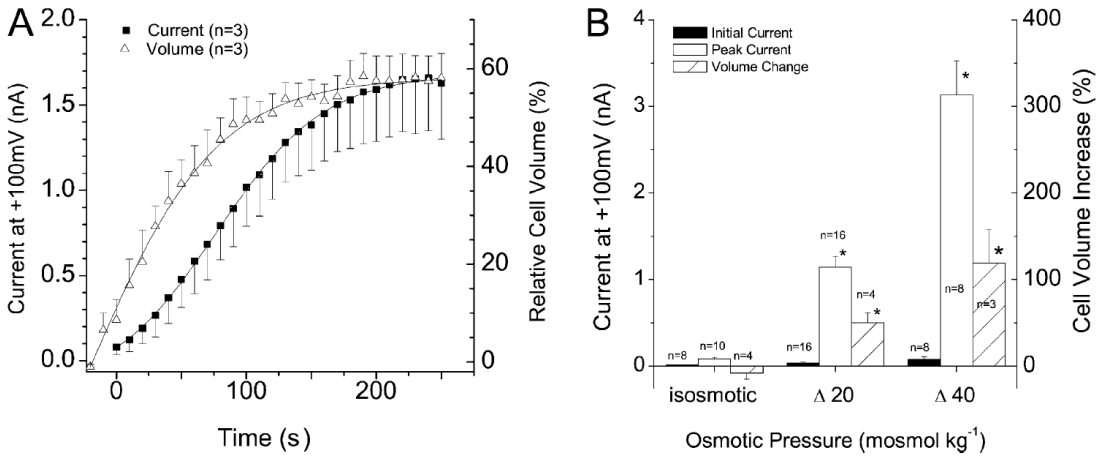

Figure 3-3: Drosophila S2 osmotically-activated Cl^- currents are correlated with cell swelling. (A) Time courses of the increase in cell volume (open triangles) and the Cl^- current amplitude after patch break at +100 mV (solid squares) with Δ20 mosmol kg^{-1} (*n* = 3). The change in cell volume was calculated as a percentage of the cell volume ~30 sec before patch break. The first data point shown is immediately after patch break. Current measurements were begun after cell capacitance and series resistance were measured, ~20 sec after patch break. (B) Mean current amplitudes at +100 mV at the onset of whole cell recording (filled bars) and after the currents had reached a peak (open bars) and the corresponding cell volume increase (hatched bars) with Δ 40 mosmol kg^{-1}, Δ 20 mosmol kg^{-1}, and Δ 0 mosmol kg^{-1}. Cell volume change is expressed as percent increase in cell volume from the initiation of whole cell recording to ~5 min after patch break when the currents had approached a steady value. For zero osmotic pressure, the cell volume change was measured 5 min after the initiation of whole cell recording. (mean ± SEM). *, significantly different from control at $P < 0.01$. Solutions were the same as used in Fig. 2.

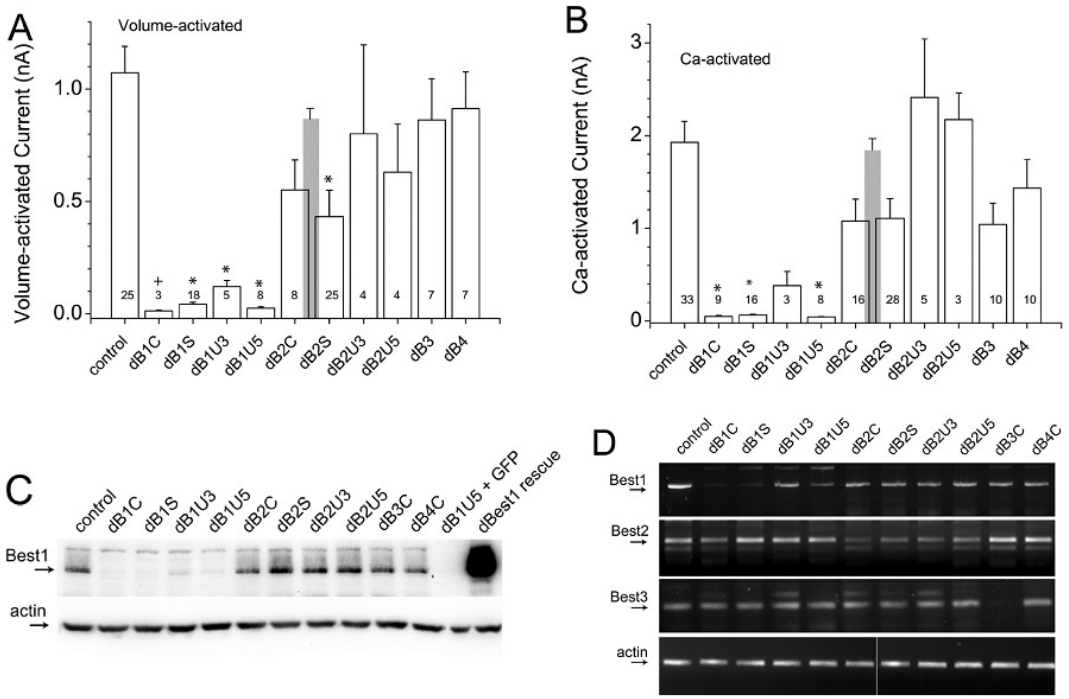

Figure 3-4: RNAi inhibition of the native S2 volume-activated Cl^- currents. S2 cells were treated with control dsRNA (from a mammalian intron) or *Drosophila* bestrophin subtype-specific RNAi before patch clamping at day 6. Mean amplitudes of Cl^- currents at +100 mV were measured for the (B) Ca^{2+}-activated currents (~4.5 μM free Ca^{2+}_i, isosmotic solutions, open bars) and the (A) volume-regulated currents (E300, nominally 0 Ca^{2+}_i I320, Δ20 mosmol kg^{-1}, red bars) after the currents had reached peak amplitude 4-5 min after patch break. (mean ± SEM). *, significantly different from control at $P < 0.01$.+, significantly different from control at $P < 0.02$. The gray bars show the mean current amplitudes of cells treated with dB2S or dB2C for which Western blot data were available to show that dBest1 protein levels were close to control. Some of the CaC currents data for

dB1S, dB1C, dB2C, dB2S, dB3C, and dB4C have previously been published (Chien *et al.*, 2006). (C) Effects of RNAi on dBest1 protein expression. S2 cells treated 6 d earlier with the indicated RNAi constructs were extracted with SDS and the Western blot was probed with dBest1 antibody. (D) RT-PCR of bestrophin transcripts from S2 cells treated with different RNAi constructs. RT-PCR was performed using the primers described in Materials and methods. RNA was extracted 6 d after RNAi treatment for dBest1 and dBest2 and 2 d after RNAi treatment for dBest3. The actin gel was composite from two different gels that were run in parallel (lanes 1-6 are from one gel and 7-11 from the second). The white line indicates that intervening lanes have been spliced out.

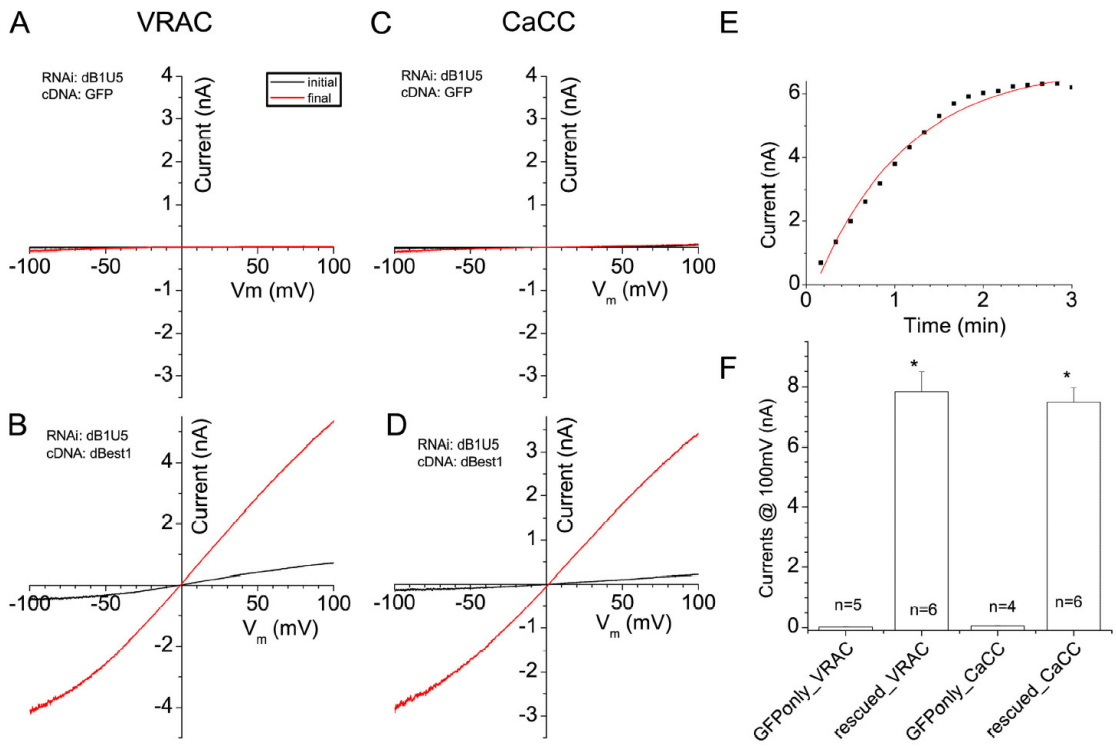

Figure 3-5: Rescue of Ca^{2+}-activated and volume-regulated currents. Cells were treated with dB1U5 RNAi for ~4 days and then transfected with either GFP alone (A and C) or GFP + dBest1 (B and D) and recorded 18-24 hrs. later. (A-D) Typical I-V curves for VRAC (A and B) and CaC (C and D) currents immediately after patch break (black) and after the current had reached maximum (red, ~2-4 min after patch break). (A and B) VRACs were recorded with nominally 0 Ca^{2+} internal solution (I320) and E300 extracellular solution. (C and D) CaC currents were recorded with ~4.5 μM internal free Ca^{2+} and isosmotic (300 mosmol kg^{-1}) solutions. (E) Time course of activation of VRAC current after patch break of a typical dBest1-rescued cell. (F) Average amplitude (mean ± SEM) of currents at +100 mV ~4-5 min after patch break corresponding to the conditions in A-D. *, significantly different from GFP alone, $P < 0.01$.

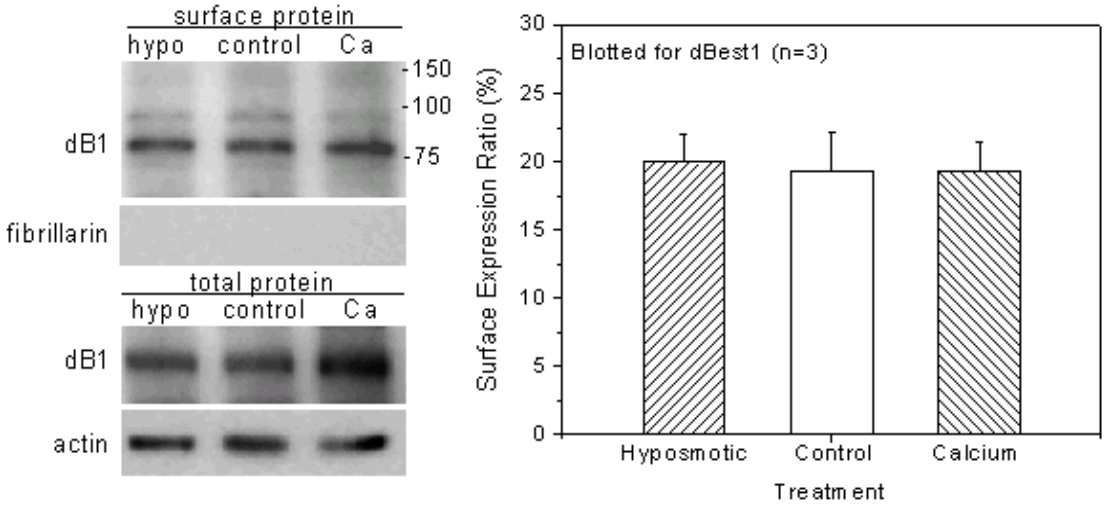

Figure 3-6: Semi-quantification of surface level of dBest1. S2 cells were treated with either 40 mosmol kg^{-1} (E300 then E260 extracellular solutions) hyposmotic shock or incubated in standard extracellular solution containing Calcimycin (Ca^{2+} ionophore) for 5 minutes. Intact cells were then incubated with membrane-impermeable biotinylation reagent. Total protein was collected from whole cell extract, whereas surface protein was isolated from the whole cell extract by pulling down the biotinylated proteins with avidin-coated agarose beads. Equal amount of proteins were loaded and Western blotting was performed to label dBest1. (A) Blots of dBest1 from surface protein fraction (fibrillarin as the loading control) and from total cell extract (actin as the loading control). (B) Densitometry quantification result of the relative surface expression level of dBest1. Data are presented as mean $\pm$ S.E.M from a total of three independent experiments.

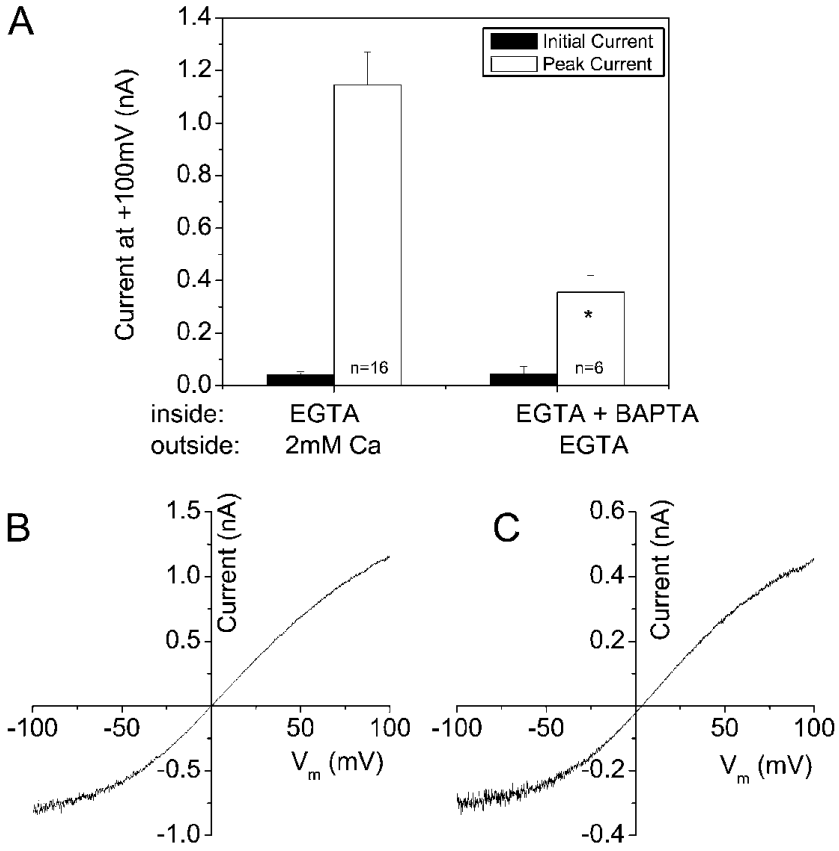

Figure 3-7: Volume-activated Cl^- currents are Ca^{2+} independent. (A) Average amplitudes of S2 volume-activated Cl^- currents at +100 mV at the onset of whole cell recording (filled bars) and after the currents had reached peak values (open bars) with Δ20 mosmol kg^{-1}. Bars on the left were recorded in the normal solutions with 2 mM extracellular Ca^{2+} (E300) and 10 mM intracellular EGTA (I320). Cells on the right were recorded with I320 intracellular solution with 5 mM BAPTA added and a nominally 0 Ca^{2+} extracellular solution prepared by substituting external Ca^{2+} with equimolar of Mg^{2+} and adding 1 mM EGTA. *, significantly different from control at $P < 0.01$. (B) I-V curve from a voltage ramp for current corresponding to the left bars in A. (C) I-V curve for current corresponding to right bars in A.

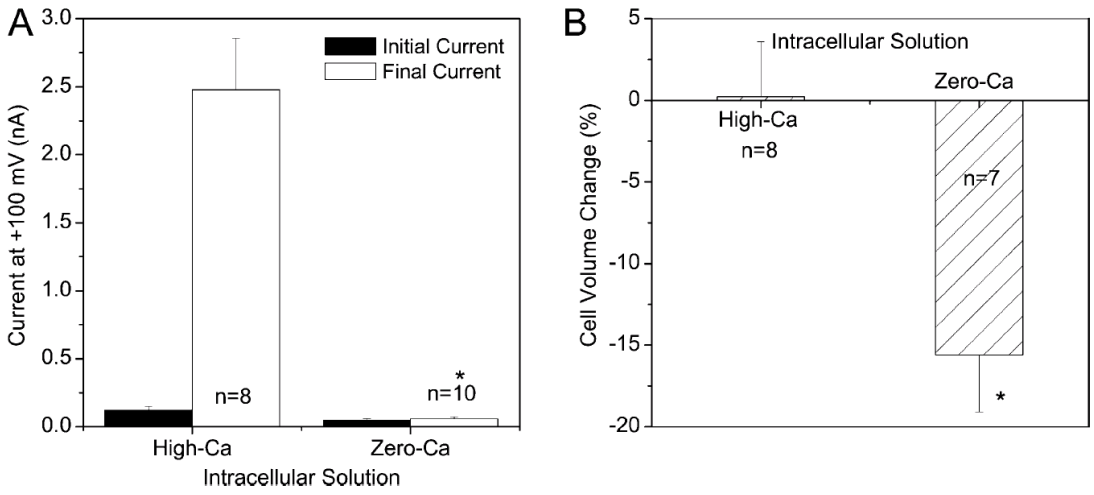

Figure 3-8: The S2 Ca^{2+}-activated Cl^- current is not correlated with cell swelling. (A) Mean current amplitudes at +100 mV at the onset of whole cell recording (filled bars) and after the currents had reached steady states (open bars) in cells recorded with high intracellular Ca^{2+} solution (~4.5 μM) or nominally Ca^{2+}-free (<20 nM) intracellular solution. (B) Changes in cell volume (%) after the currents had reached steady state in cells recorded with high intracellular Ca^{2+} solution (~4.5 μM) or nominally Ca^{2+}-free (<20 nM) intracellular solution. Cell volumes were normalized to the basal cell volume measured at the initiation of the whole cell patch clamping. The data are represented as mean $\pm$ SEM. *,significantly different from high Ca^{2+} at $P < 0.01$.

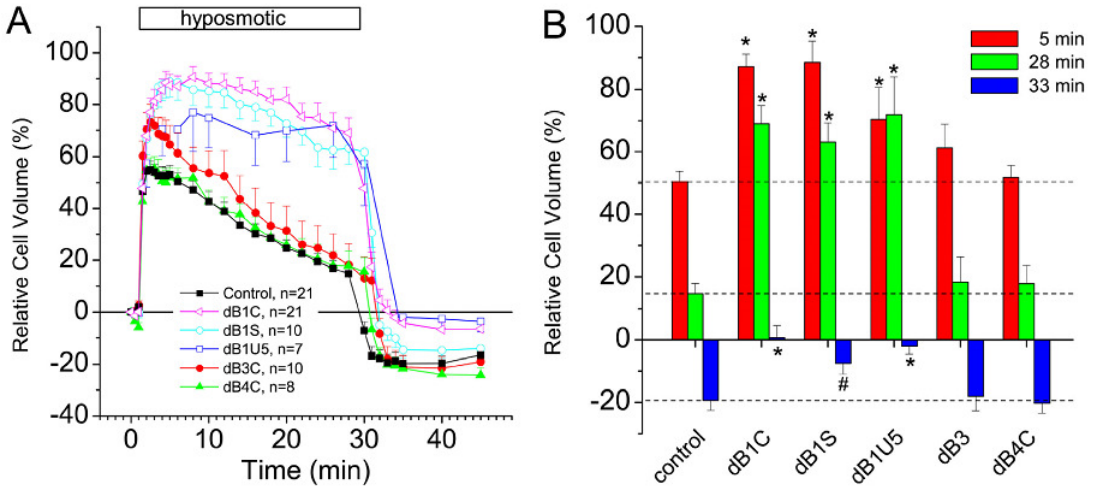

Figure 3-9: Regulatory volume decrease is inhibited by knockdown of dBest1. S2 cells were treated with RNAi specific to each *Drosophila* bestrophin subtype as described in Materials and methods for 6 days before quantification of RVD. RNAi-treated cells were pre-incubated in *Drosophila* saline (330 mosmol kg^{-1}) for 15 min before imaging. The *Drosophila* saline was replaced by a diluted solution of the same saline (1:1 with $_{H2O}$, 166 mosmol kg^{-1}) 1 min after the initiation of imaging. Cells were monitored by time lapse imaging for 30 min and cell volume was quantified with MetaMorph as described in Materials and methods. (A) Time course of increase in cell volume. Cell volumes were normalized to the initial volume and the time course of increase in cell volume (%) plotted as mean $\pm$ SEM. (B) Mean cell volume increase (%) near peak of cell swelling (red bars, ~4 min in hyposmotic solution), at the end of RVD (green bars, ~27 min in hyposmotic solution), and ~3 min after returning to isosmotic solution (blue bars). *, significantly different from control at $P < 0.01$; #, significantly different from control at $P < 0.05$.

Table 3-1. RNAi primer design and possible off-target genes.

Primer	Sequence	Size	Off-target genes
dB1C	Forward:5'-GCAACGCCCAGTCAGGA-3' Reverse:5'-TCATCGTCGAATTGGAGAAC-3'	793 bp	CG4623 (20/20) CG8831 (18/18) CG16711 (18/18)
dB1S	Forward:5'-TGATGCCAGTGGCATTCAC-3' Reverse:5'-CGCCAGGTGGAAATAGGTT-3'	509 bp	CG4623 (20/20) CG16711 (18/18)
dB1U3	Forward:5'-CCGCTGACATATACTGGACAT-3' Reverse:5'-ATTTGGCATTTCATTTTTATTT-3'	411 bp	Sif (19/19)
dB1U5	Forward:5'-TGTTTGTCTAAGCCCTTCTACCTC-3' Reverse:5'-ATTGCTGTTCTTCTTTCCGACTGT-3'	206 bp	Indy (22/22) CG33691 (23/24)
dB2C	Forward:5'-CCAGCTCGGTCCTAATG-3' Reverse:5'-CCTCTCCGGTCTTTTGTT-3'	798 bp	ninaE (18/18)
dB2S	Forward:5'-AAACATCACCACTCTGTCGT-3' Reverse:5'-TTGAGGGGGCCGAGGAT-3'	503 bp	ninaE (18/18)
dB2U3	Forward:5'-CATTGTGCCACCCAGAACC-3' Reverse:5'-GCAAGTGCCAAAACAATAAGTCA-3'	340 bp	CG14864 (21/22)
dB2U5	Forward:5'-GAGCGCAGTTTGGTTGAGTTTGTC-3' Reverse:5'-AAGGCCGAATTGTTGTTGTTTGAT-3'	289 bp	Pncr004 (19/19)
dB3C	Forward:5'-GATCGGGATATTAAGCACTACA-3' Reverse:5'-GTCCTCCTCCTTTCTCTTTTTC-3'	783 bp	CG8932 (21/22)
dB4C	Forward:5'-TGGCCACGTACTCCTTCTTCCT-3' Reverse:5'-GCTCTGTCCCCCGCTTCCT-3'	784 bp	dBest1 (49/53)

T7 sites (5'-CTAATACGACTCACTATAGGGAG-3') were added to 5' ends of all primers for in vitro RNAi synthesis. Off-target hits were identified by BLASTn against the *Drosophila* genome. Numbers in parentheses indicate number of identical nucleotides within a stretch of x nucleotides. Only homologies > 17 bp are shown. The Harvard *Drosophila* RNAi Screening Center has chosen 19-bp homology as the critical threshold for off-target effects (Kulkarni et al., 2006).

CHAPTER 4

FUNCTIONAL EVIDENCE OF DBEST1 IN FORMING THE PORE OF THE Cl^- CHANNEL

Summary

Bestrophins are a new family of Cl^- channels that are activated by cytosolic Ca^{2+} and cell swelling. Previously, we showed that treatment of *Drosophila* S2 cells with RNAi to dBest1 abolished both the Ca^{2+}-activated Cl^- current and the volume-regulated Cl^- current (VRAC). Both type of Cl^- currents could be rescued by expressing dBest1 in cells pre-treated with dB1U5 RNAi. However, our previous rescue experiment was not sufficient to demonstrate that dBest1 is indeed a pore-forming subunit of the Cl^- channel because rescuing an essential regulator of a Cl^- channel would also produce the same result. In this report, we rescued VRAC currents in dBest1 RNAi-treated S2 cells with a mutant dBest1 (F81C, F81E, and F81L) with altered biophysical properties. Like the native VRAC, the F81C-rescued VRAC was sensitive to osmotic pressure differences: the current was inhibited by isosmotic and augmented by hyposmotic extracellular solutions. The F81C-rescued current exhibited different properties than the native or wild type-rescued VRAC current as expected if F81 is located at the pore of the channel. Whereas the native current exhibited an S-shaped IV curve and was slightly inhibited by $MTSET^+$, the F81C current outwardly rectified and was stimulated 5- to 15-fold by $MTSET^+$. Furthermore, the $MTSES^-$- modified F81C current consistently showed a shift of reversal potential (E_{rev}) in the negative direction (~ -20 mV), suggesting that the channel had become more permeable to cations. This hypothesis was quantitatively examined by dilution potential experiments using fixed concentration of intracellular CsCl or NaCl while altering extracellular [CsCl] or [NaCl]. P_{cation}/P_{Cl} was calculated from the Goldman-Hodgkin-Katz equation. P_{Cs}/P_{Cl} for $MTSES^-$- treated native dBest1 was 0.25, whereas for F81C P_{Cs}/P_{Cl} became 2.38. $MTSES^-$-treated native dBest1 was exclusively permeable to Cl^- than Na^+ while F81C was almost

equally permeable to these two ions. The fact that the VRAC was rescued by dBest1 F81C and F81E mutants with different biophysical properties provides definitive evidence that dBest1 is a component of the pore of the S2 Cl^- channel and not just a regulator or an auxiliary subunit of a native S2 Cl^- channel. To test whether bestrophins are VRACs in mammalian cells, we compared VRACs in peritoneal macrophages from wild type mice and mice with both bestrophin-1 and bestrophin-2 disrupted ($best1^{-/-}/best2^{-/-}$). VRACs were identical in wild type and $best1^{-/-}/best2^{-/-}$ mice, showing that bestrophins are unlikely to be the canonical VRAC in mammalian cells.

Introduction

In previous Chapters, we have shown that *Drosophila* Bestrophin 1 (dBest1) is a Cl^- channel that is dually activated by cytoplasmic Ca^{2+} and by cell swelling. The swell-activated dBest1 current is independent of intracellular Ca^{2+}, but Ca^{2+} can facilitate the volume-regulated dBest1 Cl^- current. The functional consequence of activated dBest1 is to regulate cell volume homeostasis by mediating the process of regulatory volume-decrease (RVD). We have demonstrated that five different dBest1 RNAi constructs all abolished endogenous Cl^- currents activated by intracellular Ca^{2+} or by swelling. The loss of these currents was be rescued by over-expression of wild type dBest1 cDNA. However, the RNAi and rescue experiment alone do not formally prove that dBest1 is the pore-forming subunit of the S2 VRAC channel, because over-expression of an essential regulator or accessory subunit of an endogenous Cl^- channel might exhibit the same effect.

In this Chapter, we directly investigate if dBest1 comprises the ion-conducting pore of the Cl^- channel by rescuing VRAC in dBest1 RNAi-treated S2 cells using a mutant dBest1 that has altered biophysical properties. To do this, we mutated a putative pore-forming amino acid residue in the second transmembrane domain of dBest1. Residue F81 was chosen for this purpose because F81 (F80 in vertebrates) is one of the most conserved amino acids among bestrophins from different species and mutation of F80 in mouse and human bestrophins has been shown to alter the relative anion permeability and conductance (Chien *et al.*, 2006, Qu & Hartzell, 2004, Tsunenari *et al.*, 2003). In addition, membrane impermeable charged sulfhydryl (MTS) reagents alter the properties of F80C mutant mBest2 and hBest1 currents in characteristic ways (Qu *et al.*, 2006a, Qu & Hartzell, 2004, Tsunenari *et al.*, 2003).

Here we show that the rescued dBest1-F81C current is volume-sensitive but differs from the wild type current in the shape (rectification) of the I-V curve, the responsiveness to MTS reagents, and most importantly, the anion-cation selectivity after $MTSES^-$ treatment. These findings provide strong support that dBest1 is indeed the pore-forming domain of the Cl^- channel. However, VRACs are normal in peritoneal macrophages from mice with both mBest1 and mBest2 disrupted, suggesting that bestrophins are not responsible for the classical mammalian VRAC.

Results

Rescue of VRAC Currents in S2 Cells by Expressing dBest1 Mutants

Our first attempt to test if dBest1 forms the ion-conducting part of the VRAC channel in *Drosophila* S2 cells and not simply a regulator of an endogenous VRAC was to examine whether VRAC currents could be rescued by expressing a mutant dBest1 that had altered biophysical properties. To do this, endogenous dBest1 was first knocked down by double-stranded RNA to a portion of the 5'UTR of dBest1, as previously described in Chapter 3. Cells were tested in each experiment to verify that dBest1 current was abolished. Then dBest1 cDNAs (wild type, F81C, F81E, and F81L) was expressed in the RNAi- treated cells by transient transfection. The macroscopic VRAC currents expressed by the transfected S2 cells were recorded with solutions in which the extracellular solution was 40 mosmol kg^{-1} hyposmotic relative to the internal solution (I340/E300). Transfection with the F81L mutant did not elicit measurable currents (67.0 ±26.3 pA, n=5). Expression of F81C produced Cl^- currents that were volume- sensitive. Immediately after patch break, the F81C currents were 0.4 ± 0.1 nA at +100 mV. The currents then activated slowly to a

mean plateau amplitude of 1.0 ± 0.3 nA (n=7) with an average half time of ~1.5 min (Fig. 4-1A). The activation of the F81C current was coupled to cell swelling. On average, F81C cells swelled 33.6 ± 0.7 % (n=7) when their currents were fully activated with Δ40 mosmol kg^{-1} osmotic pressure (Fig. 4-1B). F81C currents were clearly volume-sensitive because in isosmotic condition (Δ0 mosmol kg^{-1}, E300/I300), the current remained smaller than 0.3 nA (n=6) throughout the ~5 minute of recording. Instead of swelling, their volume decreased 13.8 ± 2.7 % at the end of the recording. The native dBest1 VRAC current showed a slightly outwardly-rectifying S-shaped I-V relationship. However, the F81C current was inwardly-rectifying (Fig. 4-1C and 4-5D), similar to the Ca^{2+}-activated dBest1-F81C current expressed heterologously in HEK cells described in Chapter 2. These data showed clearly that the S2 VRAC current was rescued by expressing the mutant dBest1-F81C that exhibit different properties than the native VRAC current.

Opposite Effect of $MTSET^+$ on Native and Mutant dBest1 VRAC Currents

The substituted-cysteine accessibility method (Akabas *et al.*, 1992, Karlin & Akabas, 1998) is widely used to map the topology and to identify the pore of an ion channel. This approach employs membrane-impermeable charged MTS reagents that could covalently bound to the sulfhydryl group of native or engineered Cys residues, therefore, modifying the charged state of that Cys residue. The idea is that if a specific pore-lining amino acid is Cys, the sulfhydryl side chain of this Cys will be accessible to the membrane impermeant charged MTS (methanethiosulfonate) reagent applied through the recording solutions. As a result, if the biophysical properties of the current are altered as a result of MTS modification, the site where the engineered Cys is located at is very likely to line the

ion-conducting pore of the channel (Karlin & Akabas, 1998). We expected that the rescued F81C dBest1 current would respond differently than the wild type dBest1 VRAC currents to extracellularly- applied membrane-impermeant MTS reagents, provided that F81C is located in the pore and accessible to the reagent. To begin with, we compared the effect of positively charged $MTSET^+$ (2-(trimethyl- ammonium) ethylmethane thiosulfonate) reagent on the F81C and the wild type VRAC current. We discovered that $MTSET^+$ had opposite effects on native VRAC current then the rescued dBest1-F81C current. I-V curves and the time course of current development from typical cells are shown in Fig. 4-2. $MTSET^+$ caused a mean ~ 35 % reduction in the amplitude of the native dBest1 VRAC currents (Fig. 4-2A and C) over 8-10 minutes. The effect of $MTSET^+$ in native cells was not reversible by 5 mM reducing agent DTT. In contrast, $MTSET^+$ caused a dramatic augmentation in the F81C current. On average, the current was transiently increased 15-fold followed by a gradual decrease to a level which was still elevated ~ 4- to 7- fold compared to the F81C currents before $MTSET^+$ (Fig. 4-2B and D). The stimulation by $MTSET^+$ was at least partly reversible by DTT in F81C-rescued cells. In addition to stimulating the current, $MTSET^+$ converted the F81C current from slightly inwardly-rectifying to slightly outwardly-rectifying (Fig. 4-5C). These opposite biophysical responses to $MTSET^+$ between F81C and the wild type VRAC currents suggest that dBest1 is the pore-forming subunit of the S2 VRAC channel.

$MTSES^-$ Increased the Cation Permeability of Mutant dBest1-F81C

The effect of negatively charged $MTSES^-$ ((2-sulfonatoethyl)methane thiosulfonate) on the I-V relationships of native and F81C-rescued cells is shown in Fig. 4-3 A and B. The

osmotically-activated F81C currents were reduced ~60% by $MTSES^-$, compared to ~20% reduction for native dBest1 (Fig. 4-5A and B). More importantly, $MTSES^-$ consistently produced a shift of -19.9 ± 1.2 mV (n=12) in the reversal potential of F81C cells but not in native cells (Fig. 4-3A and B and Fig. 4-5C). This shift of E_{rev} towards more negative values could be explained by a changed ionic selectivity of the channel. It is worth re-emphasizing here that the $[Cl^-]$ was intentionally made the same in both the intracellular and the extracellular solutions, so a pure Cl^- current would be expected to have $E_{Cl} = E_{rev} =$ 0 mV. It should be noted that the primary cation in the internal solution is Cs^+ and the major cation in the external solution is Na^+. Therefore, the $MTSES^-$-induced negative shift in E_{rev} could be explained by an increased permeability to cations with a relative cation permeability of $P_{Cs} > P_{Na}$. This hypothesis was first qualitatively tested by replacing extracellular Na^+ with either Cs^+ or $NMDG^+$ in the E300 solution while maintaining Cs^+ as the major intracellular cation (I340). The result from a typical F81C-rescued cell is shown in Fig 4-3C. Initially, F81C VRAC currents recorded with symmetrical Cl^- and primarily Cs^+ inside and Na^+ outside had an E_{rev} of ~ 0 mV, as would be predicted if the F81C current was selectively carried by Cl^-. After $MTSES^-$ was applied, E_{rev} shifted to -25.1 mV. When extracellular Na^+ was replaced with Cs^+, E_{rev} changed to 1.7 mV. Replacement of extracellular Cs^+ with the membrane impermeant cation $NMDG^+$ produced a shift in E_{rev} to -38 mV. These observations suggested that the F81C current had become more permeable to Cs^+ and, less so, to Na^+ after $MTSES^-$ modification.

Quantification of Cation Permeability in $MTSES^-$-Modified dBest1-F81C

To quantify the relative $cation^+/Cl^-$ permeability, we performed dilution potential

experiments (Franciolini & Nonner, 1987) for both native and mutant dBest1 currents. All solutions were made isosmotic and high-Ca^{2+}_i was used to activate dBest1 currents because swelling-activated dBest1 current often runs down 0.5-1 minute after the current has reached a plateau. Whole cell recording was initiated with recording solutions containing equal amount of CsCl (150 mM). $MTSES^-$ was applied extracellularly after the Ca^{2+}-activated bestrophin current had stabilized at plateau values. E_{rev} was then measured with fixed [CsCl] (150 mM) inside and varied [CsCl] at the extracellular side. I-V curves recorded with 10, 50, and 150 mM external CsCl from the same cells are superimposed in Fig. 4-4A-C. For native dBest1 currents (Fig. 4-4A), E_{rev} moved toward positive values as external [CsCl] was decreased, as would be predicted if dBest1 is selectively permeable to Cl^-. In addition, the conductance in the outward direction at +100 mV increased significantly with increasing external [CsCl], consistent with Cl^- carrying the majority of the outward current. In contrast, the E_{rev} of F81C shifted towards negative potentials with decreasing external [CsCl] (Fig. 4-4B). This negative shift in E_{rev} showed that F81C had become more selective to Cs^+ than to Cl^- after $MTSES^-$ modification. The augmented inward rectification with increasing external [CsCl] was also consistent with a higher Cs^+ conductance relative to Cl^- after $MTSES^-$ treatment.

Relative Cs^+/Cl^- permeability was calculated by fitting the plots of E_{rev} vs. $[CsCl]_o$ to the Goldman-Hodgkin-Katz (GHK) equation. As shown in Fig. 4-4D, the mean E_{rev} in native S2 cells shifted +33.3 ± 3.2 mV with a 15-fold decrease in $[CsCl]_o$ (filled circles). This data were well-fitted by the GHK equation assuming that Cl^- was four-fold more permeable than Cs^+ ($P_{Cs}/P_{Cl} = 0.25$). dBest1-F81C, on the other hand, showed an opposite shift of -22.8 ± 2.7 mV with a 15-fold decrease in $[CsCl]_o$ (filled triangles), which was

fitted with $P_{Cs}/P_{Cl} = 2.38$. The P_{Cs}/P_{Cl} ratio in S2 cells over-expressing wild type dBest1 ($P_{Cs}/P_{Cl} = 0.24$) was virtually the same as the native S2 current regardless of $MTSES^-$ treatment (data not shown), indicating that the reversed ionic selectivity in F81C currents was not due to an up-regulation of an endogenous cation channel by expressing dBest1.

The dilution potential experiment was repeated with recording solutions containing fixed concentration (150 mM) of NaCl in the pipet and varied [NaCl]o. The native dBest1 channel was highly selective for Cl^- and was fitted with a P_{Na}/P_{Cl} ratio of 0.03 (Fig. 4-3D). $MTSES^-$ modified F81C, on the other hand, was almost equally permeable to Cl^- and Na^+ (P_{Na}/P_{Cl}=0.83) (Fig. 4-3D). Overall, these data showed that the ionic selectivity of dBest1 channel was altered from anionic to cationic after $MTSES^-$ modification, and the $MTSES^-$ -labeled F81C exhibited a permeability sequence of $P_{Cs}>P_{Na}>P_{Cl}$. Such dramatic alteration in the key intrinsic biophysical property of dBest1 when the charge at the site of a putative pore-lining domain is changed provide definitive evidences that dBest1 is a substantial component of the ion-conducting pore of the Cl^- channel.

The role of dBest1 in forming the pore of the channel was further tested in HEK cells transfected with either wild-type dBest1 or F81C. The dilution potential experiment was repeated in transfected HEK cells either with or without $MTSES^-$ treatment (Fig. 4-6). Wild-type dBest1 in the presence or absence of $MTSES^-$ and F81C dBest1 in the absence of $MTSES^-$ exhibited similar P_{Cs}/P_{Cl} ratios (~0.1). In contrast, the $MTSES^-$ -modified F81C channel exhibited a significantly elevated cation permeability ($P_{Cs}/P_{Cl} = 0.50$). Despite the observation that the change in relative Cs^+/Cl^- permeability is smaller when F81C is expressed in HEK cells than in S2 cells, $MTSES^-$ modification still caused a significant shift of ionic selectivity of heterologously-expressed F81C toward the direction

of cations. We do not understand why there is a quantitative difference between HEK cells and S2 cells. It is possible that there may be different factors or subunits in these two types of cell that contribute to channel selectivity.

Mimicking the Electrostatic Effect of $MTSES^-$ by Expressing F81E

To test the hypothesis that the effect of $MTSES^-$ on the ionic selectivity of F81C was mediated by an electrostatic effect at this location, we replaced the F81 residue with the negatively charged amino acid, glutamic acid (E) to mimic the negative charge of $MTSES^-$. We discovered that the F81E VRAC current rectified inwardly (Fig 4-5D) and reversed at –9.4 ± 1.2 mV, which is significantly different from the native wild-type dBest1 current (0.2 ± 0.2 mV) (Fig. 4-5C). P_{Cs}/P_{Cl} for F81E was calculated to be 1.33 from the dilution potential experiments (Fig. 4-4C and D). The fact that F81E recapitulated most of the properties of $MTSES^-$-modified F81C currents indicated that residue F81 is in vicinity to the ion selectivity filter of the dBest1 Cl^- channel and further supported that and that dBest1 forms the integral part of the channel and is not merely a regulatory subunit of another channel.

VRAC in Primary Culture of Mouse Microglia and Macrophages

Our data demonstrated that at native dBest1 is a Cl^- channel that is dually regulated by cytoplasmic Ca^{2+} and by cell swelling using *Drosophila* S2 cells as the model system. To test whether bestrophins are responsible for the VRAC currents in mammals, we measured VRAC in adult mouse peritoneal macrophages and in newborn (postnatal day 1-2) mouse microglia. Cells were purified from wild type mice and mice that had both mBest1 and

mBest2 genes disrupted (Fig. 4-7). The whole cell recording was initiated with an intracellular solution that was 306 mosm kg^{-1} and an extracellular solution that was 326 mosm kg^{-1}. The VRAC current was then stimulated by replacing the extracellular solution with the one that was 234 mosm kg^{-1}. Virtually all electrophysiological properties of VRAC currents in the wild type and knockout animals were statistically the same. In addition to adult mouse peritoneal macrophages, the same experiment was performed on newborn mouse microglia (data not shown). Both results did not show significant differences between the VRAC currents generated by the wild-type and the mBest1/mBest2 double aberrant mice. These data suggested that channels other than bestrophins are responsible for the classical VRAC current in mouse cells.

Discussion

dBest1 forms the integral part of the S2 VRAC channel

Previously, we showed that treating *Drosophila* S2 cells with RNAi to dBest1 abolished both the Cl^- currents activated by cytosolic Ca^{2+} and by cell swelling. We have also shown that dBest1 plays an essential role in maintaining cell volume homeostasis in S2 cells, because RNAi knockdown of dBest1 significantly impaired regulatory volume decrease (RVD) (Chien & Hartzell, 2007). Therefore, we concluded that dBest1 is a novel member to the VRAC channel family. However, our previous data did not formally elucidate that dBest1 is the integral component of the ion-conducting pore of the Cl^- channel. This is mainly because knocking down an essential regulator or a beta subunit of a Cl^- channel by RNAi would produce similar effect as knocking down the channel itself. To establish that dBest1 forms the pore of the ion channel, it was necessary to rescue the

current with a channel that had a biophysical signature that was readily separable from the wild type channel.

Our results described in this chapter provide solid support that dBest1 is indeed the volume regulated anion channel in *Drosophila* S2 cells, because we were able to rescue the volume sensitive current by over-expressing a mutant dBest1 (F81C) with altered biophysical properties. Like the native VRAC current, the F81C-rescued VRAC current was sensitive to osmotic pressure differences: the current was inhibited by hyperosmotic bath solution and augmented by hyposmotic extracellular solutions. Moreover, the stimulation of F81C current was coupled with cell swelling. The F81C-rescued current exhibited several hallmark features that are different from the wild type VRAC current, as expected if F81C is located in the ion-conducting pore of the dBest1 channel: (1) Whereas the native or wild-type dBest1 current exhibited an S-shaped IV relationship, the F81C current inwardly rectified; (2) F81C current amplitude was greatly enhanced by $MTSET^{+}$, whereas the wild type dBest1 current was slightly decreased; (3) Most strikingly, the $MTSES^{-}$-modified F81C current exhibited altered ionic selectivity so that the channel became more permeable to cations than to Cl^{-}. These distinguishing features clearly show that the rescued current is mediated by dBest1-F81C. The data obtained with F81E mutant provide additional support to the results obtained with F81C, because mimicking the negative charge of $MTSES^{-}$ at F81 residue by Glu also manifested an increased permeability to cations compared to the wild type dBest1 VRAC current. It would be difficult to imagine how dBest1 could produce these remarkable effects if dBest1 were merely a regulator or an auxiliary subunit but not the integral part of an ion channel.

The specificity of the effect of $MTSES^-$ on dBest1 currents

We show here that the reversal potential of dBest1-F81C Cl^- current was shifted after modification of the Cys by $MTSES^-$. The most straightforward explanation is that the ionic selectivity of dBest1 Cl^- channel has changed from anionic to cationic. However, after $MTSES^-$ treatment, the amplitude of F81C current also reduced significantly to values (~200-400 pA) close to the residual currents in cells treated with dBest1 RNAi. This raises a concern if the altered ionic selectivity was due to unmasking of an endogenous cation current. However, we feel that this concern is minimized because the same as the $MTSES^-$-modified native S2 Cl^- current, the E_{rev} of the background current in dBest1 RNAi-treated S2 cells shifted toward positive direction after $MTSES^-$ treatment (data not shown). This showed that the S2 cell background current is unlikely to account for the increased cation permeability observed in $MTSES^-$–modified F81C currents, which shifted toward negative values. In addition, mimicking the effect of $MTSES^-$ on F81 by replacing F81 with negatively charged glutamate reversed the charge selectivity of Cl^- to cation, too. This lends additional support that the charge state at F81 interferes with the ionic selectivity of dBest1 channel.

On the other hand, it is also possible that the change in ionic selectivity in F81C currents after $MTSES^-$ treatment is caused by an up-regulation of a native cation channel in S2 cells as a result of over-expression. We feel that this concern is minimized because the E_{rev} of the over-expressed wild-type dBest1 currents shifted to the opposite direction than the $MTSES^-$–treated F81C currents. These data provide additional support to our conclusion.

Altered volume sensitivity of the rescued F81C current

The volume sensitivity of the rescued current (both wild type and F81C) is slightly different than the native VRAC current that we reported previously (Chien & Hartzell, 2007). Typically, the native VRAC current immediately after breaking the patch to initiate whole-cell recording is ~ 0.1 nA or less at +100 mV, whereas with the F81C mutant the initial current is ~0.4 nA. Because the osmotic pressure difference develops only after the patch is broken, the observation that the initial F81C current is larger than native current suggests that the F81C current is partially activated before patch break. Furthermore, the rescued currents seem to activate more quickly than the native current. We believe that these differences are an artifact of over-expression: the channel may be partially uncoupled from its regulatory mechanisms and exhibit a different "set-point". This is supported by the observation that the apparent uncoupling is related to the level of over-expression, because with high levels of over-expression of wild type dBest1, volume-sensitive dBest1 currents were observed even under isosmotic conditions (data not shown).

Conversion of ionic selectivity in dBest1 and other Cl^- Channels

The ability to change the anionic selectivity of dBest1 from anionic to cationic by a point mutation followed by $MTSES^-$ modification is inspiring. The $MTSES^-$-modified F81C current exhibited a P_{Na}/P_{Cl} ratio of 0.83 and a P_{Cs}/P_{Cl} ratio of 2.38, which implies a permeability sequence of $P_{Cs} > P_{Cl} > P_{Na}$. This is supported by the observation that E_{rev} shifted to more negative values when extracellular Cs^+ was replaced with the impermeant $NMDG^+$ than with Na^+. Other examples of ion channels in which the ionic selectivity has been reversed by mutagenesis of pore-lining amino acids include the nicotinic

acetylcholine receptor (Galzi *et al.*, 1992), the GABAA receptor (Wang *et al.*, 1999), and the glycine receptor (Keramidas *et al.*, 2000, Keramidas *et al.*, 2002). Keramidas *et al.* have converted the Cl^- selective glycine receptor to cation selective by replacing a residue within the M2 pore-forming domain, A251, with negatively charged glutamate. The cation permeability is further augmented by deleting proline 250 in the A251E background. Whereas the glycine receptor double mutant has a P_{Na}/P_{Cl} ratio of 7.70, the single A251E mutant exhibits a relatively modest P_{Na}/P_{Cl} ratio of 2.94 (Keramidas *et al.*, 2002). The $MTSES^-$-treated dBest1-F81C mutant only showed a P_{Na}/P_{Cl} ratio of 0.83. The selectivity filter of mBest2 is estimated to distribute over ~20 amino acids within the transmembrane domain 2 (Qu *et al.*, 2006a). Perhaps mutation of additional amino acids in the vicinity of dBest1-F81C may produce larger effects.

Replacing F81 with the negatively charged Glutamic acid (E) mimicked the effect of $MTSES^-$ on the ionic selectivity of F81C currents. The ionic selectivity also reversed in F81E, but to a lesser extent than the shift in $MTSES^-$-modified F81C. This may be explained by the fact that $MTSES^-$ is a relatively large molecule (1.2 nm x 0.6 nm (Kaplan *et al.*, 2000)) compared to the dimensions of glutamate or cysteine (side chain length < 0.5 nm). Thus, the negative charge provided by $MTSES^-$ is likely to be located at a different location than the negative charge provided by glutamate. The conversion in charge selectivity produced by $MTSES^-$, therefore, may involve other regions of dBest1 in addition to transmembrane domain 2, where F81 is located. This raises the possibility that the region of the channel that interacts with the permeant ion is actually located as much as 1.2 nm from F81. It is also possible that the incorporation of the $MTSES^-$ moiety disrupts the structure of the pore and changes its diameter or other properties.

Materials and Methods

Solutions for Whole Cell Recording

The component of the whole cell recording solutions is the same as that mentioned in Chapter 3. Unless indicated otherwise, the osmotically-sensitive Cl^- current was routinely activated by Δ40 mosmol kg^{-1} osmotic pressure (E300/I340). These combinations of solutions set the calculated E_{Cl} to 0 mV, while cation currents carried by Cs^+ or Na^+ would have very negative or positive E_{rev}, respectively. The major cation in the intracellular solution was Cs^+ while the standard extracellular cation was Na^+ unless specified otherwise. Stock solutions of 100 mM $MTSET^+$ (2-trimethylammonioethylmethane-thiosulfonate, bromide salt) and $MTSES^-$ [sodium (2-sulfonatoethyl) methanethio-sulfonate] (Toronto Research Chemicals) were prepared in water and stored at -80 °C. Aliquots of the MTS stock solution were thawed and kept on ice no longer than 10 min. 1 mM working solution was prepared by diluting the stock with the external recording solution immediately before use. Working solutions of DTT (dithiothreitol) (Sigma) were prepared freshly from frozen 1 M stock solutions. To determine relative $cation^+/Cl^-$ permeabilities, we used a high Ca^{2+} intracellular solution containing 150 mM CsCl (or NaCl), 10 mM HEPES (pH7.2 with NMDG), and 5 mM Ca-EGTA-NMDG and extracellular solutions containing different CsCl (or NaCl) (150, 100, 50, 20, or 10 mM), 10 mM HEPES, and 1 mM $CaCl_2$. All solutions were pH 7.2 and adjusted to 304 mosmol kg^{-1} with mannitol.

Site-Directed Mutagenesis

Residue F81 was mutated to cysteine, glutamate, or leucine by a PCR-based site-directed

mutagenesis method (Quickchange; Stratagene). The F81C mutation was introduced by PCR primers (forward) 5'-CATACCCCTGTCCTGCGTGCTTGGTTTC -3' and (reverse) 5'-GAAACCAAGCACGCAGGACAGGGGTATG-3'. The F81E mutation was introduced by primers (forward) 5'-CATACCCCTGTCCGAAGTGCT TGGTTTC-3' and (reverse) 5'-GAAACCAAGCACTTCGGACAGGGGTATG-3'. The F81L mutation was introduced by primers (forward) 5'-CATACCCCTGTCCCTCGTGCTTGGTTTC-3' and (reverse) 5'-GAAACCAAGCACGAGGGACAGGGGTATG-3'. dBest1 open reading frame in pAc5.1/V5-HisA was used as the template for high fidelity PCR amplification with *Pfu* DNA polymerase. The methylated template was digested with the endonuclease Dpn-1 and the non-methylated PCR product was transformed into XL-1 blue *E. coli* for amplification. DNA was sequenced to confirm the mutation.

Rescue of dBest1 in S2 Cells

Drosophila S2 cells were cultured in Schneider's *Drosophila* Medium (GIBCO BRL) supplemented with 10% heat-inactivated FBS (GIBCO BRL) and 50 U/ml penicillin and 50 μg/ml streptomycin (GIBCO BRL) at room temperature. The open reading frame of dBest1 was introduced into pAc5.1/V5-HisA *Drosophila* expression vector (Invitrogen) as described previously (Chien et al., 2006; Chien and Hartzell, 2007). Residue F81 was mutated to cysteine by a PCR-based site-directed mutagenesis method (Quickchange; Stratagene). The F81C mutation was introduced by PCR primers (up:5'-CATACCCCTGTCCTGCGTGCTTGGTTTC-3'; down:5'-GAAACCAAGCACG CAGGACAGGGGTATG-3'). pAc5.1-dBest1ORF was used as the template for high fidelity PCR amplification with Pfu DNA polymerase. The methylated template was

digested with the endonuclease Dpn-1 and the non-methylated PCR product was transformed into XL-1 blue *E. coli* for amplification. DNA was sequenced to confirm the mutation. For the rescue experiment, 2.1×10^5 S2 cells were treated with 8.3 µg of double stranded RNA against the 5' UTR of dBest1 (5UdB1) for 4 days as mentioned in previous chapter. The RNAi-treated cells were then transfected with a mixture of pAc5.1-dBest1 or dBest1-F81C DNA and pAc5.1-EGFP in 2:1 ratio using calcium phosphate. Green cells were recorded 2 to 4 days after transfection.

Electrophysiology, cell volume determination, and Data Analysis

S2 cells were allowed to adhere to the bottom of the recording chamber for ~10 min and were then washed and incubated with extracellular solution for ~10 min before whole cell recording. Fire-polished pipettes pulled from borosilicate glass (Sutter Instrument Co.) had resistances of 2–3 MΩ when filled with intracellular solution. For whole-cell recording, cells were voltage clamped with ~1-s duration ramps from −100 to +100 mV run at 10-s intervals as mentioned in Chapter 3. Whole cell recording data were filtered at 2–5 kHz and sampled at 5–10 kHz by an Axopatch 200A amplifier controlled by Clampex 8.2 via a Digidata 1322A data acquisition system (Axon Instruments Inc.). Data were not corrected for liquid junction potentials when quantifying relative Cs/Cl permeability, which were calculated to be < 0.6 mV. For NaCl solutions, the liquid junction potential was calculated and corrected using Liquid Junction Potential utility in pClamp (the maximum liquid junction potential, for 150 mM NaCl inside and 10 mM NaCl outside was -12.6 mV). Series resistance compensation was not routinely employed. Phase contrast images of the cells were taken with MetaMorph Imaging software (Universal Imaging Co.)

immediately after patch break and when the currents stabilized. The volume of the cell was calculated from the measured circumference assuming that the shape of S2 cells is spherical. Relative X/Cl permeability was determined by measuring the shift of E_{rev} upon changing the solution on the extracellular side of the membrane from the one containing 150 mM XCl to 100, 50, 20, and 10 mM. The relative X:Cl permeability ratio was then estimated by fitting the measured mean E_{rev} differences with the Goldman-Hodgkin-Katz (GHK) equation (Hille, 2001), assuming that the movement of anions is independent of cations,

$$P_X/P_{Cl} = \exp(\Delta E_{rev}F/RT),$$

where ΔE_{rev} is the difference between the reversal potential with the test XCl concentration and that observed with symmetrical [XCl] ($E_{rev} = 0$ mV) and F, R, and T have their normal thermodynamic meanings. All data were analyzed using pClamp 8.2 software and Origin 7.0 and are expressed as mean ± SEM.

Measurement of VRAC in Peritoneal Macrophages and Microglia.

Adult mouse peritoneal macrophages were isolated by peritoneal lavage. 5 ml of cold RPMI medium containing 10% fetal bovine serum was injected intraperitoneally into a mouse that had just been euthanized by an overdose of isoflurane anesthesia. The abdomen was massaged for several minutes and the fluid was withdrawn and plated onto glass coverslips and cultured at 37^{o}C in a 5% CO_2 – 95% air environment. Round macrophages were patch clamped 2 hr to 2 days after isolation at room temperature. Primary cultures of mouse microglia cells were prepared from postnatal day 2-3 mice according to Nicole et al. (Nicole *et al.*, 2005). After one week of in vitro culture, microglia was isolated from the

mixed astroglial culture by vigorous shaking. Detached microglial cells were seeded onto poly-L-Lys-coated glass coverslips for whole cell recording the next day. The intracellular solution was (in mM) 95 Cs-aspartate, 40 CsCl, 1 $MgCl_2$, 10 HEPES pH 7.4, 4 Na/K-ATP, 5 EGTA, and $CaCl_2$ added to give approximately 50 nM free Ca^{2+}. The hyposmotic extracellular solution was 105 NaCl, 6 CsCl, 1 $MgCl_2$, 1.5 $CaCl_2$, 10 HEPES (pH 7.4), and 10 glucose (234 mosmol kg^{-1}). Isosmotic and hyperosmotic solutions were made by adding mannitol to the hyposmotic solution to make 266, 306, and 326 mosmol kg^{-1} solutions. Recording pipettes had 3–6 MΩ of resistances when filled with intracellular solution and the averaged cell capacitance was 12.73 $\pm$ 0.89 pF (n=20). Wild type mice were C57B. The mBest1-mBest2 double knockout mice were made by breeding mBest1 knockout mice (Merck & Co.) with mBest2 knockout mice (Bakall *et al.*, 2008). The mBest1 knockout mice were generated by homologous recombination that resulted in deletion of exons 5 -9 of mBest1.

.

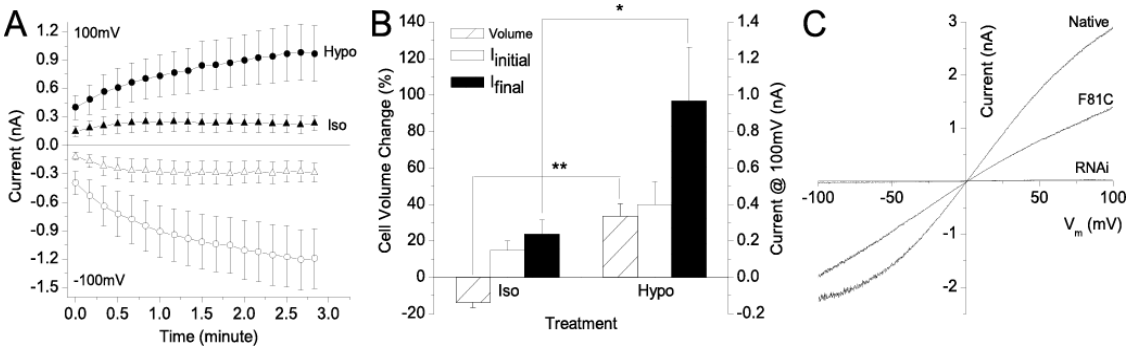

Figure 4-1: Rescue of the volume-regulated Cl^- current in S2 cells by expression of dBest1-F81C. Endogenous dBest1 in S2 cells was knocked down by dB1U5 RNAi, and these cells were transfected with dBest1-F81C and EGFP constructs. RNAi treated cells had no currents. Green cells were patch-clamped in a whole-cell configuration with a 10-sec interval voltage ramps from -100 mV to +100 mV from a holding potential of 0 mV. (A) Time course of activation of VRAC in S2 cells rescued with dBest1-F81C. The currents shown were measured at -100 mV (open symbols) and +100 mV (solid symbols) under isosmotic (I300/E300, triangles, n=6) or hyposmotic (I340/E300, circles, n=7) conditions. (B) Mean current amplitudes at 100 mV at the onset of whole cell recording (Initial current, open bars) and after the currents had reached a peak (Final currents, filled bars) and the corresponding cell volume alterations (hatched bars) with hyposmotic (Δ40 mosmol kg^{-1}) and isosmotic solutions. Changes in cell volume are expressed as percent change in cell volume from the initiation of whole cell recording to ~3-5 min after patch break (isosmotic, n=6) or when the currents had approached a steady value (hyposmotic, n=7). Data are represented in mean ± SEM. *, significantly different at $p<0.05$ and ** at $p<0.01$ level. (C) I-V curve of dBest1 currents in native, dBest1-F81C-rescued, and RNAi-only S2 cells stimulated with Δ 40 mosmol kg^{-1} hyposmotic solutions.

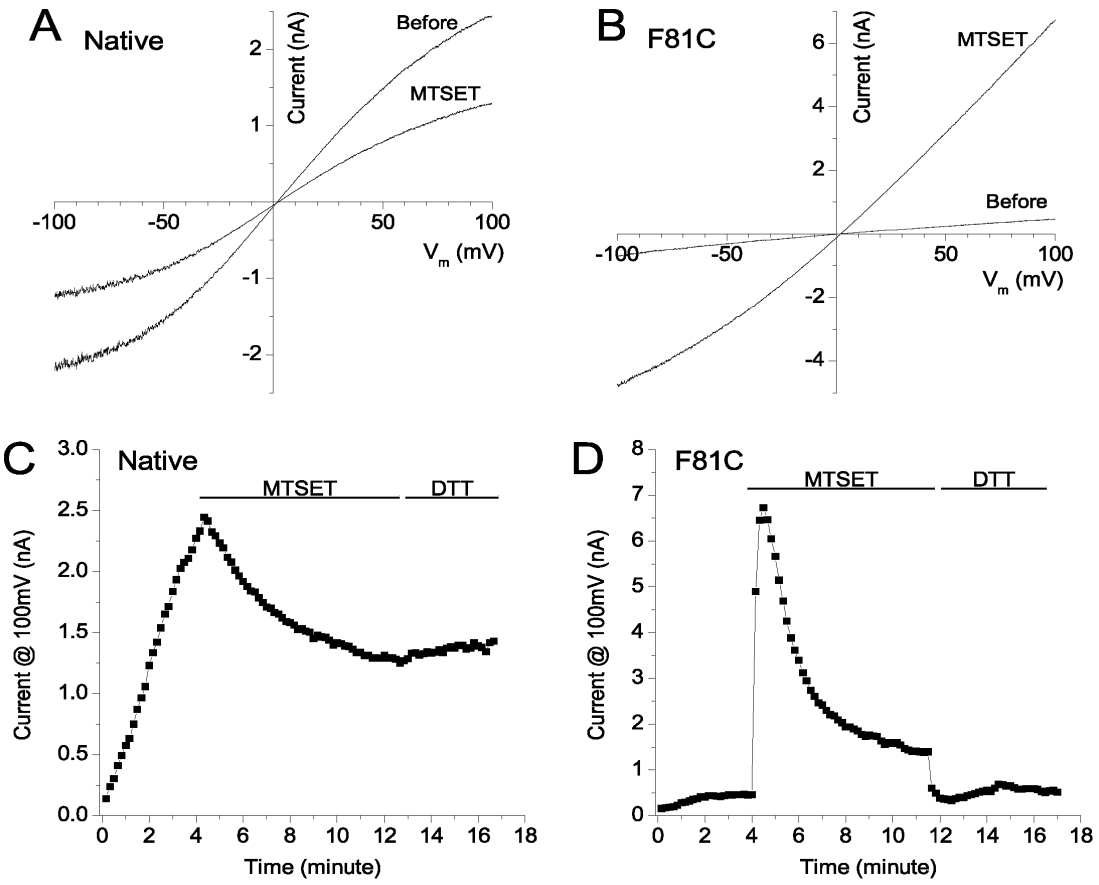

Figure 4-2: dBest1-F81C rescued cells respond differently to $MTSET^+$ modification than native S2 cells. Whole cell VRAC currents were established in hyposmotic solutions (I340/E300, Δ40 mosmol kg^{-1}) and were recorded with voltage ramps from -100mV to 100mV. 1 mM $MTSET^+$ was applied to the bath solution (E300) after the volume-sensitive current was fully activated. The bath was then replaced with 5 mM DTT to check if the effect of $MTSET^+$ was reversible. (A and B). Current-voltage relationships in native (A) and dBest1-F81C rescued (B) S2 cells before and after $MTSET^+$ modification. (C and D) Time course of the effect of $MTSET^+$ modification on native (C) and dBest1-F81C rescued (D) VRAC currents. These time course data were collected from the same cells shown in (A) and (B).

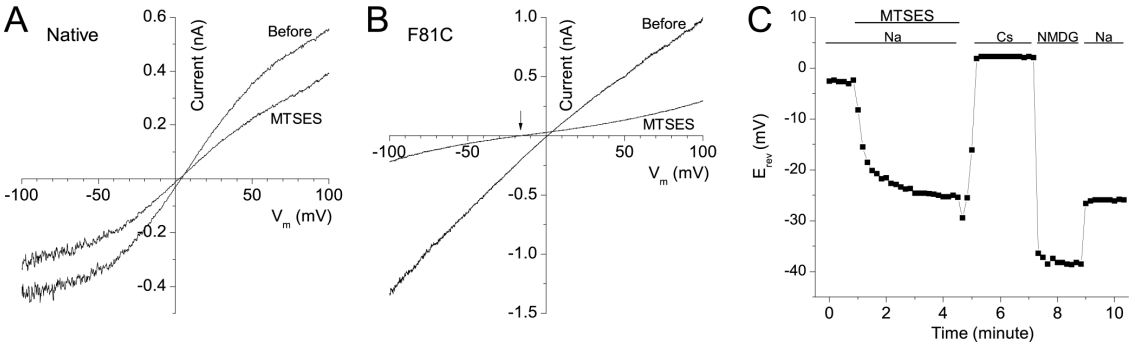

Figure 4-3: MTSES$^-$ increases the cation permeability of F81C currents. Current-voltage relationships from a typical native S2 cell (A) and a S2 cell rescued with dBest1-F81C (B) before and after MTSES$^-$ modification. Currents were activated with Δ 40 mosmol kg^{-1} hyposmotic solutions. (C) Changes in E_{rev} of F81C currents under different ionic conditions. The record begins after the dBest1 current had stabilized under hyposmotic solutions (I340/E300, Δ 40 mosmol kg^{-1}). MTSES$^-$ was then applied in the bath. Extracellular solution containing symmetrical Cl^- and Na^+ as the major cation (E300) was then replaced by solutions with Cs^+ or $NMDG^+$ as the major cations as indicated. The osmolality of all the extracellular solutions was 300 mosmol kg^{-1}.

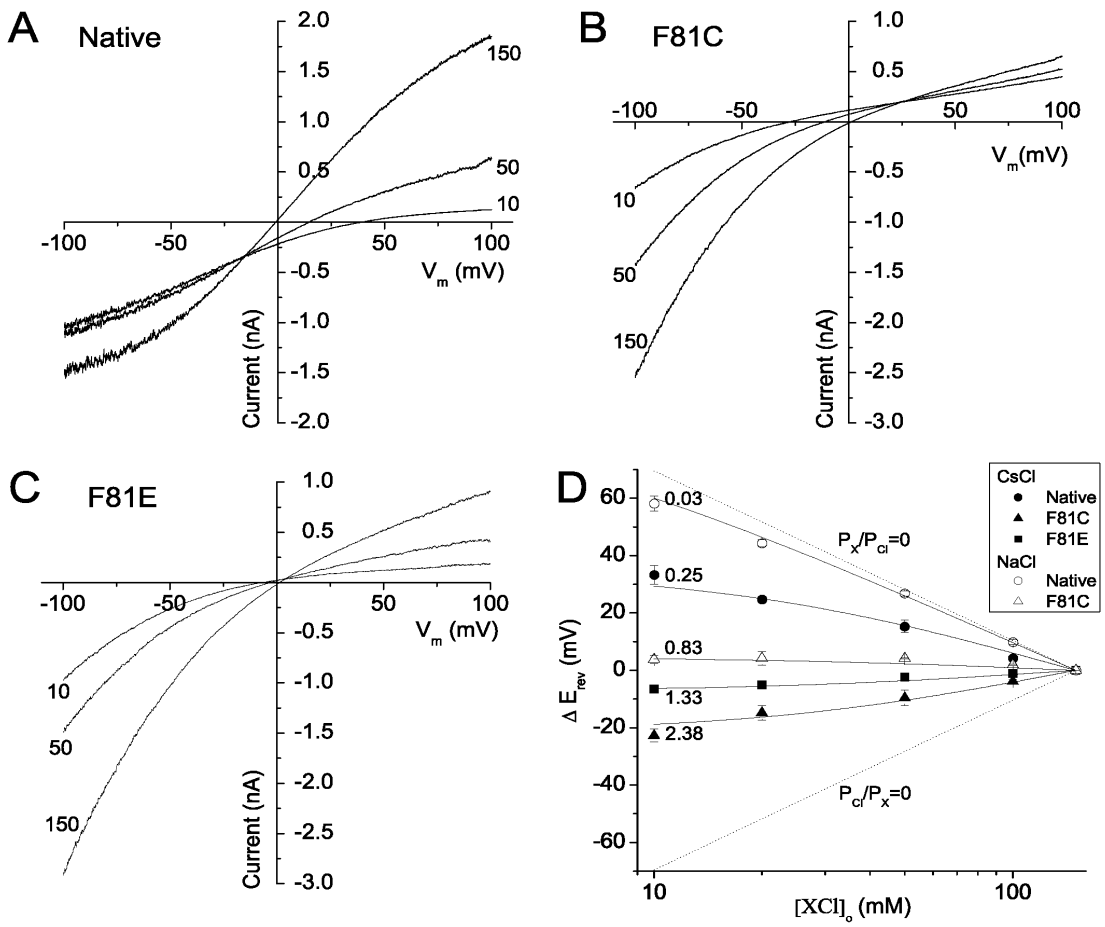

Figure 4-4: Quantification of relative cation/chloride permeability. Current-voltage relationships of $MTSES^-$-modified native dBest1 (A) and dBest1-F81C (B) currents and non-MTSES modified dBest1-F81E currents (C) in response to different external [CsCl]. Whole cell currents were activated under isosmotic condition (304 mosmol kg^{-1}) with high Ca^{2+} in the pipette and symmetrical CsCl in the bath (150 mM). The extracellular solution was replaced by solutions containing varied [CsCl] as indicated. (D) Changes in E_{rev} (ΔE_{rev}) as a function of extracellular salt concentration. ΔE_{rev} is E_{rev} at the indicated salt concentration minus the E_{rev} with 150 mM extracellular salt. Salt is either CsCl or NaCl as

indicated. Each data point represents the mean $E_{rev} \pm$ SEM of two to nine cells. Dashed lines were calculated from the Goldman-Hodgkin-Katz equation ($\Delta E_{rev} = 25.7 \cdot \ln [([X^+]_o + [Cl^-]_i \cdot P_{Cl}/P_X) / ([X^+]_i + [Cl^-]_o \cdot P_{Cl}/P_X)]$), assuming that the channel is exclusively permeable to Cl^- ($P_X/P_{Cl}=0$) or to the cation X^+ ($P_{Cl}/P_X=0$). Filled symbols: CsCl solutions. Filled circles: $MTSES^-$-treated native dBest1 (n=2-7); filled triangles: $MTSES^-$-modified F81C (n= 4-9); filled squares: F81E (n=2-5). Open symbols: NaCl solutions. Open circles: $MTSES^-$-treated native dBest1 (n=3-5); open triangles: F81C (n=3-8).

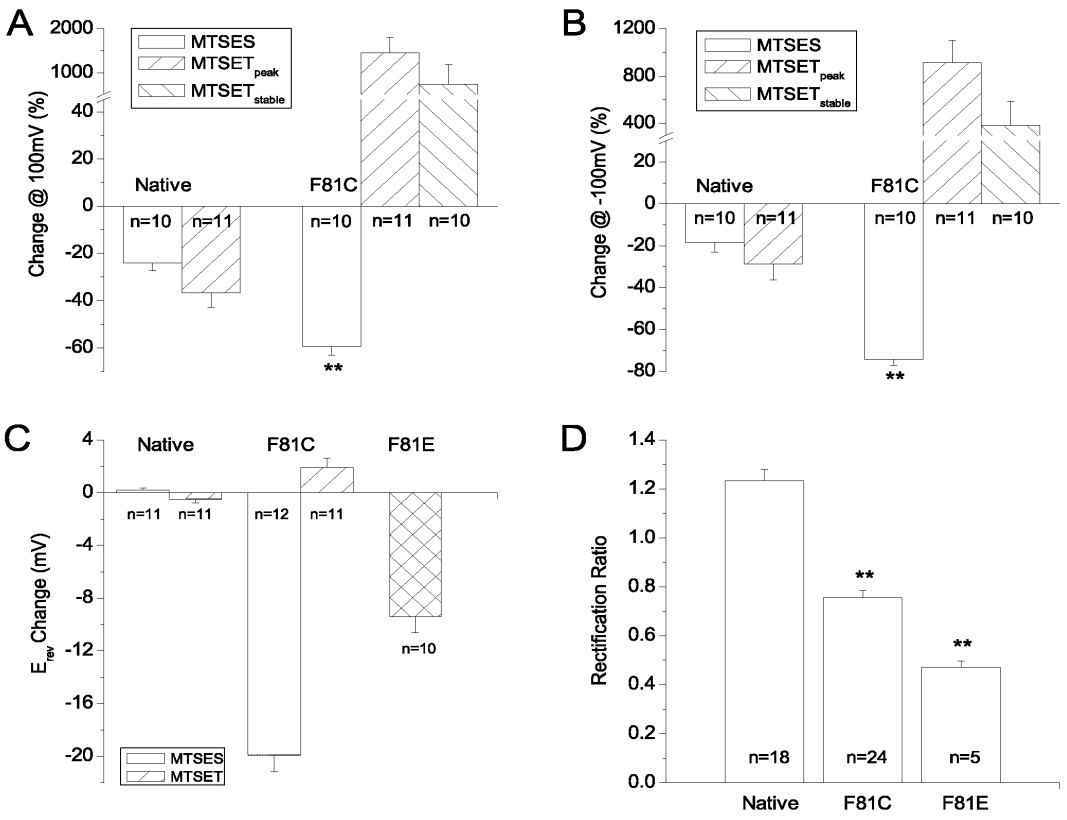

Figure 4-5: Summary of the effect of sulfhydryl modifications and rectification ratio. The change was calculated using the following equation: $(I_{MTS} - I_{before}) / I_{before} \times 100\%$ for steady state VRAC currents measured at 100mV (A) and -100mV (B) respectively. The effect of $MTSES^-$ is shown in open bars, the peak stimulation after applying $MTSET^+$ is shown as $MTSET_{peak}$, and the stabilized level in $MTSET^+$ is shown as $MTSET_{stable}$. (C) Effect of MTS treatment on E_{rev}. The change in E_{rev} is the difference between E_{rev} before and after MTS treatment. The reversal potential of F81E currents (without MTS treatment) is shown with a crossed bar. (D) Rectification ratio of native, F81C, and F81E VRAC currents. The rectification ratio was calculated as the absolute value of the VRAC current at +100mV divided by the current at -100 mV for native, F81C, and F81E currents. Data are represented in mean ± SEM. **, significantly different at $p<0.01$ level.

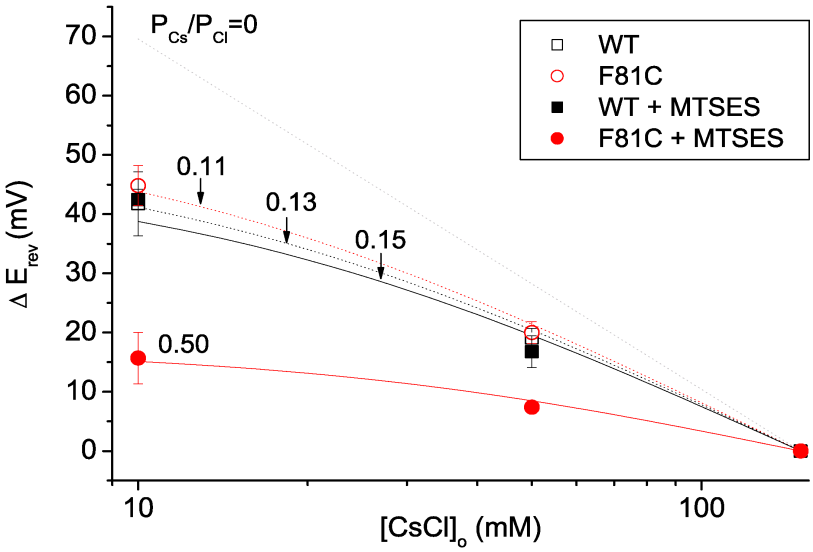

Figure 4-6: Quantification of relative Cs^+/Cl^- permeability in HEK cells transfected with dBest1. Whole cell current was measured in wild-type dBest1 or dBest1-F81C over-expressed HEK cells. Changes in E_{rev} (ΔE_{rev}) as a function of extracellular CsCl concentration was plotted for cells with and without $MTSES^-$ treatment. Each data point represents the mean E_{rev} ± SEM of two to seven cells. Gray dashed line was calculated from the Goldman-Hodgkin-Katz equation assuming that the channel is exclusively permeable to Cl^- ($P_{Cs}/P_{Cl} = 0$). Filled symbols: $MTSES^-$-treated. Filled circles: F81C (n= 2-7); filled squares: wild-type dBest1 (n= 3-4). Open symbols: without $MTSES^-$ treatment. Open circles: wild-type dBest1 (n= 5); open squares: F81C (n= 3).

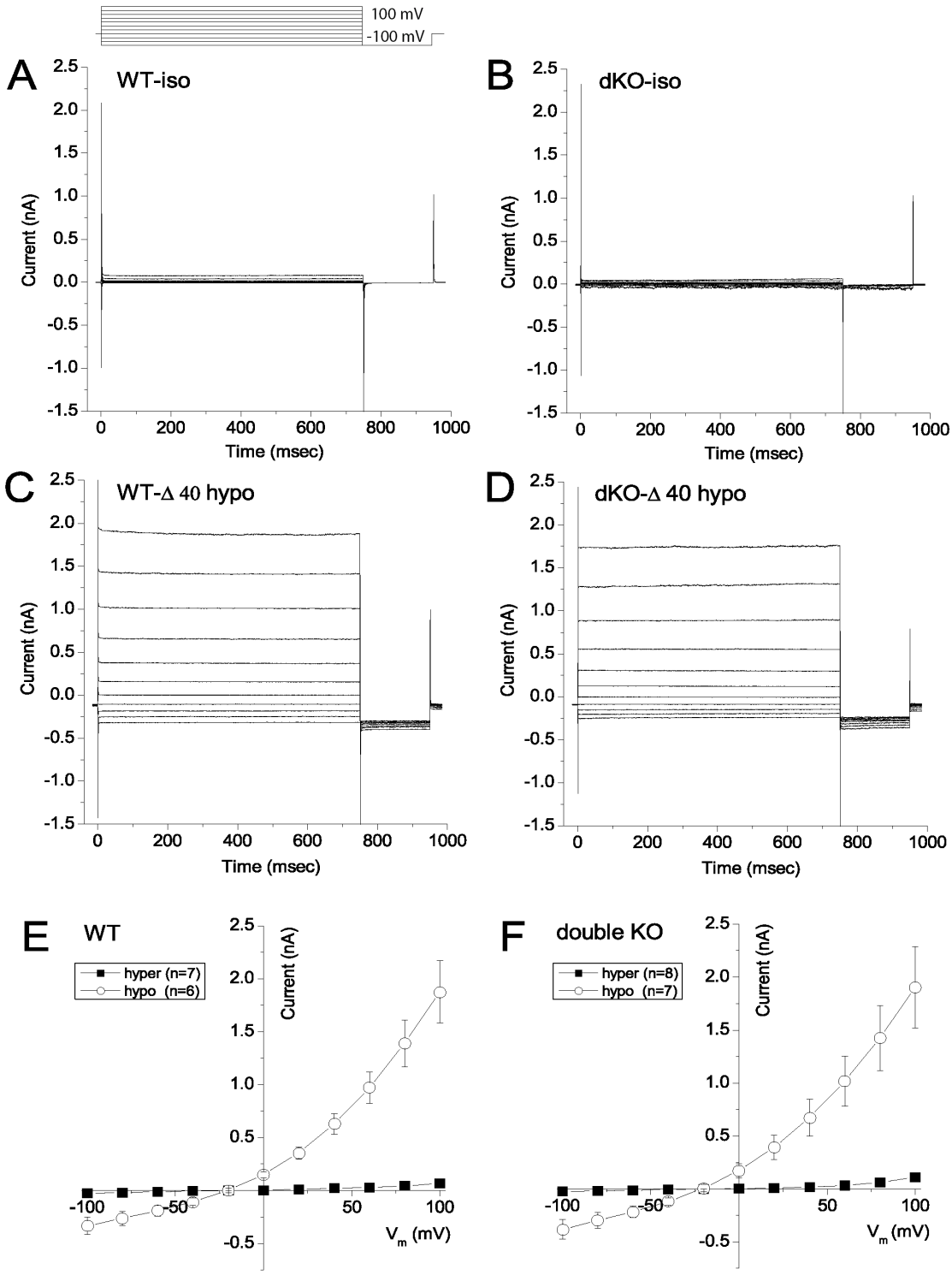

Figure 4-7: VRAC in peritoneal macrophages from wild type and mBest1-/- -mBest2

-/- mice. (A,C, and E) Wild type mice. (B,D, and F) mBest1$^{-/-}$-mBest2$^{-/-}$ mice. The intracellular solution of all recordings was held constant at 306 mosmol kg^{-1} while the osmolality of the extracellular solution was altered to achieve different osmotic pressures. (A and B) Current traces under isosmotic conditions. (C and D) Current traces in Δ40 mosmol kg^{-1} hyposmotic conditions (266 mosmol kg^{-1} extracellular). (E and F) Average current-voltage relationships under Δ 70 mosmol kg^{-1} hyposmotic (open symbols; 234 mosmol kg^{-1}extracellular) and -Δ 20 mosmol kg^{-1} hyperosmotic (filled symbols; 326 mosmol kg^{-1}extracellular) conditions.

CHAPTER 5

A POTENTIAL ROLE FOR DBEST1 IN ADULT FLIES

Summary

At the molecular level, we have demonstrated that endogenous dBest1 encodes for Cl^- channels that are dually regulated by Ca^{2+} and by cell volume. At the cellular level, we have elucidated the involvement of dBest1 in the process of regulatory volume decrease (RVD) in response to hyposmotic cell swelling. To investigate possible roles of dBest1 in intact animals, we examined its expression. Real-time PCR showed that dBest1 is the most abundantly expressed gene among all fly bestrophins. dBest1 protein expression profile determined by Western blotting revealed that dBest1 is distributed in various tissues such as the Malpighian tubule and the crop. By immunofluorescent staining, dBest1 signal is found to be enriched in the hindgut, and confocal microscopy analysis further refined the subcellular localization of dBest1 to the basolateral membrane in the Malpighian tubule. The Malpighian tubule and the hindgut together function as the major excretory organs in insects. The enrichment of dBest1 in these tissues implies a potential role of dBest1 in osmoregulation. Our preliminary data showing that flies with suppressed dBest1 expression exhibited elevated mortality when raised on food containing NaCl supports this hypothesis. More efforts are required in the future to fully characterize the role of dBest1 in animals. This work will be invaluable in illuminating the physiology of bestrophin in animals and may shed lights on the pathogenesis of the Best Disease.

Introduction

Our comprehensive analysis described in Chapters II to IV have substantiated the molecular function of endogenous dBest1 as a Cl^- channel and have elucidated the cellular function of dBest1 in regulating cell volume (Chien & Hartzell, 2007, Chien *et al.*, 2006). However, a phenotype that is related to defective bestrophin has not been described. *Drosophila melanogaster* is a well-established model organism that is well suited for reverse genetics. One of the most popular mutagenesis approaches in flies involves the insertion of a 8-10 kb transposon (P-element) to disrupt the sequence of the target gene. The p-element can also be used to induce excision of the target gene because of its ability in hijacking a portion of the gene flanking the transposon by the catalytic activity of a transposase.

To investigate possible roles of dBest1 in animals, dBest1 mutant lines have been created. Among these, a deletion mutant of *dBest1* (*dBest1*$^{1-2}$), in which the entire dBest1 gene has been removed by P-element transposase-mediated deletion of genomic DNA between two P-elements that flank the dBest1 locus, has been made (Tavsanli *et al.*, 2001). The flies homozygous for the dBest1 deletion are fertile and have normal lifespan. They do not exhibit gross morphological abnormalities. In addition, these flies have eye morphology and electroretinogram readings that are indistinguishable from that of the wild type flies (at all age). The lack of eye phenotype is not unexpected, considering the great divergence in embryology and morphology between eyes in human and flies. However, dBest1 may exhibit more obvious phenotypes in tissues other than the eye, especially where it is most abundantly expressed.

To explore the potential role of dBest1 in the fly, we collected the dBest1 knockout

line described above (from Dr. Edward Blumenthal, originally made by Dr. Graeme Mardon) and several other mutant lines with a P-element randomly inserted in the dBest1 gene (from Bloomington Fly Stock Center). In the wild type fly, dBest1 is the most abundantly expressed bestrophin isoform, and dBest1 protein is found in various tissues including the major excretory tissues of the fly that mediate osmoregulation. Our preliminary data showing that flies with suppressed dBest1 expression die quickly in a high-salt diet but not in a sorbitol-rich diet is consistent with the Cl^- transport function of dBest1. Although the precise site of dBest1 action and the exact mechanism of the salt sensitivity remain to be studied, the phenotype implicates a potential role of dBest1 in regulating Cl^- homeostasis in intact animals.

Results

To explore the potential roles of *Drosophila* bestrophin gene products in the physiology of the fly, we first used real-time PCR to quantify the relative expression level of the bestrophin genes. PCR from whole-fly cDNA showed that dBest1 and dBest2 are roughly expressed at the same level in the adult fly, with expression levels approximately two-fold higher than that of dBest3 (Figure 5-1). dBest4 expression is not detectable, and it might be a pseudo gene (personal correspondence, Dr. Edward Blumenthal).

Adult fly dBest1 protein expression profile was also systematically examined. To do so, we generated polyclonal anti-dBest1 antibody (described in Chapter 2) and compared the expression of dBest1 between the wild type (Canton S) and the knockout fly tissues by Western blotting. The blots elicit the expression of dBest1 protein (79 kDa) in the Malpighian tubule, crop, eye, ovary, fat body, and to a lesser extent in testis of the wild

type fly (Canton S) but not in the dBest1 knockout fly (dBest$^{1\text{-}2}$) (Figure 5-2). In addition to these tissues, dBest1 signal is also enriched in the hindgut, as determined by immunofluorescent staining (Figure 5-3). Confocal microscopy analysis further shows a basolateral localization of dBest1 in the Malpighian tubule (Figure 5-3). The protein expression profile for dBest1 is in agreement with the mRNA expression profile provided by the University of Glasgow *Drosophila* Adult Expression Database (http://www.flyatlas.org/), which shows that dBest1 mRNA is highly expressed in the crop, Malpighian tubules, and the hindgut, and to a basal extent in the ovary, male accessory gland, and the larval fat body when compared to the whole fly.

We further examined the expression level of dBest1 in all of our dBest1 mutant lines and a dBest1 rescued line. Tissue extracts were collected from the Malpighian tubule and were subjected to Western blotting for dBest1 (Figure 5-4). The 79-kDa dBest1 protein is detected in the wild type fly (Canton S), whereas this band is significantly suppressed in the p-element inserted *dBest1* mutant line (*dBest1*^{C04106}). dBest1 level is not detectable in the dBest1 knockout fly (*dBest1*$^{1\text{-}2}$), whereas dBest1 expression is rescued in a line in which the entire *dBest1* gene is reinserted into the genome of the dBest1 null fly(*λ5; dBest*$^{1\text{-}2}$). This experiment showed that both dBest1 knockout and p-element inserted mutant lines do not express detectable dBest1 protein, while dBest1 expression is successfully rescued in the *λ5; dBest*$^{1\text{-}2}$ line. We did not test the protein level for dBest2 and dBest3 because of the lack of antibody to these two bestrophin paralogs.

Given that many of these dBest1-enriched fly tissues, such as Malpighian tubules, crop, and hindgut have been implicated in electrolyte and fluid homeostasis and for osmoregulation (Dow *et al.*, 1994, O'Donnell *et al.*, 1998, Riegel *et al.*, 1999), it is

tempting to speculate that at least part of dBest1's role in the fly is to mediate osmoregulation by controlling Cl^- homeostasis. To explore the possible function of dBest1 in Cl^- homeostasis, we tested the ability of the *dBest1* mutant flies to survive on food containing significant levels of salt. As shown in Figure 5-5 A, dBest1 knockout flies displayed a profoundly reduced ability to survive on food prepared with 0.4M NaCl, with 80% of the flies dead after 7 days. Under these same conditions, wild-type flies did not exhibit significant mortality, and in fact can survive on salt concentrations as high as 0.6M ((Huang *et al.*, 2002), and data not shown). A similar high mortality as the dBest1 knockout flies was also observed in flies carrying the $dBest1^{c04106}$ insertion mutant allele of *dBest1*, with ~75% of the homozygotes died on the salty food after 7 days. The salt sensitivity caused by disruption of *dBest1* is fully rescued in the $\lambda 5;\ dbest1^{1-2}$ line, which exhibited the same degree of tolerance to dietary salt as the wild type fly.

To test whether the effect of dBest1 knockout was a direct effect of dBest1 expression or was related to other genes in the genetic background, flies were backcrossed to the wild type flies. Despite the fact that the dBest1 knockout line exhibited the salt sensitive phenotype, these flies lost their salt sensitivity once backcrossed to the wild type. This raises a doubt on the causal relationship between disruption of *dBest1* and the salt sensitivity, because the simplest explanation for the loss of the phenotype would be that the salt sensitivity is mediated by a second gene in the original background of these lines but not by dBest1. However, both the backcrossed $dBest1^{C04106}$ mutant line and the transheterozygous $dBest1^{1-2}/dBest1^{c04106}$ flies also exhibit significant mortality on 0.4M NaCl (data not shown). Moreover, dBest1 knockout and dBest1 C04106 mutant flies were generated in different genetic backgrounds and both exhibit salt sensitivity. These data

support a direct genetic relationship between defective dBest1 to the phenotype.

In contrast to their sensitivity to high salt, *dBest1* mutant flies were able to survive on food containing 0.8M sorbitol (Figure 5-6 B). This shows that the disruption of *dBest1* does not cause the fly to be generally osmosensitive, rather, the flies are specifically sensitive to salt, as might be expected to result from a defect in Cl^- transport.

Discussion

The data presented above demonstrate that dBest1 is expressed in the excretory tissues and the gonads of the adult fly. The elevated susceptibility to dietary salt in dBest1-null flies has elucidated an evident phenotype caused by defective bestrophins in intact animals for the first time. This phenotype has raised the possibility that dBest1 is involved in regulating Cl^- homeostasis in animals. Future experiments such as testing the fly viability on food containing Cl^- salts other than NaCl and Na^+ salts with different anions will help to establish a direct correlation between defective dBest1 to dysfunctional Cl^- homeostasis in the animal.

As mentioned above, the loss of phenotype in the backcrossed dBest1 knockout flies raised the concern that the phenotype was irrelevant to defective dBest1. Instead, the phenotype could likely be mediated by another gene. In fact, the dBest1 knockout flies were derived from a background stock with the mutant rosy eye-color, in which 90% of the structural gene for xanthine dehydrogenase is deleted (MacIntyre & O'Brien, 1976). It has been demonstrated that the xanthine oxidase activity is peroxisomal in the Malpighian tubule and the gut, tissues that contain abundant peroxisomes to maintain proper metabolism (Beard & Holtzman, 1987). Therefore, instead of defective dBest1, the mutant

rosy might be contributing to the phenotype in the dBest1 knockout line. The observation that the expressivity of the phenotype of dBest1 is sensitive to the background genetic component raised a possible explanation for the varied penetrance of Best Disease in human; whether carriers of mutant *hBest1* actually develop the disease may be partially determined by their genetic background. The enrichment of dBest1 in the excretory tissues of the adult fly together with the salt sensitive phenotype have prompted the speculation that dBest1 is important for the physiology of anion excretion. The Malpighian tubules and the hindgut together comprise the insect equivalent of a kidney and are important in osmoregulation. The tubules are composed of a single layer of secretory epithelial cells that are responsible for generating the primary urine, and the hindgut selectively reabsorbs water, ions, and desired solutes (Dow & Davies, 2006).

The Malpighian tubule is the most extensively investigated excretory organ in the fly and is one of the simplest epithelial model for the study of transport phenotypes in animals (Sozen *et al.*, 1997, Dow & Davies, 2006, Dow *et al.*, 1994). A great deal of effort has particularly been invested in characterizing both the mechanism of urine production by the Malpighian tubules and in identifying the regulation of fluid/osmolyte secretion by neuropeptides (Beyenbach, 2003, Beyenbach & Liu, 1996, Coast, 1996, Dow & Davies, 2003, O'Donnell & Spring, 2000). The diuretic agent leucokinin stimulates fluid secretion via activation of a CaC conductance at the plasma membrane of the tubule (O'Donnell *et al.*, 1996, O'Donnell *et al.*, 1998, Radford *et al.*, 2002, Blumenthal, 2003). The basolateral localization of dBest1 in the Malpighian tubule raises the possibility that dBest1 may mediate Cl^- transport in the tubules. Future experiments could aim at examining the causal relationship of dBest1 to the renal function in the tubules. These experiments could include

tissue-specific driving of dBest1 expression in the tubule to determine whether putting dBest1 back to the tubules could rescue the salt sensitivity, electrophysiological recording for Cl^- currents in the tubule cell isolated from dBest1 mutant lines to determine if dBest1 mediates this current, and urine secretion studies on the mutants to uncover the relationship of dBest1 to renal function.

Alternatively, the salt-sensitivity of flies with disrupted dBest1 could be due to dysfunction of Cl^- channels elsewhere, for example, in the hindgut. Therefore, it is also worthwhile to examine the role of dBest1 in tissues other than the tubules that are important in osmoregulation. Furthermore, dysfunctional dBest1 could lead to the phenotype by means other than affecting the Cl^- secretion. Alternatively, the phenotype could be caused by defective cell volume regulation or bicarbonate transport (Qu & Hartzell, 2008) in the dBest1 knockout fly. Whatever the ultimate explanation of our findings, this study identifies a phenotype associated with defective dBest1 in an animal model convenient for future genetic study.

Materials and Methods

Knockout and Mutant Flies

We used Canton S flies as the wild type fly. dBest1 knockout flies were made by excising the two P-elements that flank the dBest1 locus by transposase activity (Tavsanli *et al.*, 2001). P-element inserted mutant dBest1 line (*dBest1*^{C04106}) was made by insertion of a piggyback transposon into the fifth intron of the dBest1 gene. This mutant line was purchased from the Bloomington Fly Stock Center. The dBest1 rescued line (*λ5; dBest*$^{1\text{-}2}$) was made by reinsertion of a transposon containing an 18kb dBest1 genomic fragment into the genome of the dBest1 knockout fly, and this line is generated by Dr. Edward Blumenthal.

Real-Time PCR

Real-time PCR was performed on cDNA generated by reverse transcriptase of RNA isolated from tissues of adult fly using the SYBR Green method (Applied Biosystems). Detailed real-time PCR primer sequences are listed in table 5-1.

Western Blotting

Fly tissues (Malpighian tubules, brain, crop, testis, ovary, intestine, eye, fat body, and legs) were collected from both the wild type and dBest1 knockout adult flies. Tissues were homogenized by sonication in a lysis buffer containing (in mM) 150 NaCl, 5 EDTA, 50 Hepes pH7.2, and 1% Triton X. The sonicated samples were centrifuged with 15,000 rpm for 10 min to remove insoluble debris. Samples were loaded equally (25 μg or 5, 10, or 30 μl) for protein separation by SDS-PAGE. dBest1 protein was detected using the polyclonal

rabbit anti-dBest1 antibody at 1:5000 dilution ratio. 1:2000 goat polyclonal beta-tubulin antibody (Santa Cruz Inc.) was used for loading control for some of the experiments.

Immunofluorescent Staining of dBest1

Adult fly Malpighian tubules attached to the hindgut were isolated and fixed in 4 % paraformaldehyde in 0.2M phosphate buffer (pH 7.4) for 20 minutes at room temperature. The tissue was then permeablized for 20 minutes in 0.3 % Triton in PBS supplemented with 10 % normal goat serum. The permeablized tissue was labeled with the polyclonal dBest1 antibody (1:2000) containing 10 % goat serum and 8 % PBST for >16 hrs. at room temperature before washed extensively with 0.1 % PBST. The tissues were then incubated with a secondary antibody (anti-rabbit IgG Alexa 567, 1:1000, Invitrogen) for > 16 hrs at 4 °C. The tissue was washed and incubated in 0.5 % n-propyl gallate in glycerol at room temperature for an overnight before mounted with the same solution for confocal microscopy analysis.

Salt Sensitivity Test

Male flies that were 7 or fewer days after eclosion were selected for experiment. The fly food containing 0.4M NaCl was prepared by mixing appropriate amount of NaCl to the standard food recipe that contains 143 g/l cornmeal, 57 g/l yeast, 12 g/l agar, 143 ml/l molasses, 29 ml/l 10% methyl paraben, and 12 ml/l propionic acid. For control experiment, NaCl was replaced by 0.8M sorbitol. Each vial contained 20-30 male flies. The survival ratio of flies was counted on a daily basis for up to 30 days. Data were collected from 3 independent repeats and the fly survival ratio (%) is shown as mean $\pm$ SEM.

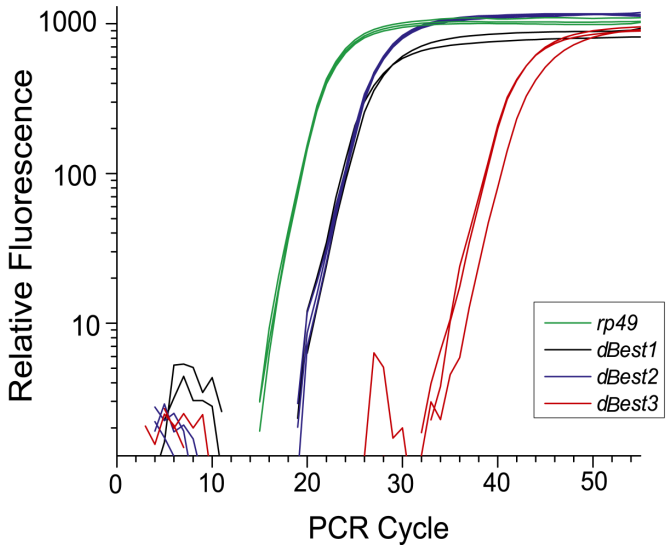

Figure 5-1: dBest1 is the most abundantly expressed bestrophin paralog in the adult fruit fly. Real-Time PCR was performed to quantify the relative expression level of *Drosophila* bestrophin paralogs. The wild type whole fly cDNA was used as template for real-time PCR analysis. In the whole fly, the mRNA level of dBest1 (black line) and dBest2 (blue line) are similar while dBest3 (red line) expression level is approximately 1.7 fold less than the levels of dBest1 and dBest2. Ribosomal protein rp49 (green line) is a housekeeping gene that is used as an internal control in the RT-PCR reaction.

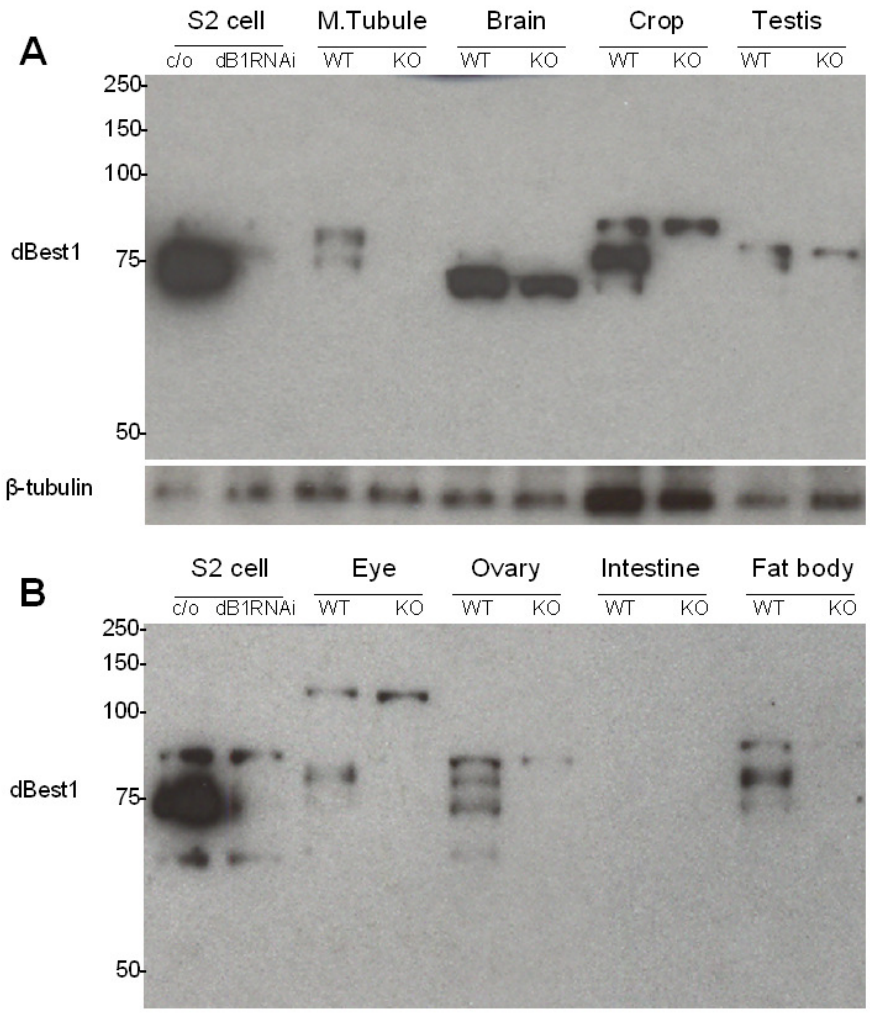

Figure 5-2: Expression profile of dBest1 protein in the *Drosophila melanogaster*. Approximately fifty wild type flies (Canton S) and dBest1 knockout flies (*dBest1*$^{1-2}$) were dissected and tissues were collected for western blotting. Equal amount (5 µg) of tissue lysates were loaded to the SDS gel and probed for dBest1 using polyclonal dBest1 antibody. WT: Canton S flies; KO: dBest1 knockout flies (*dBest1*$^{1-2}$).

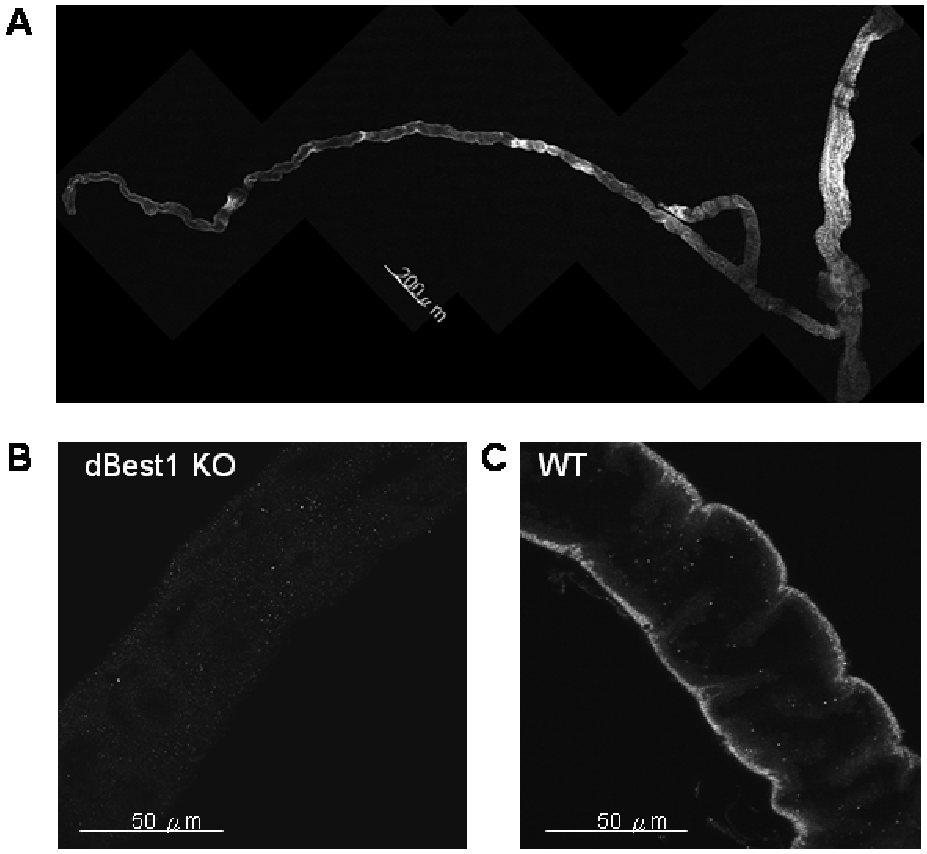

Figure 5-3: dBest1 protein is distributed in adult *Drosophila melanogaster* hindgut and the basolateral membrane of the Malpighian tubules. The tissue was dissected and labeled with polyclonal dBest1 antibody followed by a secondary antibody that is conjugated with green fluorescence. (A) The distribution of dBest1 signal under low magnification (20X). Images were taken along the entire renal tubule and the hindgut with the same exposure criteria by confocal microscopy and were aligned to reconstruct the original structure of the tissues with Photoshop. (B-C) The blow-up view of the Malpighian tubule at the initial bifurcated region. The tubules from a dBest1 knockout (*dBest1*$^{1-2}$) fly (B) and a wild type fly (Canton S) (C) were collected on the same day and processed in parallel. The images were taken with 100X oil lens by confocal microscopy.

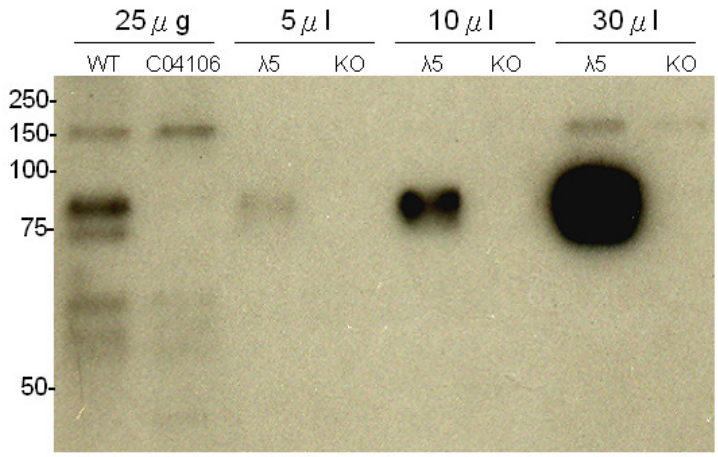

Figure 5-4: Expression of dBest1 in the adult *Drosophila* Malpighian tubules. Western blot for dBest1 protein in adult fly Malpighian tubules. Malpighian tubule extracts were collected from wild type flies (WT; Canton S), dBest1 mutant flies (C04106; $dBest1^{c04106}$), rescued dBest1 knockout flies ($\lambda 5$; $dBest1^{1-2}$), and dBest1 knockout flies (KO; $dBest1^{1-2}$). The tissue extract loading amount is indicated in the figure. dBest1 protein is 79 kDa in size.

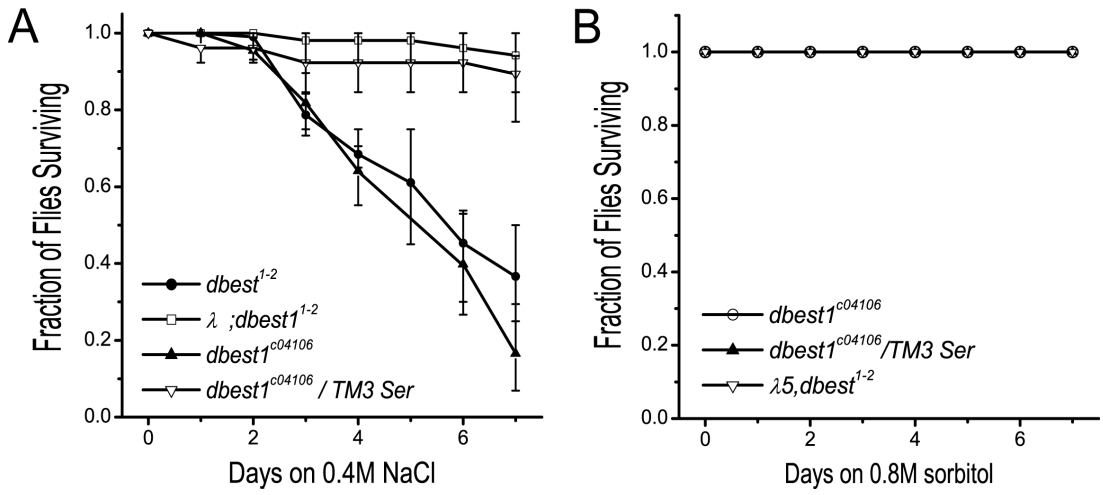

Figure 5-5: Salt sensitivity of *Drosophila* with dBest1 gene disrupted. The fly food was supplemented with 0.4M of NaCl or 0.8M of sorbitol. Male *Drosophila melanogasters* that were seven or fewer days after eclosion were selected for salt sensitivity test. Each vial contained 20 to 30 flies. The number of living flies was counted every 24 hours for up to one month. Fly survival fraction is the quotient of the number of living flies divided by the total number of flies in the vial, and the fractions of flies surviving during the first seven days are shown. (A) Survival of flies raised on food containing 0.4M NaCl. (B) Survival of flies raised on food containing 0.8 M sorbitol. Filled diamonds: dBest1 knockout flies (*dBest1*$^{1-2}$); filled circles: dBest1 mutant flies (*dBest1*^{c04106}); open triangles: rescued dBest1 knockout flies (*λ5; dBest1*$^{1-2}$); open squares: heterozygous mutant dBest1 flies (*dBest1*^{c04106}*/TM3 Ser*). Data are presented as mean $\pm$ S.E.M.

Table 5-1. Real-time PCR primer sequences.

Primer	Exon	Sequence	Product Size
dBest1	1	Forward: 5'-CGGCAACGAAAACGTAAAAT-3' Reverse: 5'-TGTGCATGTTGTTGTTGTGG-3'	197 bp
dBest2	2	Forward: 5'-ACAACAACAATTCGGCCTTC-3' Reverse: 5'-CTTCCAGAAACAGCCAAAGC-3'	201 bp
dBest3	4	Forward: 5'-CATGACGAAAAGCGAAGTCA-3' Reverse: 5'-CGGTCAAAGTCGTCCTTGTT-3'	240 bp
dBest4	1	Forward: 5'-CCGATGATAGAGCCAGGGTA-3' Reverse: 5'-GCAGAAAGCCAGCCTCAATA-3'	141 bp
rp49		Forward: 5'-AAGATCGTGAAGAAGCGCACCAA-3' Reverse: 5'-CTGTTGTCGATACCCTTGGGCTT-3'	101 bp

Acknowledgement

I especially thank our collaborator, Dr. Edward Blumenthal, for initiating the search for phenotypes caused by dBest1 mutation and for his openness in sharing his experimental results and ideas with us. I thank Jennifer Krueger for performing the whole fly real-time PCR. I also thank Yihan Yang and many of my dear TSA fellows at Georgia Institute of Technology in assisting the laborious fly count while I was on vacation. They have especially contributed in the identification of the optimal NaCl concentration and in the screening of the most salt-sensitive dBest1 mutant lines.

CHAPTER 6

DISCUSSION AND FUTURE DIRECTIONS

Summary of Findings

In this dissertation, I have extended our understanding of the molecular function and regulation of bestrophins in native cells by incorporating multi-disciplinary approaches including electrophysiology, molecular biology, biochemistry, and cell biology. In addition, my dissertation illuminates the field of bestrophin biology by demonstrating that the cell volume is regulated by dBest1. The findings presented in Chapters 2 to 5 demonstrate that:

1) Endogenous *Drosophila* bestrophin 1 is a Ca^{2+}-activated Cl^- channel.

2) dBest1 functions as a volume-regulated anion channel in *Drosophila* S2 cells.

3) dBest1 regulates cell volume homeostasis by mediating regulatory volume decrease.

4) dBest1 may play a role in osmoregulation by mediating Cl^- homeostasis in the fly.

In this chapter, I will address the significance of this work, provide a comparison between dBest1 CaC currents and typical CaC currents, compare between dBest1 VRAC currents and canonical VRAC currents, discuss the implications of these findings for understanding the molecular basis of Best Disease, and deliberate possible physiological roles of bestrophins in various types of tissues other than the eye. Finally I will provide a brief description of potential future directions.

Significance of the dissertation

In chapter 2, I demonstrate for the first time that bestrophins function as Ca^{2+}-activated Cl^- channels physiologically. The native CaC currents expressed by *Drosophila* S2 cells are abolished when bestrophins expression are silenced post-transcriptionally by interfering RNA. The combination of functional assessment and reverse genetic

approaches successfully bypassed the use of problematic pharmacological reagents for identifying Cl^- channels. In addition, cloning and expression of *Drosophila* bestrophin 1 in HEK cells induce Cl^- currents that recapitulate key phenotypic characteristics of the native S2 CaC currents. Moreover, mutations to a putative pore-lining amino acid of dBest1 altered the biophysical properties of the dBest1 Cl^- currents. Taken together, these findings have provided additional support to compliment previous studies of the function of vertebrate bestrophins as CaC channels and have successfully established a physiological cell model for future elucidations of the physiology of bestrophin.

The work presented in Chapter 3 further extends the regulatory mechanism from cytoplasmic Ca^{2+} to hyposmotic cell swelling. In addition to demonstrating the correlation between the native S2 CaC/VRAC currents and the expression of dBest1 protein by RNAi, I have provided evidence to confirm the specificity of the dBest1 RNAi by showing that both the CaC and VRAC currents are rescued by expressing dBest1 cDNA in S2 cells pre-treated with dBest1 RNAi. Furthermore, the data showing that the S2 cell regulatory volume decrease (RVD) is mediated by dBest1 illuminate the biological process that bestrophin is involved. These data together elicit a novel role for bestrophins in regulating cell volume and provide new testable hypothesis that implies VRAC channel dysfunction in the pathogenic mechanisms of Best Disease.

In Chapter 4, I have demonstrated that dBest1 is indeed a component of the ion conducting pore of the ion channel by demonstrating that many intrinsic biophysical properties of dBest1 current were altered if a putative pore-forming amino acid was mutated. The most dramatic outcome of all is the inversion of the ionic selectivity from anionic to cationic when negative charges were introduced to the site of F81. The dilution

potential experiment further provides a quantifiable comparison, which confirms the opposite ionic selectivity between the wild-type and $MTSES^-$-modified F81C current. These data suggest that the electrostatic effect at the site of or in the vicinity of residue F81 underlies the ionic selectivity of dBest1 Cl^- channel. Taken together, these findings provide substantial support that dBest1 is indeed an ion channel, but not just an essential auxiliary subunit or regulator of an endogenous Cl^- channel.

The preliminary data presented in Chapter 5 further extends the knowledge of dBest1 to intact organisms. In addition to characterizing the expression profile of dBest1 protein in adult flies, we have demonstrated the correlation between disrupted dBest1 expressions to increased adult fly mortality on food containing salt. This phenotype suggests a potential role of dBest1 in osmoregulation by mediating Cl^- homeostasis in intact animals. Overall, these studies provide important insights into the possible role of bestrophins in macular degeneration.

Comparison of dBest1 CaC and classical CaC Currents

CaC channels are transmembrane proteins that conduct Cl^- in response to elevated intracellular Ca^{2+}. Experimentally, CaC currents are stimulated by direct application of constant amounts of Ca^{2+} through the recording pipette, photoreleasing of caged Ca^{2+}, increasing Ca^{2+} release from intracellular storage by IP_3, or by enhancing Ca^{2+} entry by application of Ca^{2+} ionophores (Arreola *et al.*, 1996, Evans & Marty, 1986, Giovannucci *et al.*, 2002, Hartzell, 1996, Kuruma & Hartzell, 2000, Nilius *et al.*, 1997b, Okada *et al.*, 1995). The classical vertebrate CaC current displays an anion selectivity sequence of $SCN^- > NO_3^- > I^- > Br^- > Cl^- > F^-$ (Evans & Marty, 1986, Kidd & Thorn, 2000, Large & Wang,

1996, Nilius *et al.*, 1997b). The CaC currents mediated by bestrophins exhibit similar anionic permeation sequence (Qu *et al.*, 2004). The comprehensively studied vertebrate CaC current is outwardly-rectifying (voltage-dependent) and activates at positive voltages in a time-dependent manner at low levels (<1 μ M) of $[Ca^{2+}]_i$ and becomes time- and voltage-independent when $[Ca^{2+}]_i$ is saturating (Kuruma & Hartzell, 2000).

Unlike the classical vertebrate CaC currents and mBest2 currents that exhibit linear current-voltage relationship when intracellular $[Ca^{2+}]$ is saturating (Arreola *et al.*, 1996, Evans & Marty, 1986, Kuruma & Hartzell, 2000, Qu *et al.*, 2004), dBest1 macroscopic CaC currents display slight voltage-dependence at $\pm$ 100 mVs (Chien & Hartzell, 2007). hBest1 current is slightly outwardly-rectifying (Sun *et al.*, 2002, Tsunenari *et al.*, 2003).A few of the other bestrophins including hBest3, hBest4 and *Caenorhabditis elegans* bestrophin 1 exhibit Cl^- currents that are both time- and voltage- dependent (Sun *et al.*, 2002, Tsunenari *et al.*, 2003). These findings demonstrate that there is heterogeneity in channel kinetics among bestrophins (Tsunenari *et al.*, 2006). This heterogeneity in voltage dependence among bestrophins implies heterogeneity in the gating mechanism for each bestrophin homolog.

Among all bestrophins and other CaC channels that have been studied so far, seldom has a CaC current been examined at both macroscopic and single channel levels. The CaC current encoded by dBest1 is an exception. Single channel analysis of endogenous dBest1 channel elicits a linear I-V relationship (voltage independence), whereas the macroscopic dBest1 current exhibits a sigmoidal I-V relationship. This difference suggests that the sigmoid nature of the macroscopic dBest1 current is related to channel gating (Chien *et al.*, 2006). In addition, the activation rate for both macroscopic and single channel dBest1

currents is similar, both required minutes for full channel activation. This implies an indirect activation mechanism by Ca^{2+}, probably through a Ca^{2+}-dependent kinase pathway as mentioned below. Moreover, the single channel conductance of dBest1 currents is estimated to be 2 pS, which is very similar to a subset of CaC channels that have been described in cardiac myocytes (Collier *et al.*, 1996), arterial smooth muscle (Hirakawa *et al.*, 1999, Klockner, 1993, Piper & Large, 2003), A6 kidney cells (Marunaka & Eaton, 1990), endocrine cells (Taleb *et al.*, 1988), and *Xenopus* oocytes (Takahashi *et al.*, 1987).

The detailed mechanism of the slow run-up of dBest1 current is not fully understood. Our data suggest that phosphorylation is involved in regulating the dBest1 current. In brief, the activation of dBest1 CaC current is accelerated when ATP is applied to the cytoplasm of S2 cells in addition to Ca^{2+}. Conversely, when ATP is introduced in the absence of Ca^{2+}, dBest1 CaC current does not activate. In addition, kinase inhibitors suppress dBest1 CaC currents, whereas phosphatase inhibitors bypassed the slow run-up. These results indicate that Ca^{2+} is a pre-requisite for dBest1 activation and that the slow run-up of dBest1 CaC currents might involve an indirect action of Ca^{2+}, probably through a Ca^{2+}-sensitive kinase pathway such as CaMKII. Indirect activation of CaC currents by the Ca^{2+} through CaMKII has been shown in cells from the human colonic tumor cell line T84 (Chan *et al.*, 1994, Kaetzel *et al.*, 1994, Worrell & Frizzell, 1991, Xie *et al.*, 1998), airway epithelia (Wagner *et al.*, 1991), T lymphocytes (Nishimoto *et al.*, 1991), human macrophages (Holevinsky *et al.*, 1994), biliary epithelial cells (Schlenker & Fitz, 1996), and cystic fibrosis-derived pancreatic epithelial cells (Chao *et al.*, 1995) by the use of inhibitors of calmodulin or CaMKII or by cell dialysis with the purified enzyme. Our preliminary analysis also implied a similar indirect activation mechanism because dBest1 CaC current was prevented from

activating by pre-treating the S2 cell with a CaMKII inhibitor. More efforts are required to fully elucidate the regulatory factors and the exact signaling pathway that activate dBest1 current.

Comparison of dBest1 VRAC and canonical VRAC

VRAC channels belong to the group of transporters that activates when cell volume deviates from its steady state volume. The canonical VRAC current is outwardly-rectifying (voltage-dependent), inactivates at positive potentials in a time-dependent manner, and is stimulated by different maneuvers including hyposmotic swelling, membrane stretching, inflation by positive pressure, shear stress, reduction of intracellular ionic strength, and intracellular application of GTPγS (Nilius *et al.*, 1997a, Sorota, 1992, Sorota, 1995, Sorota & Du, 1998, Tseng, 1992). The classical VRAC channel exhibits an anion selectivity sequence of $SCN^- > I^- > NO_3^- > Br^- > Cl^- >$ gluconate$^-$ (Nilius *et al.*, 1996, Okada, 1997, Strange *et al.*, 1996). This sequence is very similar to what was described for bestrophins (Qu et al., 2004). At the single channel level, both endogenous and heterologously expressed dBest1 exhibit a single channel conductance of ~ 2pS (Chien *et al.*, 2006). This is very similar to the single channel conductance of VRAC currents in endothelial cells, neutrophils, chromaffin cells, and T lymphocytes by stationary noise analysis (Nilius *et al.*, 1997a).

Unlike many VRAC currents that are outwardly rectifying and inactivate at positive potentials, dBest1 currents exhibit relatively little to slight outward rectification and inactivates only slightly at positive potentials. However, VRACs' dependence on voltage and time seems to depend on the recording conditions, the cell type, and the differentiation

state of the cells (Tseng, 1992). For example, in endothelial cells, parotid acinar cells, T lymphocytes neutrophils, skate hepatocytes, rabbit ventricular cardiomyocytes (Jalonen, 1993), apical membranes of cultured renal cortical collecting tubule cells (RCCT-28A) (Schwiebert *et al.*, 1994), neuroblastoma cells (Falke & Misler, 1989), dog atrial myocytes (Sorota, 1992, Tseng, 1992), *Xenopus* oocytes (Souktani *et al.*, 2000), and rat microglial cells, inactivation is small or even completely absent. Our measurements of VRAC currents in adult mouse peritoneal macrophages and in newborn mouse microglial cells (data not shown) also exhibit subtle voltage- and time- dependence.

dBest1 VRAC currents in S2 cells can activate independently of intracellular Ca^{2+} (Chien & Hartzell, 2007). This is consistent with previous reports that showed that the activation of VRAC does not require an increase of cytoplasmic Ca^{2+} in some types of cell (Doroshenko & Neher, 1992, Hazama & Okada, 1988). However, dBest1 VRAC current can be potentiated by Ca^{2+}_i. This is similar to some reports that show a low level (~50-100 nM) of cytoplasmic Ca^{2+} is required for fully activation of VRAC channels (Altamirano *et al.*, 1998, Chen *et al.*, 2007, Nilius *et al.*, 1997a, Park *et al.*, 2007, Szucs *et al.*, 1996). One example is hBest1 has an EC_{50} for Ca^{2+} of ~150 nM, which is very close to the permissive level for VRAC activation.

Despite the finding that dBest1 can be activated by elevated cytoplasmic Ca^{2+} without cell swelling and by cell swelling in nominally zero Ca^{2+} condition, it is still possible that these two activation mechanisms can converge at some point. An example is the VRAC in astrocytes. In astrocytes, sub-micromolar of cytoplasmic Ca^{2+} is required to activate VRAC channels (Mongin & Kimelberg, 2005). This Ca^{2+}-dependence is further supported by the demonstration that the VRAC activity is blocked by intracellular application of Ca^{2+}

chelator. Furthermore, VRAC channels in these cells are also subjected to regulations by phosphorylation through a Ca^{2+}-dependent pathway because application of calmodulin inhibitors suppressed the astrocyte VRAC activity (Mongin & Kimelberg, 2005, Takano *et al.*, 2005). It remains to be characterized the detailed interplay of cell swelling and Ca^{2+} in activating dBest1 Cl^- currents.

Despite our highly compelling data showing that dBest1 is the VRAC channel in *Drosophila* S2 cells, mouse bestrophins do not seem to constitute the VRAC family in peritoneal macrophages and microglial cells. Because VRACs are ubiquitously expressed, one might expect that bestrophins would be ubiquitously expressed. However, the expression pattern of bestrophins has not yet been fully characterized. Publicly available microarray and electronic Northern database (www.genecards.org) are limited, and published reports on bestrophin expression profile determined by RT-PCR, Northern, and immuno-blotting or immuno-staining do not often agree with one another (Hartzell *et al.*, 2008). At this point in time, the most conservative interpretation is that bestrophins belong to one of many different kinds of VRAC channels (Lang *et al.*, 1998, Nilius *et al.*, 1996, Strange *et al.*, 1996) that play a role in cell volume regulation.

Implications for Best Disease

Best Disease patients exhibit defect EOG component that reflects a Ca^{2+}-sensitve Cl^- conductance (Joseph & Miller, 1992, Ueda & Steinberg, 1994), and most disease-causing mutations in hBest1 affect the Cl^- channel function. The most straightforward interpretation, therefore, is that Best Disease is a Cl^- channelopathy resulting from dysfunctioning hBest1. Other lines of evidence have depicted the restricted distribution of

hBest1 in plasma membrane of the REP cells in the eye (Marmorstein *et al.*, 2000). These comprehensive analyses of the Cl^- conducting function of bestrophins and the specified distribution of bestrophins in the RPE cells together have resulted in the hypothesis that bestrophins are crucial for the function and survival of photoreceptors, such as maintaining the optimal RPE-retina interface by modulating electrolyte composition and the hydration status in the sub-retinal microenvironment.

The RPE is a highly specialized single layer of epithelial cells that lies adjacent to the photoreceptor outer segments in the retina. The RPE plays a central role in retinal homeostasis (Strauss, 2005) and in regulating the microenvironment surrounding the photoreceptors in the outer retina, where the events of photo-transduction take place. Critical functions of the RPE that contribute to these process include control of the volume and composition of the fluid in the subretinal space by mediating the transport of ions, fluid, and metabolites (Adorante & Miller, 1990, Bialek & Miller, 1994, Hughes *et al.*, 1987, Hughes *et al.*, 1984, Kenyon *et al.*, 1994, la Cour *et al.*, 1994), maintaining the vital turnover of the photosensitive membrane of photoreceptor outer segment discs by phagocytosis (Besharse *et al.*, 1982, LaVail, 1983, Nguyen-Legros & Hicks, 2000), mediating vitamin A transport and metabolism (the retinoid or visual cycle of visual pigment regeneration) (Bok, 1990, Chader, 1989, Rando, 1992, Saari & Bredberg, 1990), and providing the "retinal-blood barrier" to protect the retina from exposure to substances that leak out from the choroidal vessels (Marmor & Dalal, 1993, Marmor & Yao, 1994, Pederson & Cantrill, 1984, Tsuboi, 1990).

Bestrophins have been shown to act directly as a CaC channel, to exhibit sensitivity to changes in cell volume, and to modulate other kinds of ion channel (Chien & Hartzell,

2007, Chien *et al.*, 2006, Fischmeister & Hartzell, 2005, Hartzell *et al.*, 2008, Marmorstein *et al.*, 2006, Qu *et al.*, 2004, Qu *et al.*, 2003, Rosenthal *et al.*, 2006, Sun *et al.*, 2002, Tsunenari *et al.*, 2003, Yu *et al.*, 2008). These properties of bestrophins could possibly underlie many of the physiological functions of the RPE described above. In addition, a defective RPE Cl^- transport function may also underlie the prominent lipofuscin deposition in the subretinal space in Best Disease patients. A direct link between dysfunctioning bestrophin to lipofuscin formation is proposed based on the findings obtained from a choroidal melanoma cancer patient. With normal hBest1 gene, this patient still developed, Best Disease associated EOG manifestations and lipofuscin deposition in the macula. Interestingly, auto-antibodies to hBest1 were also discovered from this patient (Eksandh *et al.*, 2008). The result of auto-antibodies to hBest1 would be expected to cause a loss of hBest1 function. Therefore, it is intriguing to speculate that the formation of lipofuscin in Best Disease patients is at least partly caused by dysfunctioning hBest1. Indirect evidences that link the defective Cl^- channel activity to lipofuscin formation arise from the findings that the lipofuscin-like material is accumulated in the brain of animals that are null of some types of ClC channels (Cooper *et al.*, 2006, Hartzell *et al.*, 2005b, Kasper *et al.*, 2005, Poet *et al.*, 2006, Steward, 2003, Yoshikawa *et al.*, 2002). Lipofuscin deposition in the subretinal space could possibly interfere with the visual ability by weakening the photoreceptor-REP interface. Therefore, it is possible that part of RPE dysfunction in Best Disease might involve abnormal RPE transport function.

The discovery that bestrophins is a subfamily of the VRAC channel has provided another platform for more testable hypothesis. We have previously shown that RPE expresses a volume-sensitive Cl^- current that is in many aspects resembles bestrophin

currents (Fischmeister & Hartzell, 2005), and other investigators have demonstrated that RPE cells possess the appropriate ion channel and transport machineries to respond to hyposmotic cell swelling by regulatory volume decrease or hyperosmsotic cell shrinkage (Adorante, 1995, Civan *et al.*, 1994, Kennedy, 1994, La Cour & Zeuthen, 1993). RPE cells are subjected to stimuli such as changes in ionic composition and phagocytosis of shed photoreceptor outer discs that would induce deviations to the steady state cell volume. The involvement of VRAC channel in both cell volume regulation and phagocytosis is apparent because phagocytosis is often accompanied by a large change in cell volume (Bos & de Souza, 2001). Bestrophins could possibly mediate osmolyte efflux to compensate for phagocytosis-induced cell volume increase as described previously in other cell type (Warskulat *et al.*, 1996). This hypothesis is supported by the finding that the release of cell volume homeostasis-relevant organic osmolyte such as betaine, taurine, and inositol during phagocytosis is inhibited by the application of Cl^- channel blockers (Wettstein *et al.*, 2000). In addition, phagocytosis requires the cell volume to be optimally controlled, because phagocytosis is greatly suppressed when cells shrink (Warskulat *et al.*, 1996). Taken together, it is tempting to speculate that at least part of the pathogenic mechanism of Best Disease involves altered RPE cell volume regulation and/or defective phagocytosis as a consequence of altered bestrophin VRAC channel function.

Similar to the function of CaC channels, VRAC channels can also mediate Cl^- transport. VRAC channels have been reported to mediate vectorial Cl^- transport and salt and fluid secretion in RPE and in other polarized cells (Hoffmann & Dunham, 1995, McEwan *et al.*, 1993, Strange *et al.*, 1996, Zhang & Jacob, 1997, Strange, 1992). Therefore, similar to the proposed pathogenic model by defective hBest1 CaC activity, it is also

tempting to speculate that a portion of the pathogenic mechanism of Best Disease might involve altered RPE transport function resulted from defective hBest1 VRAC channel function.

In addition, it is known that various types of plasma membrane Cl^- channels can also mediate intracellular pH regulation (Eggermont *et al.*, 2001, Nilius *et al.*, 1997a). Phagocytic cells like RPE have prominent acidic lysosome compartments that require the import of intracellular Cl^- channels to neutralize the proton. Because a portion of bestrophins locates in the intracellular compartment, defective bestrophins function may also underlie Best Disease by affecting intracellular pH regulation.

Possible roles of bestrophins in other cell types

Although bestrophins' roles as CaC and VRAC channels provide intriguing platforms for testable hypothesis for the pathogenic of Best Disease, the attempts at understanding the mechanism by which hBest1 mutations cause Best Disease have been complicated because both mBest1 knockout mice and dBest1 knockout flies do not display visual deficit or retinal pathology (Marmorstein *et al.*, 2006, Tavsanli *et al.*, 2001). Efforts have already been extended to the understanding of the physiological processes that bestrophin are involved in tissues other than the eye.

One of the physiological processes that CaC channels are involved in is olfactory transduction. Binding of olfactory molecules to olfactory receptors on the cilia of olfactory sensory neurons (OSNs) induces an increase in cytoplasmic Ca^{2+} by Ca^{2+} entry from the cyclic nucleotide-gated channel (CNG). The degree of depolarization is then amplified by the Cl^- efflux through CaC channels. Piferri *et al.* has demonstrated that mBest2 is

expressed in the OSNs and that mBest2 co-localizes with the principle CNG channel in the cilia of OSNs (Pifferi *et al.*, 2006). At the functional level, a great majority of the electrophysiological properties including anionic selectivity sequence, single channel conductance, rectification ratio, and sensitivity to Cl^- channel blockers of the CaC current in the OSN resemble the CaC current induced by mBest2 in HEK cells. Therefore, the authors concluded that mBest2 comprises the molecular component of the CaC channel in the OSNs. Despite the compelling conclusion drawn from this report, the Ca^{2+} sensitivity between the native and over-expressed mBest2 current differs an order of magnitude. Similar as native CNG channels (Kaupp & Seifert, 2002), OSN mBest2 channels may be composed of additional proteins. The major limitation of this report is the lack of direct evidence showing that the OSN endogenous CaC current is indeed mediated by mBest2. A detailed investigation on the OSN CaC current and the olfactory function in mBest2 knockout animal is worth elucidating in the future in order to provide definitive support to the conclusion that mBest2 is the CaC channel that mediates olfactory transduction.

Another important function of CaC channels is fluid secretion. Ca^{2+}-activated Cl^- secretion pathways have been described in a variety of cells including salivary gland and airway and colonic epithelial cells (Hartzell *et al.*, 2005a). Recently, Sorria *et al.* showed that endogenous CaC currents coincide with the native expression of mBest1 and hBest1 in various types of cells from airway, kidney, and colon (Barro Soria *et al.*, 2006, Kunzelmann *et al.*, 2007). They have also shown that both the protein level of hBest1 and the native CaC currents induced by extracellular application of ATP are suppressed by hBest1 small interference RNAi treatment in colonic cancer cell line HT29. Therefore, the authors conclude that bestrophins enable Ca^{2+}-activated Cl^{2+} conduction in epithelial cells.

It remains to be studied in the future to test if bestrophins mediate secretion in animals.

Bestrophins have also been implicated in mediating homeostatic cell volume regulation and phagocytosis in microglia (brain immune cells). The shape and volume of microglia change during brain inflammation and become migratory and phagocytic (Eder *et al.*, 1998, Rappert *et al.*, 2002). Ducharme *et al.* identified that the expression of four mBests parallels the VRAC currents in rat microglial culture (Ducharme *et al.*, 2007). The microglial VRAC currents exhibit various key characteristics similar to bestrophin currents, including volume sensitivity (Chien & Hartzell, 2007, Fischmeister & Hartzell, 2005), voltage-independence (Fischmeister & Hartzell, 2005, Qu *et al.*, 2004), halide permeability sequence of $I^- > Br^- > Cl^-$ (Pifferi *et al.*, 2006, Qu *et al.*, 2004), single channel conductance of ~2 pS (Chien *et al.*, 2006), and sensitivity to pharmacological blockers such as SITS (4-acetamido- 4'isiothiocyanostilbene-2,2'-disulphonic acid) and DIDS (Pifferi *et al.*, 2006, Sun *et al.*, 2002). These data suggest that bestrophins are mediating regulatory volume decrease (RVD), homeostatic cell volume regulation, and phagocytosis in the central nervous system. Direct correlations between the expression of bestrophins and the Cl^- channel phenotypes still await to be described.

A recent study on a colonic cancer cell line that exhibits accelerated cell proliferation rate and loss of cell polarity and contact inhibition has suggested novel roles for bestrophins in cell proliferation (Spitzner *et al.*, 2008). Spitzner *et al.* discovered an association between up-regulation of hBest1 expression level and Ca^{2+}-activated Cl^- currents. Functionally, the increased level of hBest1 and CaC currents coincide with the cancerous proliferation phenotype. Data that demonstrate the direct contribution of bestrophins to cell proliferation await to be depicted.

Given the often numerous Cl^- candidate genes in many types of cells, the poor pharmacological reagents available, and the often inefficient RNAi-mediated gene silencing in primary cultures, it has been difficult to ascribe a specific physiological function to a certain type of Cl^- channel. Therefore, it seems that bestrophin knockout animals are indispensable for future studies to provide definitive confidence that bestrophins are involved in these different physiological processes mentioned above.

Possible roles for bestrophins other than conducting Cl^-

Despite the definitive evidence presented in Chapter IV that led to the conclusion that dBest1 is a substantial Cl^- conducting ion channel, bestrophins' roles as Cl^- channels have been challenged. The existence of CaC currents in the RPE of mBest1 knockout mice (Marmorstein *et al.*, 2006) has served as the most compelling argument for some investigators to question the role of hBest1 as a CaC channel (Marmorstein *et al.*, 2004, Marmorstein *et al.*, 2006, Rosenthal & Brown, 2007). This observation together with the finding that hBest1 can regulate voltage-gated Ca^{2+} channels in RPE cell lines (Rosenthal & Brown, 2007) and in HEK cells (Yu *et al.*, 2008) have led to the suggestion that hBest1 is not a Cl^- channel but rather is a regulator of cation channels (Marmorstein *et al.*, 2006).

Perhaps bestrophins belong to those Cl^- channels that also serve functions other than conducting Cl^-. In fact, bestrophins is not the only Cl^- channel that exhibit functions other than conducting Cl^-. CFTR Cl^- channel (cystic fibrosis transmembrane conductance regulator) is another example. Mutations in CFTR lead to hereditary cystic fibrosis in which deficit in the exocrine function in the lung, liver, pancreas, and intestine causes thick mucus production followed by incompetent immune function. In fact, comparing CFTR

with bestrophins reveal several significant parallels. First of all, CFTR is clearly a Cl^- channel (Bear *et al.*, 1992), but it also regulates other plasma membrane transport proteins, including the epithelial Na^+ channel (ENaC) (Mall *et al.*, 2004, Mehta, 2005, Schwiebert *et al.*, 1999). Secondly, CFTR knockout mice do not exhibit any lung pathology as expected. This is partly because other Cl^- channels in the lung subserve the role of CFTR (Grubb & Boucher, 1999, Kowdley *et al.*, 1994, Mall *et al.*, 2004). Last but not least, disease-causing mutations are described to scatter both the CFTR (1525 mutations) and bestrophin (100 mutations) genes.

Like CFTR, bestrophins may also exhibit regulatory roles to other transport machinery in addition to conducting Cl^-. It remains to be examined whether the macular degeneration caused by mutations in hBest1 can be solely attributed to the loss of Cl^- channel activity of bestrophins or whether, like CFTR, other functions come into play (Hartzell *et al.*, 2008).

Conclusion and Future Direction

Our comprehensive analysis described in Chapters 2 to 5 together have substantiated the molecular function of dBest1 and have elicited the cellular process that dBest1 is regulating. At the molecular level, our analysis of the molecular function of dBest1 revealed clearly that dBest1 is a Cl^- channel that is dually regulated by cytoplasmic Ca^{2+} and by hyposmotic cell swelling (Chien & Hartzell, 2007, Chien *et al.*, 2006). At the cellular level, activated dBest1 current is mediating regulatory volume decrease to maintain homeostatic volume. In adult flies, lack of dBest1 protein expression is associated with a salt sensitive phenotype, which may be explained by a dysregulated Cl^- homeostasis.

Two weeks after I've finished writing my thesis, two independent articles describing the identification of the TMEM16A protein as a new family of Cl^- channels are published (Caputo *et al.*, 2008, Yang *et al.*, 2008). When expressed in HEK cell, the TMEM16A protein induces a Ca^{2+}-activated Cl^- current with a single channel conductance of 8.5 pS. The phenotype of the current as well as the ionic permeability was changed when conserved positively charged amino acids in the putative TM5 and 6 were mutated to glutamate. Both the biophysical properties and the pharmacological profile of the current mediated by TMEM16A are in full agreement with native CaC currents. In addition, TMEM16A is distribute in tissues in which endogenous CaC currents have been reported previously. These tissues include various secretory epithelia (in lung, kidney, pancreas, and submandibular gland) and the neuron in the retina and in the dorsal root ganglion. Moreover, knocking down the TMEM16A in mouse by RNAi markedly reduced both the CaC currents and the production of saliva in the salivary gland. These data together have provided strong evidence that TMEM16A encodes the classical CaC channels. The identification of a novel protein as the long sought classical CaC channels is inspiring. It is tempting to study in the future if bestrophins have any interaction with this new family of CaC channels, or these two channels contribute to different aspects of Ca^{2+}-activated Cl^- flux in different types of signaling pathways or cells.

REFERENCE

Ackerman, M.J., Wickman, K.D. & Clapham, D.E. (1994) Hypotonicity activates a native chloride current in Xenopus oocytes. *J Gen Physiol,* 103**,** 153-79.

Adorante, J.S. (1995) Regulatory volume decrease in frog retinal pigment epithelium. *Am J Physiol,* 268**,** C89-100.

Adorante, J.S. & Miller, S.S. (1990) Potassium-dependent volume regulation in retinal pigment epithelium is mediated by Na,K,Cl cotransport. *J Gen Physiol,* 96**,** 1153-76.

Akabas, M.H., Stauffer, D.A., Xu, M. & Karlin, A. (1992) Acetylcholine receptor channel structure probed in cysteine-substitution mutants. *Science,* 258**,** 307-10.

Allikmets, R., Seddon, J.M., Bernstein, P.S., Hutchinson, A., Atkinson, A., Sharma, S., Gerrard, B., Li, W., Metzker, M.L., Wadelius, C., Caskey, C.T., Dean, M. & Petrukhin, K. (1999) Evaluation of the Best disease gene in patients with age-related macular degeneration and other maculopathies. *Hum Genet,* 104**,** 449-53.

Altamirano, J., Brodwick, M.S. & Alvarez-Leefmans, F.J. (1998) Regulatory volume decrease and intracellular Ca2+ in murine neuroblastoma cells studied with fluorescent probes. *J Gen Physiol,* 112**,** 145-60.

Anderson, J.W., Jirsch, J.D. & Fedida, D. (1995) Cation regulation of anion current activated by cell swelling in two types of human epithelial cancer cells. *J Physiol,* 483 (Pt 3)**,** 549-57.

Andre, S., Boukhaddaoui, H., Campo, B., Al-Jumaily, M., Mayeux, V., Greuet, D., Valmier, J. & Scamps, F. (2003) Axotomy-induced expression of calcium-activated chloride current in subpopulations of mouse dorsal root ganglion neurons. *J Neurophysiol,* 90**,** 3764-73.

Arellano, R.O. & Miledi, R. (1995) Functional role of follicular cells in the generation of osmolarity-dependent Cl- currents in Xenopus follicles. *J Physiol,* 488 (Pt 2)**,** 351-7.

Arreola, J., Begenisich, T., Nehrke, K., Nguyen, H.V., Park, K., Richardson, L., Yang, B., Schutte, B.C., Lamb, F.S. & Melvin, J.E. (2002) Secretion and cell volume regulation by salivary acinar cells from mice lacking expression of the Clcn3 Cl- channel gene. *J Physiol,* 545**,** 207-16.

Arreola, J., Melvin, J.E. & Begenisich, T. (1996) Activation of calcium-dependent chloride channels in rat parotid acinar cells. *J Gen Physiol,* 108**,** 35-47.

Asmild, M. & Willumsen, N.J. (2000) Chloride channels in the plasma membrane of a foetal Drosophila cell line, S2. *Pflugers Arch,* 439**,** 759-64.

Attali, B., Guillemare, E., Lesage, F., Honore, E., Romey, G., Lazdunski, M. & Barhanin, J. (1993) The protein IsK is a dual activator of K+ and Cl- channels. *Nature,* 365**,** 850-2.

Bader, C.R., Bertrand, D. & Schlichter, R. (1987) Calcium-activated chloride current in cultured sensory and parasympathetic quail neurones. *J Physiol,* 394**,** 125-48.

Bader, C.R., Bertrand, D. & Schwartz, E.A. (1982) Voltage-activated and calcium-activated currents studied in solitary rod inner segments from the salamander retina. *J Physiol,* 331**,** 253-84.

Bakall, B., Marknell, T., Ingvast, S., Koisti, M.J., Sandgren, O., Li, W., Bergen, A.A., Andreasson, S., Rosenberg, T., Petrukhin, K. & Wadelius, C. (1999) The mutation spectrum of the bestrophin protein--functional implications. *Hum Genet,* 104**,** 383-9.

Bakall, B., Marmorstein, L.Y., Hoppe, G., Peachey, N.S., Wadelius, C. & Marmorstein, A.D. (2003) Expression and localization of bestrophin during normal mouse development. *Invest Ophthalmol Vis Sci,* 44**,** 3622-8.

Bakall, B., Mclaughlin, P., Stanton, J.B., Zhang, Y., Hartzell, H.C., Marmorstein, L.Y. & Marmorstein, A.D. (2008) Bestrophin-2 is involved in the generation of intraocular pressure. *Invest Ophthalmol Vis Sci,* 49**,** 1563-70.

Banderali, U. & Ehrenfeld, J. (1996) Heterogeneity of volume-sensitive chloride channels in basolateral membranes of A6 epithelial cells in culture. *J Membr Biol,* 154**,** 23-33.

Banderali, U. & Roy, G. (1992) Activation of K+ and Cl- channels in MDCK cells during volume regulation in hypotonic media. *J Membr Biol,* 126**,** 219-34.

Barish, M.E. (1983) A transient calcium-dependent chloride current in the immature Xenopus oocyte. *J Physiol,* 342**,** 309-25.

Barnes, S. (1994) After transduction: response shaping and control of transmission by ion channels of the photoreceptor inner segments. *Neuroscience,* 58**,** 447-59.

Barnes, S. & Bui, Q. (1991) Modulation of calcium-activated chloride current via pH-induced changes of calcium channel properties in cone photoreceptors. *J Neurosci,* 11**,** 4015-23.

Barnes, S. & Hille, B. (1989) Ionic channels of the inner segment of tiger salamander cone photoreceptors. *J Gen Physiol,* 94**,** 719-43.

Barro Soria, R., Spitzner, M., Schreiber, R. & Kunzelmann, K. (2006) Bestrophin 1 enables Ca2+ activated Cl- conductance in epithelia. *J Biol Chem*.

Bass, R.B., Strop, P., Barclay, M. & Rees, D.C. (2002) Crystal structure of Escherichia coli MscS, a voltage-modulated and mechanosensitive channel. *Science,* 298**,** 1582-7.

Bear, C.E., Li, C.H., Kartner, N., Bridges, R.J., Jensen, T.J., Ramjeesingh, M. & Riordan, J.R. (1992) Purification and functional reconstitution of the cystic fibrosis transmembrane conductance regulator (CFTR). *Cell,* 68**,** 809-18.

Beard, M.E. & Holtzman, E. (1987) Peroxisomes in wild-type and rosy mutant Drosophila melanogaster. *Proc Natl Acad Sci U S A,* 84**,** 7433-7.

Begenisich, T. & Melvin, J.E. (1998) Regulation of chloride channels in secretory epithelia. *J Membr Biol,* 163**,** 77-85.

Besharse, J.C., Dunis, D.A. & Burnside, B. (1982) Effects of cyclic adenosine 3',5'-monophosphate on photoreceptor disc shedding and retinomotor movement. Inhibition of rod shedding and stimulation of cone elongation. *J Gen Physiol,* 79**,** 775-90.

Beyenbach, K.W. (2003) Regulation of tight junction permeability with switch-like speed. *Curr Opin Nephrol Hypertens,* 12**,** 543-50.

Beyenbach, K.W. & Liu, P.L. (1996) Mechanism of fluid secretion common to aglomerular and glomerular kidneys. *Kidney Int,* 49**,** 1543-8.

Bialek, S. & Miller, S.S. (1994) K+ and Cl- transport mechanisms in bovine pigment epithelium that could modulate subretinal space volume and composition. *J Physiol,* 475**,** 401-17.

Birmingham, A., Anderson, E.M., Reynolds, A., Ilsley-Tyree, D., Leake, D., Fedorov, Y., Baskerville, S., Maksimova, E., Robinson, K., Karpilow, J., Marshall, W.S. & Khvorova, A. (2006) 3' UTR seed matches, but not overall identity, are associated with RNAi off-targets. *Nat Methods,* 3**,** 199-204.

Blodi, C.F. & Stone, E.M. (1990) Best's vitelliform dystrophy. *Ophthalmic Paediatr Genet,* 11**,** 49-59.

Blumenthal, E.M. (2003) Regulation of chloride permeability by endogenously produced tyramine in the Drosophila Malpighian tubule. *Am J Physiol Cell Physiol,* 284**,** C718-28.

Boese, S.H., Wehner, F. & Kinne, R.K. (1996) Taurine permeation through swelling-activated anion conductance in rat IMCD cells in primary culture. *Am J Physiol,* 271**,** F498-507.

Bok, D. (1990) Processing and transport of retinoids by the retinal pigment epithelium. *Eye,* 4 (Pt 2)**,** 326-32.

Bond, T.D., Ambikapathy, S., Mohammad, S. & Valverde, M.A. (1998) Osmosensitive C1- currents and their relevance to regulatory volume decrease in human intestinal T84 cells: outwardly vs. inwardly rectifying currents. *J Physiol,* 511 (Pt 1)**,** 45-54.

Bos, H. & De Souza, W. (2001) Morphometrical Method for Estimating Mean Cell Volume of Phagocytosing Cells. *Microsc Microanal,* 7**,** 39-47.

Bosl, M.R., Stein, V., Hubner, C., Zdebik, A.A., Jordt, S.E., Mukhopadhyay, A.K., Davidoff, M.S., Holstein, A.F. & Jentsch, T.J. (2001) Male germ cells and

photoreceptors, both dependent on close cell-cell interactions, degenerate upon ClC-2 Cl(-) channel disruption. *EMBO J,* 20**,** 1289-99.

Botelho, S.Y. & Dartt, D.A. (1980) Effect of calcium antagonism or chelation on rabbit lacrimal gland secretion and membrane potentials. *J Physiol,* 304**,** 397-403.

Boucher, R.C., Cheng, E.H., Paradiso, A.M., Stutts, M.J., Knowles, M.R. & Earp, H.S. (1989) Chloride secretory response of cystic fibrosis human airway epithelia. Preservation of calcium but not protein kinase C- and A-dependent mechanisms. *J Clin Invest,* 84**,** 1424-31.

Braley, A.E. (1966) Dystrophy of the macula. *Am J Ophthalmol,* 61**,** 1-24.

Brecher, R. & Bird, A.C. (1990) Adult vitelliform macular dystrophy. *Eye,* 4 (Pt 1)**,** 210-5.

Burgess, R., Millar, I.D., Leroy, B.P., Urquhart, J.E., Fearon, I.M., De Baere, E., Brown, P.D., Robson, A.G., Wright, G.A., Kestelyn, P., Holder, G.E., Webster, A.R., Manson, F.D. & Black, G.C. (2008) Biallelic mutation of BEST1 causes a distinct retinopathy in humans. *Am J Hum Genet,* 82**,** 19-31.

Buyse, G., Trouet, D., Voets, T., Missiaen, L., Droogmans, G., Nilius, B. & Eggermont, J. (1998) Evidence for the intracellular location of chloride channel (ClC)-type proteins: co-localization of ClC-6a and ClC-6c with the sarco/endoplasmic-reticulum Ca2+ pump SERCA2b. *Biochem J,* 330 (Pt 2)**,** 1015-21.

Caldwell, G.M., Kakuk, L.E., Griesinger, I.B., Simpson, S.A., Nowak, N.J., Small, K.W., Maumenee, I.H., Rosenfeld, P.J., Sieving, P.A., Shows, T.B. & Ayyagari, R. (1999) Bestrophin gene mutations in patients with Best vitelliform macular dystrophy. *Genomics,* 58**,** 98-101.

Caputo, A., Caci, E., Ferrera, L., Pedemonte, N., Barsanti, C., Sondo, E., Pfeffer, U., Ravazzolo, R., Zegarra-Moran, O. & Galietta, L.J. (2008) TMEM16A, A Membrane Protein Associated With Calcium-Dependent Chloride Channel Activity. *Science*.

Chader, G.J. (1989) Interphotoreceptor retinoid-binding protein (IRBP): a model protein for molecular biological and clinically relevant studies. Friedenwald lecture. *Invest*

Ophthalmol Vis Sci, 30**,** 7-22.

Chan, H.C., Kaetzel, M.A., Gotter, A.L., Dedman, J.R. & Nelson, D.J. (1994) Annexin IV inhibits calmodulin-dependent protein kinase II-activated chloride conductance. A novel mechanism for ion channel regulation. *J Biol Chem,* 269**,** 32464-8.

Chang, G., Spencer, R.H., Lee, A.T., Barclay, M.T. & Rees, D.C. (1998) Structure of the MscL homolog from Mycobacterium tuberculosis: a gated mechanosensitive ion channel. *Science,* 282**,** 2220-6.

Chao, A.C., Kouyama, K., Heist, E.K., Dong, Y.J. & Gardner, P. (1995) Calcium- and CaMKII-dependent chloride secretion induced by the microsomal Ca(2+)-ATPase inhibitor 2,5-di-(tert-butyl)-1,4-hydroquinone in cystic fibrosis pancreatic epithelial cells. *J Clin Invest,* 96**,** 1794-801.

Chen, B., Nicol, G. & Cho, W.K. (2007) Role of calcium in volume-activated chloride currents in a mouse cholangiocyte cell line. *J Membr Biol,* 215**,** 1-13.

Cheng, L.W. & Portnoy, D.A. (2003) Drosophila S2 cells: an alternative infection model for Listeria monocytogenes. *Cell Microbiol,* 5**,** 875-85.

Chien, L.T. & Hartzell, H.C. (2007) Drosophila bestrophin-1 chloride current is dually regulated by calcium and cell volume. *J Gen Physiol,* 130**,** 513-24.

Chien, L.T., Zhang, Z.R. & Hartzell, H.C. (2006) Single Cl- channels activated by Ca2+ in Drosophila S2 cells are mediated by bestrophins. *J Gen Physiol,* 128**,** 247-59.

Chou, C.Y., Shen, M.R. & Wu, S.N. (1995) Volume-sensitive chloride channels associated with human cervical carcinogenesis. *Cancer Res,* 55**,** 6077-83.

Christensen, O. & Hoffmann, E.K. (1992) Cell swelling activates K+ and Cl- channels as well as nonselective, stretch-activated cation channels in Ehrlich ascites tumor cells. *J Membr Biol,* 129**,** 13-36.

Christensen, O., Simon, M. & Randlev, T. (1989) Anion channels in a leaky epithelium. A patch-clamp study of choroid plexus. *Pflugers Arch,* 415**,** 37-46.

Chung, M.M., Oh, K.T., Streb, L.M., Kimura, A.E. & Stone, E.M. (2001) Visual outcome following subretinal hemorrhage in Best disease. *Retina,* 21**,** 575-80.

Civan, M.M., Marano, C.W., Matschinsky, F.W. & Peterson-Yantorno, K. (1994) Prolonged incubation with elevated glucose inhibits the regulatory response to shrinkage of cultured human retinal pigment epithelial cells. *J Membr Biol,* 139**,** 1-13.

Clemens, J.C., Worby, C.A., Simonson-Leff, N., Muda, M., Maehama, T., Hemmings, B.A. & Dixon, J.E. (2000) Use of double-stranded RNA interference in Drosophila cell lines to dissect signal transduction pathways. *Proc Natl Acad Sci U S A,* 97**,** 6499-503.

Coast, G.M. (1996) Neuropeptides implicated in the control of diuresis in insects. *Peptides,* 17**,** 327-36.

Collier, M.L., Levesque, P.C., Kenyon, J.L. & Hume, J.R. (1996) Unitary Cl- channels activated by cytoplasmic Ca2+ in canine ventricular myocytes. *Circ Res,* 78**,** 936-44.

Cooper, J.D., Russell, C. & Mitchison, H.M. (2006) Progress towards understanding disease mechanisms in small vertebrate models of neuronal ceroid lipofuscinosis. *Biochim Biophys Acta,* 1762**,** 873-89.

Cooper, P.R., Nowak, N.J., Higgins, M.J., Simpson, S.A., Marquardt, A., Stoehr, H., Weber, B.H., Gerhard, D.S., De Jong, P.J. & Shows, T.B. (1997) A sequence-ready high-resolution physical map of the best macular dystrophy gene region in 11q12-q13. *Genomics,* 41**,** 185-92.

Coulombe, A. & Coraboeuf, E. (1992) Large-conductance chloride channels of new-born rat cardiac myocytes are activated by hypotonic media. *Pflugers Arch,* 422**,** 143-50.

Cowan, S.W., Schirmer, T., Rummel, G., Steiert, M., Ghosh, R., Pauptit, R.A., Jansonius, J.N. & Rosenbusch, J.P. (1992) Crystal structures explain functional properties of two E. coli porins. *Nature,* 358**,** 727-33.

Cullen, B.R. (2006) Enhancing and confirming the specificity of RNAi experiments. *Nat Methods,* 3**,** 677-81.

Cully, D.F., Paress, P.S., Liu, K.K., Schaeffer, J.M. & Arena, J.P. (1996) Identification of a Drosophila melanogaster glutamate-gated chloride channel sensitive to the antiparasitic agent avermectin. *J Biol Chem,* 271**,** 20187-91.

Cunningham, S.A., Awayda, M.S., Bubien, J.K., Ismailov, Ii, Arrate, M.P., Berdiev, B.K., Benos, D.J. & Fuller, C.M. (1995) Cloning of an epithelial chloride channel from bovine trachea. *J Biol Chem,* 270**,** 31016-26.

Currie, K.P., Wootton, J.F. & Scott, R.H. (1995) Activation of Ca(2+)-dependent Cl- currents in cultured rat sensory neurones by flash photolysis of DM-nitrophen. *J Physiol,* 482 (Pt 2)**,** 291-307.

De Jong, P.T. (2006) Age-related macular degeneration. *N Engl J Med,* 355**,** 1474-85.

Delay, R.J., Dubin, A.E. & Dionne, V.E. (1997) A cyclic nucleotide-dependent chloride conductance in olfactory receptor neurons. *J Membr Biol,* 159**,** 53-60.

Delgado, R., Barla, R., Latorre, R. & Labarca, P. (1989) L-glutamate activates excitatory and inhibitory channels in Drosophila larval muscle. *FEBS Lett,* 243**,** 337-42.

Deutman, A.F. (1969) Electro-oculography in families with vitelliform dystrophy of the fovea. Detection of the carrier state. *Arch Ophthalmol,* 81**,** 305-16.

Doroshenko, P. & Neher, E. (1992) Volume-sensitive chloride conductance in bovine chromaffin cell membrane. *J Physiol,* 449**,** 197-218.

Dow, J.A. & Davies, S.A. (2006) The Malpighian tubule: rapid insights from post-genomic biology. *J Insect Physiol,* 52**,** 365-78.

Dow, J.A., Maddrell, S.H., Gortz, A., Skaer, N.J., Brogan, S. & Kaiser, K. (1994) The malpighian tubules of Drosophila melanogaster: a novel phenotype for studies of fluid secretion and its control. *J Exp Biol,* 197**,** 421-8.

Dow, J.T. & Davies, S.A. (2003) Integrative physiology and functional genomics of epithelial function in a genetic model organism. *Physiol Rev,* 83**,** 687-729.

Doyle, D.A., Morais Cabral, J., Pfuetzner, R.A., Kuo, A., Gulbis, J.M., Cohen, S.L., Chait,

B.T. & Mackinnon, R. (1998) The structure of the potassium channel: molecular basis of K+ conduction and selectivity. *Science,* 280**,** 69-77.

Duan, D., Winter, C., Cowley, S., Hume, J.R. & Horowitz, B. (1997) Molecular identification of a volume-regulated chloride channel. *Nature,* 390**,** 417-21.

Ducharme, G., Newell, E.W., Pinto, C. & Schlichter, L.C. (2007) Small-conductance Cl- channels contribute to volume regulation and phagocytosis in microglia. *Eur J Neurosci,* 26**,** 2119-30.

Duta, V., Szkotak, A.J., Nahirney, D. & Duszyk, M. (2004) The role of bestrophin in airway epithelial ion transport. *FEBS Lett,* 577**,** 551-4.

Duy, D., Soll, J. & Philippar, K. (2007) Solute channels of the outer membrane: from bacteria to chloroplasts. *Biol Chem,* 388**,** 879-89.

Echeverri, C.J., Beachy, P.A., Baum, B., Boutros, M., Buchholz, F., Chanda, S.K., Downward, J., Ellenberg, J., Fraser, A.G., Hacohen, N., Hahn, W.C., Jackson, A.L., Kiger, A., Linsley, P.S., Lum, L., Ma, Y., Mathey-Prevot, B., Root, D.E., Sabatini, D.M., Taipale, J., Perrimon, N. & Bernards, R. (2006) Minimizing the risk of reporting false positives in large-scale RNAi screens. *Nat Methods,* 3**,** 777-9.

Eder, C., Klee, R. & Heinemann, U. (1998) Involvement of stretch-activated Cl- channels in ramification of murine microglia. *J Neurosci,* 18**,** 7127-37.

Eggermont, J., Trouet, D., Carton, I. & Nilius, B. (2001) Cellular function and control of volume-regulated anion channels. *Cell Biochem Biophys,* 35**,** 263-74.

Eisenman, G. & Horn, R. (1983) Ionic selectivity revisited: the role of kinetic and equilibrium processes in ion permeation through channels. *J Membr Biol,* 76**,** 197-225.

Eksandh, L., Bakall, B., Bauer, B., Wadelius, C. & Andreasson, S. (2001) Best's vitelliform macular dystrophy caused by a new mutation (Val89Ala) in the VMD2 gene. *Ophthalmic Genet,* 22**,** 107-15.

Elble, R.C., Widom, J., Gruber, A.D., Abdel-Ghany, M., Levine, R., Goodwin, A., Cheng, H.C. & Pauli, B.U. (1997) Cloning and characterization of lung-endothelial cell

adhesion molecule-1 suggest it is an endothelial chloride channel. *J Biol Chem,* 272**,** 27853-61.

Eldred, G.E. & Lasky, M.R. (1993) Retinal age pigments generated by self-assembling lysosomotropic detergents. *Nature,* 361**,** 724-6.

Elleder, M., Drahota, Z., Lisa, V., Mares, V., Mandys, V., Muller, J. & Palmer, D.N. (1995) Tissue culture loading test with storage granules from animal models of neuronal ceroid-lipofuscinosis (Batten disease): testing their lysosomal degradability by normal and Batten cells. *Am J Med Genet,* 57**,** 213-21.

Elwell, C. & Engel, J.N. (2005) Drosophila melanogaster S2 cells: a model system to study Chlamydia interaction with host cells. *Cell Microbiol,* 7**,** 725-39.

Evans, M.G. & Marty, A. (1986) Calcium-dependent chloride currents in isolated cells from rat lacrimal glands. *J Physiol,* 378**,** 437-60.

Fahlke, C. (2001) Ion permeation and selectivity in ClC-type chloride channels. *Am J Physiol Renal Physiol,* 280**,** F748-57.

Falke, L.C. & Misler, S. (1989) Activity of ion channels during volume regulation by clonal N1E115 neuroblastoma cells. *Proc Natl Acad Sci U S A,* 86**,** 3919-23.

Felbor, U., Schilling, H. & Weber, B.H. (1997) Adult vitelliform macular dystrophy is frequently associated with mutations in the peripherin/RDS gene. *Hum Mutat,* 10**,** 301-9.

Finnemann, S.C., Leung, L.W. & Rodriguez-Boulan, E. (2002) The lipofuscin component A2E selectively inhibits phagolysosomal degradation of photoreceptor phospholipid by the retinal pigment epithelium. *Proc Natl Acad Sci U S A,* 99**,** 3842-7.

Firestein, S. & Shepherd, G.M. (1995) Interaction of anionic and cationic currents leads to a voltage dependence in the odor response of olfactory receptor neurons. *J Neurophysiol,* 73**,** 562-7.

Fischmeister, R. & Hartzell, H.C. (2005) Volume sensitivity of the bestrophin family of chloride channels. *J Physiol,* 562**,** 477-91.

Forsman, K., Graff, C., Nordstrom, S., Johansson, K., Westermark, E., Lundgren, E., Gustavson, K.H., Wadelius, C. & Holmgren, G. (1992) The gene for Best's macular dystrophy is located at 11q13 in a Swedish family. *Clin Genet,* 42**,** 156-9.

Franciolini, F. & Nonner, W. (1987) Anion and cation permeability of a chloride channel in rat hippocampal neurons. *J Gen Physiol,* 90**,** 453-78.

Franciolini, F. & Nonner, W. (1994) A multi-ion permeation mechanism in neuronal background chloride channels. *J Gen Physiol,* 104**,** 725-46.

Francois, J., De Rouck, A. & Fernandez-Sasso, D. (1967) Electro-oculography in vitelliform degeneration of the macula. *Arch Ophthalmol,* 77**,** 726-33.

Fraser, S.P., Djamgoz, M.B., Usherwood, P.N., O'brien, J., Darlison, M.G. & Barnard, E.A. (1990) Amino acid receptors from insect muscle: electrophysiological characterization in Xenopus oocytes following expression by injection of mRNA. *Brain Res Mol Brain Res,* 8**,** 331-41.

Friedrich, T., Breiderhoff, T. & Jentsch, T.J. (1999) Mutational analysis demonstrates that ClC-4 and ClC-5 directly mediate plasma membrane currents. *J Biol Chem,* 274**,** 896-902.

Frings, S., Reuter, D. & Kleene, S.J. (2000) Neuronal Ca2+ -activated Cl- channels--homing in on an elusive channel species. *Prog Neurobiol,* 60**,** 247-89.

Frizzell, R.A., Rechkemmer, G. & Shoemaker, R.L. (1986) Altered regulation of airway epithelial cell chloride channels in cystic fibrosis. *Science,* 233**,** 558-60.

Furukawa, T., Ogura, T., Katayama, Y. & Hiraoka, M. (1998) Characteristics of rabbit ClC-2 current expressed in Xenopus oocytes and its contribution to volume regulation. *Am J Physiol,* 274**,** C500-12.

Gallemore, R.P. & Steinberg, R.H. (1993) Light-evoked modulation of basolateral membrane Cl- conductance in chick retinal pigment epithelium: the light peak and fast oscillation. *J Neurophysiol,* 70**,** 1669-80.

Galzi, J.L., Devillers-Thiery, A., Hussy, N., Bertrand, S., Changeux, J.P. & Bertrand, D. (1992) Mutations in the channel domain of a neuronal nicotinic receptor convert

ion selectivity from cationic to anionic. *Nature,* 359**,** 500-5.

Gandhi, R., Elble, R.C., Gruber, A.D., Schreur, K.D., Ji, H.L., Fuller, C.M. & Pauli, B.U. (1998) Molecular and functional characterization of a calcium-sensitive chloride channel from mouse lung. *J Biol Chem,* 273**,** 32096-101.

Gaspar, K.J., Racette, K.J., Gordon, J.R., Loewen, M.E. & Forsyth, G.W. (2000) Cloning a chloride conductance mediator from the apical membrane of porcine ileal enterocytes. *Physiol Genomics,* 3**,** 101-11.

George, A.L., Jr., Crackower, M.A., Abdalla, J.A., Hudson, A.J. & Ebers, G.C. (1993) Molecular basis of Thomsen's disease (autosomal dominant myotonia congenita). *Nat Genet,* 3**,** 305-10.

Giles, D. & Usherwood, P.N. (1985) The effects of putative amino acid neurotransmitters on somata isolated from neurons of the locust central nervous system. *Comp Biochem Physiol C,* 80**,** 231-6.

Giovannucci, D.R., Bruce, J.I., Straub, S.V., Arreola, J., Sneyd, J., Shuttleworth, T.J. & Yule, D.I. (2002) Cytosolic Ca(2+) and Ca(2+)-activated Cl(-) current dynamics: insights from two functionally distinct mouse exocrine cells. *J Physiol,* 540**,** 469-84.

Gomez-Hernandez, J.M., Stuhmer, W. & Parekh, A.B. (1997) Calcium dependence and distribution of calcium-activated chloride channels in Xenopus oocytes. *J Physiol,* 502 (Pt 3)**,** 569-74.

Gomez, A., Cedano, J., Oliva, B., Pinol, J. & Querol, E. (2001) The gene causing the Best's macular dystrophy (BMD) encodes a putative ion exchanger. *DNA Seq,* 12**,** 431-5.

Gong, W., Xu, H., Shimizu, T., Morishima, S., Tanabe, S., Tachibe, T., Uchida, S., Sasaki, S. & Okada, Y. (2004) ClC-3-independent, PKC-dependent activity of volume-sensitive Cl channel in mouse ventricular cardiomyocytes. *Cell Physiol Biochem,* 14**,** 213-24.

Gosling, M., Smith, J.W. & Poyner, D.R. (1995) Characterization of a volume-sensitive chloride current in rat osteoblast-like (ROS 17/2.8) cells. *J Physiol,* 485 (Pt 3)**,** 671-82.

Grinstein, S., Rothstein, A., Sarkadi, B. & Gelfand, E.W. (1984) Responses of lymphocytes to anisotonic media: volume-regulating behavior. *Am J Physiol,* 246**,** C204-15.

Grubb, B.R. & Boucher, R.C. (1999) Pathophysiology of gene-targeted mouse models for cystic fibrosis. *Physiol Rev,* 79**,** S193-214.

Grubb, B.R. & Gabriel, S.E. (1997) Intestinal physiology and pathology in gene-targeted mouse models of cystic fibrosis. *Am J Physiol,* 273**,** G258-66.

Gruber, A.D., Elble, R.C., Ji, H.L., Schreur, K.D., Fuller, C.M. & Pauli, B.U. (1998) Genomic cloning, molecular characterization, and functional analysis of human CLCA1, the first human member of the family of Ca2+-activated Cl- channel proteins. *Genomics,* 54**,** 200-14.

Gutman, I., Walsh, J.B. & Henkind, P. (1982) Vitelliform macular dystrophy and butterfly-shaped epithelial dystrophy: a continuum? *Br J Ophthalmol,* 66**,** 170-3.

Guziewicz, K.E., Zangerl, B., Lindauer, S.J., Mullins, R.F., Sandmeyer, L.S., Grahn, B.H., Stone, E.M., Acland, G.M. & Aguirre, G.D. (2007) Bestrophin gene mutations cause canine multifocal retinopathy: a novel animal model for best disease. *Invest Ophthalmol Vis Sci,* 48**,** 1959-67.

Hamill, O.P., Marty, A., Neher, E., Sakmann, B. & Sigworth, F.J. (1981) Improved patch-clamp techniques for high-resolution current recording from cells and cell-free membrane patches. *Pflugers Arch,* 391**,** 85-100.

Hamill, O.P. & Mcbride, D.W., Jr. (1994) The cloning of a mechano-gated membrane ion channel. *Trends Neurosci,* 17**,** 439-43.

Han, X. & Ferrier, G.R. (1992) Ionic mechanisms of transient inward current in the absence of Na(+)-Ca2+ exchange in rabbit cardiac Purkinje fibres. *J Physiol,* 456**,** 19-38.

Han, X. & Ferrier, G.R. (1996) Transient inward current is conducted through two types of channels in cardiac Purkinje fibres. *J Mol Cell Cardiol,* 28**,** 2069-84.

Hartzell, C., Putzier, I. & Arreola, J. (2005a) Calcium-activated chloride channels. *Annu Rev Physiol,* 67**,** 719-58.

Hartzell, C., Qu, Z., Putzier, I., Artinian, L., Chien, L.T. & Cui, Y. (2005b) Looking chloride channels straight in the eye: bestrophins, lipofuscinosis, and retinal degeneration. *Physiology (Bethesda),* 20**,** 292-302.

Hartzell, H.C. (1996) Activation of different Cl currents in Xenopus oocytes by Ca liberated from stores and by capacitative Ca influx. *J Gen Physiol,* 108**,** 157-75.

Hartzell, H.C., Qu, Z., Yu, K., Xiao, Q. & Chien, L.T. (2008) Molecular physiology of bestrophins: multifunctional membrane proteins linked to best disease and other retinopathies. *Physiol Rev,* 88**,** 639-72.

Hazama, A. & Okada, Y. (1988) Ca2+ sensitivity of volume-regulatory K+ and Cl- channels in cultured human epithelial cells. *J Physiol,* 402**,** 687-702.

Helix, N., Strobaek, D., Dahl, B.H. & Christophersen, P. (2003) Inhibition of the endogenous volume-regulated anion channel (VRAC) in HEK293 cells by acidic di-aryl-ureas. *J Membr Biol,* 196**,** 83-94.

Hermoso, M., Satterwhite, C.M., Andrade, Y.N., Hidalgo, J., Wilson, S.M., Horowitz, B. & Hume, J.R. (2002) ClC-3 is a fundamental molecular component of volume-sensitive outwardly rectifying Cl- channels and volume regulation in HeLa cells and Xenopus laevis oocytes. *J Biol Chem,* 277**,** 40066-74.

Herness, M.S. & Sun, X.D. (1999) Characterization of chloride currents and their noradrenergic modulation in rat taste receptor cells. *J Neurophysiol,* 82**,** 260-71.

Hirakawa, Y., Gericke, M., Cohen, R.A. & Bolotina, V.M. (1999) Ca(2+)-dependent Cl(-) channels in mouse and rabbit aortic smooth muscle cells: regulation by intracellular Ca(2+) and NO. *Am J Physiol,* 277**,** H1732-44.

Hodgkin, A.L. & Huxley, A.F. (1952a) Currents carried by sodium and potassium ions through the membrane of the giant axon of Loligo. *J Physiol,* 116**,** 449-72.

Hodgkin, A.L. & Huxley, A.F. (1952b) A quantitative description of membrane current and its application to conduction and excitation in nerve. *J Physiol,* 117**,** 500-44.

Hoffmann, E.K. & Dunham, P.B. (1995) Membrane mechanisms and intracellular signalling in cell volume regulation. *Int Rev Cytol,* 161**,** 173-262.

Hoffmann, E.K. & Simonsen, L.O. (1989) Membrane mechanisms in volume and pH regulation in vertebrate cells. *Physiol Rev,* 69**,** 315-82.

Hoffmann, E.K., Simonsen, L.O. & Sjoholm, C. (1979) Membrane potential, chloride exchange, and chloride conductance in Ehrlich mouse ascites tumour cells. *J Physiol,* 296**,** 61-84.

Holevinsky, K.O., Jow, F. & Nelson, D.J. (1994) Elevation in intracellular calcium activates both chloride and proton currents in human macrophages. *J Membr Biol,* 140**,** 13-30.

Horseman, B.G., Seymour, C., Bermudez, I. & Beadle, D.J. (1988) The effects of L-glutamate on cultured insect neurones. *Neurosci Lett,* 85**,** 65-70.

Hu, J. & Bok, D. (2001) A cell culture medium that supports the differentiation of human retinal pigment epithelium into functionally polarized monolayers. *Mol Vis,* 7**,** 14-9.

Huang, X., Huang, Y., Chinnappan, R., Bocchini, C., Gustin, M.C. & Stern, M. (2002) The Drosophila inebriated-encoded neurotransmitter/osmolyte transporter: dual roles in the control of neuronal excitability and the osmotic stress response. *Genetics,* 160**,** 561-9.

Hughes, B.A., Miller, S.S. & Farber, D.B. (1987) Adenylate cyclase stimulation alters transport in frog retinal pigment epithelium. *Am J Physiol,* 252**,** C385-95.

Hughes, B.A., Miller, S.S. & Machen, T.E. (1984) Effects of cyclic AMP on fluid absorption and ion transport across frog retinal pigment epithelium. Measurements in the open-circuit state. *J Gen Physiol,* 83**,** 875-99.

Hunter, M., Smith, P.A. & Case, R.M. (1983) The dependence of fluid secretion by mandibular salivary gland and pancreas on extracellular calcium. *Cell Calcium,* 4**,** 307-17.

Hussy, N. (1992) Calcium-activated chloride channels in cultured embryonic Xenopus spinal neurons. *J Neurophysiol,* 68**,** 2042-50.

Ingber, D.E. (1997) Tensegrity: the architectural basis of cellular mechanotransduction.

Annu Rev Physiol, 59**,** 575-99.

Jackson, A.L., Burchard, J., Schelter, J., Chau, B.N., Cleary, M., Lim, L. & Linsley, P.S. (2006) Widespread siRNA "off-target" transcript silencing mediated by seed region sequence complementarity. *RNA,* 12**,** 1179-87.

Jackson, P.S. & Strange, K. (1993) Volume-sensitive anion channels mediate swelling-activated inositol and taurine efflux. *Am J Physiol,* 265**,** C1489-500.

Jackson, P.S. & Strange, K. (1995) Characterization of the voltage-dependent properties of a volume-sensitive anion conductance. *J Gen Physiol,* 105**,** 661-76.

Jacob, T.C., Moss, S.J. & Jurd, R. (2008) GABA(A) receptor trafficking and its role in the dynamic modulation of neuronal inhibition. *Nat Rev Neurosci,* 9**,** 331-43.

Jager, R.D., Mieler, W.F. & Miller, J.W. (2008) Age-related macular degeneration. *N Engl J Med,* 358**,** 2606-17.

Jalonen, T. (1993) Single-channel characteristics of the large-conductance anion channel in rat cortical astrocytes in primary culture. *Glia,* 9**,** 227-37.

Jentsch, T.J., Poet, M., Fuhrmann, J.C. & Zdebik, A.A. (2005) Physiological functions of CLC Cl- channels gleaned from human genetic disease and mouse models. *Annu Rev Physiol,* 67**,** 779-807.

Jentsch, T.J., Steinmeyer, K. & Schwarz, G. (1990) Primary structure of Torpedo marmorata chloride channel isolated by expression cloning in Xenopus oocytes. *Nature,* 348**,** 510-4.

Jiang, Y., Lee, A., Chen, J., Cadene, M., Chait, B.T. & Mackinnon, R. (2002) Crystal structure and mechanism of a calcium-gated potassium channel. *Nature,* 417**,** 515-22.

Jiang, Y., Lee, A., Chen, J., Ruta, V., Cadene, M., Chait, B.T. & Mackinnon, R. (2003) X-ray structure of a voltage-dependent K+ channel. *Nature,* 423**,** 33-41.

Jones-Davis, D.M. & Macdonald, R.L. (2003) GABA(A) receptor function and

pharmacology in epilepsy and status epilepticus. *Curr Opin Pharmacol,* 3**,** 12-8.

Jordt, S.E. & Jentsch, T.J. (1997) Molecular dissection of gating in the ClC-2 chloride channel. *EMBO J,* 16**,** 1582-92.

Joseph, D.P. & Miller, S.S. (1992) Alpha-1-adrenergic modulation of K and Cl transport in bovine retinal pigment epithelium. *J Gen Physiol,* 99**,** 263-90.

Kaetzel, M.A., Chan, H.C., Dubinsky, W.P., Dedman, J.R. & Nelson, D.J. (1994) A role for annexin IV in epithelial cell function. Inhibition of calcium-activated chloride conductance. *J Biol Chem,* 269**,** 5297-302.

Kaplan, R.S., Mayor, J.A., Brauer, D., Kotaria, R., Walters, D.E. & Dean, A.M. (2000) The yeast mitochondrial citrate transport protein. Probing the secondary structure of transmembrane domain iv and identification of residues that likely comprise a portion of the citrate translocation pathway. *J Biol Chem,* 275**,** 12009-16.

Karlin, A. & Akabas, M.H. (1998) Substituted-cysteine accessibility method. *Methods Enzymol,* 293**,** 123-45.

Kasper, D., Planells-Cases, R., Fuhrmann, J.C., Scheel, O., Zeitz, O., Ruether, K., Schmitt, A., Poet, M., Steinfeld, R., Schweizer, M., Kornak, U. & Jentsch, T.J. (2005) Loss of the chloride channel ClC-7 leads to lysosomal storage disease and neurodegeneration. *EMBO J,* 24**,** 1079-91.

Katz, M.L., Rice, L.M. & Gao, C.L. (1999) Reversible accumulation of lipofuscin-like inclusions in the retinal pigment epithelium. *Invest Ophthalmol Vis Sci,* 40**,** 175-81.

Kaupp, U.B. & Seifert, R. (2002) Cyclic nucleotide-gated ion channels. *Physiol Rev,* 82**,** 769-824.

Kawano, S., Hirayama, Y. & Hiraoka, M. (1995) Activation mechanism of Ca(2+)-sensitive transient outward current in rabbit ventricular myocytes. *J Physiol,* 486 (Pt 3)**,** 593-604.

Kennedy, B.G. (1994) Volume regulation in cultured cells derived from human retinal pigment epithelium. *Am J Physiol,* 266**,** C676-83.

Kenyon, E., Yu, K., La Cour, M. & Miller, S.S. (1994) Lactate transport mechanisms at apical and basolateral membranes of bovine retinal pigment epithelium. *Am J Physiol,* 267**,** C1561-73.

Keramidas, A., Moorhouse, A.J., French, C.R., Schofield, P.R. & Barry, P.H. (2000) M2 pore mutations convert the glycine receptor channel from being anion- to cation-selective. *Biophys J,* 79**,** 247-59.

Keramidas, A., Moorhouse, A.J., Pierce, K.D., Schofield, P.R. & Barry, P.H. (2002) Cation-selective mutations in the M2 domain of the inhibitory glycine receptor channel reveal determinants of ion-charge selectivity. *J Gen Physiol,* 119**,** 393-410.

Khan, J.C., Shahid, H., Thurlby, D.A., Yates, J.R. & Moore, A.T. (2008) Charles Bonnet syndrome in age-related macular degeneration: the nature and frequency of images in subjects with end-stage disease. *Ophthalmic Epidemiol,* 15**,** 202-8.

Kidd, J.F. & Thorn, P. (2000) Intracellular Ca2+ and Cl- channel activation in secretory cells. *Annu Rev Physiol,* 62**,** 493-513.

Kirk, K., Ellory, J.C. & Young, J.D. (1992) Transport of organic substrates via a volume-activated channel. *J Biol Chem,* 267**,** 23475-8.

Kleene, S.J. & Gesteland, R.C. (1991) Calcium-activated chloride conductance in frog olfactory cilia. *J Neurosci,* 11**,** 3624-9.

Klockner, U. (1993) Intracellular calcium ions activate a low-conductance chloride channel in smooth-muscle cells isolated from human mesenteric artery. *Pflugers Arch,* 424**,** 231-7.

Koch, M.C., Steinmeyer, K., Lorenz, C., Ricker, K., Wolf, F., Otto, M., Zoll, B., Lehmann-Horn, F., Grzeschik, K.H. & Jentsch, T.J. (1992) The skeletal muscle chloride channel in dominant and recessive human myotonia. *Science,* 257**,** 797-800.

Kornak, U., Kasper, D., Bosl, M.R., Kaiser, E., Schweizer, M., Schulz, A., Friedrich, W., Delling, G. & Jentsch, T.J. (2001) Loss of the ClC-7 chloride channel leads to osteopetrosis in mice and man. *Cell,* 104**,** 205-15.

Koumi, S., Sato, R. & Aramaki, T. (1994) Characterization of the calcium-activated chloride channel in isolated guinea-pig hepatocytes. *J Gen Physiol,* 104**,** 357-73.

Kowdley, G.C., Ackerman, S.J., John, J.E., 3rd, Jones, L.R. & Moorman, J.R. (1994) Hyperpolarization-activated chloride currents in Xenopus oocytes. *J Gen Physiol,* 103**,** 217-30.

Kramer, F., Mohr, N., Kellner, U., Rudolph, G. & Weber, B.H. (2003) Ten novel mutations in VMD2 associated with Best macular dystrophy (BMD). *Hum Mutat,* 22**,** 418.

Kramer, F., Stohr, H. & Weber, B.H. (2004) Cloning and characterization of the murine Vmd2 RFP-TM gene family. *Cytogenet Genome Res,* 105**,** 107-14.

Kramer, F., White, K., Pauleikhoff, D., Gehrig, A., Passmore, L., Rivera, A., Rudolph, G., Kellner, U., Andrassi, M., Lorenz, B., Rohrschneider, K., Blankenagel, A., Jurklies, B., Schilling, H., Schutt, F., Holz, F.G. & Weber, B.H. (2000) Mutations in the VMD2 gene are associated with juvenile-onset vitelliform macular dystrophy (Best disease) and adult vitelliform macular dystrophy but not age-related macular degeneration. *Eur J Hum Genet,* 8**,** 286-92.

Kubo, M. & Okada, Y. (1992) Volume-regulatory Cl- channel currents in cultured human epithelial cells. *J Physiol,* 456**,** 351-71.

Kunzelmann, K., Milenkovic, V.M., Spitzner, M., Soria, R.B. & Schreiber, R. (2007) Calcium-dependent chloride conductance in epithelia: is there a contribution by Bestrophin? *Pflugers Arch,* 454**,** 879-89.

Kuo, A., Gulbis, J.M., Antcliff, J.F., Rahman, T., Lowe, E.D., Zimmer, J., Cuthbertson, J., Ashcroft, F.M., Ezaki, T. & Doyle, D.A. (2003) Crystal structure of the potassium channel KirBac1.1 in the closed state. *Science,* 300**,** 1922-6.

Kurahashi, T. & Yau, K.W. (1994) Olfactory transduction. Tale of an unusual chloride current. *Curr Biol,* 4**,** 256-8.

Kuruma, A. & Hartzell, H.C. (1999) Dynamics of calcium regulation of chloride currents in Xenopus oocytes. *Am J Physiol,* 276**,** C161-75.

Kuruma, A. & Hartzell, H.C. (2000) Bimodal control of a Ca(2+)-activated Cl(-) channel

by different Ca(2+) signals. *J Gen Physiol,* 115**,** 59-80.

La Cour, M., Lin, H., Kenyon, E. & Miller, S.S. (1994) Lactate transport in freshly isolated human fetal retinal pigment epithelium. *Invest Ophthalmol Vis Sci,* 35**,** 434-42.

La Cour, M. & Zeuthen, T. (1993) Osmotic properties of the frog retinal pigment epithelium. *Exp Eye Res,* 56**,** 521-30.

Lachapelle, P., Quigley, M.G., Polomeno, R.C. & Little, J.M. (1988) Abnormal dark-adapted electroretinogram in Best's vitelliform macular degeneration. *Can J Ophthalmol,* 23**,** 279-84.

Lang, F., Busch, G.L. & Volkl, H. (1998) The diversity of volume regulatory mechanisms. *Cell Physiol Biochem,* 8**,** 1-45.

Lapunzina, P., Sanchez, J.M., Cabrera, M., Moreno, A., Delicado, A., De Torres, M.L., Mori, A.M., Quero, J. & Lopez Pajares, I. (2003) Hyperekplexia (startle disease): a novel mutation (S270T) in the M2 domain of the GLRA1 gene and a molecular review of the disorder. *Mol Diagn,* 7**,** 125-8.

Large, W.A. & Wang, Q. (1996) Characteristics and physiological role of the Ca(2+)-activated Cl- conductance in smooth muscle. *Am J Physiol,* 271**,** C435-54.

Lavail, M.M. (1983) Outer segment disc shedding and phagocytosis in the outer retina. *Trans Ophthalmol Soc U K,* 103 (Pt 4)**,** 397-404.

Lewis, R.S., Ross, P.E. & Cahalan, M.D. (1993) Chloride channels activated by osmotic stress in T lymphocytes. *J Gen Physiol,* 101**,** 801-26.

Li, X., Shimada, K., Showalter, L.A. & Weinman, S.A. (2000) Biophysical properties of ClC-3 differentiate it from swelling-activated chloride channels in Chinese hamster ovary-K1 cells. *J Biol Chem,* 275**,** 35994-8.

Li, X., Wang, T., Zhao, Z. & Weinman, S.A. (2002) The ClC-3 chloride channel promotes acidification of lysosomes in CHO-K1 and Huh-7 cells. *Am J Physiol Cell Physiol,* 282**,** C1483-91.

Lin, X., Ruan, X., Anderson, M.G., Mcdowell, J.A., Kroeger, P.E., Fesik, S.W. & Shen, Y. (2005) siRNA-mediated off-target gene silencing triggered by a 7 nt complementation. *Nucleic Acids Res,* 33**,** 4527-35.

Loewenstein, A., Godel, V., Godel, L. & Lazar, M. (1993) Variable phenotypic expressivity of Best's vitelliform dystrophy. *Ophthalmic Paediatr Genet,* 14**,** 131-6.

Long, S.B., Campbell, E.B. & Mackinnon, R. (2005) Crystal structure of a mammalian voltage-dependent Shaker family K+ channel. *Science,* 309**,** 897-903.

Lotery, A.J., Munier, F.L., Fishman, G.A., Weleber, R.G., Jacobson, S.G., Affatigato, L.M., Nichols, B.E., Schorderet, D.F., Sheffield, V.C. & Stone, E.M. (2000) Allelic variation in the VMD2 gene in best disease and age-related macular degeneration. *Invest Ophthalmol Vis Sci,* 41**,** 1291-6.

Lowe, G. & Gold, G.H. (1993) Contribution of the ciliary cyclic nucleotide-gated conductance to olfactory transduction in the salamander. *J Physiol,* 462**,** 175-96.

Macintyre, R.J. & O'brien, S.J. (1976) Interacting gene-enzyme systems in Drosophila. *Annu Rev Genet,* 10**,** 281-318.

Mall, M., Grubb, B.R., Harkema, J.R., O'neal, W.K. & Boucher, R.C. (2004) Increased airway epithelial Na+ absorption produces cystic fibrosis-like lung disease in mice. *Nat Med,* 10**,** 487-93.

Mankodi, A., Takahashi, M.P., Jiang, H., Beck, C.L., Bowers, W.J., Moxley, R.T., Cannon, S.C. & Thornton, C.A. (2002) Expanded CUG repeats trigger aberrant splicing of ClC-1 chloride channel pre-mRNA and hyperexcitability of skeletal muscle in myotonic dystrophy. *Mol Cell,* 10**,** 35-44.

Manolopoulos, G.V., Prenen, J., Droogmans, G. & Nilius, B. (1997) Thrombin potentiates volume-activated chloride currents in pulmonary artery endothelial cells. *Pflugers Arch,* 433**,** 845-7.

Mansfield, B.E., Dionne, M.S., Schneider, D.S. & Freitag, N.E. (2003) Exploration of host-pathogen interactions using Listeria monocytogenes and Drosophila melanogaster. *Cell Microbiol,* 5**,** 901-11.

Marchant, D., Gogat, K., Dureau, P., Sainton, K., Sternberg, C., Gadin, S., Dollfus, H., Brasseur, G., Hache, J.C., Dumur, V., Puech, V., Munier, F., Schorderet, D.F., Marsac, C., Menasche, M., Dufier, J.L. & Abitbol, M. (2002) Use of denaturing HPLC and automated sequencing to screen the VMD2 gene for mutations associated with Best's vitelliform macular dystrophy. *Ophthalmic Genet,* 23**,** 167-74.

Marchant, D., Yu, K., Bigot, K., Roche, O., Germain, A., Bonneau, D., Drouin-Garraud, V., Schorderet, D.F., Munier, F., Schmidt, D., Le Neindre, P., Marsac, C., Menasche, M., Dufier, J.L., Fischmeister, R., Hartzell, C. & Abitbol, M. (2007) New VMD2 gene mutations identified in patients affected by Best vitelliform macular dystrophy. *J Med Genet,* 44**,** e70.

Maricq, A.V. & Korenbrot, J.I. (1988) Calcium and calcium-dependent chloride currents generate action potentials in solitary cone photoreceptors. *Neuron,* 1**,** 503-15.

Marmor, M.F. & Dalal, R. (1993) Irregular retinal and RPE damage after pressure-induced ischemia in the rabbit. *Invest Ophthalmol Vis Sci,* 34**,** 2570-5.

Marmor, M.F. & Yao, X.Y. (1994) Conditions necessary for the formation of serous detachment. Experimental evidence from the cat. *Arch Ophthalmol,* 112**,** 830-8.

Marmorstein, A.D. & Kinnick, T.R. (2007) Focus on molecules: bestrophin (best-1). *Exp Eye Res,* 85**,** 423-4.

Marmorstein, A.D., Marmorstein, L.Y., Rayborn, M., Wang, X., Hollyfield, J.G. & Petrukhin, K. (2000) Bestrophin, the product of the Best vitelliform macular dystrophy gene (VMD2), localizes to the basolateral plasma membrane of the retinal pigment epithelium. *Proc Natl Acad Sci U S A,* 97**,** 12758-63.

Marmorstein, A.D., Stanton, J.B., Yocom, J., Bakall, B., Schiavone, M.T., Wadelius, C., Marmorstein, L.Y. & Peachey, N.S. (2004) A model of best vitelliform macular dystrophy in rats. *Invest Ophthalmol Vis Sci,* 45**,** 3733-9.

Marmorstein, L.Y., Mclaughlin, P.J., Stanton, J.B., Yan, L., Crabb, J.W. & Marmorstein, A.D. (2002) Bestrophin interacts physically and functionally with protein phosphatase 2A. *J Biol Chem,* 277**,** 30591-7.

Marmorstein, L.Y., Wu, J., Mclaughlin, P., Yocom, J., Karl, M.O., Neussert, R., Wimmers, S., Stanton, J.B., Gregg, R.G., Strauss, O., Peachey, N.S. & Marmorstein, A.D. (2006) The light peak of the electroretinogram is dependent on voltage-gated calcium channels and antagonized by bestrophin (best-1). *J Gen Physiol,* 127**,** 577-89.

Marquardt, A., Stohr, H., Passmore, L.A., Kramer, F., Rivera, A. & Weber, B.H. (1998) Mutations in a novel gene, VMD2, encoding a protein of unknown properties cause juvenile-onset vitelliform macular dystrophy (Best's disease). *Hum Mol Genet,* 7**,** 1517-25.

Martin, D.K. (1993) Small conductance chloride channels in acinar cells from the rat mandibular salivary gland are directly controlled by a G-protein. *Biochem Biophys Res Commun,* 192**,** 1266-73.

Marunaka, Y. & Eaton, D.C. (1990) Chloride channels in the apical membrane of a distal nephron A6 cell line. *Am J Physiol,* 258**,** C352-68.

Matsumura, Y., Uchida, S., Kondo, Y., Miyazaki, H., Ko, S.B., Hayama, A., Morimoto, T., Liu, W., Arisawa, M., Sasaki, S. & Marumo, F. (1999) Overt nephrogenic diabetes insipidus in mice lacking the CLC-K1 chloride channel. *Nat Genet,* 21**,** 95-8.

Mcbride, D.W., Jr. & Roper, S.D. (1991) Ca(2+)-dependent chloride conductance in Necturus taste cells. *J Membr Biol,* 124**,** 85-93.

Mccarty, N.A. & O'neil, R.G. (1992) Calcium signaling in cell volume regulation. *Physiol Rev,* 72**,** 1037-61.

Mcewan, G.T., Brown, C.D., Hirst, B.H. & Simmons, N.L. (1993) Characterisation of volume-activated ion transport across epithelial monolayers of human intestinal T84 cells. *Pflugers Arch,* 423**,** 213-20.

Mehta, A. (2005) CFTR: more than just a chloride channel. *Pediatr Pulmonol,* 39**,** 292-8.

Melvin, J.E., Koek, L. & Zhang, G.H. (1991) A capacitative Ca2+ influx is required for sustained fluid secretion in sublingual mucous acini. *Am J Physiol,* 261**,** G1043-50.

Melvin, J.E., Yule, D., Shuttleworth, T. & Begenisich, T. (2005) Regulation of fluid and

electrolyte secretion in salivary gland acinar cells. *Annu Rev Physiol,* 67**,** 445-69.

Miledi, R. (1982) A calcium-dependent transient outward current in Xenopus laevis oocytes. *Proc R Soc Lond B Biol Sci,* 215**,** 491-7.

Milenkovic, V.M., Langmann, T., Schreiber, R., Kunzelmann, K. & Weber, B.H. (2008) Molecular evolution and functional divergence of the bestrophin protein family. *BMC Evol Biol,* 8**,** 72.

Milenkovic, V.M., Rivera, A., Horling, F. & Weber, B.H. (2007) Insertion and topology of normal and mutant bestrophin-1 in the endoplasmic reticulum membrane. *J Biol Chem,* 282**,** 1313-21.

Miller, C. & White, M.M. (1980) A voltage-dependent chloride conductance channel from Torpedo electroplax membrane. *Ann N Y Acad Sci,* 341**,** 534-51.

Moffat, J., Reiling, J.H. & Sabatini, D.M. (2007) Off-target effects associated with long dsRNAs in Drosophila RNAi screens. *Trends Pharmacol Sci,* 28**,** 149-51.

Mongin, A.A. & Kimelberg, H.K. (2005) ATP regulates anion channel-mediated organic osmolyte release from cultured rat astrocytes via multiple Ca2+-sensitive mechanisms. *Am J Physiol Cell Physiol,* 288**,** C204-13.

Moreland, J.G., Davis, A.P., Bailey, G., Nauseef, W.M. & Lamb, F.S. (2006) Anion channels, including ClC-3, are required for normal neutrophil oxidative function, phagocytosis, and transendothelial migration. *J Biol Chem,* 281**,** 12277-88.

Morris, A.P. & Frizzell, R.A. (1993) Ca(2+)-dependent Cl- channels in undifferentiated human colonic cells (HT-29). II. Regulation and rundown. *Am J Physiol,* 264**,** C977-85.

Nakamoto, T., Srivastava, A., Romanenko, V.G., Ovitt, C.E., Perez-Cornejo, P., Arreola, J., Begenisich, T. & Melvin, J.E. (2007) Functional and molecular characterization of the fluid secretion mechanism in human parotid acinar cells. *Am J Physiol Regul Integr Comp Physiol,* 292**,** R2380-90.

Nakayama, T. & Fozzard, H.A. (1988) Adrenergic modulation of the transient outward current in isolated canine Purkinje cells. *Circ Res,* 62**,** 162-72.

Neher, E. & Sakmann, B. (1976) Single-channel currents recorded from membrane of denervated frog muscle fibres. *Nature,* 260**,** 799-802.

Nguyen-Legros, J. & Hicks, D. (2000) Renewal of photoreceptor outer segments and their phagocytosis by the retinal pigment epithelium. *Int Rev Cytol,* 196**,** 245-313.

Nicholson, B.J., Weber, P.A., Cao, F., Chang, H., Lampe, P. & Goldberg, G. (2000) The molecular basis of selective permeability of connexins is complex and includes both size and charge. *Braz J Med Biol Res,* 33**,** 369-78.

Nilius, B. & Droogmans, G. (2003) Amazing chloride channels: an overview. *Acta Physiol Scand,* 177**,** 119-47.

Nilius, B., Eggermont, J., Voets, T., Buyse, G., Manolopoulos, V. & Droogmans, G. (1997a) Properties of volume-regulated anion channels in mammalian cells. *Prog Biophys Mol Biol,* 68**,** 69-119.

Nilius, B., Eggermont, J., Voets, T. & Droogmans, G. (1996) Volume-activated Cl- channels. *Gen Pharmacol,* 27**,** 1131-40.

Nilius, B., Oike, M., Zahradnik, I. & Droogmans, G. (1994) Activation of a Cl- current by hypotonic volume increase in human endothelial cells. *J Gen Physiol,* 103**,** 787-805.

Nilius, B., Prenen, J., Szucs, G., Wei, L., Tanzi, F., Voets, T. & Droogmans, G. (1997b) Calcium-activated chloride channels in bovine pulmonary artery endothelial cells. *J Physiol,* 498 (Pt 2)**,** 381-96.

Nilius, B., Sehrer, J., De Smet, P., Van Driessche, W. & Droogmans, G. (1995) Volume regulation in a toad epithelial cell line: role of coactivation of K+ and Cl- channels. *J Physiol,* 487 (Pt 2)**,** 367-78.

Nilius, B., Viana, F. & Droogmans, G. (1997c) Ion channels in vascular endothelium. *Annu Rev Physiol,* 59**,** 145-70.

Nishimoto, I., Wagner, J.A., Schulman, H. & Gardner, P. (1991) Regulation of Cl- channels by multifunctional CaM kinase. *Neuron,* 6**,** 547-55.

Nordstrom, S. & Barkman, Y. (1977) Hereditary maculardegeneration (HMD) in 246 cases traced to one gene-source in central Sweden. *Hereditas,* 84**,** 163-76.

O'donnell, M.J., Dow, J.A., Huesmann, G.R., Tublitz, N.J. & Maddrell, S.H. (1996) Separate control of anion and cation transport in malpighian tubules of Drosophila Melanogaster. *J Exp Biol,* 199**,** 1163-75.

O'donnell, M.J., Rheault, M.R., Davies, S.A., Rosay, P., Harvey, B.J., Maddrell, S.H., Kaiser, K. & Dow, J.A. (1998) Hormonally controlled chloride movement across Drosophila tubules is via ion channels in stellate cells. *Am J Physiol,* 274**,** R1039-49.

O'donnell, M.J. & Spring, J.H. (2000) Modes of control of insect Malpighian tubules: synergism, antagonism, cooperation and autonomous regulation. *J Insect Physiol,* 46**,** 107-117.

Ohno-Matsui, K., Mori, K., Ichinose, S., Sato, T., Wang, J., Shimada, N., Kojima, A., Mochizuki, M. & Morita, I. (2006) In vitro and in vivo characterization of iris pigment epithelial cells cultured on amniotic membranes. *Mol Vis,* 12**,** 1022-32.

Okada, T., Horiguchi, H. & Tachibana, M. (1995) Ca(2+)-dependent Cl- current at the presynaptic terminals of goldfish retinal bipolar cells. *Neurosci Res,* 23**,** 297-303.

Okada, Y. (1997) Volume expansion-sensing outward-rectifier Cl- channel: fresh start to the molecular identity and volume sensor. *Am J Physiol,* 273**,** C755-89.

Okada, Y., Oiki, S., Hazama, A. & Morishima, S. (1998) Criteria for the molecular identification of the volume-sensitive outwardly rectifying Cl- channel. *J Gen Physiol,* 112**,** 365-7.

Opsahl, L.R. & Webb, W.W. (1994) Transduction of membrane tension by the ion channel alamethicin. *Biophys J,* 66**,** 71-4.

Park, J.K., Kim, Y.C., Sim, J.H., Choi, M.Y., Choi, W., Hwang, K.K., Cho, M.C., Kim, K.W., Lim, S.W. & Lee, S.J. (2007) Regulation of membrane excitability by intracellular pH (pHi) changers through Ca2+-activated K+ current (BK channel) in single smooth muscle cells from rabbit basilar artery. *Pflugers Arch,* 454**,** 307-19.

Pauli, B.U., Abdel-Ghany, M., Cheng, H.C., Gruber, A.D., Archibald, H.A. & Elble, R.C. (2000) Molecular characteristics and functional diversity of CLCA family members. *Clin Exp Pharmacol Physiol,* 27**,** 901-5.

Paulmichl, M., Li, Y., Wickman, K., Ackerman, M., Peralta, E. & Clapham, D. (1992) New mammalian chloride channel identified by expression cloning. *Nature,* 356**,** 238-41.

Pederson, J.E. & Cantrill, H.L. (1984) Experimental retinal detachment. V. Fluid movement through the retinal hole. *Arch Ophthalmol,* 102**,** 136-9.

Petrukhin, K., Koisti, M.J., Bakall, B., Li, W., Xie, G., Marknell, T., Sandgren, O., Forsman, K., Holmgren, G., Andreasson, S., Vujic, M., Bergen, A.A., Mcgarty-Dugan, V., Figueroa, D., Austin, C.P., Metzker, M.L., Caskey, C.T. & Wadelius, C. (1998) Identification of the gene responsible for Best macular dystrophy. *Nat Genet,* 19**,** 241-7.

Phipps, D.J., Branch, D.R. & Schlichter, L.C. (1996) Chloride-channel block inhibits T lymphocyte activation and signalling. *Cell Signal,* 8**,** 141-9.

Picollo, A., Liantonio, A., Didonna, M.P., Elia, L., Camerino, D.C. & Pusch, M. (2004) Molecular determinants of differential pore blocking of kidney CLC-K chloride channels. *EMBO Rep,* 5**,** 584-9.

Picollo, A. & Pusch, M. (2005) Chloride/proton antiporter activity of mammalian CLC proteins ClC-4 and ClC-5. *Nature,* 436**,** 420-3.

Pifferi, S., Pascarella, G., Boccaccio, A., Mazzatenta, A., Gustincich, S., Menini, A. & Zucchelli, S. (2006) Bestrophin-2 is a candidate calcium-activated chloride channel involved in olfactory transduction. *Proc Natl Acad Sci U S A,* 103**,** 12929-34.

Pilewski, J.M. & Frizzell, R.A. (1999) Role of CFTR in airway disease. *Physiol Rev,* 79**,** S215-55.

Piper, A.S., Greenwood, I.A. & Large, W.A. (2002) Dual effect of blocking agents on Ca2+-activated Cl(-) currents in rabbit pulmonary artery smooth muscle cells. *J Physiol,* 539**,** 119-31.

Piper, A.S. & Large, W.A. (2003) Multiple conductance states of single Ca2+-activated Cl- channels in rabbit pulmonary artery smooth muscle cells. *J Physiol,* 547**,** 181-96.

Poet, M., Kornak, U., Schweizer, M., Zdebik, A.A., Scheel, O., Hoelter, S., Wurst, W., Schmitt, A., Fuhrmann, J.C., Planells-Cases, R., Mole, S.E., Hubner, C.A. & Jentsch, T.J. (2006) Lysosomal storage disease upon disruption of the neuronal chloride transport protein ClC-6. *Proc Natl Acad Sci U S A,* 103**,** 13854-9.

Pollack, K., Kreuz, F.R. & Pillunat, L.E. (2005) [Best's disease with normal EOG. Case report of familial macular dystrophy]. *Ophthalmologe,* 102**,** 891-4.

Ponjavic, V., Eksandh, L., Andreasson, S., Sjostrom, K., Bakall, B., Ingvast, S., Wadelius, C. & Ehinger, B. (1999) Clinical expression of Best's vitelliform macular dystrophy in Swedish families with mutations in the bestrophin gene. *Ophthalmic Genet,* 20**,** 251-7.

Pusch, M. (2002) Myotonia caused by mutations in the muscle chloride channel gene CLCN1. *Hum Mutat,* 19**,** 423-34.

Qu, Z., Chien, L.T., Cui, Y. & Hartzell, H.C. (2006a) The anion-selective pore of the bestrophins, a family of chloride channels associated with retinal degeneration. *J Neurosci,* 26**,** 5411-9.

Qu, Z., Cui, Y. & Hartzell, C. (2006b) A short motif in the C-terminus of mouse bestrophin 3 [corrected] inhibits its activation as a Cl channel. *FEBS Lett,* 580**,** 2141-6.

Qu, Z., Fischmeister, R. & Hartzell, C. (2004) Mouse bestrophin-2 is a bona fide Cl(-) channel: identification of a residue important in anion binding and conduction. *J Gen Physiol,* 123**,** 327-40.

Qu, Z. & Hartzell, C. (2004) Determinants of anion permeation in the second transmembrane domain of the mouse bestrophin-2 chloride channel. *J Gen Physiol,* 124**,** 371-82.

Qu, Z. & Hartzell, H.C. (2000) Anion permeation in Ca(2+)-activated Cl(-) channels. *J Gen Physiol,* 116**,** 825-44.

Qu, Z. & Hartzell, H.C. (2001) Functional geometry of the permeation pathway of

Ca2+-activated Cl-channels inferred from analysis of voltage-dependent block. *J Biol Chem,* 276**,** 18423-9.

Qu, Z. & Hartzell, H.C. (2008) Bestrophin Cl- channels are highly permeable to HCO3. *Am J Physiol Cell Physiol,* 294**,** C1371-7.

Qu, Z., Wei, R.W., Mann, W. & Hartzell, H.C. (2003) Two bestrophins cloned from Xenopus laevis oocytes express Ca(2+)-activated Cl(-) currents. *J Biol Chem,* 278**,** 49563-72.

Qu, Z.Q., Yu, K., Cui, Y.Y., Ying, C. & Hartzell, C. (2007) Activation of bestrophin Cl-channels is regulated by C-terminal domains. *J Biol Chem,* 282**,** 17460-7.

Radford, J.C., Davies, S.A. & Dow, J.A. (2002) Systematic G-protein-coupled receptor analysis in Drosophila melanogaster identifies a leucokinin receptor with novel roles. *J Biol Chem,* 277**,** 38810-7.

Rak, D.J., Hardy, K.M., Jaffe, G.J. & Mckay, B.S. (2006) Ca++-switch induction of RPE differentiation. *Exp Eye Res,* 82**,** 648-56.

Ramet, M., Manfruelli, P., Pearson, A., Mathey-Prevot, B. & Ezekowitz, R.A. (2002) Functional genomic analysis of phagocytosis and identification of a Drosophila receptor for E. coli. *Nature,* 416**,** 644-8.

Rando, R.R. (1992) Molecular mechanisms in visual pigment regeneration. *Photochem Photobiol,* 56**,** 1145-56.

Rappert, A., Biber, K., Nolte, C., Lipp, M., Schubel, A., Lu, B., Gerard, N.P., Gerard, C., Boddeke, H.W. & Kettenmann, H. (2002) Secondary lymphoid tissue chemokine (CCL21) activates CXCR3 to trigger a Cl- current and chemotaxis in murine microglia. *J Immunol,* 168**,** 3221-6.

Reinsprecht, M., Rohn, M.H., Spadinger, R.J., Pecht, I., Schindler, H. & Romanin, C. (1995) Blockade of capacitive Ca2+ influx by Cl- channel blockers inhibits secretion from rat mucosal-type mast cells. *Mol Pharmacol,* 47**,** 1014-20.

Reisert, J., Bauer, P.J., Yau, K.W. & Frings, S. (2003) The Ca-activated Cl channel and its control in rat olfactory receptor neurons. *J Gen Physiol,* 122**,** 349-63.

Riegel, J.A., Farndale, R.W. & Maddrell, S.H. (1999) Fluid secretion by isolated Malpighian tubules of Drosophila melanogaster Meig.: effects of organic anions, quinacrine and a diuretic factor found in the secreted fluid. *J Exp Biol,* 202**,** 2339-48.

Robinson, N.C., Huang, P., Kaetzel, M.A., Lamb, F.S. & Nelson, D.J. (2004) Identification of an N-terminal amino acid of the CLC-3 chloride channel critical in phosphorylation-dependent activation of a CaMKII-activated chloride current. *J Physiol,* 556**,** 353-68.

Rosenthal, N. & Brown, S. (2007) The mouse ascending: perspectives for human-disease models. *Nat Cell Biol,* 9**,** 993-9.

Rosenthal, R., Bakall, B., Kinnick, T., Peachey, N., Wimmers, S., Wadelius, C., Marmorstein, A. & Strauss, O. (2006) Expression of bestrophin-1, the product of the VMD2 gene, modulates voltage-dependent Ca2+ channels in retinal pigment epithelial cells. *FASEB J,* 20**,** 178-80.

Rovner, B.W. (2006) The Charles Bonnet syndrome: a review of recent research. *Curr Opin Ophthalmol,* 17**,** 275-7.

Roy, G. (1995) Amino acid current through anion channels in cultured human glial cells. *J Membr Biol,* 147**,** 35-44.

Saari, J.C. & Bredberg, D.L. (1990) Acyl-CoA:retinol acyltransferase and lecithin:retinol acyltransferase activities of bovine retinal pigment epithelial microsomes. *Methods Enzymol,* 190**,** 156-63.

Sackin, H. (1995) Mechanosensitive channels. *Annu Rev Physiol,* 57**,** 333-53.

Sardini, A., Amey, J.S., Weylandt, K.H., Nobles, M., Valverde, M.A. & Higgins, C.F. (2003) Cell volume regulation and swelling-activated chloride channels. *Biochim Biophys Acta,* 1618**,** 153-62.

Sato, K. & Suzuki, N. (2000) The contribution of a Ca(2+)-activated Cl(-) conductance to amino-acid-induced inward current responses of ciliated olfactory neurons of the rainbow trout. *J Exp Biol,* 203**,** 253-62.

Scheel, O., Zdebik, A.A., Lourdel, S. & Jentsch, T.J. (2005) Voltage-dependent electrogenic chloride/proton exchange by endosomal CLC proteins. *Nature,* 436**,** 424-7.

Schlenker, T. & Fitz, J.G. (1996) Ca(2+)-activated C1- channels in a human biliary cell line: regulation by Ca2+/calmodulin-dependent protein kinase. *Am J Physiol,* 271**,** G304-10.

Schlichter, R., Bader, C.R., Bertrand, D., Dubois-Dauphin, M. & Bernheim, L. (1989) Expression of substance P and of a Ca2+-activated Cl- current in quail sensory trigeminal neurons. *Neuroscience,* 30**,** 585-94.

Schmieder, S., Lindenthal, S., Banderali, U. & Ehrenfeld, J. (1998) Characterization of the putative chloride channel xClC-5 expressed in Xenopus laevis oocytes and comparison with endogenous chloride currents. *J Physiol,* 511 (Pt 2)**,** 379-93.

Schneider, I. (1972) Cell lines derived from late embryonic stages of Drosophila melanogaster. *J Embryol Exp Morphol,* 27**,** 353-65.

Schofield, P.R., Darlison, M.G., Fujita, N., Burt, D.R., Stephenson, F.A., Rodriguez, H., Rhee, L.M., Ramachandran, J., Reale, V., Glencorse, T.A. & Et Al. (1987) Sequence and functional expression of the GABA A receptor shows a ligand-gated receptor super-family. *Nature,* 328**,** 221-7.

Schumacher, P.A., Sakellaropoulos, G., Phipps, D.J. & Schlichter, L.C. (1995) Small-conductance chloride channels in human peripheral T lymphocytes. *J Membr Biol,* 145**,** 217-32.

Schutt, F., Ueberle, B., Schnolzer, M., Holz, F.G. & Kopitz, J. (2002) Proteome analysis of lipofuscin in human retinal pigment epithelial cells. *FEBS Lett,* 528**,** 217-21.

Schwiebert, E.M., Benos, D.J., Egan, M.E., Stutts, M.J. & Guggino, W.B. (1999) CFTR is a conductance regulator as well as a chloride channel. *Physiol Rev,* 79**,** S145-66.

Schwiebert, E.M., Mills, J.W. & Stanton, B.A. (1994) Actin-based cytoskeleton regulates a chloride channel and cell volume in a renal cortical collecting duct cell line. *J Biol Chem,* 269**,** 7081-9.

Scott, R.H., Mcguirk, S.M. & Dolphin, A.C. (1988) Modulation of divalent cation-activated chloride ion currents. *Br J Pharmacol,* 94**,** 653-62.

Seddon, J.M., Afshari, M.A., Sharma, S., Bernstein, P.S., Chong, S., Hutchinson, A., Petrukhin, K. & Allikmets, R. (2001) Assessment of mutations in the Best macular dystrophy (VMD2) gene in patients with adult-onset foveomacular vitelliform dystrophy, age-related maculopathy, and bull's-eye maculopathy. *Ophthalmology,* 108**,** 2060-7.

Shamsi, F.A. & Boulton, M. (2001) Inhibition of RPE lysosomal and antioxidant activity by the age pigment lipofuscin. *Invest Ophthalmol Vis Sci,* 42**,** 3041-6.

Shimbo, K., Brassard, D.L., Lamb, R.A. & Pinto, L.H. (1995) Viral and cellular small integral membrane proteins can modify ion channels endogenous to Xenopus oocytes. *Biophys J,* 69**,** 1819-29.

Snouwaert, J.N., Brigman, K.K., Latour, A.M., Malouf, N.N., Boucher, R.C., Smithies, O. & Koller, B.H. (1992) An animal model for cystic fibrosis made by gene targeting. *Science,* 257**,** 1083-8.

Solc, C.K. & Wine, J.J. (1991) Swelling-induced and depolarization-induced C1-channels in normal and cystic fibrosis epithelial cells. *Am J Physiol,* 261**,** C658-74.

Sorota, S. (1992) Swelling-induced chloride-sensitive current in canine atrial cells revealed by whole-cell patch-clamp method. *Circ Res,* 70**,** 679-87.

Sorota, S. (1995) Tyrosine protein kinase inhibitors prevent activation of cardiac swelling-induced chloride current. *Pflugers Arch,* 431**,** 178-85.

Sorota, S. & Du, X.Y. (1998) Delayed activation of cardiac swelling-induced chloride current after step changes in cell size. *J Cardiovasc Electrophysiol,* 9**,** 825-31.

Souktani, R., Berdeaux, A., Ghaleb, B., Giudicelli, J.F., Guize, L., Le Heuzey, J.Y. & Henry, P. (2000) Induction of apoptosis using sphingolipids activates a chloride current in Xenopus laevis oocytes. *Am J Physiol Cell Physiol,* 279**,** C158-65.

Sozen, M.A., Armstrong, J.D., Yang, M., Kaiser, K. & Dow, J.A. (1997) Functional domains are specified to single-cell resolution in a Drosophila epithelium. *Proc*

Natl Acad Sci U S A, 94**,** 5207-12.

Sparrow, J.R. & Cai, B. (2001) Blue light-induced apoptosis of A2E-containing RPE: involvement of caspase-3 and protection by Bcl-2. *Invest Ophthalmol Vis Sci,* 42**,** 1356-62.

Spitzner, M., Martins, J.R., Soria, R.B., Ousingsawat, J., Scheidt, K., Schreiber, R. & Kunzelmann, K. (2008) Eag1 and Bestrophin 1 are up-regulated in fast-growing colonic cancer cells. *J Biol Chem,* 283**,** 7421-8.

Srivastava, A., Romanenko, V.G., Gonzalez-Begne, M., Catalan, M.A. & Melvin, J.E. (2008) A Variant of the Ca(2+)-Activated Cl Channel Best3 is Expressed in Mouse Exocrine Glands. *J Membr Biol*.

Stanton, J.B., Goldberg, A.F., Hoppe, G., Marmorstein, L.Y. & Marmorstein, A.D. (2006) Hydrodynamic properties of porcine bestrophin-1 in Triton X-100. *Biochim Biophys Acta,* 1758**,** 241-7.

Stapleton, S.R., Scott, R.H. & Bell, B.A. (1994) Effects of metabolic blockers on Ca(2+)-dependent currents in cultured sensory neurones from neonatal rats. *Br J Pharmacol,* 111**,** 57-64.

Steinberg, R.H. (1985) Interactions between the retinal pigment epithelium and the neural retina. *Doc Ophthalmol,* 60**,** 327-46.

Steinmeyer, K., Ortland, C. & Jentsch, T.J. (1991) Primary structure and functional expression of a developmentally regulated skeletal muscle chloride channel. *Nature,* 354**,** 301-4.

Steinmeyer, K., Schwappach, B., Bens, M., Vandewalle, A. & Jentsch, T.J. (1995) Cloning and functional expression of rat CLC-5, a chloride channel related to kidney disease. *J Biol Chem,* 270**,** 31172-7.

Steward, C.G. (2003) Neurological aspects of osteopetrosis. *Neuropathol Appl Neurobiol,* 29**,** 87-97.

Stoddard, J.S., Steinbach, J.H. & Simchowitz, L. (1993) Whole cell Cl- currents in human neutrophils induced by cell swelling. *Am J Physiol,* 265**,** C156-65.

Stohr, H., Marquardt, A., Rivera, A., Cooper, P.R., Nowak, N.J., Shows, T.B., Gerhard, D.S. & Weber, B.H. (1998) A gene map of the Best's vitelliform macular dystrophy region in chromosome 11q12-q13.1. *Genome Res,* 8**,** 48-56.

Stone, E.M., Nichols, B.E., Streb, L.M., Kimura, A.E. & Sheffield, V.C. (1992) Genetic linkage of vitelliform macular degeneration (Best's disease) to chromosome 11q13. *Nat Genet,* 1**,** 246-50.

Strange, K. (1992) Regulation of solute and water balance and cell volume in the central nervous system. *J Am Soc Nephrol,* 3**,** 12-27.

Strange, K., Emma, F. & Jackson, P.S. (1996) Cellular and molecular physiology of volume-sensitive anion channels. *Am J Physiol,* 270**,** C711-30.

Strange, K. & Jackson, P.S. (1995) Swelling-activated organic osmolyte efflux: a new role for anion channels. *Kidney Int,* 48**,** 994-1003.

Strauss, O. (2005) The retinal pigment epithelium in visual function. *Physiol Rev,* 85**,** 845-81.

Sun, H., Tsunenari, T., Yau, K.W. & Nathans, J. (2002) The vitelliform macular dystrophy protein defines a new family of chloride channels. *Proc Natl Acad Sci U S A,* 99**,** 4008-13.

Suzuki, M. & Mizuno, A. (2004) A novel human Cl(-) channel family related to Drosophila flightless locus. *J Biol Chem,* 279**,** 22461-8.

Suzuki, M., Morita, T. & Iwamoto, T. (2006) Diversity of Cl(-) channels. *Cell Mol Life Sci,* 63**,** 12-24.

Szucs, G., Heinke, S., Droogmans, G. & Nilius, B. (1996) Activation of the volume-sensitive chloride current in vascular endothelial cells requires a permissive intracellular Ca2+ concentration. *Pflugers Arch,* 431**,** 467-9.

Takahashi, T., Neher, E. & Sakmann, B. (1987) Rat brain serotonin receptors in Xenopus oocytes are coupled by intracellular calcium to endogenous channels. *Proc Natl Acad Sci U S A,* 84**,** 5063-7.

Takano, T., Kang, J., Jaiswal, J.K., Simon, S.M., Lin, J.H., Yu, Y., Li, Y., Yang, J., Dienel, G., Zielke, H.R. & Nedergaard, M. (2005) Receptor-mediated glutamate release from volume sensitive channels in astrocytes. *Proc Natl Acad Sci U S A,* 102**,** 16466-71.

Taleb, O., Feltz, P., Bossu, J.L. & Feltz, A. (1988) Small-conductance chloride channels activated by calcium on cultured endocrine cells from mammalian pars intermedia. *Pflugers Arch,* 412**,** 641-6.

Tavsanli, B.C., Pappu, K.S., Mehta, S.Q. & Mardon, G. (2001) Dbest1, a Drosophila homolog of human Bestrophin, is not required for viability or photoreceptor integrity. *Genesis,* 31**,** 130-6.

Terman, A. & Brunk, U.T. (1998) On the degradability and exocytosis of ceroid/lipofuscin in cultured rat cardiac myocytes. *Mech Ageing Dev,* 100**,** 145-56.

Thiemann, A., Grunder, S., Pusch, M. & Jentsch, T.J. (1992) A chloride channel widely expressed in epithelial and non-epithelial cells. *Nature,* 356**,** 57-60.

Thoreson, W.B. & Burkhardt, D.A. (1991) Ionic influences on the prolonged depolarization of turtle cones in situ. *J Neurophysiol,* 65**,** 96-110.

Tominaga, M., Tominaga, T., Miwa, A. & Okada, Y. (1995) Volume-sensitive chloride channel activity does not depend on endogenous P-glycoprotein. *J Biol Chem,* 270**,** 27887-93.

Tseng, G.N. (1992) Cell swelling increases membrane conductance of canine cardiac cells: evidence for a volume-sensitive Cl channel. *Am J Physiol,* 262**,** C1056-68.

Tsuboi, S. (1990) Fluid movement across the blood-retinal barrier: a review of studies by vitreous fluorophotometry. *Jpn J Ophthalmol,* 34**,** 133-41.

Tsunenari, T., Nathans, J. & Yau, K.W. (2006) Ca2+-activated Cl- current from human bestrophin-4 in excised membrane patches. *J Gen Physiol,* 127**,** 749-54.

Tsunenari, T., Sun, H., Williams, J., Cahill, H., Smallwood, P., Yau, K.W. & Nathans, J. (2003) Structure-function analysis of the bestrophin family of anion channels. *J Biol Chem,* 278**,** 41114-25.

Tzounopoulos, T., Maylie, J. & Adelman, J.P. (1995) Induction of endogenous channels by high levels of heterologous membrane proteins in Xenopus oocytes. *Biophys J,* 69**,** 904-8.

Ueda, Y. & Steinberg, R.H. (1994) Chloride currents in freshly isolated rat retinal pigment epithelial cells. *Exp Eye Res,* 58**,** 331-42.

Valverde, M.A., Diaz, M., Sepulveda, F.V., Gill, D.R., Hyde, S.C. & Higgins, C.F. (1992) Volume-regulated chloride channels associated with the human multidrug-resistance P-glycoprotein. *Nature,* 355**,** 830-3.

Van Gelder, R.N., Von Zastrow, M.E., Yool, A., Dement, W.C., Barchas, J.D. & Eberwine, J.H. (1990) Amplified RNA synthesized from limited quantities of heterogeneous cDNA. *Proc Natl Acad Sci U S A,* 87**,** 1663-7.

Van Renterghem, C. & Lazdunski, M. (1993) Endothelin and vasopressin activate low conductance chloride channels in aortic smooth muscle cells. *Pflugers Arch,* 425**,** 156-63.

Vandewalle, A., Cluzeaud, F., Bens, M., Kieferle, S., Steinmeyer, K. & Jentsch, T.J. (1997) Localization and induction by dehydration of ClC-K chloride channels in the rat kidney. *Am J Physiol,* 272**,** F678-88.

Villaz, M., Cinniger, J.C. & Moody, W.J. (1995) A voltage-gated chloride channel in ascidian embryos modulated by both the cell cycle clock and cell volume. *J Physiol,* 488 (Pt 3)**,** 689-99.

Voets, T., Buyse, G., Tytgat, J., Droogmans, G., Eggermont, J. & Nilius, B. (1996) The chloride current induced by expression of the protein pICln in Xenopus oocytes differs from the endogenous volume-sensitive chloride current. *J Physiol,* 495 (Pt 2)**,** 441-7.

Voets, T., Szucs, G., Droogmans, G. & Nilius, B. (1995) Blockers of volume-activated Cl- currents inhibit endothelial cell proliferation. *Pflugers Arch,* 431**,** 132-4.

Voets, T., Wei, L., De Smet, P., Van Driessche, W., Eggermont, J., Droogmans, G. & Nilius, B. (1997) Downregulation of volume-activated Cl- currents during muscle differentiation. *Am J Physiol,* 272**,** C667-74.

Wabbels, B., Preising, M.N., Kretschmann, U., Demmler, A. & Lorenz, B. (2006) Genotype-phenotype correlation and longitudinal course in ten families with Best vitelliform macular dystrophy. *Graefes Arch Clin Exp Ophthalmol,* 244**,** 1453-66.

Wafford, K.A., Lummis, S.C. & Sattelle, D.B. (1989) Block of an insect central nervous system GABA receptor by cyclodiene and cyclohexane insecticides. *Proc R Soc Lond B Biol Sci,* 237**,** 53-61.

Wagner, J.A., Cozens, A.L., Schulman, H., Gruenert, D.C., Stryer, L. & Gardner, P. (1991) Activation of chloride channels in normal and cystic fibrosis airway epithelial cells by multifunctional calcium/calmodulin-dependent protein kinase. *Nature,* 349**,** 793-6.

Wajima, R., Chater, S.B., Katsumi, O., Mehta, M.C. & Hirose, T. (1993) Correlating visual acuity and electrooculogram recordings in Best's disease. *Ophthalmologica,* 207**,** 174-81.

Wang, C.T., Zhang, H.G., Rocheleau, T.A., Ffrench-Constant, R.H. & Jackson, M.B. (1999) Cation permeability and cation-anion interactions in a mutant GABA-gated chloride channel from Drosophila. *Biophys J,* 77**,** 691-700.

Wang, Q., Wang, Y.X., Yu, M. & Kotlikoff, M.I. (1997) Ca(2+)-activated Cl- currents are activated by metabolic inhibition in rat pulmonary artery smooth muscle cells. *Am J Physiol,* 273**,** C520-30.

Warskulat, U., Zhang, F. & Haussinger, D. (1996) Modulation of phagocytosis by anisoosmolarity and betaine in rat liver macrophages (Kupffer cells) and RAW 264.7 mouse macrophages. *FEBS Lett,* 391**,** 287-92.

Weber, B.H., Walker, D., Muller, B. & Mar, L. (1994) Best's vitelliform dystrophy (VMD2) maps between D11S903 and PYGM: no evidence for locus heterogeneity. *Genomics,* 20**,** 267-74.

Weiss, M.S., Abele, U., Weckesser, J., Welte, W., Schiltz, E. & Schulz, G.E. (1991) Molecular architecture and electrostatic properties of a bacterial porin. *Science,* 254**,** 1627-30.

Wettstein, M., Peters-Regehr, T., Kubitz, R., Fischer, R., Holneicher, C., Monnighoff, I. &

Haussinger, D. (2000) Release of osmolytes induced by phagocytosis and hormones in rat liver. *Am J Physiol Gastrointest Liver Physiol,* 278**,** G227-33.

White, K., Marquardt, A. & Weber, B.H. (2000) VMD2 mutations in vitelliform macular dystrophy (Best disease) and other maculopathies. *Hum Mutat,* 15**,** 301-8.

White, M.M. & Aylwin, M. (1990) Niflumic and flufenamic acids are potent reversible blockers of Ca2(+)-activated Cl- channels in Xenopus oocytes. *Mol Pharmacol,* 37**,** 720-4.

Worrell, R.T., Butt, A.G., Cliff, W.H. & Frizzell, R.A. (1989) A volume-sensitive chloride conductance in human colonic cell line T84. *Am J Physiol,* 256**,** C1111-9.

Worrell, R.T. & Frizzell, R.A. (1991) CaMKII mediates stimulation of chloride conductance by calcium in T84 cells. *Am J Physiol,* 260**,** C877-82.

Xie, W., Solomons, K.R., Freeman, S., Kaetzel, M.A., Bruzik, K.S., Nelson, D.J. & Shears, S.B. (1998) Regulation of Ca2+-dependent Cl- conductance in a human colonic epithelial cell line (T84): cross-talk between Ins(3,4,5,6)P4 and protein phosphatases. *J Physiol,* 510 (Pt 3)**,** 661-73.

Yanagi, Y., Sekine, H. & Mori, M. (2002) Identification of a novel VMD2 mutation in Japanese patients with Best disease. *Ophthalmic Genet,* 23**,** 129-33.

Yang, Y.D., Cho, H., Koo, J.Y., Tak, M.H., Cho, Y., Shim, W.S., Park, S.P., Lee, J., Lee, B., Kim, B.M., Raouf, R., Shin, Y.K. & Oh, U. (2008) TMEM16A confers receptor-activated calcium-dependent chloride conductance. *Nature*.

Yardley, J., Leroy, B.P., Hart-Holden, N., Lafaut, B.A., Loeys, B., Messiaen, L.M., Perveen, R., Reddy, M.A., Bhattacharya, S.S., Traboulsi, E., Baralle, D., De Laey, J.J., Puech, B., Kestelyn, P., Moore, A.T., Manson, F.D. & Black, G.C. (2004) Mutations of VMD2 splicing regulators cause nanophthalmos and autosomal dominant vitreoretinochoroidopathy (ADVIRC). *Invest Ophthalmol Vis Sci,* 45**,** 3683-9.

Yoshikawa, M., Uchida, S., Ezaki, J., Rai, T., Hayama, A., Kobayashi, K., Kida, Y., Noda, M., Koike, M., Uchiyama, Y., Marumo, F., Kominami, E. & Sasaki, S. (2002) CLC-3 deficiency leads to phenotypes similar to human neuronal ceroid lipofuscinosis. *Genes Cells,* 7**,** 597-605.

Young, R.W. (1987) Pathophysiology of age-related macular degeneration. *Surv Ophthalmol,* 31**,** 291-306.

Yu, K., Cui, Y. & Hartzell, H.C. (2006) The bestrophin mutation A243V, linked to adult-onset vitelliform macular dystrophy, impairs its chloride channel function. *Invest Ophthalmol Vis Sci,* 47**,** 4956-61.

Yu, K., Qu, Z., Cui, Y. & Hartzell, H.C. (2007) Chloride channel activity of bestrophin mutants associated with mild or late-onset macular degeneration. *Invest Ophthalmol Vis Sci,* 48**,** 4694-705.

Yu, K., Xiao, Q., Cui, G., Lee, A. & Hartzell, H.C. (2008) The best disease-linked Cl- channel hBest1 regulates Ca V 1 (L-type) Ca2+ channels via src-homology-binding domains. *J Neurosci,* 28**,** 5660-70.

Zhang, G.H., Arreola, J. & Melvin, J.E. (1995) Inhibition by thiocyanate of muscarinic-induced cytosolic acidification and Ca2+ entry in rat sublingual acini. *Arch Oral Biol,* 40**,** 111-8.

Zhang, J.J. & Jacob, T.J. (1997) Three different Cl- channels in the bovine ciliary epithelium activated by hypotonic stress. *J Physiol,* 499 (Pt 2)**,** 379-89.

Zygmunt, A.C. (1994) Intracellular calcium activates a chloride current in canine ventricular myocytes. *Am J Physiol,* 267**,** H1984-95.

Zygmunt, A.C., Goodrow, R.J. & Weigel, C.M. (1998) INaCa and ICl(Ca) contribute to isoproterenol-induced delayed after depolarizations in midmyocardial cells. *Am J Physiol,* 275**,** H1979-92.